

**Engineering Properties of High Performance Concrete
Containing Large Volume of Class C Fly Ash**

A Thesis

Submitted to the Faculty of Graduate Studies and Research
in Partial Fulfillment of the Requirements

for the Degree of

Doctor of Philosophy

in the

Department of Civil Engineering

University of Saskatchewan, Canada

by

Elli Makrides-Saravanos

Saskatoon, Saskatchewan, Canada

Fall, 1995



National Library
of Canada

Acquisitions and
Bibliographic Services

395 Wellington Street
Ottawa ON K1A 0N4
Canada

Bibliothèque nationale
du Canada

Acquisitions et
services bibliographiques

395, rue Wellington
Ottawa ON K1A 0N4
Canada

Your file *Votre référence*

Our file *Notre référence*

The author has granted a non-exclusive licence allowing the National Library of Canada to reproduce, loan, distribute or sell copies of this thesis in microform, paper or electronic formats.

The author retains ownership of the copyright in this thesis. Neither the thesis nor substantial extracts from it may be printed or otherwise reproduced without the author's permission.

L'auteur a accordé une licence non exclusive permettant à la Bibliothèque nationale du Canada de reproduire, prêter, distribuer ou vendre des copies de cette thèse sous la forme de microfiche/film, de reproduction sur papier ou sur format électronique.

L'auteur conserve la propriété du droit d'auteur qui protège cette thèse. Ni la thèse ni des extraits substantiels de celle-ci ne doivent être imprimés ou autrement reproduits sans son autorisation.

0-612-23904-7

UNIVERSITY OF SASKATCHEWAN

College of Graduate Studies and Research

SUMMARY OF DISSERTATION

Submitted in Partial Fulfillment
of the Requirements for the

DEGREE OF DOCTOR OF PHILOSOPHY

by

ELLI MAKRIDES-SARAVANOS

Department of Civil Engineering
University of Saskatchewan

Spring 1996

EXAMINATION COMMITTEE:

Dr. D. Norum	Dean/Associate Dean/ Dean's Designate, Chair, College of Graduate Studies and Research
Dr. D.E. Pufahl	Department of Civil Engineering
Dr. K.W. Nasser	Supervisor, Department of Civil Engineering
Dr. T. Rezansoff	Department of Civil Engineering
Dr. V.V. Neis	Department of Civil Engineering
Dr. G. Sparks	Department of Civil Engineering
Dr. J. Postlethwaite	Department of Chemical Engineering
Dr. S. Yannacopoulos	Department of Mechanical Engineering

EXTERNAL EXAMINER

Dr. Michael Ward
The Dean' Office of Engineering
University of Calgary
Calgary, Alberta, Canada T2N 1N4

ENGINEERING PROPERTIES OF HIGH PERFORMANCE CONCRETE CONTAINING LARGE VOLUME OF CLASS C FLY ASH

This investigation for the use of large volume of fly ash in concrete in combination with superplasticizer, was for the purpose of optimizing its mechanical properties while reducing its cost. Several concrete mixtures using coarse/fine aggregate ratio of 1.22 and aggregate/binder ratio of 5.1 were investigated. Fly ash was used as a partial replacement of type 10 Portland cement at levels ranging between 20 - 60% by weight of the total cementitious materials in the mixture. Use of superplasticizer allowed a reduction of the water/binder ratio to 0.28 - 0.33, while the K-slump of fresh concrete was kept at a practical level of 25%. The effect of fly ash on the development of the compressive strength of the hardened concrete was determined.

The selection of a concrete mixture with an optimum fly-ash/cement ratio was based on compressive strength results and cost. Concrete with compressive strength levels of 50 MPa, applicable to mid-rise buildings, mine structural components and bridge construction, was obtained by taking advantage of the water reducing properties of superplasticizers, and by replacing 50% of the cement with Class C fly ash. The 28-day compressive strength of the resultant concrete was approximately 80% of the strength of the identical control mixture containing no fly ash replacement of the cement; at 56 and 91 days, the strength of the resultant mixture improved and eventually became identical to that of the control mixture. The above results were achieved with a 10% reduction in cost, which is a significant savings for the construction industry.

The selected mixture was tested for its engineering properties of strength, elasticity, shrinkage and creep, and the results were compared to the same properties of a control mixture.

Creep and shrinkage are important concrete properties in prestressed and reinforced concrete structures. Time-dependent deformation of concrete due to creep and shrinkage, results in partial loss of the prestress force and produces significant changes in deflection. In reinforced concrete structures a slow growth of deflection with time may lead to eventual unsatisfactory performance of the structure. Creep and shrinkage of concrete are affected by time, stress intensity, temperature and humidity. In the present study it is indicated that fly ash concrete under sustained loads at room temperature while its creep increased with a rise in sustained temperatures.

Durability tests were performed using freezing-and-thawing and sulphate resistance experiments. The results were compared to the same properties of a control mixture containing superplasticizer and 100% type 10 Portland cement. The frost resistance of fly ash concrete was found to be comparable to the control mixture. The presence of a large volume of fly ash improved the sulphate resistance of the hardened concrete.

Microstructural studies were concurrently conducted in order to determine and explain the effects of superplasticizer and fly ash in producing high performance concrete.

The author has agreed that the Library, University of Saskatchewan, may make this thesis freely available for inspection. Moreover, the author has agreed that permission for extensive copying of this thesis for scholarly purposes may be granted by the professor or professors who supervised the thesis work recorded herein or, in their absence, by the Head of the Department or the Dean of the College in which the thesis work was done. It is understood that due recognition will be given to the author of this thesis and to the University of Saskatchewan in any use of the material in this thesis. Copying or publication or any other use of the thesis for financial gain without approval by the University of Saskatchewan and the author's written permission is prohibited.

Requests for permission to copy or to make any other use of material in this thesis in whole or in part should be addressed to:

Head of the Department of Civil Engineering
University of Saskatchewan
Saskatoon, Saskatchewan, Canada.



**UNIVERSITY OF SASKATCHEWAN
COLLEGE OF GRADUATE STUDIES AND RESEARCH**

Saskatoon

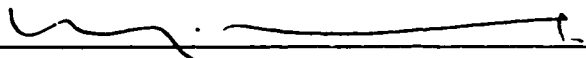
CERTIFICATION OF THESIS WORK

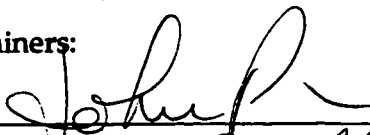
We, the undersigned, certify that **Elli MAKRIDES-SARAVANOS**, candidate for the degree of Doctor of Philosophy has presented a thesis with the following title: ***"Engineering Properties of High Performance Concrete Containing Large Volumes of Class C Fly Ash."***

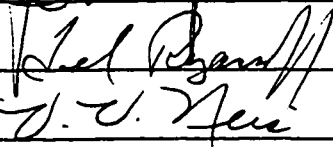
We consider that the thesis is acceptable in form and content, and that a satisfactory knowledge of the field covered by the thesis was demonstrated by the candidate through an oral examination held on September 25, 1995.

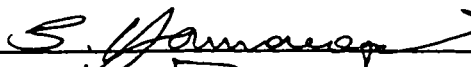
External Examiner: Dr. Michael Ward
Dean's Office of Engineering
University of Calgary


Internal Examiners:

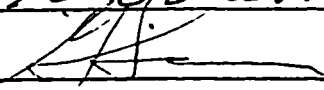












ABSTRACT

This investigation for the use of large volume of fly ash in concrete in combination with superplasticizer, was for the purpose of optimizing its mechanical properties while reducing its cost. Several concrete mixtures using coarse/fine aggregate ratio of 1.22 and aggregate/binder ratio of 5.1 were investigated. Fly ash was used as a partial replacement of type 10 Portland cement at levels ranging between 20 - 60 % by weight of the total cementitious materials in the mixture. Use of superplasticizer allowed a reduction of the water/binder ratio to 0.28 - 0.33, while the K-slump of fresh concrete was kept at a practical level of 25%. The effect of fly ash on the development of the compressive strength of the hardened concrete was determined.

The selection of a concrete mixture with an optimum fly-ash/cement ratio was based on compressive strength results and cost. Concrete with compressive strength levels of 50 MPa, applicable to mid-rise buildings, mine structural components and bridge construction, was obtained by taking advantage of the water reducing properties of superplasticizers, and by replacing 50% of the cement with Class C fly ash. The 28-day compressive strength of the resultant concrete was approximately 80% of the strength of the identical control mixture containing no fly ash replacement of the cement; at 56 and 91 days, the strength of the resultant mixture improved and eventually became identical to that of the control mixture. The above results were achieved with a 10% reduction in cost, which is a significant savings for the construction industry.

The selected mixture was tested for its engineering properties of strength, elasticity, shrinkage and creep, and the results were compared to the same properties of a control mixture.

Creep and shrinkage are important concrete properties in prestressed and reinforced concrete structures. Time-dependent deformation of concrete due to creep and shrinkage, results in partial loss of the prestress force and produces significant changes in deflection. In reinforced concrete structures a slow growth of deflection with time may lead to eventual unsatisfactory performance of the structure. Creep and shrinkage of concrete are affected by time, stress intensity, temperature and humidity. In the present study it is indicated that fly ash concrete produced lower creep and drying shrinkage strains than the control concrete under sustained loads at room temperature while its creep increased with a rise in sustained temperatures.

Durability tests were performed using freezing-and-thawing and sulphate resistance experiments. The results were compared to the same properties of a control mixture containing superplasticizer and 100% type 10 Portland cement. The frost resistance of fly ash concrete was found to be comparable to the control mixture. The presence of a large volume of fly ash improved the sulphate resistance of the hardened concrete.

Microstructural studies were concurrently conducted in order to determine and explain the effects of superplasticizer and fly ash in producing high performance concrete.

ACKNOWLEDGEMENTS

For the support and freedom I was given, to develop leadership skills in scientific research, I wish to express my most sincere gratitude to my supervisor Dr. K. W. Nasser. I wish to also express my appreciation to the members of my advisory committee for their positive contribution towards my research, and Dr. M. Bickis for his interest in my work and many helpful discussions on statistics.

Special thanks to Tom Bonli for his help with the microstructural investigation and also to Dan, Alex and my fellow graduate students for their help with the experiments.

My family's graceful assistance that led to the completion of this work, deserves special recognition.

Table of Contents

ABSTRACT	i
AKNOWLEDGEMENTS	iii
TABLE OF CONTENTS	iv
LIST OF TABLES	viii
LIST OF FIGURES	ix
1. INTRODUCTION.....	1
1.1 GENERAL	1
1.2 ADVANTAGES OF FLY ASH IN CONCRETE	3
1.3 OBJECTIVES AND SCOPE OF THIS STUDY	4
<i>1.3.1 Background</i>	4
<i>1.3.2 Objectives</i>	6
2. LITERATURE REVIEW	8
2.1 GENERAL	8
2.2 PORTLAND CEMENT AND GELS IN GENERAL.....	9

2.3 THE STRUCTURE AND FUNDAMENTAL PROPERTIES OF GELS	9
2.4 PORTLAND CEMENT COMPOSITION	13
2.5 PORTLAND CEMENT HYDRATION.....	14
2.6 STRUCTURE OF THE CEMENT PASTE.....	22
2.7 SUPERPLASTICIZERS.....	24
2.8 USE OF FLY ASH IN CONCRETE	28
2.9 STRUCTURE OF FLY ASH PARTICLES.....	30
2.10 POZZOLAN - CEMENT INTERACTION AND ITS MICROSTRUCTURE	32
2.11 EFFECT OF FLY ASH ON THE RHEOLOGY OF FRESH CONCRETE.....	34
2.12 EFFECT OF FLY ASH ON THE MECHANICAL PROPERTIES OF CONCRETE	35
2.12.1 <i>Compressive Strength and Static Elastic Modulus</i>	35
2.12.2 <i>Long-Term Deformation: Creep and Drying Shrinkage</i>	38
2.12.3 <i>Frost Resistance</i>	40
2.12.4 <i>Resistance to Sulphate Attack</i>	41
 3. TEST PROGRAM AND PROCEDURE	43
3.1 GENERAL OUTLINE OF PROGRAM	43
3.2 MATERIALS.....	45
3.3 PREPARATION AND PROPORTIONING OF THE CONCRETE MIXTURES	47
3.4 PREPARATION AND CURING OF CONCRETE TEST SPECIMENS.....	50
3.4.1 <i>Concrete Cylinders for Compressive Strength Testing</i>	52
3.4.2 <i>Concrete Cylinders for Creep and Shrinkage Testing</i>	53
3.4.3 <i>Concrete Prisms for Freezing-Thawing Durability Testing</i>	57
3.4.4 <i>Concrete Prisms for Sulphate Resistance Testing</i>	58
3.5 APPARATUS AND TESTING PROCEDURES.....	59
3.5.1 <i>Compressive Strength Tests</i>	59

3.5.2 Long Term Deformation Testing.....	60
3.5.3 Freezing-Thawing Durability Testing	68
3.5.4 Sulphate Resistance Tests	70
3.6 MICROSTRUCTURAL EXAMINATION	73
3.6.1 General	73
3.6.2 The Atomic Theory.....	74
3.6.3 Operation of the Scanning Electron Microscope (SEM)	76
3.6.4 Electron - Specimen Interactions.....	81
3.6.5 SEM Specimen Preparation.....	84
 4. EXPERIMENTAL RESULTS.....	 87
4.1 INTRODUCTION	87
4.2 WORKABILITY OF FRESH CONCRETE MIXTURES.....	87
4.3 COMPRESSIVE STRENGTH TEST RESULTS.....	90
4.4 MODULUS OF ELASTICITY TEST RESULTS	98
4.5 LONG-TERM DEFORMATION TEST RESULTS	100
4.5.1 Moisture Influence on Shrinkage Characteristics	100
4.5.2 Moisture Influence on Creep Characteristics.....	102
4.5.3 Moisture Influence on Creep Recovery.....	110
4.5.4 Temperature Influence on Creep Characteristics.....	111
4.6 FROST RESISTANCE.....	116
4.7 SULPHATE RESISTANCE	121
 5. MICROSTRUCTURAL ANALYSIS.....	 123
5.1 INTRODUCTION	123

5.2 COMPRESSIVE STRENGTH AND STATIC MODULUS OF ELASTICITY	124
5.3 LONG-TERM DEFORMATION	130
<i>5.3.1 Moisture Influence on Creep Characteristics.....</i>	<i>131</i>
<i>5.3.2 Temperature Influence on Creep Characteristics.....</i>	<i>142</i>
5.4 FROST RESISTANCE.....	154
5.5 RESISTANCE TO SULPHATE ATTACK	161
 6. CONCLUSIONS AND RECOMMENDATIONS.....	176
6.1 SUMMARY	176
6.2 CONCLUSIONS.....	178
6.3 RECOMMENDATIONS	181
<i>6.3.1 Optimum Mixture Using Class C Fly Ash.....</i>	<i>181</i>
<i>6.3.2 Recommendations for Future Research.....</i>	<i>182</i>
 7. REFERENCES.....	184
 APPENDIX A.....	194
CHEMICAL AND PHYSICAL PROPERTIES OF MATERIALS	
 APPENDIX B	199
STATISTICAL ANALYSIS OF COMPRESSIVE STRENGTH	
 APPENDIX C	219
FREEZING-AND-THAWING RESULTS	

List of Tables

<i>Table 2.1</i>	<i>Market Prices of Cement and Mineral Admixtures</i>	<i>5</i>
<i>Table 2.1</i>	<i>Portland Cement - Chemical Composition.....</i>	<i>13</i>
<i>Table 2.2</i>	<i>Chemical composition of some fly ashes high in CaO (Taylor, 1990).</i>	<i>30</i>
<i>Table 3.1</i>	<i>Concrete Mixture Design.....</i>	<i>48</i>
<i>Table 3.2</i>	<i>Summary of the various tests and their specimens as they were used in this study.</i>	<i>50</i>
<i>Table 4.1</i>	<i>Properties of fresh and hardened concrete.....</i>	<i>89</i>
<i>Table A.1</i>	<i>Chemical Analysis and Physical Properties of Portland Cement.</i>	<i>195</i>
<i>Table A.2</i>	<i>Chemical Analysis and Physical Properties of Class C Fly Ash (Sundance, Alberta)</i>	<i>196</i>
<i>Table A.3</i>	<i>Chemical Analysis of anhydrous sodium sulphate (supplied by manufacturer)</i>	<i>197</i>
<i>Table A.4</i>	<i>Chemical Analysis of Tap Water Used for Mixing</i>	<i>198</i>
<i>Table C.1</i>	<i>Air void characteristics of hardened fly ash and control concretes, measured according to ASTM C-457 standard.</i>	<i>220</i>
<i>Table C.2</i>	<i>Density and K-Slump of fresh concrete.</i>	<i>220</i>

List of Figures

<i>Figure 2.1</i>	<i>Electrical double layer and potential fall in layers. The potential drop in the diffuse or mobile layer is called the zeta-potential (Jastrzebski, 1987).....</i>	<i>11</i>
<i>Figure 2.2</i>	<i>Formation of gel. (a) Colloidal dispersion. (b) Gel structure; colloidal particles form a connected structure interpenetrated by dispersing liquid (Jastrzebski, 1987).</i>	<i>11</i>
<i>Figure 2.3</i>	<i>Development of microstructure during the hydration of portland cement (Scrivener, 1984).....</i>	<i>21</i>
<i>Figure 2.4</i>	<i>Scanning Electron Micrograph of portland cement showing grain morphology (Magnification 400x).</i>	<i>32</i>
<i>Figure 2.5</i>	<i>Scanning Electron Micrograph of fly ash showing particle morphology (Magnification 400x).</i>	<i>32</i>
<i>Figure 3.1</i>	<i>Steel molds clamped to vibrating table for preparation of creep and shrinkage test specimens.</i>	<i>55</i>
<i>Figure 3.2</i>	<i>Stress-and-moisture interaction experimental set-up.</i>	<i>62</i>
<i>Figure 3.3</i>	<i>Creep apparatus with partial view of experimental set-up at room temperature of 21^o C (70^o F).</i>	<i>63</i>
<i>Figure 3.4</i>	<i>Partial view of the high temperature creep equipment.....</i>	<i>65</i>
<i>Figure 3.5</i>	<i>Stress-and-temperature interaction experimental set-up.....</i>	<i>66</i>
<i>Figure 3.6</i>	<i>Concrete specimens inside metal containers in the freezing-thawing tank.....</i>	<i>68</i>

<i>Figure 3.7 Experimental set-up for sulphate resistance of fly ash and control concrete.</i>	72
<i>Figure 3.8 Sulphate resistance test specimens immersed in Na₂SO₄ solution.</i>	72
<i>Figure 3.9 Schematic representation of Bohr's hydrogen model.</i>	75
<i>Figure 3.10 Relationship between wavelength (l) and atomic number (Z) (Goldstein and Yakowitz, 1975).</i>	78
<i>Figure 3.11 Interaction volumes for various electron specimen interactions (Goldstein and Yakowitz, 1975).</i>	79
<i>Figure 3.12 Schematic effect of accelerating voltage and specimen composition on the volume of excitation (Robertson, 1990).</i>	80
<i>Figure 3.13 The effect of surface irregularities on X-ray photon energy.</i>	85
<i>Figure 3.14 The effect of surface irregularities on the number of backscattered electrons that may reach the detector.</i>	86
<i>Figure 4.1 Compressive strength development of concrete made with Rheobuild 1000 superplasticizer for various contents of Class C fly ash.</i>	92
<i>Figure 4.2 K-5 accelerated strength development test results for concrete made with Rheobuild 1000 superplasticizer, for various contents of Class C fly ash.</i>	92
<i>Figure 4.3 Compressive strength development of concrete made with Pozzolith 400N superplasticizer for various contents of Class C fly ash.</i>	93
<i>Figure 4.4 K-5 accelerated strength development test results for concrete made with Pozzolith 400N superplasticizer, for various contents of Class C fly ash.</i>	93
<i>Figure 4.5 Relative cost of concrete based on compressive strength and fly ash content.</i>	96
<i>Figure 4.6 Compressive strength development of control mixture and concrete containing 50% fly ash using Rheobuild 1000 superplasticizer.</i>	96

<i>Figure 4.7</i>	<i>Compressive strength of 50% fly ash concrete, following completion of creep tests (sealed test specimens), as a percentage of the strength at the initial application of external stress.</i>	<i>97</i>
<i>Figure 4.8</i>	<i>Comparison of modulus of elasticity for plain and fly ash concretes.</i>	<i>99</i>
<i>Figure 4.9</i>	<i>Shrinkage data for unsealed specimens of fly ash and control concretes.</i>	<i>101</i>
<i>Figure 4.10</i>	<i>Basic creep data for sealed specimens of control and fly ash concrete under applied stress of 13.8 MPa (2000 psi).</i>	<i>103</i>
<i>Figure 4.11</i>	<i>Basic creep data for sealed specimens of control and fly ash concrete under applied stress of 8.3 MPa (1200 psi).</i>	<i>104</i>
<i>Figure 4.12</i>	<i>Basic creep data for sealed specimens of control and fly ash concrete under applied stress of 5.5 MPa (800 psi).</i>	<i>104</i>
<i>Figure 4.13</i>	<i>Basic creep data for 50% fly ash concrete indicating dependence on the intensity of the stress level.</i>	<i>105</i>
<i>Figure 4.14</i>	<i>Drying creep data for unsealed specimens of control and fly ash concrete under applied stress of 13.8 MPa (2000 psi).</i>	<i>107</i>
<i>Figure 4.15</i>	<i>Drying creep data for unsealed specimens of control and fly ash concrete under applied stress of 8.3 MPa (1200 psi).</i>	<i>107</i>
<i>Figure 4.16</i>	<i>Drying creep data for unsealed specimens of control and fly ash concrete under applied stress of 5.5 MPa (800 psi).</i>	<i>108</i>
<i>Figure 4.17</i>	<i>Drying creep data for 50% fly ash concrete indicating proportionality to the intensity of the stress level.</i>	<i>108</i>
<i>Figure 4.18</i>	<i>Comparison of total drying creep strains for control and fly ash concrete with respect to the stress-strength ratio.</i>	<i>109</i>
<i>Figure 4.19</i>	<i>Comparison between basic and drying creep for 50% fly ash concrete for all stress intensity levels used in the study (the Pickett effect).</i>	<i>109</i>
<i>Figure 4.20</i>	<i>Creep recovery of 50% fly ash concrete after 372 days of creep loading under sealed and unsealed conditions.</i>	<i>110</i>

<i>Figure 4.21</i>	<i>Total strain data for 50% fly ash concrete under external applied stress of 13.8 MPa (2000 psi) for various levels of high temperature.</i>	<i>112</i>
<i>Figure 4.22</i>	<i>Total strain data for 50% fly ash concrete under external applied stress of 8.3 MPa (1200 psi) for various levels of high temperature.</i>	<i>112</i>
<i>Figure 4.23</i>	<i>Total strain data for 50% fly ash concrete under external applied stress of 5.5 MPa (800 psi) for various levels of high temperature.</i>	<i>113</i>
<i>Figure 4.24</i>	<i>Effect of temperature on the total creep of 50% fly ash concrete for the external applied stresses used in this study under sealed conditions.</i>	<i>114</i>
<i>Figure 4.25</i>	<i>Comparison of the total creep strains of 50% fly ash concrete, for various temperature levels, with respect to the stress-strength ratio.</i>	<i>115</i>
<i>Figure 4.26</i>	<i>Performance of non-air-entrained concrete exposed to rapid freezing-and-thawing according to ASTM C-666 standard.</i>	<i>117</i>
<i>Figure 4.27</i>	<i>Performance of air-entrained fly ash and control concrete exposed to 300 cycles of rapid freezing-and-thawing according to ASTM C-666 standard.</i>	<i>119</i>
<i>Figure 4.28</i>	<i>Durability Factors of air-entrained fly ash and control concretes following exposure to 300 cycles of freezing-and-thawing according to ASTM C-666 standard.</i>	<i>119</i>
<i>Figure 4.29</i>	<i>Comparison of the freezing-thawing durability of air- and non-air-entrained fly ash and control concrete.</i>	<i>120</i>
<i>Figure 4.30</i>	<i>Comparison of the linear expansion of fly ash and control concretes in sulphate solution.</i>	<i>122</i>
<i>Figure 4.31</i>	<i>Comparison of the percent weight gain of fly ash and control concretes in sulphate solution.</i>	<i>122</i>
<i>Figure 5.1</i>	<i>Secondary electron image micrograph of cement paste, in contact with quartz aggregate, in concrete containing 50% fly ash (Magnification 150x).</i>	<i>126</i>
<i>Figure 5.2</i>	<i>Secondary electron image micrograph of bulk paste of 100% portland cement concrete (Magnification 150x).</i>	<i>126</i>

Figure 5.3	Secondary electron image micrograph of bulk paste at a paste/aggregate interface of 100% portland cement concrete (Magnification 400x).	127
Figure 5.4	SEI micrograph of an air void interior of 100% portland cement concrete showing a massive deposition of $\text{Ca}(\text{OH})_2$ crystals (Magnification 200x).	127
Figure 5.5	Secondary electron image micrograph at a paste/aggregate interface of a concrete specimen containing 50% fly ash (Magnification 1000x).	128
Figure 5.6	SEI micrograph of an air void interior of a concrete specimen containing 50% fly ash showing a minimal amount of $\text{Ca}(\text{OH})_2$ crystals (Magnification 150x).	128
Figure 5.7	Backscattered electron micrograph of a polished surface of fly ash concrete. Specimen was unsealed and tested at 13.8 MPa (Magnification 150x).	133
Figure 5.8	Backscattered electron micrograph of a control concrete polished surface. Specimen was unsealed and tested at 13.8 MPa (Magnification 150x).	133
Figure 5.9	EDS spectrum of hydrated cement paste from a polished surface of a control concrete specimen.	134
Figure 5.10	EDS spectrum of anhydrous cement grains from a polished surface of a control concrete specimen.	135
Figure 5.11	EDS spectrum of hydrated cement paste from a polished surface of a 50% fly ash concrete specimen.	136
Figure 5.12	SEI micrograph of a polished surface of fly ash concrete showing fly ash particles being resistant to polishing (Magnification 100x).	138
Figure 5.13	SEI micrograph of a polished surface of fly ash concrete showing fly ash particles being resistant to polishing (Magnification 400x).	138
Figure 5.14	Backscattered electron micrograph of a polished surface of fly ash concrete. Specimen was sealed and tested at 13.8 MPa (Magnification 150x).	140
Figure 5.15	Backscattered electron micrograph of a control concrete polished surface. Specimen was sealed and tested at 13.8 MPa (Magnification 150x).	140

<i>Figure 5.16</i>	<i>SEI micrograph of a fractured surface of the control concrete. Specimen was tested sealed at 8.3 MPa (Magnification 400x).....</i>	<i>141</i>
<i>Figure 5.17</i>	<i>SEI micrograph of a fractured surface of the fly ash concrete. Specimen was tested sealed at 13.8 MPa (Magnification 400x).....</i>	<i>141</i>
<i>Figure 5.18</i>	<i>BEI micrograph of a polished surface of fly ash concrete at 1490 C (Magnification 150x)</i>	<i>144</i>
<i>Figure 5.19</i>	<i>BEI micrograph of a polished surface of fly ash concrete. Specimen was tested sealed at 210 C and 5.5 MPa (Magnification 400x).</i>	<i>144</i>
<i>Figure 5.20</i>	<i>BEI micrograph of a polished surface of fly ash concrete. Specimen was tested sealed at 710 C and 5.5 MPa (Magnification 400x).</i>	<i>145</i>
<i>Figure 5.21</i>	<i>BEI micrograph of a polished surface of fly ash concrete. Specimen was tested sealed at 710 C and 13.8 MPa (Magnification 400x).</i>	<i>145</i>
<i>Figure 5.22</i>	<i>BEI micrograph of a polished surface of fly ash concrete. Specimen was tested sealed at 1770 C and zero stress (Magnification 400x).</i>	<i>146</i>
<i>Figure 5.23</i>	<i>BEI micrograph of a polished surface of fly ash concrete. Specimen was tested sealed at 1770 C and 13.8 MPa (Magnification 400x).</i>	<i>146</i>
<i>Figure 5.24</i>	<i>BEI micrograph of a polished surface of fly ash concrete. Specimen was tested sealed at 1770 C and 13.8 MPa (Magnification 1000x).</i>	<i>147</i>
<i>Figure 5.25</i>	<i>EDS spectrum of hydrated cement paste from a polished surface of a 50% fly ash concrete. Specimen was subjected to 1490 C.....</i>	<i>149</i>
<i>Figure 5.26</i>	<i>EDS spectrum of hydrated cement paste from a fractured surface of a 50% fly ash concrete. Specimen was subjected to 1770 C.....</i>	<i>150</i>
<i>Figure 5.27</i>	<i>SEI micrograph of a fractured surface from 50% fly ash concrete tested for creep at 710 C and a stress level of 13.8 MPa (Magnification 400x).....</i>	<i>151</i>
<i>Figure 5.28</i>	<i>SEI micrograph of a fractured surface from 50% fly ash concrete tested for creep at 710 C and a stress level of 13.8 MPa (Magnification 2000x).....</i>	<i>151</i>

<i>Figure 5.29</i>	<i>SEI micrograph of a fractured surface from 50% fly ash concrete tested at 232° C and a zero stress level (Magnification 1000x).</i>	<i>152</i>
<i>Figure 5.30</i>	<i>EDS spectrum of calcium hydroxide crystals from the fractured surface of fly ash concrete shown in Figure 5.29. Specimen was subjected to 232° C.</i>	<i>153</i>
<i>Figure 5.31</i>	<i>SEI micrograph of a fractured surface of non-air-entrained fly ash concrete following freezing-and-thawing (Magnification 400x).</i>	<i>157</i>
<i>Figure 5.32</i>	<i>SEI micrograph of a fractured surface of air-entrained control concrete following 300 cycles of freezing-and-thawing (Magnification 400x).</i>	<i>157</i>
<i>Figure 5.33</i>	<i>SEI micrograph of a fractured surface of air-entrained fly ash concrete following 300 cycles of freezing-and-thawing (Magnification 400x).</i>	<i>158</i>
<i>Figure 5.34</i>	<i>SEI micrograph of a fractured surface of air-entrained fly ash concrete following 300 cycles of freezing-and-thawing (Magnification 1500x).</i>	<i>158</i>
<i>Figure 5.35</i>	<i>EDS spectrum of the fibrous material of Figure 5.34.</i>	<i>159</i>
<i>Figure 5.36</i>	<i>EDS spectrum of ettringite.</i>	<i>160</i>
<i>Figure 5.37</i>	<i>SEI micrograph of a fractured surface of the control concrete. Specimen was immersed in Na₂SO₄ solution for 330 days. (Magnification 400x).</i>	<i>163</i>
<i>Figure 5.38</i>	<i>SEI micrograph of a fractured surface of the control concrete. Specimen was immersed in distilled water for 330 days. (Magnification 400x).</i>	<i>163</i>
<i>Figure 5.39</i>	<i>SEI micrograph of a fractured surface of fly ash concrete. Specimen was immersed in Na₂SO₄ solution for 330 days. (Magnification 400x).</i>	<i>165</i>
<i>Figure 5.40</i>	<i>SEI micrograph of a fractured surface of fly ash concrete. Specimen was immersed in Na₂SO₄ solution for 330 days. (Magnification 1500x).</i>	<i>165</i>
<i>Figure 5.41</i>	<i>EDS spectrum of the sheet-like material shown in Figure 5.40 in a fly ash concrete specimen that was immersed in Na₂SO₄ solution for 330 days.</i>	<i>166</i>
<i>Figure 5.42</i>	<i>SEI micrograph of a fractured surface of fly ash concrete. Specimen was immersed in distilled water for 330 days. (Magnification 400x).</i>	<i>167</i>

<i>Figure 5.43 EDS spectrum of the sheet-like material shown in Figure 5.42 in a fly ash concrete specimen that was immersed in distilled water for 330 days.</i>	<i>168</i>
<i>Figure 5.44 BEI micrograph of a polished surface from the inner core of control concrete. Specimen was immersed in Na₂SO₄ solution for 330 days (Magnification 200x).</i>	<i>170</i>
<i>Figure 5.45 X-ray map of sulphur corresponding to the BEI micrograph above (Magnification 200x).</i>	<i>170</i>
<i>Figure 5.46 BEI micrograph of a polished surface from the outer edge of control concrete. Specimen was immersed in Na₂SO₄ solution for 330 days (Magnification 200x).</i>	<i>171</i>
<i>Figure 5.47 X-ray map of sulphur corresponding to the BEI micrograph above (Magnification 200x).</i>	<i>171</i>
<i>Figure 5.48 BEI micrograph of a polished surface from the outer edge of control concrete. Specimen was immersed in distilled water for 330 days (Magnification 200x).</i>	<i>172</i>
<i>Figure 5.49 X-ray map of sulphur corresponding to the BEI micrograph above (Magnification 200x).</i>	<i>172</i>
<i>Figure 5.50 BEI micrograph of a polished surface from the inner core of fly ash concrete. Specimen was immersed in Na₂SO₄ solution for 330 days (Magnification 200x).</i>	<i>173</i>
<i>Figure 5.51 X-ray map of sulphur corresponding to the BEI micrograph above (Magnification 200x).</i>	<i>173</i>
<i>Figure 5.52 BEI micrograph of a polished surface from the outer edge of fly ash concrete. Specimen was immersed in Na₂SO₄ solution for 330 days (Magnification 200x).</i>	<i>174</i>
<i>Figure 5.53 X-ray map of sulphur corresponding to the BEI micrograph above (Magnification 200x).</i>	<i>174</i>

<i>Figure 5.54</i>	<i>BEI micrograph of a polished surface from the outer edge of fly ash concrete. Specimen was immersed in distilled water for 330 days (Magnification 200x).</i>	<i>175</i>
<i>Figure 5.55</i>	<i>X-ray map of sulphur corresponding to the BEI micrograph above (Magnification 200x).</i>	<i>175</i>
<i>Figure A.1</i>	<i>Grading curve for 19 mm (3/4") Saskatchewan coarse aggregate.</i>	<i>194</i>
<i>Figure A.2</i>	<i>Grading curve for Saskatchewan fine aggregate.</i>	<i>194</i>
<i>Figure C.1</i>	<i>Durability factors of air-entrained fly ash and control concretes following exposure to 270 cycles of freezing-and-thawing according to ASTM C-666 standard. Testing was performed at the PFRA laboratory, on the UofS campus.</i>	<i>219</i>

CHAPTER 1

Introduction

1.1 General

Concrete as it is known today came into use in 1824 with the invention of portland cement (Mehta, 1987). Until then, pozzolan-lime mortars and concretes were used throughout the world. The term pozzolan is used to indicate a material which reacts with lime to make a product with cementitious properties. However, their relatively slow setting and hardening characteristics was the reason for their gradual decline. The main technical advantage of portland cement is its considerably faster rate of setting and hardening, even under water.

Environmental and economic reasons require the revision of present concrete making methods. Mineral admixtures have been used successfully to partially replace energy consuming portland cement. These inorganic substances take part in the hydration reactions; consequently, they make a substantial contribution to the hydration products and the structure of the cement paste. The technical advantage of replacing portland cement with mineral admixtures is the modification of the mechanical properties of the fresh and hardened concrete. This includes faster or slower rates of setting and hardening, lower heat of hydration, improved durability in acidic environments and higher ultimate strength (Mehta, 1987).

In various parts of the world, the concrete production industry utilizes natural pozzolans which are derived directly from volcanic rocks and minerals by crushing, grinding and size separation. Some examples are Italy, Japan, Greece and Germany. Pozzolanic materials are high in SiO_2 , low in CaO and they possess little or no cementitious value in themselves. However, in a finely divided form they are sufficiently reactive, that in the presence of water, will combine chemically with calcium hydroxide at ordinary temperatures to produce compounds with cementitious properties (C-S-H). Therefore, they are acting as hydraulic cements. In the case of portland-pozzolan cement, the required Ca(OH)_2 is provided from the crystalline by-product of the hydration reaction of di-calcium (C_2S) and tri-calcium silicates (C_3S).

Industrial by-products that would otherwise be discarded as harmful environmental pollutants, are being widely used as cement replacements in concrete. For economic and environmental reasons industrial by-products are fast becoming a vital source of mineral admixtures in portland cement concrete. Suitable by-product materials comprise ashes from the combustion of coal and some crop residues, volatized silica and granulated slag from metallurgical operations.

Industrialized countries are among the major producers of the following most important mineral admixtures:

Pulverized fuel ash (pfa, fly-ash):

An industrial by-product from the burning of coal in power plants.

Ground granulated blast furnace slag (ggbfs):

A by-product of the blast furnace in pig-iron production.

Condensed silica fume (microsilica):

A by-product in the production of silicon or silicon alloys, by a process whereby quartz is reduced in an electric furnace. In this process, some SiO is lost as a gas. Immediately after, it oxidizes to SiO₂, and precipitates as a very fine particulate solid: microsilica.

Natural pozzolanas

Minerals of volcanic and sedimentary origin.

1.2 Advantages of Fly Ash in Concrete

The environmental and economic reasons for using fly ash as a replacement of portland cement have been stated earlier. Portland cement is the most energy-intensive component of the concrete-making materials, requiring 4000 MJ/Tonne (Malhotra, 1987). Reducing the amount of cement in the production of concrete results in significant savings in energy, hence, lowering the cost of the material. In addition, fly ash influences the properties of fresh and hardened concrete. The advantages of using fly ash may be summarized as follows:

1. The small spherical particles of the fly ash, acting as ball bearings, influence the rheology of fresh concrete. When a high volume of fly ash is used as partial replacement of the cement, it generally causes a reduction in the amount of water required for workable concrete.
2. As soon as the cement and water mix, exothermic reactions of hydration commence and the temperature rises. Fly ash contributes to the reduction of the heat of hydration. This is of particular importance in mass concrete to

reduce the temperature gradient from the exterior to the interior of a structural component.

3. Fly ash causes a gradual development in the compressive strength of concrete. The pozzolanic activity of the ash continues long after the hydration of cement. Required strength levels are attained at ages beyond 91 days. After this time, the compressive strength continues to increase and it becomes higher than that of an equivalent concrete prepared without fly ash.
4. The pozzolanic activity of the fly ash produces a denser cement paste. This reduces the concrete permeability and improves its resistance to chemical attack.
5. Fly ash produces concrete with small creep and shrinkage strains (Sivasundaram et al., 1991).

1.3 Objectives and Scope of this Study

1.3.1 Background

The unit price of concrete increases in proportion to its compressive strength up to about 30 MPa; for higher strength specialty admixtures are required and the cost takes a sharp increase. High performance concrete with very high strengths is now routinely produced by using superplasticizers to reduce water demand and condensed silica fume as partial replacement of portland cement along with other mineral and chemical admixtures (Aïtcin, 1987, Feldman and Cheng-yi, 1985, Roberts, 1989). However the commercial cost of silica fume is extremely high compared to the unit price of portland cement. The cost of silica fume concrete, is consequently much higher than concrete containing 100%

portland cement. Fly ash on the other hand, has a considerably lower cost than portland cement. Hence, replacement of the cement with fly ash reduces the unit price of concrete substantially. Market prices of these mineral admixtures in relation to portland cement, as quoted by local suppliers, are given in Table 1.1.

Table 1.1 Market prices of cement and mineral admixtures

	\$/Tonne
portland cement	140
fly ash	45
silica fume	950

Demand for economical and high performance concrete were the main reason for this research investigation. Concrete with compressive strengths in the middle range between 35 and 50 MPa (5000 and 7000 psi) is used in bridge construction as well as in medium rise buildings and in structural components for underground mines and comprises a fairly large proportion of the annual concrete volume production. In order to reduce materials cost in the production of these projects, it is important to determine whether it is possible to produce economical high performance concrete with improved properties. The present study proposes to meet this objective by using a large volume of ASTM Class C, high calcium fly ash in combination with superplasticizers to increase the strength of concrete and to optimize its mechanical properties.

Considerable research has been conducted on the use of large volume replacements of portland cement with Class F, low calcium fly ash (Sivasundaram, et al., 1991, Bisailon, et al., 1994). By comparison, limited information is available on the long term performance of concrete containing large volumes of Class C fly ash with a high content of calcium. Very high quality Class C fly ash is produced locally in Estevan, Saskatchewan and in Sundance, Alberta.

For greater use of the available fly ash in the prairie provinces of Canada, a comprehensive study was thus undertaken at the University of Saskatchewan. The object of the study was twofold:

- to reduce the required amount of the energy intensive cement, thereby, reducing the cost of concrete,
- to create an economic market for Saskatchewan fly ash by creatively disposing of this environmental pollutant.

1.3.2 Objectives

The overall objective of this study was to determine and improve the mechanical properties of concrete containing a large volume of Class C fly ash and to reduce its cost. The stages of the research project may be summarized as follows:

1. Establish an optimum cement, fly ash, water and superplasticizer content to produce concrete with high strength and good workability.
2. Study the compressive strength development, at different ages, of concrete mixtures containing various levels of fly ash replacement of portland cement. Compare the results to a control mixture containing no fly ash.

3. Select an optimum fly ash/cement ratio based on compressive strength results and cost.
4. Test the mechanical properties of the selected concrete mixture which include:
 - compressive strength,
 - modulus of elasticity,
 - durability of concrete subjected to rapid freezing and thawing as well as exposure to a sulphate environment,
 - long-term creep of concrete subjected to various combinations of stress, temperature and moisture.
5. Conduct microstructural studies using the scanning electron microscope (SEM) and the electron probe microanalyzer (EPMA) to understand and explain the observed results.
6. Recommend an optimum mixture, containing fly ash and superplasticizer, for economical concrete with improved mechanical properties.

CHAPTER 2

Literature Review

2.1 General

A large number of studies have been published on the effect of low calcium (ASTM Class F) fly ash on the engineering properties of concrete (Berry and Malhotra, 1986, Berry and Malhotra, 1987, Haque, et al., 1992, Sivasundaram, et al., 1991, Tikalsky and Carrasquillo, 1992). However, the available research on the use of high calcium (ASTM Class C) fly ash is limited. Previous studies (Nasser and Lai, 1992, Lai, 1989, Lai, 1986, Marzouk, 1979) have been undertaken to study the effect of using a large volume of high calcium fly ash replacement of portland cement in concrete. The present study has used a large volume of Class C fly ash in combination with superplasticizer in order to produce economical high performance concrete.

This chapter presents a review of the following:

- Chemical composition and hydration mechanism of ordinary portland cement and the structure of cement paste.
- Chemical composition, structure and properties of fly ash.
- Available literature on the effect of fly ash on the microstructure and mechanical properties of concrete.

2.2 Portland Cement and Gels in General

Cement is a material with adhesive and cohesive properties which make it capable of bonding mineral substances into a compact whole (Neville, 1981). Adhesive are those properties which enable the cement to bond to other materials (e.g. bonding to aggregate), whereas cohesiveness allows it to become homogeneous and strong within itself. In concrete, the cements of interest are the hydraulic cements. They are broadly classified as natural, high-alumina and portland cements and they consist mainly of silicates and aluminates of lime.

The present research project uses normal (type 10) portland cement which consists mainly of crystalline compounds of calcium, silica, alumina and iron oxide. These minerals are unstable in the presence of moisture and upon contact with water they begin to undergo dissolution at various rates. Their chemical reaction which is termed *hydration* produces gel and crystalline products.

2.3 Structure and Fundamental Properties of Gels

In general, systems which are composed of solid particles in a liquid dispersing medium are classified as gels. Dispersive systems which are composed of matter in a finely divided state (from nanometer to micrometer grain size) are called colloids. There are two phases involved in a colloidal system; the dispersed particles and the dispersing medium. The particles are termed as the *disperse* or *internal phase*, while the medium is called the *dispersing* or *continuous* or *external phase*. Colloidal dispersions are further classified according to the disperse and dispersing phases, both of which may be solid, liquid or gas in any possible combination. Due to considerable overlap of properties

among these various groups of substances, the classification of the various colloidal dispersions is difficult and therefore incomplete (Moffat et al., 1964).

Colloidal dispersions owe their stability to the presence of an electric charge on the surface of the colloidal particles that is the result of:

- the adsorption of certain ions on the particle surface, or,
- self ionization of the particles (Jastrzebski, 1987).

The electric charge on the particle surface forms an electrical double layer. The first layer has approximately the thickness of a single ion and remains almost fixed on the particle surface. The second layer extends some distance into the dispersing medium and it is diffused. A potential drop exists across this electrical layer as illustrated in Figure 2.1 (Jastrzebski, 1987). Across the fixed layer there exists a sharp potential drop. The gradual potential drop in the diffuse layer is called the zeta potential and accounts for the stability of the colloidal system. As the solid particles come close together, the repulsive forces between their double electrical layers keep them dispersed and prevent them from coalescing.

Colloidal solutions in which the solubility of the colloidal material is reduced enough so as to allow the particles to link together and form a solid framework which is interpenetrated by the liquid phase of the dispersing medium are the basis of gel forming. So, the definition of a gel may be that of a two-component system, with the mechanical properties of a solid, where the constituent phases of solid and liquid are both continuous.

Gels are formed when a large amount of the solvent liquid is mechanically trapped and immobilized by the linked structure of the colloidal particles. The liquid is trapped, either in very fine capillaries between the solid particles or in very small pores

inside the solid framework. The process of gel formation is shown schematically in Figure 2.2.

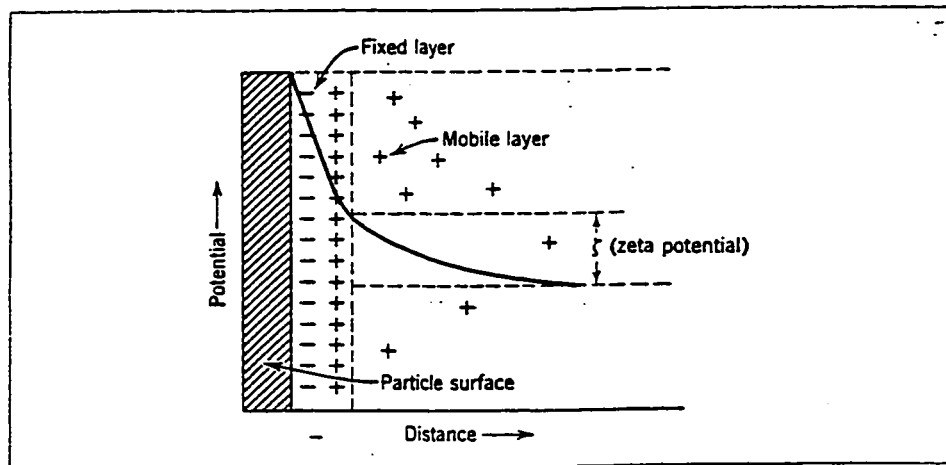


Figure 2.1 Electrical double layer and potential fall in layers. The potential drop in the diffuse or mobile layer is called the zeta-potential (Jastrzebski, 1987).

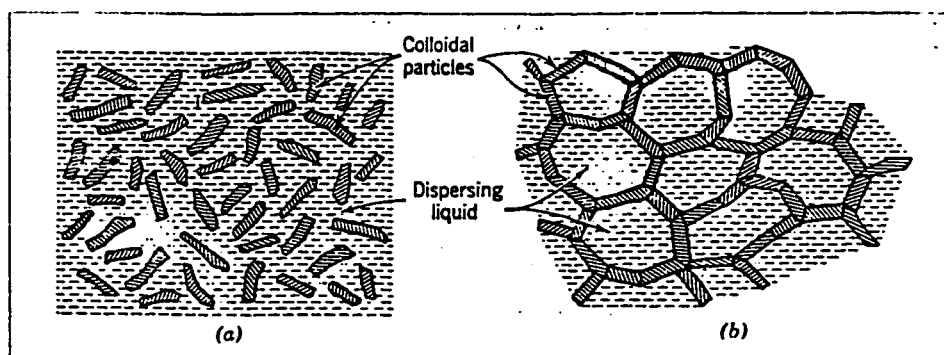


Figure 2.2 Formation of gel. (a) Colloidal dispersion. (b) Gel structure; colloidal particles form a connected structure interpenetrated by dispersing liquid (Jastrzebski, 1987).

The type of linking of the solid colloidal particles is the reason for the different structure and properties of the three main classes of gels:

1. Elastic gels (or xerogels) occur when the forces between the particles are due to secondary bonding as in van der Waals forces (dipole-dipole forces and London dispersion forces due to instantaneous dipoles). This is a weak type of bonding. For this reason, elastic gels are reversible and may be brought into solution upon moderate application of heat and reversed back to a gel upon cooling. Examples of elastic gels are gelatin, cellophane, many polymers in organic media and asphalt.
2. A second type of gels are called thixotropic which have the tendency to pass into colloidal solutions by means of mechanical shearing forces as in agitation, and they set again to the gel form when the mechanical action stops. Certain clays, such as bentonite, colloidal alumina and ferric oxide, form thixotropic gels.
3. Rigid gels form when long, flat or globular particles are chemically crosslinked forming a three-dimensional network. The bonding of the gel network structure is due to primary forces, mainly covalent bonding and for this reason the rigid gel is irreversible and cannot be brought back into solution simply by adding liquid to it. An example is portland cement that sets and hardens through the formation of a rigid gel.

2.4 Portland Cement Composition

Portland cement is composed mainly of dicalcium-silicate (C_2S), tricalcium-silicate (C_3S), tricalcium-aluminate (C_3A), and tetracalcium-alumino-ferrite (C_4AF). The composition of the four major phases in cement is outlined in Table 2.1 (Lea, 1976)¹.

Table 2.1. Portland Cement - Chemical Composition

NAME OF COMPOUND	OXIDE COMPOSITION	ABBREVIATION
TRICALCIUM SILICATE	$3CaO.SiO_2$	C_3S
DICALCIUM SILICATE	$2CaO.SiO_2$	C_2S
TRICALCIUM ALUMINATE	$3CaO.Al_2O_3$	C_3A
TETRACALCIUM ALUMINO-FERRITE	$4CaO. Al_2O_3.Fe_2O_3$	C_3AF
GYPSUM	$CaSO_4.2H_2O$	

Alite, the impure form of C_3S , is the most important component, comprising 50-70% of all normal portland cement clinkers (Taylor, 1990). During hydration, it reacts with water at a fairly quick rate. It is therefore alite which is primarily responsible for the early strength development of the cement paste up to 28 days.

¹ Cement chemistry notation:

C=CaO S=SiO₂ A=Al₂O₃ F=Fe₂O₃ CH=Ca(OH)₂ H=H₂O

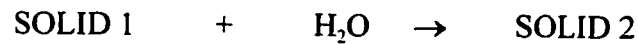
Belite, the impure form of C_2S , accounts for 15-30% of normal portland cement clinkers, and it is largely present as β - C_2S , a higher temperature (630-680° C) polymorph (Taylor, 1990). At lower temperatures (<500° C), belite assumes a different crystal structure and it stabilizes to a γ -polymorph. γ - C_2S is an undesirable formation since it scarcely reacts with water to be a meaningful cementitious material. It is desirable to stabilize the higher temperature polymorphs with foreign ions or by controlling the rate of cooling of the cement clinker, therefore, making it possible for the β - C_2S form to exist at room temperatures. β - C_2S reacts slowly with water and for this reason, contributes little to the initial strength development of the cement paste, but does so substantially after the first 28 days.

The aluminate phase (C_3A) makes up 5-10% of most portland cement clinkers, even though its presence is undesirable. It contributes little to strength development except at the very early stages. Unless gypsum is added to the cement clinker, C_3A reacts violently with water causing immediate stiffening of the cement paste (flash set).

The ferrite phase (C_4AF), making up 5-15% of the clinker, acts as a flux, together with C_3A , reducing the burning temperature of the clinker, thus reducing the cost of cement. If cost were no problem C_4AF would be removed from the clinker, and the process would result in white cement.

2.5 Portland Cement Hydration

Upon contact with water, the cement grain reacts with it forming a gel. The term hydration as applied to cement denotes the entirety of changes that occur when an anhydrous cement or one of its constituent phases is mixed with water to form a hardened cement paste. In simplified notation, hydration may be stated as:



However, the reactions that take place are more complex than this simple form.

The following definitions will aid in explaining the process of hydration:

Proportions of **water/cement** must be such that setting and hardening of the hydrated cement paste can take place.

Setting is the initial stiffening (solid product) of the cement paste, without significant strength development. This happens within a few hours after the cement is mixed with the water.

Hardening is a time dependent process, being the result of hydration. It is synonymous with strength development. Curing conditions are important for hydration to occur, and allow the strength to develop.

Curing conditions include all of the favourable ambient factors which allow the hydration of cement to proceed with time and the strength of the concrete to develop in a reasonable time interval. Such parameters include:

Temperature: Low temperatures produce a denser cement gel that eventually has a higher compressive strength, while elevated curing temperatures will produce a less dense gel.

Moisture: Hydration should be allowed to continue in a water filled environment for best development of strength of the cement paste.

Time: Strength increases with time. At 28 days of wet curing the cement paste has developed about 85% of its compressive strength.

Setting and hardening of hydraulic cements are the result of the hydration chemical reactions that occur between water and the various components of the cement. Hydration has been the subject of study for a long time in the form of experiments set up to study the degree of hydration α in relation to age or time t and the factors which influence this relationship. This study is the subject of the **kinetics** of hydration. Curves of α against t are called kinetic curves and for practical reasons they control the way in which the physical properties of the paste develop as the curing proceeds.

Kinetic curves are influenced by:

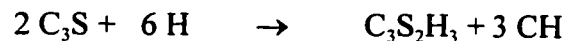
- The **composition** of the cement clinker. Not all phases hydrate with the same ease or at the same rate.
- The **fineness** of the cement, or particle size distribution. The finer the cement, the more surface area is available for hydration therefore the process is quicker with time.
- **Curing temperature and relative humidity.** Colder temperatures and high humidity produce a denser gel.
- The **water/cement** ratio. It provides the space-limiting volume where hydration may or may not be possible.
- The contents and distribution of **admixtures**.
- The **microstructure** of the cement clinker. For example the β - C_2S reacts more readily than the γ - C_2S phase.

Cement is a mixture of phases that react at different rates. For instance the C_3S phase undergoes hydration at a faster rate than C_2S . For this reason it becomes difficult to determine or even to define α for the entire system. Therefore, α is defined as the

weight fraction of cement which has hydrated irrespective of phase. The hydration reactions are summarized in the following paragraphs:

The silicate phases (C_3S and C_2S) undergo hydrolysis instead of true hydration. However the term hydration is commonly used in cement chemistry to include all reactions that lead to solid cement paste.

The tri-calcium silicate (C_3S) phase undergoes the following reaction:



The products of the above reaction are crystalline $Ca(OH)_2$ (or CH in abbreviated cement chemistry notation) and a nearly amorphous calcium silicate hydrate ($C-S-H^2$ in abbreviated form) having the properties of a rigid gel.

Hydration of the C_3S phase is responsible for the early strength development of neat cement paste. Equivalently, the C_3S phase is responsible for the development of the compressive strength of the hardened concrete during the early stages. X-ray Diffraction methods (XRD) show that 70% of the C_3S reacts with water and hydrates within 28 days, and almost all of it within a year. The C_3S content of the cement controls the rate of the strength development of the paste. For this reason, high early strength cement (or Type 30 cement) has a high content of C_3S .

Hydration of the β - C_2S phase takes place in a similar manner as the C_3S but the reaction is slower with less $Ca(OH)_2$ produced:



² **C-S-H** (with dashes) is a generic name for amorphous or poorly crystalline hydrate of the silicate phase and no particular composition is implied. In contrast **CSH** (with no dashes) denotes the hydrate with the particular composition $CaO.SiO_2.H_2O$.

Hydration of the β -C₂S is responsible for the strength developed in the paste at later stages. It has been shown that 30% of β -C₂S reacts with water and hydrates in the first 28 days and 90% of it in one year.

Reaction rates of C₃S and β -C₂S depend, among other factors, on particle size distribution (fineness of the cement). Strength development of pure C₃S and β -C₂S hydrates is comparable to that of portland cements of the same water/solid ratio and cured under the same conditions.

At any stage of hydration the hardened paste may consist of:

1. Hydrates of the various compounds, that collectively make up the **gel**.
2. Crystals of Ca(OH)₂.
3. Some minor components.
4. Unhydrated cement.
5. The remaining of the water-filled spaces called the capillary pores.
These may be empty or full of water, depending on the stage of hydration and the initial water/cement ratio.
6. Within the gel itself there exist interstitial voids (much smaller than the capillary pores) approximately 15-20Å in diameter and they firmly bond H₂O (non-evapourable water) within them. These are the gel pores and they make up 28% of the gel volume. This volume is defined as the gel porosity.

Ca(OH)₂ has a definite ordering system of Ca, H, and O atoms in a layer structure. Calcium atoms are octahedrally coordinated and oxygen atoms are tetrahedrally

coordinated. Under ideal conditions of crystallization, Ca(OH)_2 forms hexagonal plates. Crystallized hydrates (mainly calcium hydroxide) in the cement gel provide weak links in the hardened paste because of their chemical instability. Ca(OH)_2 is soluble in water, leaving behind voids, which weaken the system and have a detrimental effect on the strength and permeability of the paste. Its hexagonal structure has cleavage planes and fracture occurs easily along these. Nonetheless, the formation of Ca(OH)_2 is significant in establishing the kinetics of hydration curves. When detected by methods involving microscopy, the amount of Ca(OH)_2 present will give an indication of the degree of hydration.

Hydration is a slow, time dependent process. It is much slower than the initial setting of the cement paste, which defines a volume with only partial hydration of the cement having occurred. This is the space-limiting volume inside which hydration continues to occur with time. As the solid products are expansive by nature, full hydration is possible only if sufficient space is provided to allow it to happen accompanied by a specified proportion of pore space. Therefore, a water/cement ratio becomes very important in providing the space-limiting volume for the hydration products to grow into. A specific water/cement ratio is therefore implied for which a paste consists entirely of hydration products, including the essential pore space, and there are no residual unhydrated cement grains. Below this ratio, complete hydration is not possible. The total water content of such a paste in the saturated state is 42-44%, by weight of the cement, even though the stoichiometric equation representing the hydration of the silicate phases requires approximately 23% of water (by weight of the silicate).

Hydration is a process that begins on the outer surface of the cement grain forming a film and then propagating inward. As the products of hydration are expansive there is pressure building-up in the interior of the grain. The hydration products diffuse out from the grain surface toward larger spaces through the very fine pores of the solid

shell of previously formed hydration products around the cement grain surface. The new hydration products precipitate from the solution in air- or water-filled spaces that are large enough to allow nucleation of a new solid phase. The volume of the solid hydration products is larger than that of the unhydrated cement, but it is still less than the sum of the volumes of the unhydrated cement and water. So, there is always a fraction of capillary porosity remaining. The strength and other mechanical properties of the hardened cement paste depend primarily on the capillary porosity. The mechanism of hydration implies that the process stops when:

- no more water is available for reaction;
- no more unhydrated cement is available; and
- lack of sufficiently large space that does not allow for nucleation of new solid hydration products.

In schematic form, the hydration process of the cement grain is shown in Figure 2.3.

The hydration process results in a complex microstructure which is responsible for the physical properties of the cement paste. When one starts with a disordered suspension of cement particles of irregular shapes and varying sizes, which in turn undergoes random growth in volume because of hydration, the developing microstructure can only be expected to be complex.

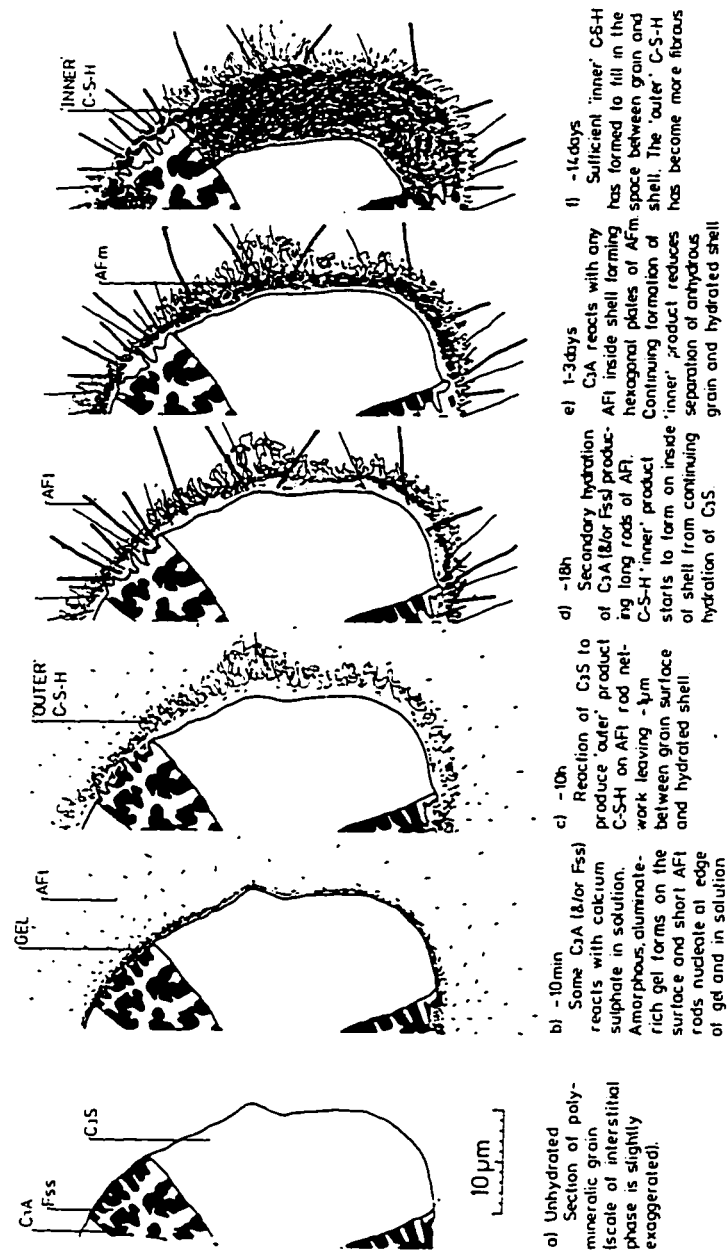


Figure 2.3 Development of microstructure during the hydration of portland cement (Scrivener, 1984).

2.6 Structure of the Cement Paste

Initially, when the cement is mixed with water, a paste is formed. Pastes are concentrated dispersions of very fine solid particles in a liquid medium. No sharp distinction exists between pastes and gels. The high concentration of the cement particles and the resulting van der Waals forces from interparticle attraction ensure that the paste acts as a single system. These forces become very important due to the high specific surface area of the cement grains. The interparticle forces may be modified by changing the water content of the paste or by adding surface-acting agents (admixtures). The structure of the fresh cement paste may then be considered as that of a weak, porous permeable solid, containing continuous capillaries filled with the aqueous solution.

By the time that all of the cement grains have hydrated to form cement gel, they have doubled their volume. Since this expansion occurs in a relatively constant external volume, it is implied that the cement gel must conform to the shape of whatever space is available to it. Studies of hardened cement paste show that the cement gel is composed of highly irregular colloidal products having a layered structure with no definite number of layers. Water is a structural part between the layers and it does not behave as normal free water.

Recent studies, making use of Scanning Electron Microscopy (SEM) confirm the following conclusions, which were arrived at in earlier times using light microscopy:

1. Calcium hydroxide (CH) grows from a few centres in the water filled space where it forms isolated masses. Much more CH is observed with C_3S than with β - C_2S .
2. C-S-H gel morphology is distinguished in the following types:
 - Type I : Observed during the early stages of hydration. It is a fibrous material, approximately 2 μm in length.

- Type II : This is also a normal early product as well, exhibiting honeycombed networks.
- Type III : Prominent in older pastes, it is more massive, consisting of tightly packed grains up to 300 μm across.
- Type IV : Observed in older pastes, it is more featureless and massive than Type III.

Whether the C_3S and $\beta\text{-C}_2\text{S}$ are studied separately as calcium silicate hydrates, or collectively as cement paste hydrates, C-S-H gel has a layer structure and together with a pore solution it forms a rigid gel with pores ranging in size from macroscopic to enlarged interlayer spaces of nanometer dimensions. In a saturated paste, that is when these pores are entirely filled with water, the most highly hydrated state exists (full hydration occurs).

Several models exist for the structure of the cement gel. The Powers-Brunauer model (Popovics, 1979) considers a very large specific surface of the grains and accepts the role of secondary van der Waals forces for the strength of the hardened paste. Even though these are weak bonds, when they are combined with a large specific surface they can be responsible for a high compressive strength in the paste. It also assumes that a small fraction of the boundary of a gel particle is chemically bonded to adjacent particles.

The Feldman-Sereda model (Popovics, 1979) is similar in that it is based on the role of physical van der Waals forces between gel particles for the strength of the paste which is considered to have a layer structure with pores as spaces between the layers.

The Tamas (Popovics, 1979) model assumes a smaller specific surface for the gel and suggests that the primary reason for the strength of the paste is chemical (cross-link) bonding which is stronger than physical forces. These bonds result from the polymerization of the calcium silicates. Hydrogen bonds and van der Waals forces

contribute as well. The type of the reactions between the calcium silicates and water is condensation polymerization, where short-chain (oligomers) of silicate anion (SiO_4^{4-}) polymers are formed through binding the SiO_4^{4-} tetrahedrons by crosslinking oxygen ions. So, the hardened calcium silicate hydrate gel is a system composed of silicate anion oligomers of different degrees of polymerization, cross-linked between them and forming an irregular three dimensional network.

A model that is based on chemical as well as physical bond forces is a more realistic representation of the structure of the cement paste. For this reason the Tamas model seems to be a more plausible alternative.

2.7 Superplasticizers

In concrete, traditionally high strength levels as well as good workability have both been desirable properties; however, they cannot be simultaneously achieved using an ideal water/cement ratio. They are both dependent on the water/cement ratio of the concrete mix but not in the same way. Workability improves with an increase in the water/cement ratio while strength is inversely proportional to it. Lowering the water/cement ratio in order to increase compressive strength and still maintaining high workability is unlikely under traditional practices, unless the effects of water reducing admixtures are considered.

Admixtures are materials other than the main ingredients of concrete (i.e. hydraulic cements, water or aggregates) which are added immediately before or during mixing (Taylor, 1990). The most important of these are the admixtures used to accelerate or retard setting or hardening of the cement paste, to decrease the amount of water

required for a given degree of workability, or air entraining agents which improve the frost resistance of the hardened concrete.

When a lower water/cement ratio is required, water-reducing admixtures (also called plasticizers) allow a certain degree of workability with a water/cement reduction of 5-15%. Water-reducers are effective in low concentrations which suggests that they act by a mechanism of adsorption at the solid-liquid interface. When adsorbed on the surfaces of growing hydration products, these admixtures interfere with growth and cause retardation. Due to this mechanism there is a wide overlap between the properties of retarders (regarding the setting of concrete) and water reducing admixtures. Many retarders can be used as water-reducers and vice-versa. An example is calcium and sodium lignosulphonates, being widely used as both, water-reducers and retarders.

The workability of a concrete mix decreases with time. This effect is called slump loss and it is more pronounced with the presence of the water-reducing admixture. The rate of slump loss of concrete containing a water-reducer is higher than in concrete with no water-reducing agent.

Slump loss is caused by the slow start of the hydration reactions and the formation of the solid products of hydration, the connectivity of which is responsible for the mechanical properties of the cement paste.

The increased rate of slump loss in the case of the admixed concrete, is due to the effect of the gradual absorption of the water-reducing agent by the products of hydration. This effect can be minimized by delaying the addition of the admixture. Water-reducing agents are most effective if added a few minutes (2- 4 minutes) after mixing. By this time, the aluminate phase of the cement has reacted with the gypsum to some degree and it consumes less water-reducer. As a result, in some cases, water-reducers are most effective with cements which are low in aluminates and alkali.

The more powerful high-range water-reducers, also called superplasticizers, allow water/cement ratio reductions of up to 30%. The ability of superplasticizers to permit lower water/cement ratios while improving workability has made the achievement of high strength concrete possible. Superplasticizers come in three principal types:

SMF : Sulphonated Melamine Formaldehyde polymers,

SNF : Sulphonated Napthalene Formaldehyde polymers, and,

Modified lignosulphonate materials.

The first two types are the ones which are most commonly used.

When compared with conventional water-reducing admixtures, superplasticizers are more effective because they can be used in higher concentrations, over 1% of the weight of the cement compared to up to 0.2% for conventional water-reducers. The properties which limit the amount of conventional water-reducers are weaker or not present in the superplasticizers. Such properties include retardation of setting, increase in air entrainment and in some cases flash setting.

The effectiveness of superplasticizers in decreasing the water/cement ratio that is required for concrete with a given workability lies in their ability to improve the dispersion of the cement grains in the mixing water.

When fine particles are suspended in a fluid, they agglomerate to form small masses called flocs. One such flocculated system occurs in fresh cement paste. Water becomes immobilized within the flocs and is not available for lubrication of the system. The importance of effective particle dispersion is the release of the immobilized fluid. Flocculation is decreased or prevented with the use of water-reducers or superplasticizers and the water which would otherwise be immobilized within the flocs is added to that in

which the particles can move giving the fresh concrete improved workability without the need to increase the water content.

In superplasticized concrete, flocculation is decreased due to the adsorption of the admixture on the hydrating cement grains in the following ways (Taylor, 1990):

1. By means of *steric hindrance*. The oriented adsorption of the non-ionic polymer superplasticizer, weakens the attraction between the solid particles.

2. There is an increase in the *z-potential* of the solid particles. The adsorbed admixture creates a negative electrical charge on the surface of the hydrating cement grains. If all of the particles have a surface charge of the same sign and sufficient magnitude, they will repel each other, and hence, they will tend to disperse in the fluid.

3. There is an increase in the *solid-liquid affinity*. When the particles are more strongly attracted to the liquid than to each other, they will tend to disperse.

Eventually the system reaches stabilization of particle dispersion and the released water becomes available for lubrication of the mix, and in this manner higher workability is reached at the same or even lower water/cement ratio. At a normal water/cement ratio the dispersing action of the superplasticizers, greatly increases the workability of the concrete mix resulting in self-leveling "flowing" concrete with a typical slump increase from 75 mm to 200 mm while the mix continues to remain cohesive.

The following are the effects of dispersion:

Stabilization is reached and the released water gives the mix a higher workability at a lower water/cement ratio.

Greater surface area is exposed, therefore the rate of hydration at the early stages is increased, and proportionately the early strength of the cement paste is increased for the same water/cement ratio.

Since the superplasticizers improve the workability for a given water/cement ratio, it follows that, for a specified workability, the lower water/cement ratio which is sufficient with the use of superplasticizers will produce concrete of higher strength.

2.8 Use of Fly Ash in Concrete

Fly ash is a fine particulate residue which is electrostatically precipitated from the exhaust fumes of coal burning power stations (Berry and Malhotra, 1986, 1987). Chemically, it is a glassy material containing compounds of silicon, aluminum, iron, calcium, and magnesium. The term glassy implies a material of amorphous structure and inconsistent chemical composition. The content of the above elements varies according to the geological type of coal which produces the fly ash. The American Society for Testing and Materials (ASTM) recognizes two general classifications of fly ash to reflect their chemical composition, mainly in the calcium content and their origin to some extent.

- Class F fly ash generally results from the combustion of anthracite and bituminous coals. It is also classified as low-calcium fly ash and it contains less than 10% CaO.

- Class C, or high calcium fly ash is normally a by-product of the combustion of lignite or sub-bituminous coals. It has a higher content of calcium, typically 15-30% and lower iron compared to Class F fly ash (Mehta, 1986).

The chemical composition of fly ash is not constant but it varies widely between different sources of power plants. Table 2.2 is an example of the chemical composition of fly ashes from various sources (Taylor, 1990).

2.9 Structure of Fly Ash Particles

Next to the mineralogical composition of the pozzolanic admixtures, including the amount of crystalline and non-crystalline phases present, the particle shape and size distribution determine the effect of the admixture on the behaviour of concrete.

Fly ash which is collected using electrostatic precipitators has a finer texture than when mechanical collectors are used alone (Berry and Malhotra, 1987). Since there is no grinding step involved in the production of fly ash, as in the production of portland cement, most of the particles occur in the form of solid spheres of glassy material. Additionally, a small number of hollow spherical particles exist, called cenospheres (from the greek *kenos* meaning empty). Occasionally the cenospheres are packed with many smaller spheres and are then called plerospheres (from the greek *pliris* meaning full) (Mehta, 1986). The spherical particles range in diameter between 1 and 150 μm , with the majority of them under 45 μm (Berry and Malhotra, 1987). They have an average diameter of 10 to 20 μm (Mehta, 1989). The cenospheres are relatively large particles while the solid spheres are smaller (Taylor, 1990).

By comparison, portland cement particles have coarser characteristics lacking the smooth spherical surface of fly ash. They are larger and of a more irregular and angular

Origin	Na ₂ O	MgO	Al ₂ O ₃	SiO ₂	SO ₃	K ₂ O	CaO	Fe ₂ O ₃	Loss	Total
Montana, USA	0.2	6.8	20.3	35.2	1.1	0.5	25.0	6.3	0.3	95.7
North Dakota, USA	7.3	7.9	12.5	30.2	9.6	0.6	23.6	4.6	1.8	98.1
North Dakota, USA	5.4	5.5	10.7	27.9	12.3	1.5	21.6	9.9	1.4	96.2
Saskatchewan, Canada	6.1	2.9	21.9	47.9	1.1	1.0	13.3	4.9	0.1	99.2

Table 2.2 Chemical composition of some fly ashes high in CaO (Taylor, 1990).

shape. The average particle diameter of cement grains is of the order of 15 to 20 μm while grains exist that are several times larger (Garboczi and Bentz, 1991, Bentz and Garboczi, 1991). A visual comparison of the particle shape and size is made in Figures 2.4 and 2.5 showing scanning electron micrographs of fly ash particles and cement grains respectively. Fly ash is not an inert filler material when blended in cement. Its main effects in concrete were briefly outlined in the previous chapter. The following sections provide a more detailed review of the mechanisms by which fly ash affects the properties of fresh and hardened concrete.

2.10 Pozzolan - Cement Interaction and its Microstructure

The chemical reactions that occur due to the interaction between portland cement and fly ash in blended cement systems have a considerable effect on the resulting microstructure.

Fly ash is one of the most commonly occurring artificial pozzolanic materials in the sense that when suitably activated, it will react with water to give products that are cementitious. According to the ASTM definition, “a pozzolan is a siliceous or siliceous and aluminous material which possesses little or no cementitious value in itself. However, in finely divided form and in the presence of moisture, it will react chemically with calcium hydroxide at ordinary temperature to form compounds possessing cementitious properties.” Pozzolan materials are high in SiO_2 and low in CaO . They are sufficiently reactive that when mixed with water and additional CaO , they will, at ordinary temperatures, produce C-S-H gel and are therefore acting as hydraulic cements. In the case of cement paste the CaO that is required to complete the pozzolanic reaction comes from the Ca(OH)_2 that has crystallized as a by-product of the hydration of di- and tri-calcium silicates. In the presence of moisture, the calcium ions react with the

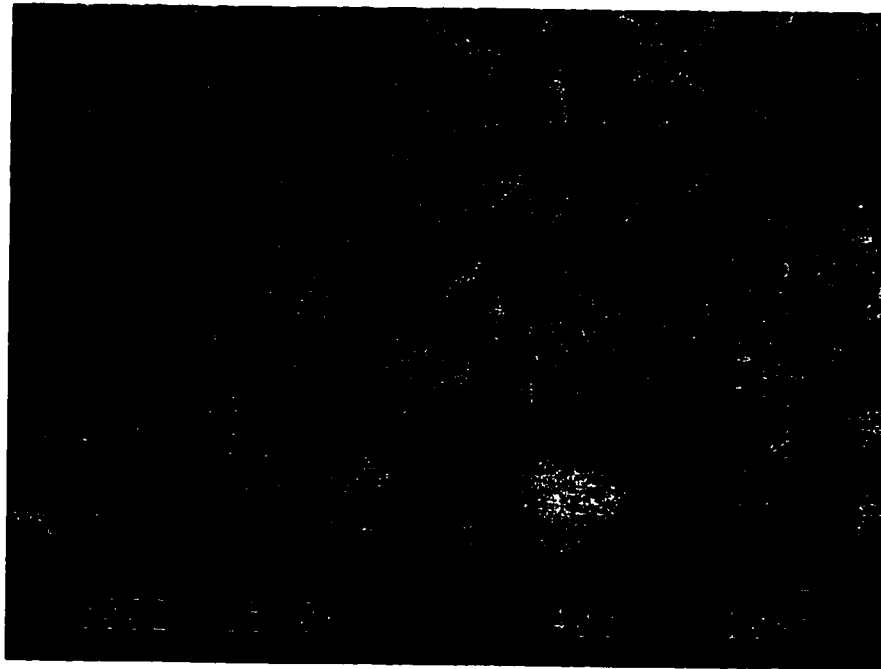


Figure 2.4 Scanning Electron Micrograph of portland cement showing grain morphology (Magnification 400x).

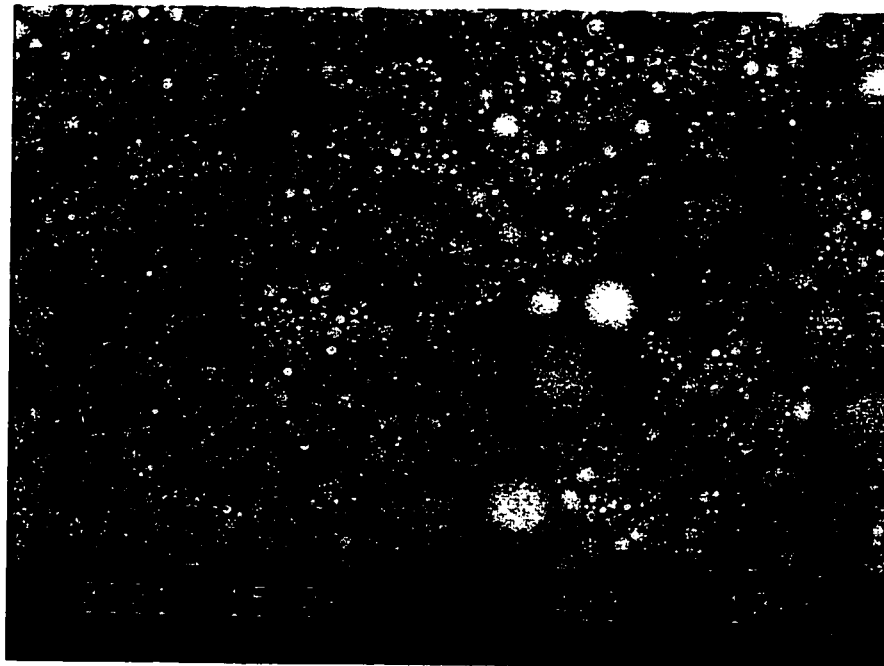


Figure 2.5 Scanning Electron Micrograph of fly ash showing particle morphology (Magnification 400x).

aluminosilicates that are present in the fly ash and they form calcium silicate hydrates with cementitious properties (Berry and Malhotra, 1987). Compared to the Class F low-calcium fly ash, the high-calcium Class C fly ash is generally more reactive since most of its calcium content is in the form of crystalline compounds, like tri-calcium aluminate (C_3A), calcium sulphate, and tetra-calcium aluminosulphate.

Fly ash used as a blending agent in cement provides preferential sites for the nucleation of hydration products especially crystals of $Ca(OH)_2$ during the initial stages of saturation of the cement / fly ash system. After the $Ca(OH)_2$ nucleates as a by-product of the hydration reaction of the constituents of portland cement, it begins to undergo a reaction due to the chemical reactivity of the SiO_2 that is contained in the fly ash and the result is the formation of additional C-S-H gel. This is termed as the pozzolanic reaction and it takes the form,



As a result of this classic pozzolanic reaction the content of $Ca(OH)_2$ that is present in blended cement pastes is lower than what is found in plain portland cement systems. However, the full range of reactions that take place due to the presence of mineral admixtures has not been fully understood. Generalization of reactions in systems containing fly ash are even more difficult to make due to the variations between different fly ashes and between different particles within the same fly ash (Glasser et al., 1987, Diamond, 1987).

One significant influence of the fly ash, as explained later, is the modification of the floc structure in the fresh cement paste. This effect is extended to the hardened paste and it influences the pore size distribution. Continuous capillary pores are replaced by finer discontinuous pores (Regourd, 1987). In the hardened cement paste this pore

refinement influences the permeability and ion diffusion and produces a more durable concrete.

Fly ash - cement systems undergo chemical reactions that later influence the mechanical properties of the hardened concrete. The process in which the reaction products are deposited is not fully understood. Diamond et al. (1980) have suggested the formation of a duplex film of reaction products around the fly ash grain. This film is composed of amorphous CH and a sparse outer layer of C-S-H gel and as it densifies, it gives rise to a hydrated shell similar to that forming around hydrating cement grains. Similar results have been published by Halse et al. (1984).

This is in agreement with research published regarding the cement paste microstructure that develops at the interfacial zone adjacent to surfaces of inclusions in concrete such as coarse or fine aggregates, steel reinforcement, other fibre reinforcements, or any other component. As water migrates toward these interfaces due to the poor local packing of the cement particle flocs, the developing microstructure is more porous than the remaining bulk paste. It is characterized by a film of hexagonal calcium hydroxide crystals that precipitate out of the supersaturated solution (Diamond, 1987, Glasser et al., 1987). The $\text{Ca}(\text{OH})_2$ then quickly reacts with the silica in solution forming a layer of C-S-H gel on the solution side of the film. Together they form the boundary or duplex film. The film thickens and forms a distinct shell.

When fly ash particles are included the formation of the shell is followed by a slow reaction between the surface of the fly ash and the inner surface of the shell. Dissolution of the glass surface of the fly ash particle leads to the formation of a narrow gap between the shell and the fly ash grain (Diamond, 1987, Clifton, 1989). Sequentially, the pozzolanic reaction takes place and the gap eventually fills with hydration products,

thus diminishing the CH content of the paste. This produces a final structure that is denser than what develops in cement systems alone.

2.11 Effect of Fly Ash on the Rheology of Fresh Concrete.

The shape and surface characteristics and the particle size distribution of the fly ash affect the behaviour of fresh and hardened concrete. The smooth spherical nature of the fly ash particles enhances the workability and influences the water requirements of the fresh concrete (Mehta, 1986). Other studies (Helmouth, 1987, Glasser et al., 1987) attribute the enhanced workability of fresh concrete to the physicochemical effects of fly ash. Adsorption of the very small fly ash particles on the surface of the cement grains creates an electrically charged envelope and causes the cement grains to disperse in the mixing water by a mechanism similar to that explained for water-reducing admixtures. This has a significant effect on the size distribution and structure of the individual flocs that comprise the fresh cement paste. This floc structure modification may be responsible for the observed decrease in water requirements rather than any supposed ball-bearing effect of the spherical fly ash particles. Modification of the flocculation behaviour, has an effect on the packing pattern of the system. This influences the pore size distribution and interconnectivity of the pores and therefore affects the permeability of the paste at later ages (Glasser et al., 1987).

Simultaneously, the particle size distribution influences the rate of progress of the hydration reactions. The smaller particles will react faster to form hydration products due to their larger surface to volume ratio (Pommersheim, 1987), thus improving the rate of strength development of the hardened concrete.

2.12 Effect of Fly Ash on the Mechanical Properties of Concrete

2.12.1 Compressive Strength and Static Elastic Modulus

The strength of the hardened paste in plain portland cement concrete is not strongly dependent on the microstructure of the C-S-H at the atomic level. Rather, it has been suggested, (Mindess, 1985), that the strength is determined by features at the mesolevel and the macrolevel. These parameters include:

- total porosity,
- pore size distribution,
- presence of "flaws" in the system, and
- the nature of the solid phase.

The detrimental effect of the total porosity on the strength of any material has been recognized historically. While a number of empirical models have been proposed for the relationship of total porosity and strength as summarized by Mindess (1985), the pore size distribution has a considerable effect on the strength of the system. For a greater proportion of finer pores, the strength is improved.

The nature of the hydration products is significant in determining the strength. It has been concluded (Jambor, 1974) that different types of hydration products develop different binding capacities. It has also been found (Feldman, and Beaudoin, 1976) that poorly aligned and ill-crystallized materials have the best bonding properties and this affects the strength as well. However, these results are not constant for large numbers of samples when all parameters are varied. It has been summarized that optimum blends of total porosity, pore size distribution and maximum pore size, crystalline and non-

crystalline phases and the nature of the solid phases are required to achieve maximum strength (Mindess, 1985).

When the system becomes more complex with inclusion of mineral admixtures, additional parameters come into play and influence the development of the compressive strength and modulus of elasticity of the hardened concrete. Fly ash influences the development of the solid phase and the hydration products and it therefore, has an effect on the strength of the material. The variables that contribute to the development of the hydration products include the chemical composition and properties of the fly ash. Also of significant importance are the particle size distribution and the chemical reactivity of the fly ash.

The pozzolanic reaction of fly ash, as stated earlier in this chapter, affects the formation of the hydration products in the hardened cement paste. The hydration products are influenced by the chemical composition of the fly ash, while the rate of the chemical reaction is dependent on the reactivity and particle size distribution of the ash. Since the pozzolanic reaction is time dependent the immediate effect of replacing cement with fly ash is one of delaying the hydration process and therefore the strength of the concrete develops at a different rate.

While data on concrete containing Class C fly ash are limited, numerous research studies have been conducted on the strength development of concrete using Class F fly ash as partial replacement of portland cement (Sivasundaram et al., 1991, Carette and Malhotra, 1987, Carette et al., 1993, Bisailon et al., 1994,). The general conclusion is that good levels of strength may be achieved in concrete containing large volumes of fly ash as partial replacements of portland cement. It is commonly reported that the effect of the fly ash is one of delaying the rate of strength development of the hardened concrete. However, significant variations in the results were observed using fly ashes of different

sources and this may be attributed to the variation in the chemical composition and the fineness of the ashes. Concrete containing fly ash with finer particles developed higher strengths with time (Sivasundaram et al., 1991). Carette and Malhotra, (1987), used fly ashes from various sources across Canada to investigate the effect of a 20% replacement of the cement on the mechanical properties of the hardened concrete. They found that at 28 days the compressive strength of fly ash concrete ranged between 70 and 90% of the strength of the control concrete. They also reported that the fly ash contribution became most significant after 56 days and at one year most of the fly ash concretes had exceeded the control in compressive strength while the remaining mixtures were only 5-10% lower.

The Young's modulus of elasticity is a mechanical property that can control the behaviour of concrete and it is of particular importance in the design of reinforced and prestressed concrete. However, unlike the measuring of the compressive strength which is quick and easy, direct measurement of the modulus of elasticity is time-consuming and, therefore, it is impractical.

The modulus of elasticity is closely related to the ultimate compressive strength of the concrete, and the different national building codes and standards have adopted various formulas for the determination of E_c as a function of the compressive strength (f'_c). This procedure is satisfactorily applicable to normal strength concrete. However, Baalbaki et al., (1992) have concluded that precise prediction of E_c of high strength concrete from its compressive strength is unreliable.

In concrete incorporating high volumes of fly ash, it has been shown that the development of the modulus of elasticity increased with time following the same pattern as the compressive strength development (Sivasundaram et al., 1991). They reported values of 41.0 and 34.9 GPa at 28 days for concretes containing 545 and 359 kg/m³ of cementitious material respectively. At 4 months the corresponding values for the

modulus of elasticity increased to 45.2 and 38.9 GPa for the same concretes. Similar results were reported by Carette and Malhotra, (1987) in a study of Canadian fly ashes where they concluded that there was no significant effect of fly ash on the modulus of elasticity. Elsewhere, Bisailon et al., (1994) have attributed the high values for the modulus of elasticity of fly ash concrete to the restraining effect of the unreacted fly ash assuming a role of a glassy fine aggregate.

2.12.2 Long-Term Deformation: Creep and Drying Shrinkage

Creep and shrinkage are important concrete properties in prestressed and reinforced concrete structures. Time-dependent deformation of concrete, due to creep and shrinkage, results in partial loss of the prestress force and produces significant changes in deflection. In reinforced concrete structures, a slow growth of deflection with time may lead to unsatisfactory performance and eventual failure. Even though data on Class C fly ash as it affects the deformation of concrete are limited, the effect of Class F fly ash on creep and drying shrinkage has been documented in various research studies (Sivasundaram et al., 1991, Carette and Malhotra, 1987, Carette et al., 1993, Bisailon et al., 1994,).

Sivasundaram et al. (1991), have reported very low creep strains in concrete incorporating a high volume of fly ash replacement. The highest value of creep strain that they reported for concrete with 155 kg/m³ cement and 215 kg/m³ fly ash was 350×10^{-6} . As the binder content of the concrete increased to 225 kg/m³ cement and 310 kg/m³ fly ash, higher creep strains were reported up to 501×10^{-6} .

Using a lower volume of fly ash (20% replacement), Carette and Malhotra (1987) found that the fly ash concrete produced lower creep strains than the control concrete by 20 to 40%.

Similar results have been published for the drying shrinkage of fly ash concrete. Bisailon et al. (1994), have shown that high volume fly ash concrete produced significantly lower drying shrinkage than concretes made with ASTM Type I cement or a modified version of ASTM Type II cement. For concrete containing only 20% fly ash as a replacement of the cement, Carette and Malhotra (1987) found slightly lower shrinkage strains in the fly ash concrete compared to the control.

Creep and shrinkage of concrete are affected by time, stress intensity, temperature and humidity. One of the objectives of the present research study is to investigate quantitative engineering information on these volumetric changes that are essential data for design engineers. The study investigates the effect of large volume of Class C fly ash on the long term deformation of concrete under various interactions of stress intensity, temperature and moisture levels.

2.12.3 Frost Resistance

The physical effect of freezing and thawing is due to the formation of ice in the pore system of the cement paste. As the water freezes and expands it disrupts the paste. Repeated cycles of freezing and thawing action weaken the paste/aggregate bond, produce microcracking within the paste, and cause eventual failure of the concrete. Theoretical studies have established that adequate air entrainment provides minute air bubbles in the paste which act as "relaxation chambers" for the pressures that develop from the ice formation.

Various studies have been performed on the effect of various types of fly ash on the frost resistance of the hardened concrete (Nasser and Lai, 1992, Bilodeau et al., 1994, Bisailon et al., 1994). Bilodeau et al., (1994) have found that all air entrained high volume fly ash concretes performed very well in an environment of repeated cycles of freezing-and-thawing. They had no difficulty in entraining air in high volume fly ash concrete and achieving satisfactory spacing factors and specific surface areas. They reported durability factors greater than 93 after 1000 cycles. Similar results were reported by Bisailon et al. (1994), and Carette and Malhotra (1987) for high-volume fly ash and control concretes after 300 cycles of rapid freezing-and-thawing. These results prove the superior performance of air entrained concrete and they indicate that incorporating high volumes of fly ash does not have any detrimental effects on the frost resistance of the hardened concrete.

2.12.4 Resistance to Sulphate Attack

Another potential cause of cracking in field concrete is due to sulphate attack. The term describes the deterioration of concrete due to the formation of calcium sulfoaluminate compounds when the material is exposed to sulphate-rich water or soil. These compounds occur when the sulphate ions from the surrounding environment react with the calcium aluminate phases and the free Ca(OH)_2 in the hardened cement paste, resulting in the formation of tricalcium-aluminate-trisulphate-hydrate ($3\text{CaO} \cdot \text{Al}_2\text{O}_3 \cdot 3\text{CaSO}_4 \cdot 31\text{H}_2\text{O}$). This is commonly called ettringite and it was identified by chemical analyses of affected concrete as early as the 19th century (Idorn et al., 1992). In addition, X-ray diffraction studies showed that gypsum (CaSO_4) is also deposited out of solution. Expansion and thereby cracking of the cement paste is attributed mainly to the formation of ettringite and to a lesser extent to that of gypsum (Taylor, 1990).

The method that is principally used to prevent sulphate attack of concrete is to change from Type 10 portland cement to Type 20 or 50 which contain a smaller amount of crystalline tricalcium aluminate (C_3A). A different way is to introduce a pozzolan. Davis et al., (1937) discovered that fly ash improved the sulphate resistance of concrete. There are two mechanisms by which fly ash improves the durability of concrete against sulphate attack. First, by using fly ash as a partial replacement of the cement, the total content of the aluminate phase is reduced. The second mechanism is due to the pozzolanic effect. Fly ash removes the free $Ca(OH)_2$ and therefore rendering it unavailable for the expansive formation of ettringite. At the same time the denser paste that is produced due to the pozzolanic reaction makes the concrete more impermeable and improves its resistance to sulphate attack.

A study on the effect of fly ash on the sulphate resistance of concrete by Tikalsky and Carrasquillo, (1992), showed that the effects of ASTM Class F fly ash on the sulphate resistance of concrete were beneficial, whereas high-calcium Class C fly ash did not always perform as well; rather, it increased the susceptibility of concrete to sulphate attack. However, in a more recent study, the same researchers (Tikalsky and Carrasquillo, 1993) have concluded that the sulphate deterioration of fly ash concrete is primarily related to the chemical composition of the glassy portion of the ash. They recommended that while fly ash containing less than 10% CaO may be used for sulphate resistant concrete, fly ash with a CaO content higher than 25% may not be used in environments rich in sulphate concentrations. Fly ash with CaO content in the intermediate range needs to be tested for sulphate exposure.

An additional objective of the present research study is to investigate the effect of high volume Class C fly ash concrete on the sulphate resistance of concrete.

CHAPTER 3

Test Program and Procedure

3.1 General Outline of Program

Economic benefits together with technical challenges stem from the use of fly ash in concrete. It became evident from the literature review in the preceding chapter that even though numerous research projects have been conducted on the use of Class F fly ash in concrete, the amount of data available on the effects of high calcium Class C fly ash on the mechanical properties of concrete is still limited. The present investigation was initiated by a demand for economical high performance concrete. The objective of this research project was to study the effect of using large volume of fly ash as a partial replacement of ordinary portland cement in combination with superplasticizer for the purpose of optimizing the mechanical properties while reducing the cost of the concrete. The fly ash selected for use in the project is Class C fly ash, available from Sundance, Alberta.

In the preliminary part of the project it was necessary to explore the possibility of using large volumes of Class C fly ash for the production of economical concrete with a high compressive strength and improved mechanical properties. For this purpose a series of studies on compressive strength and modulus of elasticity were performed using concrete mixtures with varying percentages of fly ash replacements of cement in combination with superplasticizer. An optimum ratio for water to binder (cement + fly

ash) was established that would allow the workability of the concrete to remain at a practical level. In this initial phase of the study, a concrete mixture with an optimum fly ash/cement ratio was chosen based on compressive strength results and cost.

The next portion of the experimental program consisted of the evaluation of the mechanical properties of the selected concrete mixture. For this task, a series of tests were set up to obtain data on the engineering properties of high volume fly ash concrete. For complete evaluation, a comparison was made to the same properties of a control concrete containing 100% portland cement. This part was divided into three phases outlined as follows:

Preliminary Phase: Compressive strength and modulus of elasticity

Phase One: Creep and shrinkage at elevated temperatures

Creep and shrinkage under different moisture conditions

Phase Two: Sulphate resistance

Phase Three: Freezing-thawing durability

The first phase consisted of two different test set ups to study the long term deformation of high volume fly ash concrete. The first set up was the evaluation of long term deformation of concrete at elevated temperatures. This test consisted of a study of creep of concrete under a combination of three levels of constant compressive stress and five levels of temperature. The second test investigated the effect of moisture and stress interaction on the creep of concrete under constant temperature. A zero level of stress allowed measurement of the drying shrinkage strains of fly ash concrete under the same conditions as the two experiments described above.

The second and third phases consisted of a study on the durability of fly ash concrete. In the second phase of the program the selected fly ash concrete mixture was exposed to a hostile environment of a 5% sodium sulphate solution for a period of eleven months. A simultaneous experiment was set up for concrete containing 100% portland cement in order that a comparison was made for the performance of the two concretes.

In the third phase the effect of rapid freezing-and-thawing on the durability of fly ash concrete was studied and a comparison was made again with the same property of a control concrete containing no fly ash replacement of the cement. While the majority of the experimental program was confined to non air-entrained concrete, in the third phase air-entrainment was introduced as an additional variable. A comparison was made for the frost resistance of fly ash and plain concretes, with and without an air-entraining agent.

In the preliminary phase of the project, the percentage of fly ash replacement of the cement in the mixtures was varied between the different batches of concrete. Except for the preliminary phase of the project where the percentage of fly ash replacement varied in order to establish the optimum fly ash/cement ratio, for the remainder of the program as many parameters as possible were maintained constant. These included the type of cement and fly ash, curing conditions, mixing procedure and equipment, aggregate and mix proportions, aggregate/binder and coarse/fine aggregate ratios.

3.2 Materials

The following materials were used throughout the project.

Coarse aggregate: Locally available, air-dried crushed gravel of 19 mm maximum size. Figure A.1 in Appendix A shows the grading of the coarse aggregate used.

Fine aggregate: Locally available, air-dried natural sand. Figure A.2 in Appendix A shows the grading of the fine aggregate used.

Cement: Type 10 portland cement [ASTM C-150]. Table A.1 in Appendix A provides a summary of the properties of the cement used in the program.

Fly ash: High calcium Class C fly ash [CSA Can3 A23.5 and ASTM C-618] produced in Sundance, Alberta. Table A.2 in Appendix A provides a summary of the properties of the fly ash used in the program.

Superplasticizer: Proprietary products, Rheobuild 1000 (an aqueous solution of a Ca-Napthalene Sulphonated based superplasticizer) and Pozzolith 400N (Na-Napthalene Sulphonated based superplasticizer with some organic accelerator), were used. Due to the high viscosity, the superplasticizers were dissolved with part of the mixing water prior to being added to the fresh concrete.

Chemicals: Sodium sulphate (Na_2SO_4) salt was used to prepare the solution for testing the sulphate resistance of concrete. Table A.3 in Appendix A provides a chemical analysis of the sodium sulphate used in the program.

Water: Tap water at 64° F (17° C) was used for preparing the concrete specimens. Distilled water was used in the preparation of the sulphate solution. Table A.4 in Appendix A provides a chemical analysis of the tap water.

Air-Entraining Agent: Micro-air liquid organic air entraining agent meeting ASTM C-260 specifications was used. Part of the mixing water was reserved for dissolving the air-entraining agent prior to mixing it with the fresh concrete.

The aggregates, cement and fly ash were weighed to the nearest 1/2 lb (227 g) using a Toledo Platform Scale with a weighing capacity of 800 lbs (363.2 kg). For

higher accuracy, the water was weighed to the nearest gram on a horizontal beam scale with one gram graduations. The superplasticizer was measured by volume to the nearest ml in a graduated cylinder.

3.3 Preparation and Proportioning of the Concrete Mixtures

As it was mentioned in preceding sections, the optimum concrete mixture was chosen based on economy for large utilization of fly ash and good performance in terms of high compressive strength and improved engineering properties of the concrete. A series of preliminary tests were used to determine the optimum fly ash/cement ratio.

For this purpose several concrete mixtures were prepared within a three month period, thus minimizing variability between batches of concrete due to cement, fly ash and aggregate sources. These mixtures were made using coarse/fine aggregate ratio of 1.22 and aggregate/binder ratio of 5.1. Class C fly ash was used as a partial replacement of the cement. The level of fly ash replacement ranged between 20-60% by weight of the total cementitious material (binder) in the mixture. The water/binder ratio was kept, as much as possible, constant among the various mixtures for comparison purposes; It was chosen to be low enough to produce higher compressive strengths in the hardened concrete but at the same time maintaining a good workable mixture. Workability of the concrete was evaluated using the K-slump (Nasser, 1976), a simple tubular tester which measures flow and workability in the fresh concrete. The K-slump of the concrete mixtures was kept at a practical level of 25 % which corresponds to a cone slump of 3 in (75 mm). Use of high-range water-reducing admixtures allowed a reduction of the water/binder ratio to 0.28-0.33. Two types of proprietary superplasticizers (both products of Master Builders Technologies) were used in the preliminary stages of the study. These products were Pozzolith 400N and a high early strength superplasticizer Rheobuild 1000,

both described in the preceding section. However, due to possible incompatibility of Pozzolith 400N with the fly ash, or the cement, or a combination of the two, delayed setting of the paste was observed in some of the concrete mixtures that contained a high volume of fly ash and Pozzolith 400N. This was not the case with the mixtures containing the same volume of fly ash replacement but using Rheobuild 1000 which is a high early strength superplasticizer. Delayed setting was experimentally impractical and subsequently the concrete mixtures were prepared using Rheobuild 1000. The manufacturer's recommendation for the maximum superplasticizer dosages were followed in the concrete mixtures of this study. The concrete mixture details are outlined in Table 3.1, with additional information given in Table 4.1.

Table 3.1 Concrete Mixture Design.

Materials	kg/m ³	lb/yd ³
COARSE AGGREGATE	1048	1766
FINE AGGREGATE	861	1451
CEMENT+ FLY ASH	364	630
Fly ash replacement: 20 - 60%		
SUPERPLASTICIZER	2.13 L/m ³	55 fl. oz./yd ³
WATER / BINDER RATIO	0.28 - 0.33	0.28 - 0.33
AGGR. / BINDER RATIO	5.1	5.1
K-SLUMP (5)	25±10 %	
CONE SLUMP	75±15 mm	3.0±0.5 in

For comparison purposes, control mixtures containing 100% Type 10 portland cement were also studied. For these mixtures, the mixing proportions and procedures were maintained identical as with the fly ash concrete mixtures. However, in the absence

of the fine fly ash particles, a higher water content was required in order to achieve a comparable workability in the control concrete as with the fly ash concrete. Since one of the criteria in the study was to maintain consistency in the workability, the water/cement ratio of the control mixtures was slightly adjusted and it was increased to 0.33.

The coarse and fine aggregates were used in the "saturated and surface dry" moisture conditions. Whenever the aggregates were either exceptionally wet or too dry, adjustments were made to the water content of the concrete mixtures in order that the nominal water/cement ratio was not altered due to excess water from the aggregates or due to absorption by the sand and gravel. For this purpose, samples of the aggregates were tested for their moisture content, according to the procedure described in ASTM C-127 and ASTM C-128 "Absorption of Moisture by Aggregates". Accurate adjustments were then made accordingly.

No air-entraining admixture was used in any of the concrete mixtures. An exception was the second series of concrete mixtures that were prepared for frost resistance testing.

Mixing was carried out in a pan mixer (260 lb capacity) in accordance with ASTM C-192. Prior to starting, the mixer was moistened using 100 ml of water in order to prevent mix water loss due to the absorption of the equipment and tools. The mixing sequence was as follows: Coarse aggregate, sand and part of the water were mixed and then the cement and fly ash (if any) were added. The remaining water (except the amount reserved for dissolution of the superplasticizer) was added and the mixture was worked for two minutes until it was homogeneous. The dissolved superplasticizer was then added and mixing continued for three minutes, left to rest for two minutes and then re-mixed for an additional two minutes to prevent false setting. In the case of the air-entrained mixtures, the chemical agent was added following the superplasticizer. The

properties of the fresh concrete including the K-slump, unit weight, and air content were determined prior to casting the test specimens.

3.4 Preparation and Curing of Concrete Test Specimens

As mentioned earlier, the objective of the preliminary phase of the project was to select a concrete mixture with an optimum fly ash content based on compressive strength and cost. A summary of the various tests, including a description of the size, type and number of test specimens is presented in Table 3.2.

Table 3.2 Summary of the various tests and their specimens as they were used in this study.

TEST TYPE	SPECIMENS			
	type	size	specimens per batch	number of batches
Main tests:				
compression (preliminary tests)	cylinders	75x150 mm	24	17
creep and shrinkage	cylinders	75x225 mm	12	11
frost resistance	prisms	90x115x400 mm	7	11
sulphate resistance	prisms	75x75x275 mm	4	6
Companion tests:				
K-5 accel. strength	cylinders	75x150 mm	3	
compression	cylinders	75x150 mm	12	

Seventeen preliminary concrete mixtures were prepared using varying contents of fly ash replacement of the cement. From each mixture several cylindrical specimens

were cast to be tested in compression at various ages. This allowed the study of the effect of the different fly ash levels on the development of the compressive strength. Analysis of the strength results allowed finalizing the proportions of the concrete mixture for use in the subsequent phases of the experimental program for evaluation of creep and drying shrinkage, freezing-thawing durability and sulphate resistance. For these mechanical properties various series of different types of test specimens were prepared from the selected fly ash and the control concrete mixtures. The type of the test specimens varied with the property that was to be evaluated. Following is a brief summary of the types of test specimens in this study listed according to the engineering property that was evaluated:

Compressive strength: Each of the preliminary concrete mixtures was large enough to allow casting of 27 - 75x150 mm (3x6 in) cylindrical specimens. These were tested in compression at ages ranging from 5 hours to three months. For some mixtures with a larger number of specimens, testing was also carried out at one year.

Creep and shrinkage: The specimens cast for creep and shrinkage testing consisted of 75x225 mm (3x9 in) concrete cylinders. These came from several different batches of the selected fly ash mixture. For comparison purposes identical specimens were prepared from the control concrete.

Freezing-thawing durability: Frost resistance testing was carried out in accordance with ASTM C-666 standard requiring 90x115x400 mm (3.5x4.5x16 in) concrete prisms.

Sulphate resistance: For durability of concrete against sulphate attack, the test specimens consisted of 75x75x275 mm (3x3x11 in) prisms, prepared according to ASTM C-1012.

Along with the different types of test specimens that were prepared for testing the mechanical properties, a small number of 75x150 mm cylinders were prepared simultaneously from the same batches of concrete. These specimens were tested in compression and/or splitting tension at key dates to accompany the results of long term testing as it will be described in the following sections.

3.4.1 Concrete Cylinders for Compressive Strength Testing.

Compression test specimens alone were cast from the preliminary concrete mixtures, in order to study the effect of fly ash on the strength development of the hardened concrete and to finalize the concrete mixture design. These cylinders, 75x150 mm (3x6 in), were cast in waxed cardboard molds in accordance with ASTM C-31 and C-193. They were filled in two equal layers and each layer was compacted with the use of a vibrating table with a maximum rotating speed of 6000 rpm. After being allowed to set covered for 24 hours, the test cylinders were removed from the molds and moved to a moist curing room which was kept at $23 \pm 1.7^\circ \text{C}$ ($73.4 \pm 3^\circ \text{F}$) and relative humidity of not less than 95%. The specimens were moist cured in lime saturated water for 3, 7, 14, 28, 56 and 91 days. Afterwards they were tested in compression. The cylinders that were tested for the 1-day compressive strength were not water cured; rather they were tested immediately after removing the cardboard molds. For an early indication of the 28-day potential strength of the hardened concrete, the K-5 accelerated compressive strength test (Nasser and Malhotra, 1990) was performed with each of the mixtures. For this test three additional 75x150 mm test cylinders were prepared following the same procedure that was outlined above and they were tested at five hours. These specimens were prepared in heat insulated stainless steel molds that were lined with plastic for easy removal of the hardened concrete. Immediately after casting, they were stacked vertically and mounted

onto the K-5 tester. They were then heated through a 3-hour cycle at a temperature of $149\pm 2.8^{\circ}\text{C}$ ($300\pm 5^{\circ}\text{F}$) and a pressure of $10.3\pm 0.2\text{ MPa}$ ($1500\pm 25\text{ psi}$) and afterwards they were allowed to cool for 2 hours before they were forced out of the molds and tested in compression. The details of the K-5 testing procedure are discussed in a later section. The same type of compression test cylinders were cast from each subsequent batch of the selected concrete mixture at the time of preparing the various types of specimens for evaluation of the engineering properties of the concrete in the next phases.

3.4.2 Concrete Cylinders for Creep and Shrinkage Testing.

Creep and drying shrinkage testing was carried out on test specimens from the selected fly ash concrete mixture as well as the control concrete. Two series of experiments on the long term deformation of concrete were performed to study the effects of temperature in one and the effect of moisture in the other. The test specimens were of the same size consisting of $75\times 225\text{ mm}$ ($3\times 9\text{ in}$) concrete cylinders; however, the procedure used to prepare the two types of concrete test specimens was partially different. For this reason the following two sections outline the preparation of the test specimens for the two different experiments.

Cylinders for Creep and Shrinkage Testing for Different Moisture Conditions.

High and low moisture levels were studied in combination with four levels of constant compressive stress. High moisture conditions, encountered in mass concrete, were represented by the use of sealed specimens while unsealed specimens, which were exposed to ambient temperature and humidity, simulated a dry environment.

The test cylinders for creep and drying shrinkage study were cast in 75x225 mm (3x9 in) steel molds which were fastened to a vibrating table by suitable clamps as shown in Figure 3.1. Each mold was lined with a plastic sleeve holding, at each end, three brass gauge points spaced at 120° from each other. At the time of casting, these brass studs were embedded in the fresh concrete giving a gauge length of 215 mm (8.5 in) for deformation measurements. The molds were filled in two equal layers and each layer was compacted with the use of the vibrating table. Approximately two hours after casting and while still in the steel molds the cylinders were capped with a smoothly finished surface of high strength mixture of cement paste to ensure even stress distribution during loading. After the initial setting period of 24 hours, the test cylinders were removed from the molds and moved to a moist curing room which was kept at $23 \pm 1.7^\circ \text{C}$ ($73.4 \pm 3^\circ \text{F}$) and relative humidity of not less than 95%. The specimens were moist cured in lime saturated water for 28 days.

Following this curing period they were accurately weighed to the nearest gram and then separated into sealed and unsealed specimens. For the unsealed specimens, the plastic liner was cut away leaving only the brass studs embedded in the hardened concrete. The specimens with the liners left in place, simulated mass concrete conditions. In addition to the liner, they had the top and bottom ends sealed with metal caps using a water-tight silicone adhesive under pressure application. Afterwards, all the cylinders were carefully marked and placed in specially designed spring loaded creep frames. The drying shrinkage test specimens were prepared identical to those used for creep measurements. In order that they would be tested under the same ambient conditions, they were left unloaded beside the creep frames for periodic deformation readings.



Figure 3.1 Steel molds clamped to vibrating table for preparation of creep and shrinkage test specimens.

Due to limited availability of the required number of molds, a total of three batches of the fly ash concrete were cast on three consecutive days. For comparison purposes, an equal number of concrete batches and test specimens were cast from the control mixture and an identical companion experiment was carried out.

Each batch was large enough to provide 8 specimens for testing under each of the moisture-and-stress treatment combinations as well as sealed and unsealed experimental conditions for creep and drying shrinkage. Four additional specimens were prepared from every batch of concrete in the same 75x225 mm steel molds to be used for strength and modulus of elasticity tests at the start of load application and at the end of creep loading. Twelve test cylinders were also cast from each of the batches in 75x150 mm (3x6 in) waxed cardboard molds for strength and elasticity tests at intermediate dates. These specimens were prepared and cured under the same conditions as those used for creep testing.

Cylinders for Creep and Shrinkage Testing at Elevated Temperatures.

A series of five different batches of fly ash concrete were cast on five consecutive days, to be used for creep and shrinkage testing at elevated temperatures. Twelve 75x225 mm (3x9 in) cylinders were prepared from each batch of concrete. From these, nine specimens were used for creep and one for shrinkage study in a designed arrangement that is explained in the corresponding section of this chapter. The remaining two cylinders were used for compressive strength and static modulus of elasticity testing. The concrete cylinders for creep were prepared in the same steel molds and process, as described in the previous section, but without the exterior plastic liners or the embedded brass gauge studs. The cylinders prepared for shrinkage measurements were identical except for a small diameter conduit that was placed in the centre of the cylinder in the longitudinal direction. A probe for monitoring the temperature in the interior of the test specimen was placed in the tube. Two hours after casting, the creep and shrinkage specimens were capped with a mixture of high strength cement paste to allow even stress distribution during loading.

In addition, 12 test cylinders were cast from each of the batches in 75x150 mm (3x6 in) waxed cardboard molds for strength and elasticity tests at intermediate dates. After the initial setting period these specimens were cured in water for 28 days in the same standard humid room and the same conditions of temperature and humidity as all of the other specimens described earlier.

3.4.3 Concrete Prisms for Freezing-Thawing Durability Testing.

Two series of frost resistance testing were carried out on concrete prisms from the selected fly ash concrete mixture as well as the control concrete. In the first series the concrete contained no air-entrainment. In the second set of experiments the effect of micro-air air-entraining agent on the freezing-thawing durability of the concrete was evaluated. Also, in addition to the selected fly ash and control concrete mixtures, the first series of frost resistance testing included a mixture containing an intermediate (30%) fly ash replacement of the cement. The testing and specimen preparation procedures were carried out according to ASTM C-666 standard Procedure A, for freezing and thawing in the presence of water. In order to check the reliability of the freezing-thawing equipment available in the Civil Engineering Laboratory, every batch of concrete was large enough to cast twice as many prisms as needed for one run of the experiment. The second set of specimens were tested using the freezing-thawing equipment at the PFRA Materials Laboratory located on the campus of the University of Saskatchewan.

The concrete prisms were cast in steel molds and had dimensions of 90x115x400 mm (3.5x4.5x16 in). The molds were lightly coated with form release oil for easy removal of the concrete after setting. They were then filled in two layers and each was compacted with the use of the vibrating table at 6000 rpm. The top surface was then trowelled to a smooth finish. After being allowed to set covered for 24 hours, the concrete prisms were removed from the molds, they were labeled and carefully weighed. They were then moved to the same humid room that was described in the previous sections and they were cured in lime saturated water for 28 days.

The batches of concrete were large enough to permit preparation of seven 90x115x400 mm concrete prisms. Six of these were cured for freezing-thawing testing, allowing 3 prisms to be tested in each of the independent Materials Laboratories

described above. The seventh was cut into transverse sections which were then polished for evaluation of the air void characteristics of the hardened concrete. In addition, twelve 75x150 mm (3x6 in) cylinders were prepared in waxed cardboard molds for compressive and splitting tensile strength testing. These properties were evaluated at the beginning and the end of the freezing-thawing testing.

3.4.4 Concrete Prisms for Sulphate Resistance Testing.

The batches of concrete that were used for making cylinders for testing creep and shrinkage under different moisture conditions, were proportioned to permit preparation of prisms for evaluation of the sulphate resistance of the fly ash and control concretes. The specimens for this test consisted of 75x75x275 mm (3x3x11 in) prisms, prepared according to ASTM C-1012 standard in steel molds that had been lightly oiled. Prior to casting, a stainless steel plug was threaded in the centre of each of the two end plates of the molds. After setting and hardening of the concrete the plugs remained embedded in the specimens thus allowing accurate measurement of the length change.

The molds were filled in two equal layers and each was compacted using a vibrating table. They were then allowed to set covered for 24 hours before they were removed from the molds. They were weighed, labeled and then moved to a standard humid room where they were cured in lime saturated water for 28 days under the same conditions of temperature and humidity as described earlier for all of the other test specimens. Following the same procedure as previously described, companion cylinders were prepared in 75x150 mm (3x6 in) waxed cardboard molds to be used for compressive strength testing at the start of the sulphate resistance experiment.

3.5 Apparatus and Testing Procedures

The following sections present a detailed description of the experimental set-up and testing procedure for each of the concrete properties that were studied.

3.5.1 Compressive Strength Tests

Testing was carried out on a 1335 kN (300,000 lb) capacity Baldwin Universal Testing Machine according to the ASTM C-39 standard. The testing machine was equipped with two loading ranges (0-50,000 lb and 0-300,000 lb) and the appropriate range was selected for every test. The strength of the concrete at each test time was the average of three test specimens. A 100x100 mm (4x4 in) square fibre board was used as capping material at the top and bottom surfaces of all of the tested specimens to ensure uniform load distribution. The K-5 (Nasser and Malhotra, 1990) accelerated compressive strength test was performed with each of the mixtures. In this procedure the test specimens (75x150 mm concrete cylinders) were heated through a 3-hour cycle at a temperature of $149\pm2.8^{\circ}\text{C}$ ($300\pm5^{\circ}\text{F}$) and a pressure of $10.3\pm0.2\text{ MPa}$ ($1500\pm25\text{ psi}$) and then were allowed to cool for 2 hours before they were removed from the molds and tested in compression using the same testing equipment. Nasser and Malhotra (1990) have established a correlation between the 28-day compressive strength of the hardened concrete and the strength of the heat cured concrete cylinders at 5 hours. The advantage of this test is the early indication of the 28-day potential compressive strength of the concrete.

3.5.2 Long Term Deformation Testing

Creep properties were evaluated by subjecting the specimens to constant stress intensity levels of 5.5, 8.3, and 13.8 MPa (800, 1200, and 2000 psi). A zero stress level allowed measurement of shrinkage strains in the concrete when subjected to the same ambient conditions as the creep specimens. In addition to the stress intensity levels, different conditions of moisture and high temperature were introduced in the experiments and their combined effects on the creep and shrinkage of the concrete were studied. The experimental program was set up to study these effects in two types of creep experiments. One experiment evaluated the influence of stress and high temperature on creep. In the second experiment the creep and shrinkage of concrete under stress and moisture interaction conditions were studied for a period of one year under constant temperature.

The following sections describe the experimental set-up for the two series of creep and shrinkage studies.

a. Moisture Influence on Creep and Shrinkage

The fly ash and the control concretes were tested for creep and drying shrinkage simultaneously in order to minimize variations due to the effects of ambient conditions of temperature and humidity. In order to cast the required number of cylinders to test for all of the stress and moisture combinations, three different batches of each of the two concretes were mixed. This was due to a shortage of steel molds that made it impossible to cast all of the specimens from a single batch. At the same time, three different batches meant replication of the experiment. However, strength variability was encountered between the batches and therefore, it became important to use experimental design for the arrangement of the cylinders under the different treatments.

The experiment was set up as a randomized complete block design (Montgomery, 1991, Bickis) to study the effects of moisture and stress interaction on creep and shrinkage strains of the concrete while the temperature was kept at a constant level. The statistical analysis was able to differentiate between moisture-and-stress interactions from concrete batch effects. The above analysis separated the uncontrolled batch variability from the effects of stress-and-moisture interaction and removed it from the experimental error.

High and low moisture levels were studied in combination with four levels of constant compressive stress. High moisture conditions, encountered in mass concrete, were represented by the use of sealed specimens while unsealed specimens, which were exposed to ambient temperature and humidity, simulated a dry environment. The various batches of concrete had equal representation in the treatments in terms of test specimens.

Figure 3.2 represents a diagram of the experimental set-up where every treatment is the average of three cylinders, one from each of the concrete batches making the results more accurate from a statistical sense.

Following the 28-day curing period, the test specimens were removed from the humid room and after being weighed and capped, as described in the specimen preparation section, they were ready to be fitted in spring loaded creep frames. A total of 36 frames were available. The fly ash and the control concretes were tested simultaneously by using 18 frames for each in the arrangement that is shown in the diagram of Figure 3.2.

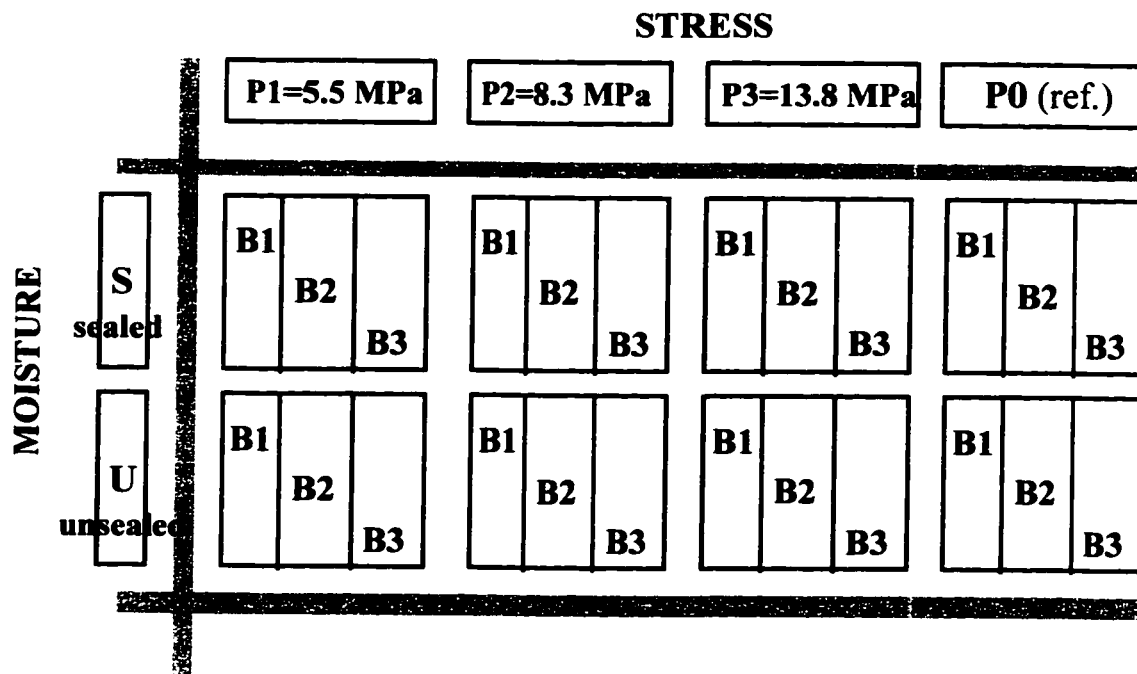


Figure 3.2 Stress-and-moisture interaction experimental set-up.

The creep testing device consisted of a steel L-shaped frame with its base fixed to the counter-top. The creep specimens were fitted with steel cup-shaped plates for the transfer of load and they were placed in the metal frames ensuring that the bottom plate rested on a 13 mm (1/2 in) ball bearing. Then a short I-beam was placed on the top of the specimen. This I-beam was fixed to the L-shaped frame at one end while at the other end it was connected to the base of the frame by means of a vertical aluminum tie rod with a diameter measuring 16 mm (5/8 in) and a length of 690 mm (27.5 in). A coiled spring was centered on the aluminum rod and it rested on top of the I-beam. The spring was topped by a small plate and a nut. The testing device is shown in Figure 3.3.

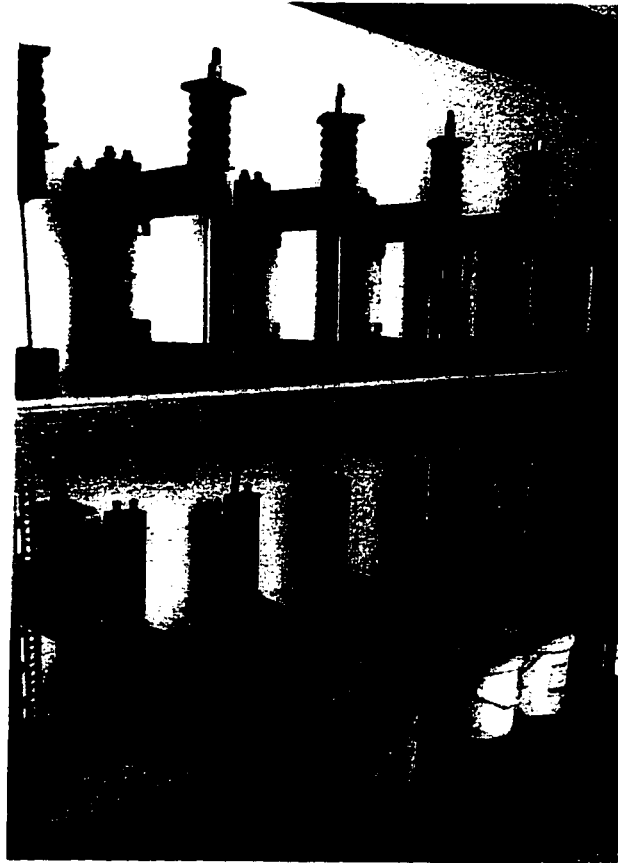


Figure 3.3 Creep apparatus with partial view of experimental set-up at room temperature of 21° C (70° F).

The required load was applied by tightening the nut and compressing the spring the desired amount and it was transferred to the specimen via the short I-beam. A graduated torque wrench that read to the nearest one-foot-pound was used to apply the load. To ensure uniform load distribution over the concrete cylinder, a 13 mm (1/2 in) steel ball bearing was positioned into spherical indentations that were machined into the loading I-beam and the cup plate that was fitted over the top of the test specimen. The load was kept constant by monitoring the strain in the aluminum tie rod. For this purpose, three gauge points at 120° to each other were impressed on the surface of the tie rod at two locations 200 mm (8 in) apart. The deformation was measured and the average

between the three pairs of gauge points was used as an indication for appropriate adjustment of the spring. Maintaining a controlled deformation in the tie rod ensured a constant load and hence, a constant stress in the concrete test specimen.

After the deformation of the tie rod was checked and any necessary adjustments to the spring were made, the deformation in the concrete specimen was read by using the two accessible pairs of brass studs that were embedded in the cylinders at the time of casting the concrete. The longitudinal deformation was measured using a portable mechanical extensometer with a least scale reading to the nearest 0.0001 inch. This process was followed the day the specimens were loaded in the creep frames and it was repeated after 1, 2, 3, and 7 days. Thereafter, the deformation was monitored every week for the first month, and then monthly for a period of one year. After this time, the specimens were unloaded by completely loosening the spring and the creep recovery of the concrete was monitored for an additional month.

Drying shrinkage was monitored at the same time intervals as creep. This was done by reading the longitudinal deformation of the shrinkage specimens using the average of three pairs of the brass studs.

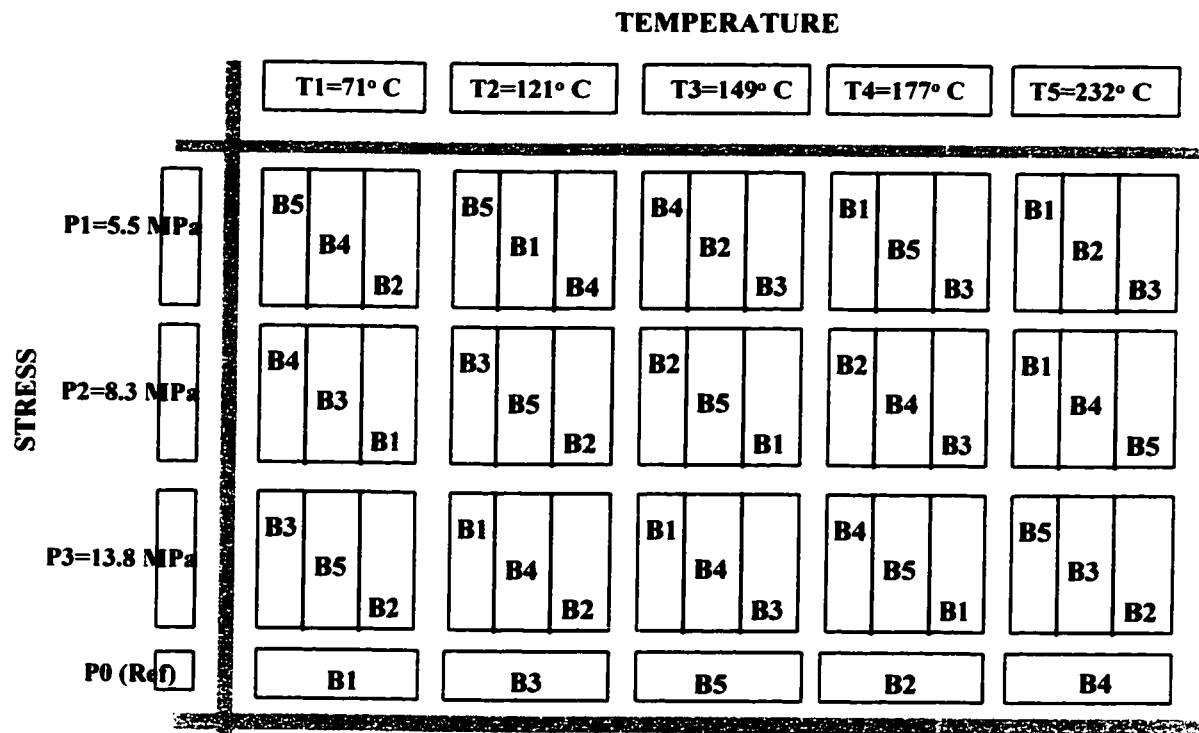
b. Temperature Influence on Creep and Shrinkage

The effects of stress and temperature interaction on the creep and shrinkage of the concrete were studied in this experiment. The testing devices are shown in Figure 3.4. The details of the high temperature creep apparatus and its operating mechanism are described in earlier studies (Marzouk, 1979, Lohtia, 1968) and are briefly described in this section.



Figure 3.4 Partial view of the high temperature creep equipment.

The same three levels of one-directional constant compressive stress that were mentioned earlier (5.5, 8.3, and 13.8 MPa) were used in combination with five levels of constant temperature. These temperatures were 71, 121, 149, 177 and 232 °C (160, 250, 300, 350 and 450 °F). Fifteen combinations of the different levels of stress and temperature were possible. Three concrete cylinders were tested under each of these combinations and each cylinder came from a different batch of concrete. The various batches of concrete had uniform representation under the different treatment combinations of stress and temperature. The diagram in Figure 3.5 represents the experimental set-up.



- B1 represents a specimen from batch 1
- B2 represents a specimen from batch 2
- B3 represents a specimen from batch 3
- B4 represents a specimen from batch 4
- B5 represents a specimen from batch 5

Figure 3.5 Stress-and-temperature interaction experimental set-up.

Following the initial 28-day curing period, the cylinders that were prepared for creep study at elevated temperatures were removed from the lime water. After washing and surface drying them, they were carefully weighed. Then, they were placed in upright, temperature and pressure controlled creep cells. Immediately after placing a gasket and a water-tight high temperature adhesive, the lid of the cell was closed and bolted in place with an air-gun and a torque wrench. The specimens were thus sealed. The thermocouples were attached to the lids of the creep cells connecting each cell to the temperature controlling equipment. The compartments that held the cylinders were insulated by filling the space between them and their exterior containers with vermiculite.

Heat was then applied gradually and the temperature was monitored for a few days until it stabilized at the required level before the pressure was pumped on. Following a small one-directional pressure application of 0.67 MPa (100 psi), the deformations were measured with a portable mechanical extensometer made from invar metal to withstand high temperatures without altering the results. This measurement served as the reference value for subsequent deformation readings. Afterwards, the pressure was pumped gradually to the required levels and immediately after, the deformations were measured again for estimation of the elastic strain. Thereafter, the deformation measuring procedure was followed at 1, 3, 7, 10 and 14 days. It was repeated weekly and later monthly until one year was completed from the pressure application date. At each time interval, three deformation measurements, at 120° from each other, were taken from each of the creep cells and their average was used for estimating the creep strain of the concrete. Creep recovery of the specimens was studied in the same creep cells for a period of three months after the pressure was released.

The cylinders that were used to study the drying shrinkage were placed in five temperature controlled cells under zero stress. They were exposed to the same levels of temperature and they were measured at the same time intervals as the creep cells.

3.5.3 Freezing-Thawing Durability Testing

Testing was carried out in accordance with ASTM C-666 Procedure A for rapid freezing and thawing in water. After 28 days of moist curing the concrete prisms were removed from the lime saturated water, washed and wiped dry. They were then weighed to the nearest gram and this would be the reference value for monitoring the weight loss due to surface scaling of the concrete or the weight gain due to internal cracking and water absorption. However, the principal cause of deterioration of the concrete due to

freezing-and-thawing is due to internal cracking of the cement paste. According to the ASTM standard, the evaluation of this effect is based on the calculation of the relative dynamic modulus of elasticity after any number of freezing-thawing cycles. This property is dependent on the propagation of sound waves through solid matter. For this reason the initial fundamental transverse frequency of the concrete is evaluated at zero cycles of freezing-and-thawing as reference and it is monitored at regular intervals subsequently. The freezing-thawing equipment is pictured in Figure 3.6.

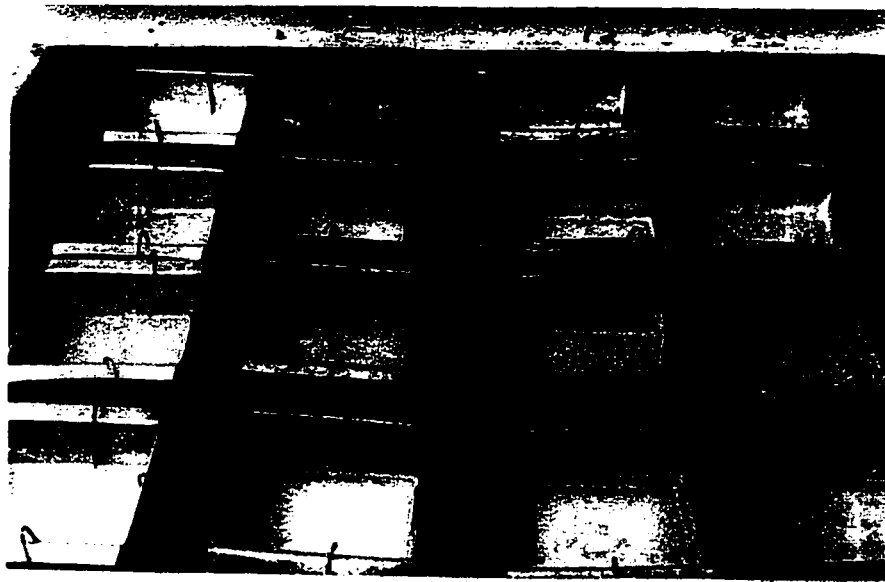


Figure 3.6 Concrete specimens inside metal containers in the freezing-thawing tank.

Sixteen containers are arranged vertically on a grid inside the tank. A solution of antifreeze circulates around the containers continuously cooling and warming their temperature between 4.4°C and -17.8°C (40°F and 0°F) in a three-hour cycle.

For the freezing-thawing study using non air-entrained concrete, two mixes using different fly ash replacements of cement, and a control mixture, as described in the

specimen preparation section were tested. Each mixture was replicated twice by using two distinct batches. Each batch of the fly ash concretes was represented by three specimens while each batch of the control concrete was tested using two specimens.

For the freezing-thawing test with air-entrainment included, only the selected fly ash and control concretes were tested. Two batches of each were used thus ensuring duplication of the results and each batch was represented by three test specimens. For the remaining containers in the freezing-thawing tank, one of the non-air entrained batches of the selected fly ash concrete was tested (using three prisms) for the effect of longer curing (70 days instead of 28 days) on the frost resistance property.

The test prisms were placed upright inside the containers, which were then filled with water. Small diameter wire spacers were inserted between each vertical face of the concrete beam and the corresponding wall of the container. This ensured that the beam was completely surrounded by approximately 3 mm (1/8 in) of water. For the same effect at the base of the beam, the bottom of each metal container was lined with wire meshing. When the containers were filled with water care was taken to cover the concrete lightly thus allowing for the expansion of the water when the temperature was lowered.

At regular intervals the test specimens were removed from the containers during the warm cycle. They were cleaned in lukewarm water with a stiff brush to remove any scaling and they were surface dried. Then, they were weighed to the nearest gram using an electronic digital scale as a means of monitoring any weight loss due to surface scaling or any weight gain due to internal cracking and water seepage. Their fundamental transverse frequency was measured using a "Sonic Star" equipped with a Type 602 Display Unit of Tektronix, Oregon, as outlined in ASTM C-666 and C-215. Afterwards, they were promptly returned to the freezing-thawing containers in time for the cold cycle to begin. At this point the prisms were turned end-for-end so that the same ends did not

always remain either at the bottom or at the top for the entire duration of the freezing-thawing test. This procedure was performed every approximately 8 cycles at the beginning, while later the test was monitored every 30 cycles. It was repeated up to 300 cycles or until the dynamic modulus of elasticity dropped to 60% of the initial value. The physical condition of the test prisms was noted every time.

3.5.4 Sulphate Resistance Tests

After being moist cured for 28 days, the 75x75x275 mm (3x3x11 in) prisms were taken out of the water bath and prepared for the experimental set-up. For this purpose, they were washed and wiped so they would be surface dry. They were weighed on an electronic digital scale to the nearest gram and this was noted as the reference weight. Since the result of deterioration of the concrete due to sulphate attack is the expansion of the paste, the data of this testing procedure reflect volumetric changes. To simplify the measuring procedure it is sufficient to record the length change of the specimen according to ASTM C-1012 standard. Therefore, the beam specimens were carefully measured for their length using a length comparator capable of measuring to the nearest 0.0001 inch. This was recorded as the reference length before the prisms were immersed in a solution of Na_2SO_4 . To evaluate the effect of the sulphate ions on the concrete identical prismatic specimens from each batch of the fly ash and the control concretes were immersed in distilled water and their length change was monitored at the same time intervals as the specimens that were immersed in the Na_2SO_4 solution.

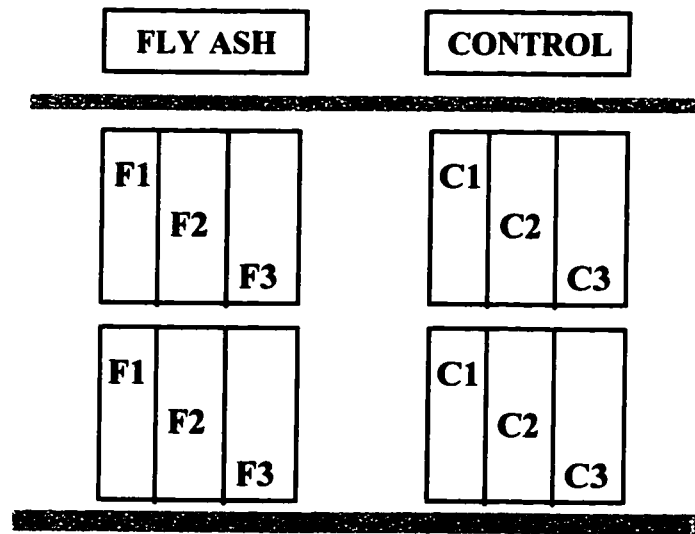
Following the ASTM specifications, the sodium sulphate solution contained 50g of Na_2SO_4 per litre of solution. A sample solution was prepared by volume using distilled water and pure sodium sulphate chemical. For this purpose 50g of Na_2SO_4 were dissolved in part of the distilled water and then additional distilled water was used to

make one litre of solution. The weight of this sample litre of solution was very accurately measured. For practical reasons the large quantity of the sulphate solution that was needed for the experiment was prepared by weight using the sample litre of solution as a basis.

The experiment was set-up as a randomized complete block design. Using the three different batches of concrete, the experiment was essentially replicated three times with two observations from each replicate. For this, two test prisms from each batch of concrete were immersed in the sulphate solution and two in distilled water for reference. In total there were two independent containers of sulphate solution for testing the fly ash and two for the control concrete prisms. Three test prisms were placed in each of the containers in an arrangement that ensured equal representation of the different batches of concrete. For example, the first container for the fly ash concrete held one test specimen from each of the three batches of fly ash concrete. Figure 3.7 represents a diagram of the four containers of the sulphate solution.

The containers were stored in the same standard humid room that was described earlier for other experiments. The prisms were positioned vertically in the containers, as shown in

Figure 3.8, ensuring that they were completely surrounded by the sulphate solution and they remained so for a period of one year. Their weight and length change were monitored periodically according to ASTM C-1012. At regular intervals, the prisms were removed from the solution and rinsed in lukewarm water to remove any scaling or surface depositions. After surface drying, they were weighed and measured for length changes. The pH of the solution was also checked at the same time and it was maintained at a constant value.



F1, F2, F3 represent specimens from batches 1, 2 and 3 of the fly ash concrete
C1, C2, C3 represent specimens from batches 1, 2 and 3 of the control concrete

Figure 3.7 Experimental set-up for sulphate resistance of fly ash and control concrete.

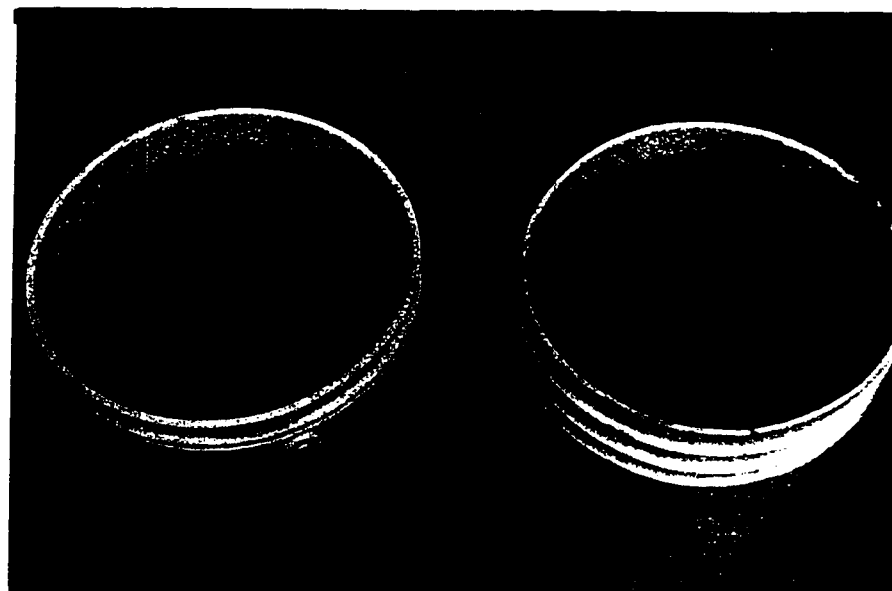


Figure 3.8 Sulphate resistance test specimens immersed in Na_2SO_4 solution.

3.6 Microstructural Examination

Following the completion of the experiments that were described above, a microstructural investigation was undertaken to explain the performance of the fly ash concrete compared to the control mixture. This study was based on the microstructure that resulted from the replacement of the cement with fly ash. The effect of the experimental conditions on the structure of the two concretes was noted. These included sustained loads at elevated temperatures or different levels of moisture; also the effects of a sulphate environment and freezing-and-thawing conditions were studied. The microstructural investigation was performed using Scanning Electron Microscopy and Electron Probe Microanalysis on fractured and polished samples respectively and the microstructural features of the two concretes were compared. The following sections contain a review of the equipment and its principles of operation, as well as the analytical techniques used and their theoretical background.

3.6.1 General

Rapidly expanding technology places strong demands on today's Materials Scientist to collect information and correctly explain phenomena that occur on a micrometer and submicrometer level. Typically, the resolution of the unaided human eye is limited to 0.1mm - 0.2mm (100-200 microns). This resolution increases by one thousand times with the aid of the light microscope. The conventional scanning electron microscope achieves practical magnifications of several hundreds of thousands of times (100 000 - 200 000x) allowing observation of features which are only a few nanometers in size.

In addition to its superior resolution and high magnification, the scanning electron microscope is capable of displaying objects in three dimensions. This is due to its extreme depth of field or depth of focus (on the order of 100 - 500 microns) compared to the optical microscope (approximately 0.08 microns). This is considered to be the feature which is of most value to the SEM user.

High resolution, high magnification and three dimensional effect provide information on the surface topography of the examined specimen. However, this is not the only goal of the microscopist. It is also desirable to analyze the chemical composition, the structural stress or strain, and in cases, the electrical properties of the sample. Many of these properties can be obtained with the use of the scanning electron microscope (SEM) and the electron probe microanalyzer (EPMA or Probe). The Probe is one of the most powerful techniques for microanalysis of materials. It is capable of giving compositional information using characteristic X-ray lines with a spatial resolution of the order of 1 μ m. Typically the SEM and the Probe are two separate instruments but after using them one finds that the two are essentially one and the same instrument. Their operation is based on the atomic theory of matter and it is reviewed in the next section.

3.6.2 The Atomic Theory

In the 5th century B.C., in ancient Greece, Democritus had set the roots for the origin of the atomic theory of matter. He proposed, for the first time, that matter is not indefinitely divisible; rather, it is composed of small indivisible particles, each called *atomo* from the greek for "indivisible". Even though Democritus's proposition was largely ignored at the time, it reemerged in the 19th century to explain the inconsistencies of the idea of indefinitely divisible matter (Brown et al., 1991). A historic development

through scientific theories led to Ernest Rutherford's establishment of the nuclear nature of the atom in 1910. In 1914, based on Max Planck's quantum theory, the Danish physicist Niels Bohr introduced the Bohr model of hydrogen. In summary, the principles of Bohr's model state that:

1. The electron of the hydrogen atom orbits the nuclear proton in a circular orbit. The electron may occupy orbits of certain radii which correspond to allowed energy states.
2. The electron can change from one allowed energy state to another either by absorbing or emitting radiation. The frequency (ν) of the radiant energy corresponds to the energy difference between the two allowed energy states.

In a schematic form the atom is shown in Figure 3.9. The figure indicates the nucleus of the atom and the allowed energy levels K, L, and M, where the electrons may be found, attracted to the nucleus. The energy that is required to remove any one electron outside the influence of the nucleus is called the ionization energy. Since the electrons of the inner shells have a stronger bond to the nucleus, the ionization energy of an electron increases as one moves from the outer to the inner shells.

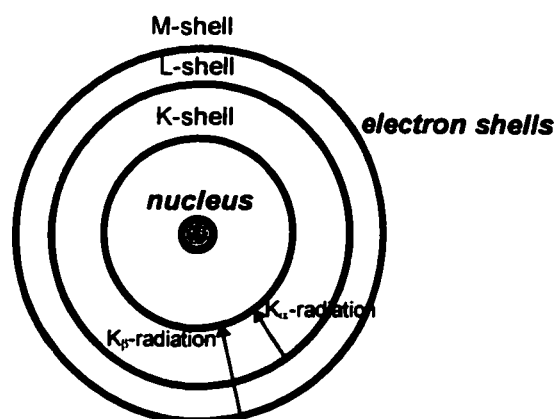


Figure 3.9 Schematic representation of Bohr's hydrogen model.

The distance of an electron from the nucleus may be used to describe its potential energy. An electron is considered to be in its lowest and most stable energy level when it is closest to the nucleus. This is called the ground state of the atom. Unlike the ionization energy of the electron, its energy state is higher as the electron's distance from the nucleus becomes greater. When an electron exists in a higher energy state, the atom is said to be in an excited state. As the second principle of Bohr's model states, the atom may interchange between the ground and the excited energy states when electrons absorb or emit radiation. The results from SEM or Probe analyses are the interpretation of these radiation signals.

3.6.3 Operation of the SEM

All SEMs operate by irradiating a sample with a finely focused static or continually rastered beam of electrons and collecting the various reflected and emitted signals which are generated from the interaction of the electron beam with the solid specimen.

The major components of the SEM are (Robertson, 1990):

- The electron gun.
- The electron column.
- The vacuum system.
- The Beam-Specimen interaction.

The electron gun consists of a wire filament (usually tungsten) which is held at a slightly negative potential relative to ground. The filament is heated inside a Wehnelt

cylinder which is held at a slightly negative potential relative to the filament. The filament and the Wehnelt cylinder are both above the anode which is held at a very high positive potential relative to the filament. As the filament is heated directly by electrical current passing through it, electrons are emitted and, as they are accelerated by high voltage at the anode, they enter the electron column. Here, they encounter a series of electromagnetic lenses and apertures which cause the electrons to converge to a single point at the beam-specimen interaction.

The entire SEM (the gun, the column and the specimen observation chamber) is operated at a very low pressure in order to prolong the filament lifetime but also to avoid destroying image quality from collisions between residual gas molecules and the primary electron beam (e-beam).

The focused e-beam has sufficient energy to eject electrons from the inner shells of an atom in the material sample. When an electron from the K-shell of the atom is ejected, the atom is a charged positive ion. However, it is different from an ion with a missing valence electron in that it is in a highly energetic state; the electrons do not reside in their lowest possible energy levels. In order for the atom to return to the ground state, an electron drops from one of the outer shells to fill the vacancy. Energy emission accompanies this process since the electron drops from a higher energy state (more distant from the nucleus) to a lower one (closer to the nucleus). The emitted signal is called X-ray photon.

The energy of the X-ray photon is a function of the difference between the initial and the final energy states of the electron. An electron may drop from the L-shell to the K-shell and the result is K_{α} radiation emission. If the transition is from the M- to the K-shell, the result is K_{β} radiation. The electrons in the M-shell are at a higher potential energy level than those of the L-shell ($E_M > E_L$). Compared to the transitions from L to K,

transitions from the M- to the K-shell will result in a higher emitted energy for the X-ray photon. Hence, K_{β} radiation is more energetic than K_{α} radiation. Higher energy means shorter wavelength, therefore, K_{β} radiation has shorter wavelength than the K_{α} . This energy or wavelength of the characteristic radiation are specific for atoms of a given atomic number (Z). During qualitative or quantitative analysis, Energy Dispersive Spectroscopy (EDS), or Wavelength Dispersive Spectroscopy (WDS) matches the above energy or wavelength to the respective properties of the element present. This is the basis for detecting the presence of a specific element in a sample compound. The general relationship is one of decreasing wavelength of the X-radiation with an increasing atomic number and it is shown in Figure 3.10.

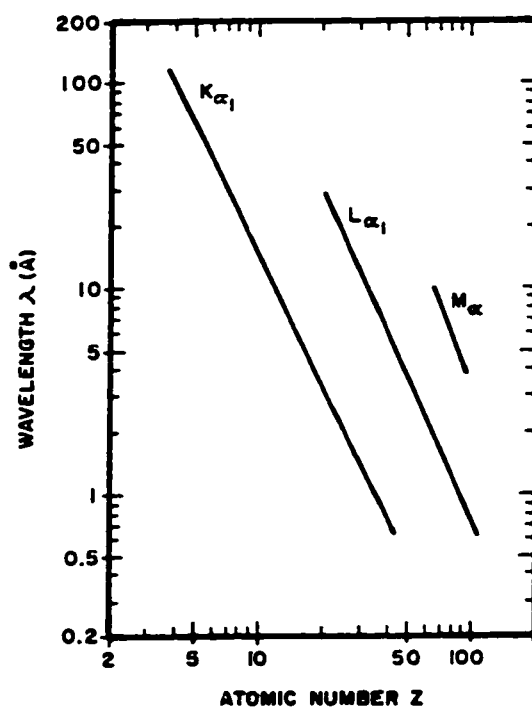


Figure 3.10 Relationship between wavelength (λ) and atomic number (Z) (Goldstein and Yakowitz, 1975)

The information required by the material scientist is collected from the beam-specimen interaction. The electrons of the beam (primary or exciting electrons) interact with the sample and they are scattered and spread. The volume in which the primary electrons interact with the sample has a characteristic onion shape as shown in Figure 3.11. Penetration into the sample results in divergence of the e-beam and consequently reduction in spatial resolution.

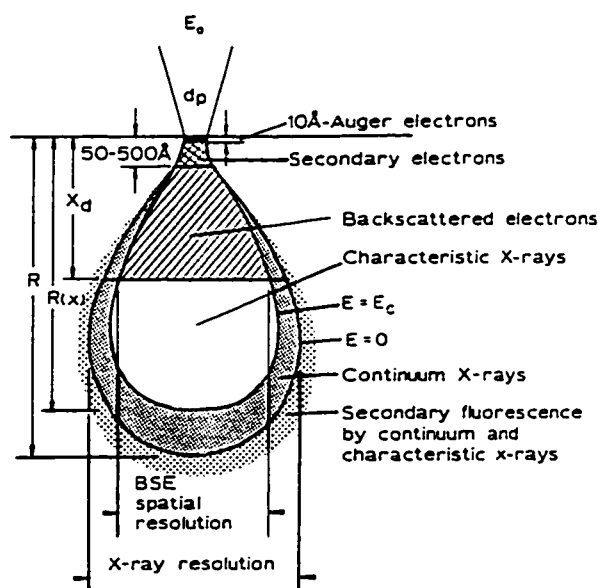


Figure 3.11 Interaction volumes for various electron specimen interactions (Goldstein and Yakowitz, 1975).

The accelerating voltage has an effect on the volume of excitation. Higher accelerating voltage produces a larger volume of excitation with poorer resolution, while lower accelerating voltage produces a smaller volume of excitation and hence better

resolution. At the same time, the element (atomic number) that is being analyzed has an effect on the required accelerating voltage. Higher accelerating voltage is needed in order to excite electrons and produce K-radiation from heavier elements with a higher atomic number. Figure 3.12 below shows these relationships schematically.

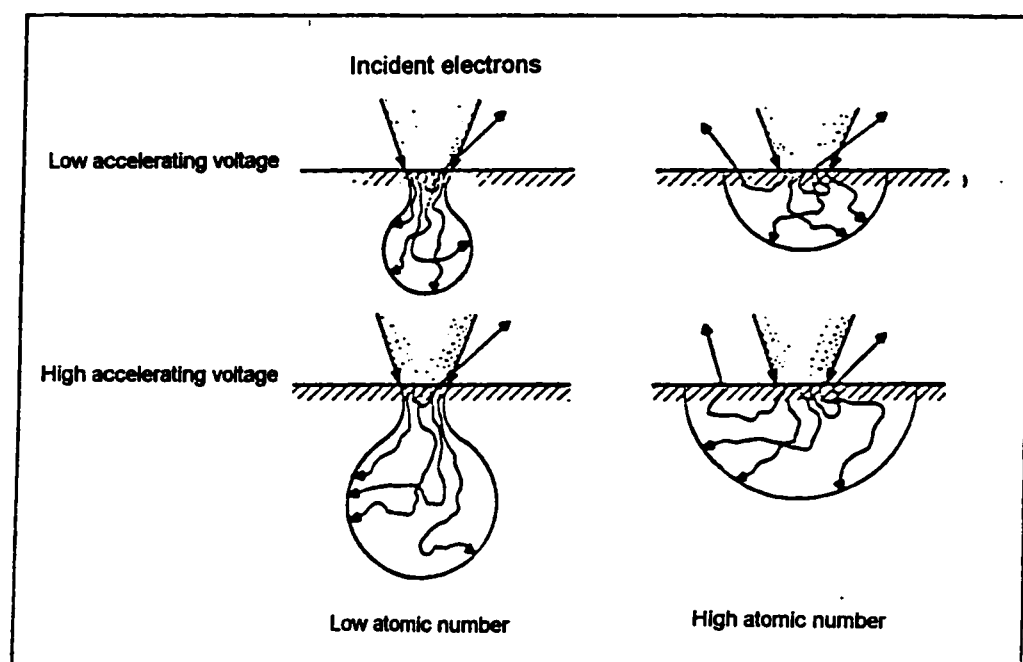


Figure 3.12 Schematic effect of accelerating voltage and specimen composition on the volume of excitation (Robertson, 1990).

The intent is to keep the volume of excitation as small as possible and at the same time to be able to excite radiation from the elements that are being analyzed. From previous research (Scrivener, et al., 1987), it was found that an accelerating voltage of 15 kV gave the best resolution with satisfactory atomic number contrast. The same voltage was used for the microstructural investigation of the present study.

As they are accelerated in the electron column, the primary electrons acquire kinetic energy. This energy is deposited in the sample and its dissipation produces a variety of signals that may be interpreted by the microscopist. These signals are the result of electron-electron or electron-nucleus collisions as they are explained in the following section.

3.6.4 Electron - Specimen Interactions

The signals from the e-beam and specimen interaction are used to reveal information about the topography and local chemistry of the material sample. These signals consist of secondary and backscattered electrons and characteristic X-rays.

Secondary electrons are produced from inelastic collisions between the primary (beam) electrons and the electrons from the sample of material being studied. During an inelastic collision some of the beam energy is transferred to the specimen's electrons. Essentially, the sample absorbs some of the high-energy beam electrons and it acquires a net negative charge. In attempting to return to its ground state the sample releases weakly bound electrons which emerge with energy that is significantly lower than that of the striking beam. Since they have only a few eV's of energy, secondary electrons can escape from the sample only if they are created near the surface. For this reason, secondary electron images (SEI) are sensitive to the topography of the sample and they provide information about it.

Also, since the secondary electrons are created near the surface before the primary beam has a chance to spread, they have very high spatial resolution compared to other signals which escape from deeper into the volume of excitation. Some of the principal uses of SEI are to provide information about:

- Fracture surface analysis,
- Grain size,
- Structural defects (cracking, voids etc.).

A different signal occurs when a primary electron interacts with the nucleus of a sample atom. This collision is elastic and the primary electron may be scattered in any direction with little loss of energy. Some of these electrons are scattered back out of the sample and they are detected. These backscattered electrons have a much higher energy than the secondary electrons and therefore they can escape from a greater depth within the sample. However, the volume of excitation is greater at this depth and for this reason a backscattered electron image (BEI) is not as highly resolved in space as SEI. Backscattered electrons do not provide as much information on sample topography.

The main influence on the strength of a BEI image is the mean atomic number of the element. The higher the atomic number, the greater the positive charge of the element's nucleus and therefore, the probability of a backscattering event is also greater. The BEI image provides some information about the sample composition. This information is qualitative and it is shown as gray colour variation between the different elements in the sample. The heavier elements with high atomic numbers produce a greater number of backscattered electrons and they appear much brighter than those with a low atomic number. This method enables identification of various phases comprising the sample as well as any reactions that have taken place.

Some of the typical applications of BEI imaging are:

- Compositional information,
- Some topographic information,

- Electron channelling to allow measurement of crystallographic properties of materials,
- Analysis of internal magnetic structure of appropriate materials.

In a backscattered electron image, differences in colour (gray level) are associated with the elemental composition of the various phases in the material. On the other hand, in secondary electron images, different levels of gray merely signify changes in topographical elevations and do not contain any compositional information.

Each point in the backscattered electron image may be analyzed using energy or wavelength dispersive spectroscopies (EDS or WDS). As mentioned above, this analysis is based on the characteristic X-radiation from the sample. When an electron is ejected from an inner shell of an atom, as described earlier, the result is an ion in the excited state. In order to return to the normal ground state, the excited ion gives up energy in the form of electromagnetic radiation, X-rays in the case of high energy transitions involving inner shells. This electromagnetic radiation is called characteristic emission or characteristic X-rays since it is a unique indication of the element from where it originated. The analysis produces an X-ray spectrum in which the positions of the peaks indicate the elemental composition of the sample. The ratio of the different elements within each phase of the material corresponds to the relative heights of the peaks.

X-rays come from a greater depth from the sample, where the electron beam has had the chance to spread widely. Their spatial resolution is then poorer compared to that of the secondary and backscattered electrons.

Examples of secondary and backscattered electron images as well as EDS spectrums are presented in Chapter 5.

3.6.5 SEM Specimen Preparation

The SEM is a surface examination tool that displays information by using backscattered and secondary electrons and other emitted signals. Unlike the case of transmission electron microscopy, the thickness of the specimen is not a real concern and its surface area is limited only by the size of the sample holder stage.

Concrete, being an insulating material, poses a special difficulty for SEM examination. When the electron beam strikes an insulator, the absorbed electrons accumulate on the surface since there exists no conducting path to ground. If the specimen is allowed to build up charge, it repels the electron beam which then becomes very unstable. This results in a severe distortion of the image and a great change in the emission of secondary electrons. To avoid charging effects, a conductive coating is applied to the sample surface of insulators. The coating may be a metallic film (gold), or a thin layer of carbon.

The carbon film must be relatively thin, but at the same time it must be thick enough to be conductive. Carbon has a low atomic weight (12.01) and it is therefore a low absorber of characteristic X-rays which are released by the specimen during study. In addition, it does not release a detectable X-ray signal of its own and hence, it does not interfere with the microprobe analysis and the EDS spectra. At the same time it does not increase the secondary electron yield. By comparison, heavy metal coatings, like gold for example, absorb low-energy and low-intensity X-rays. Additionally, they emit characteristic radiation of their own. The result is a misleading analysis of the true composition of the specimen.

For the above reasons, carbon films are used for energy dispersive spectroscopy to reveal information about the chemical composition of the material. Metal coatings that are more conductive than carbon, thus ensuring a steadier electron beam, are used for a

topographical evaluation of the microstructure. Silver paint is then used to ground the coated specimens to the holder stage.

When conducting qualitative chemical analysis using backscattered electrons and the electron probe microanalyzer, it is important to have a highly polished sample. Surface irregularities have an effect on the energy of the X-ray photons that reach the detector from a specific point in the sample material. As outlined in Figure 3.13, signal A will reach the detector unaltered, while signal B will get reabsorbed by the sample thickness above it and will be changed by the time it reaches the detector.

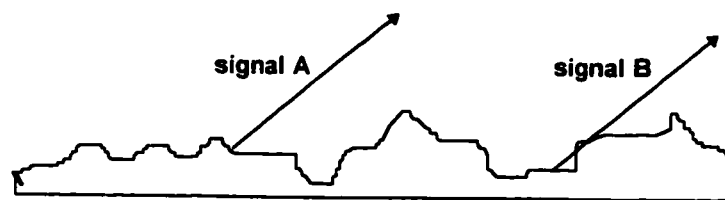


Figure 3.13 The effect of surface irregularities on X-ray photon energy.

The detector is directly above the sample surface and for this reason an uneven surface also affects the number of backscattered electrons that can reach it. Electrons scattered widely due to surface roughness, as shown in diagram B of Figure 3.14, remain undetected. A greater number of backscattered electrons will reach the detector following interaction of the e-beam with a smooth sample surface (diagram A). So, a well polished sample surface ensures backscattered electron images of high quality as well as an accurate X-ray analysis.

For topographic investigation using secondary electron images, it is sufficient to have a gold coated fractured surface of the sample (Gabriel, 1985).

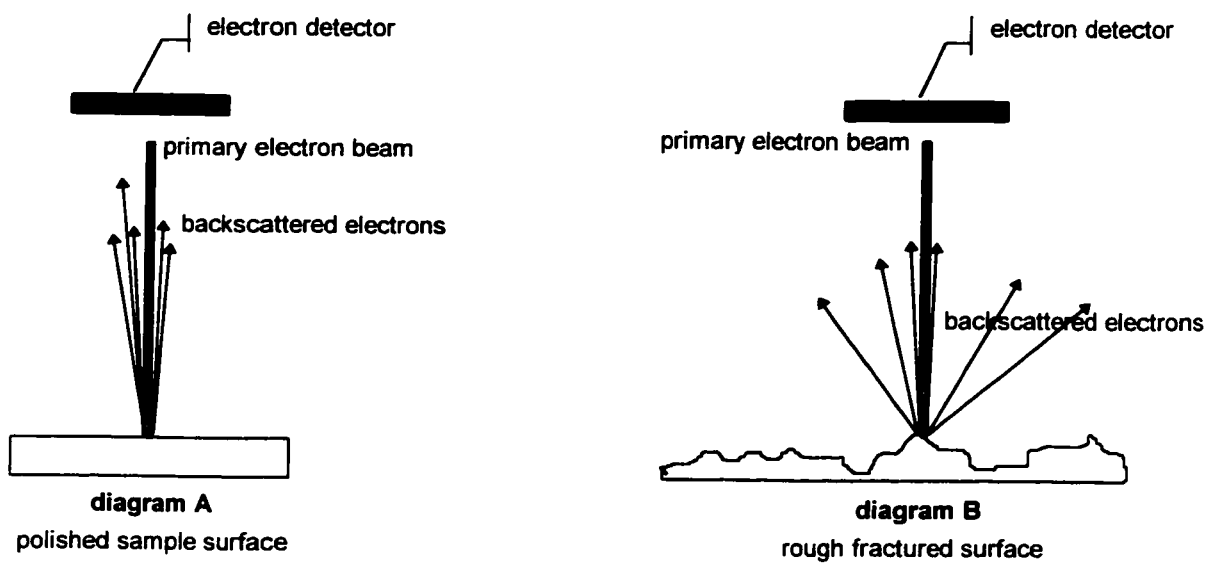


Figure 3.14 The effect of surface irregularities on the number of backscattered electrons that may reach the detector.

CHAPTER 4

Experimental Results

4.1 Introduction

The experimental results of the studies that were described in the previous chapter are presented in the following sections. These results include data on the workability of the fresh concrete and also the compressive strength, modulus of elasticity, creep, shrinkage, frost and sulphate resistance of the hardened concrete. A comparison is made between fly ash and normal portland cement concretes. Workability and compressive strength results are presented for concrete mixtures containing various percentages of fly ash replacement of the cement. Following the discussion of these results, an optimum fly ash/cement ratio is recommended. Afterwards, results on the engineering properties of the selected fly ash mixture are presented and compared to the same properties of concrete containing 100% portland cement.

4.2 Workability of Fresh Concrete Mixtures

It is understood that the workability of concrete is improved in the presence of the spherical fine fly ash particles due to their ball-bearing effect. In addition, workability increases due to the physicochemical effects of the fly ash particles on the rheology of the fresh concrete. The mechanisms by which fly ash reduces the water requirements for

fresh concrete of a given workability have been discussed in a previous chapter. It is then accepted that for a concrete mixture which is designed for a certain degree of workability, partial replacement of the cement with fly ash has favourable effects and there is a need to adjust the water content.

These results have been observed in the concrete mixtures of the present study where fly ash was used as a partial replacement of the cement at levels ranging from 20 - 60% by weight of the total cementitious material in the mixture. As the fly ash content of the mixture increased to 50% and higher there was a need to reduce the water content of the mixture in order that the workability was maintained at the design level. The slump of the concrete was used as an index of its workability and it was measured using the K-Slump apparatus. This is a simple tubular tester which measures the flow and workability of the concrete; details of its relationship to the ordinary cone slump were described by Nasser in an earlier publication (Nasser, 1976). The K-Slump values for the preliminary concrete mixtures are listed in Table 4.1.

The water-to-binder ratio was kept, as much as possible constant among the various mixtures for comparison purposes; it was chosen to be low enough to produce higher compressive strength in the hardened concrete but at the same time maintaining a good workable mixture. This ratio varied with the fly ash content of the mixture, ranging between 0.28-0.33 as it is shown in Table 4.1. Prior to mixing, the coarse and fine aggregates were tested for their moisture content and the necessary adjustments were made to the amount of the mixing water so that the aggregates were brought to the saturated and surface dry moisture condition. The water/binder ratio that is shown in the table represents the effective water that was used for the hydration of the cementitious material only; it includes the aqueous content of the superplasticizer and excludes the amount absorbed by the aggregates.

	BATCH	FLY ASH %	w/(c+f)	K- SLUMP %	COMPRESSIVE STRENGTH MPa						
					1-DAY	3-DAY	7-DAY	14-DAY	28-DAY	56-DAY	91-DAY
POZZOLITH 400-N	7	0	0.30	17	27.4	38.6	45.3	51.2	52.4	58.0	59.0
	4	20	0.30	25	14.9	24.1	30.8	39.7	46.6	53.8	48.1
	5	40	0.30	29	0.5	17.6	23.1	29.0	39.0	42.1	43.4
	6	50	0.28	25	6.8	19.3	27.3	35.0	42.8	54.0	56.3
RHEOBUILD 1000	11	0	0.33	21	27.9	38.4	48.6	54.3	57.4	60.2	61.5
	17	0	0.33	17	33.3	41.8	49.4	55.9	64.2	64.9	66.2
	8	20	0.30	17	24.4	39.2	41.1	52.7	63.4	73.3	76.1
	12	30	0.33	17	15.6	31.2	38.8	44.8	56.1	62.3	64.7
	9	40	0.30	15	10.0	19.0	24.0	29.5	37.2	42.9	44.9
	13	50	0.31	21	9.9	22.4	30.5	40.9	47.0	55.0	58.0
	15	50	0.31	21	10.8	23.2	28.8	38.0	48.9	52.9	62.2
	16	50	0.31	19	11.0	24.0	30.2	41.0	46.7	54.6	55.9
	10	60	0.30	28	2.0	8.0	14.2	15.2	18.2	20.7	26.2

Note: The air content of the above concrete mixtures ranged between 1.0 - 1.5 %. No air-entraining agent was used.
The value of the K-slump in % corresponds to centimeters as follows: 25% = 3 cm

50% = 6 cm

In addition, the value of the K-slump in centimeters corresponds approximately to the same value of the cone slump test in inches.

The density of the fresh concrete was as follows: 50% fly ash concrete: 2460 kg/m³ (153 lb/ft³)
control concrete: 2530 kg/m³ (158 lb/ft³)

Table 4.1 Properties of fresh and hardened concrete.

In order to avoid any misleading results due to the effects of possible systematic errors, the concrete mixtures were not prepared in any particular order; rather they were randomly selected for the fly ash content. Additionally, the preliminary concrete mixtures, containing varying levels of fly ash replacement, were prepared within a three month period, thus minimizing variability between batches due to cement, fly ash and aggregate sources.

4.3 Compressive Strength Test Results

The effect of the level of cement replacement with fly ash on the development of the compressive strength of the hardened concrete was investigated and compared with the control mixture. The results were based on the testing of 75x150 mm (3x6 in) cylindrical test specimens. The influence of the size of test specimens on the measured compressive strength has long been the subject of study in concrete technology. It has been shown that under standard curing conditions, 75-mm cylinders can be used as a replacement for 150-mm cylinders for confident evaluation of the compressive strength when the aggregate does not exceed a maximum size of 25 mm (1 in) (Nasser and Al-Manasser, 1987, Nasser and Kenyon, 1984). Day and Haque (1993) have extended the study of the influence of cylinder size to include fly ash concrete exposed to a variety of curing and testing conditions. For strengths up to 50 MPa (7250 psi), they reported statistical equivalence in the results between 75-mm and 150-mm cylinders. They also found no significant influence from the mold-type, whether they used tin, steel or cardboard.

Following these suggestions, it was deemed appropriate to use 75x150 mm test specimens, prepared in waxed cardboard molds. For equivalent comparisons the same test specimen size was used for all concrete mixtures for evaluation of the compressive

strength. The advantages of using the smaller 75x150 mm specimens in this study were: (a) lower required capacity of the testing machine, (b) smaller required storage space for curing, (c) economic advantages of reduced costs for molds and concrete, and, (d) ease in handling.

The compressive strength development of the hardened concrete was studied at ages of 5 hours following accelerated curing and also after 1, 3, 7, 14, 28, 56 and 91 days of standard curing. Details of the test results for this series of mixtures are summarized in Table 4.1. Comparison of the strength development of the same mixtures is shown in Figures 4.1 and 4.3 for the two types of superplasticizer. In Figure 4.1, the compressive strength values for the control and 50% fly ash mixtures represent the averages of two and three replicate mixtures respectively.

Initially, up to 14 days, the concrete which was prepared with 100% portland cement developed higher strength than all of the mixtures containing fly ash as partial cement replacement.

The 20% fly ash concrete mixtures containing Rheobuild 1000 developed a compressive strength equal to that of the control mixture at the age of 14 days. The strength of concrete aged beyond this point continued to increase in strength at a faster rate compared to that of the control mixture. At 91-days, the compressive strength of the concrete with 20% fly ash was 25% higher than that of the control mixture. The compressive strength of the 30% and 50% fly ash concrete mixtures followed a similar pattern and their 91-day strength was similar to that of the control mixture. The mixture with 60% fly ash replacement had, by comparison, a lower rate of compressive strength increase. At 91 days, its strength was below that of the control mixture at 1-day. In addition, the 60% fly ash mixture had a delayed setting time exceeding 24 hours; the performance of the 60% fly ash mixture makes it unsuitable for any practical applications

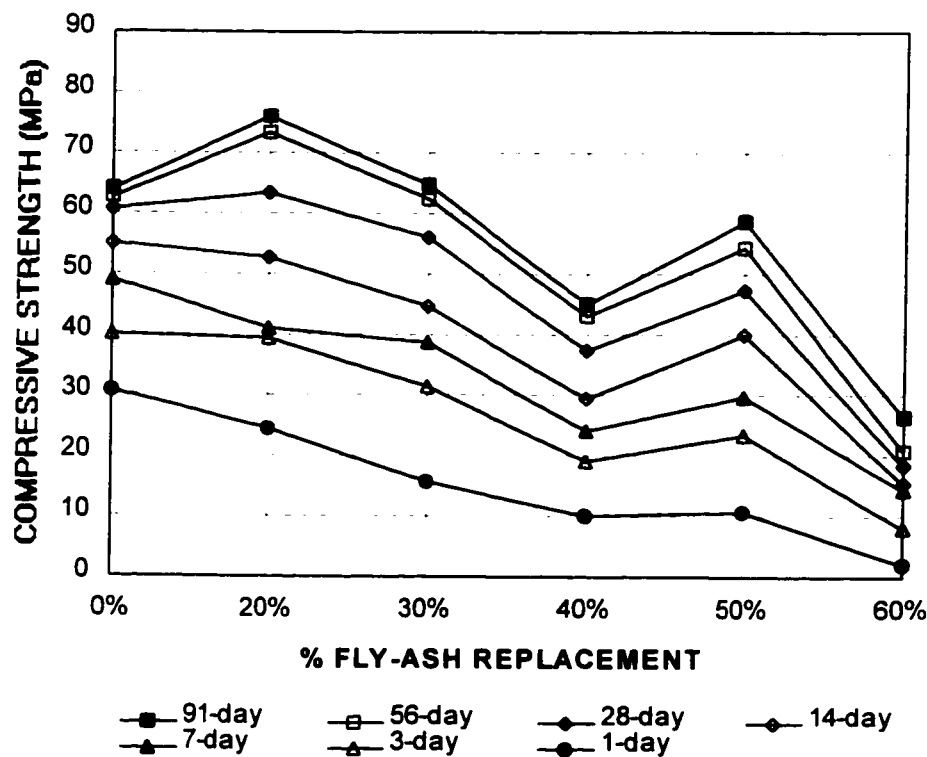


Figure 4.1 Compressive strength development of concrete made with Rheobuild 1000 superplasticizer for various contents of Class C fly ash.

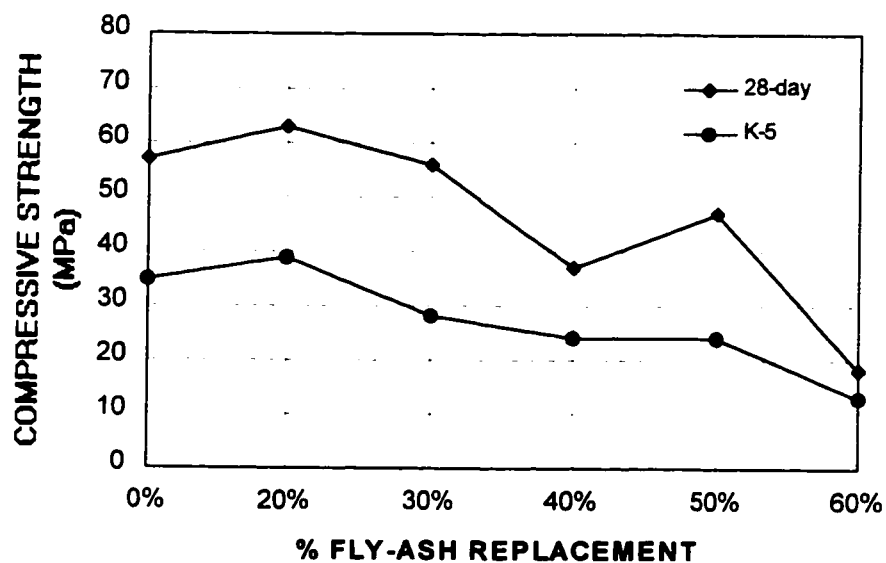


Figure 4.2 K-5 accelerated strength development test results for concrete made with Rheobuild 1000 superplasticizer, for various contents of Class C fly ash.

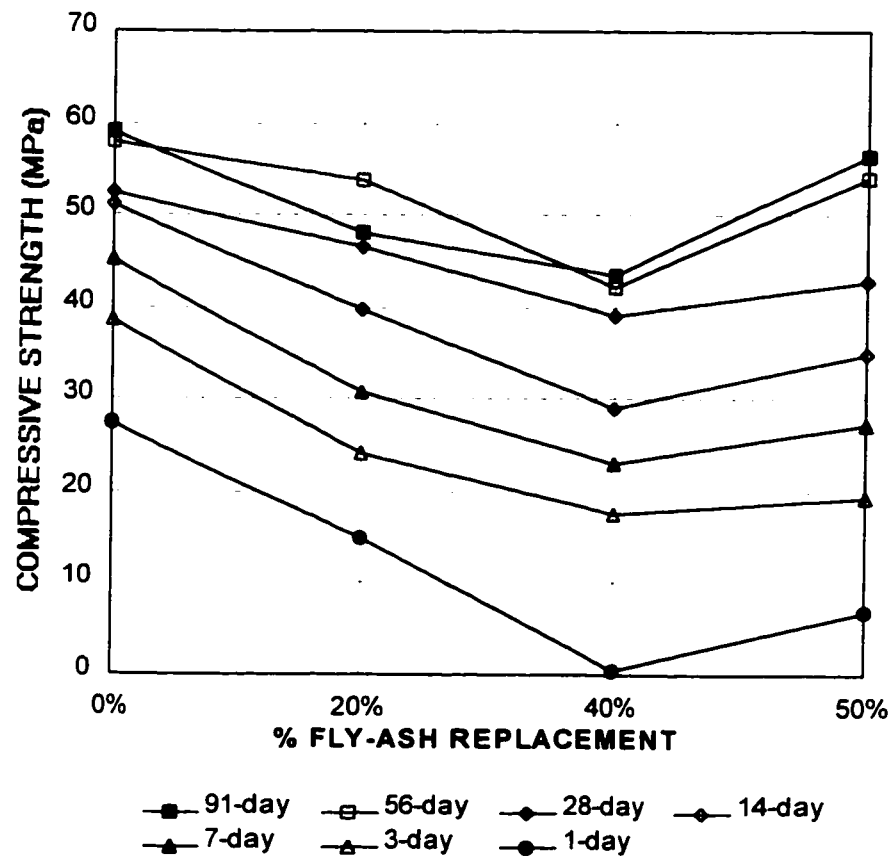


Figure 4.3 Compressive strength development of concrete made with Pozzolith 400N superplasticizer for various contents of Class C fly ash.

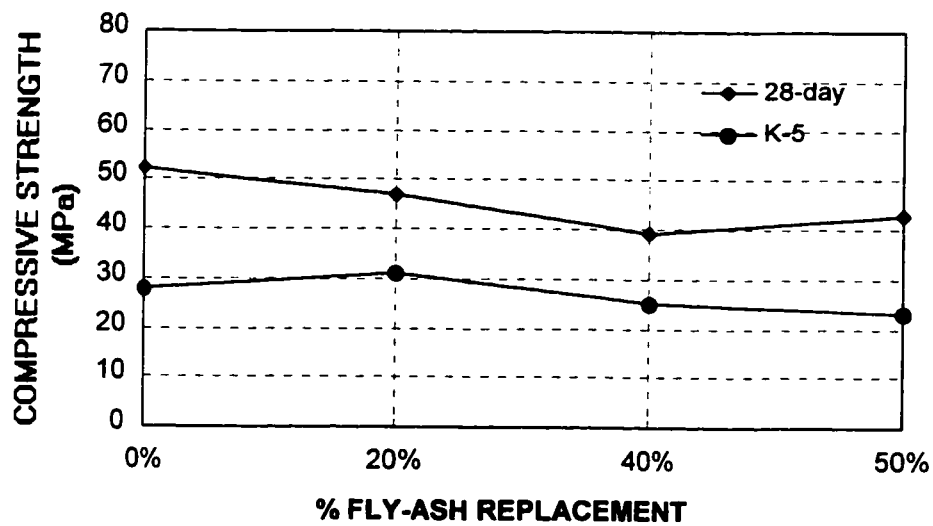


Figure 4.4 K-5 accelerated strength development test results for concrete made with Pozzolith 400N superplasticizer, for various contents of Class C fly ash.

with the chemical admixtures used in this study. The mixtures made with 40% fly ash also had a delayed setting time when Pozzolith 400N was used. The compressive strength of the 40% fly ash mixtures did not follow the pattern of the 30% and 50% fly ash concretes; its strength was inferior at all ages with either one of the superplasticizers.

The results of the K-5 accelerated strength test are compared to the 28-day compressive strength for the various mixtures in Figures 4.2 and 4.4 for the two types of superplasticizer. Good prediction of the compressive strength of concrete is possible with the K-5 accelerated strength test. On the average, the strength of concrete using the K-5 test is between 50 - 60 % of its compressive strength at 28 days.

A cost analysis indicates that concrete with 50% fly ash replacement results in about 10% cost reduction. Based on compressive strength results from Table 4.1, the cost of the concrete for each of the fly ash mixtures relative to that of the control mixture was estimated and is shown in Figure 4.5. This figure was generated based on the assumption that concretes with $\pm 10\%$ difference in compressive strength may be considered of the same population and their relative cost varied in proportion to the fly ash content. To achieve higher strength, other chemical and/or mineral admixtures are needed and this will make the cost higher. This initial investigation indicates that concrete containing 50% fly ash is a likely choice for economical high performance concrete utilizing large volumes of fly ash replacement of the cement.

A comparison of the strength development of the control concrete and the mixture containing 50% fly ash, is shown in Figure 4.6. To indicate strength variability within each of the concrete mixtures, Figure 4.6 represents a plot of each test specimen separately. It can be seen that concrete with 50% fly ash replacement has a 28-day strength which is approximately 80% of the strength of the control mixture at the same age, while at 56 and 91 days, the strength is over 85% and 90% respectively. Statistical

analysis of variance points out significant differences between the strength of the two concretes up to 28 days; the difference becomes less significant at 28 and 56 days and later the two strengths are statistically of the same population. This analysis was done by writing a program in Statistical Analysis System (SAS) on the VAX/VMS mainframe computer. The program and the results are included in Appendix B.

Table 4.1 indicates that the average compressive strength of the 50% fly ash concrete at 28 days is 47.5 MPa (6890 psi), while at 91 days the strength of this concrete is 58.7 MPa (8510 psi). Sivasundaram et al. (1991), reported lower strength levels for concrete mixtures with comparable proportions as the mixtures of this study but utilizing 58% Class F fly ash replacement. They reported an average 28-day compressive strength of 31.2 MPa (4520 psi) between seven different sources of low calcium fly ash while the average strength at 91 days was 42.3 MPa (6130 psi).

Based on cost considerations and compressive strength, concrete containing equal weights of cement and fly ash is the most economical mixture. Assessment of other mechanical properties such as elasticity, shrinkage, creep, durability and sulphate resistance is needed before a final recommendation is made regarding the commercial application of concrete containing 50% Class C fly ash. These properties were evaluated in the subsequent phases of the present study and the results are presented in the following sections.

The effect of sustained high temperature and pressure on the compressive strength of fly ash concrete was also studied. For this purpose the 75x225 mm (3x9 in) cylinders were tested in compression following the completion of the high temperature creep tests.

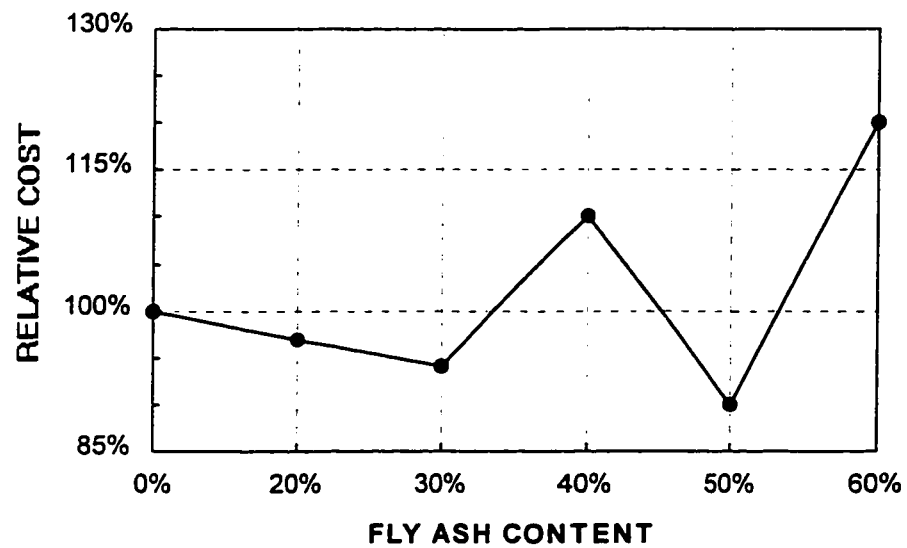


Figure 4.5 Relative cost of concrete based on compressive strength and fly ash content.

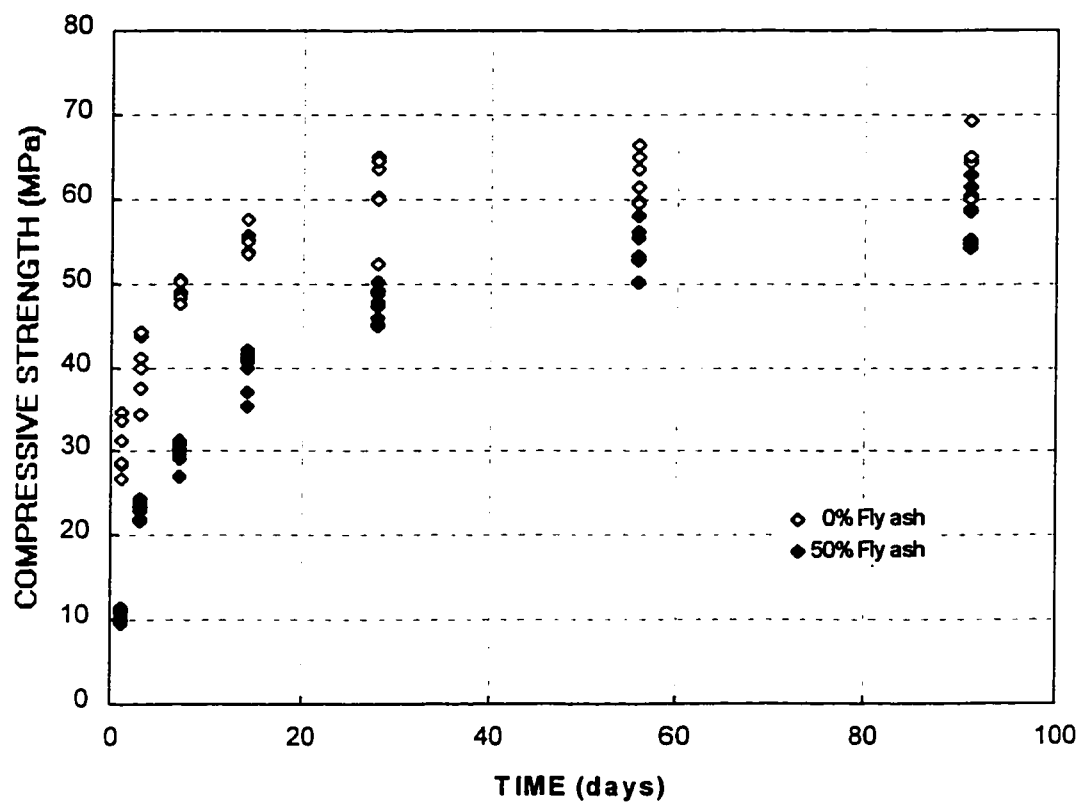


Figure 4.6 Compressive strength development of control mixture and concrete containing 50% fly ash using Rheobuild 1000 superplasticizer.

Their strength is shown in Figure 4.7 as a percentage of the 28-day compressive strength of the same fly ash concrete cured under standard conditions of temperature and humidity. The graph indicates that, on the average, the compressive strength of concrete containing equal weights of cement and fly ash was about 10% higher due to sustained pressures and high temperatures. A similar study (Ghosh, 1994) was completed using concrete containing 10% silica fume in addition to low and high contents of Class C fly ash. The study showed that for a 20% fly ash content, the rise in temperature caused a gradual loss in the compressive strength of the concrete. However, as the amount of fly ash replacement increased to 60%, a much less pronounced decrease in the compressive strength was observed for all levels of sustained pressure.

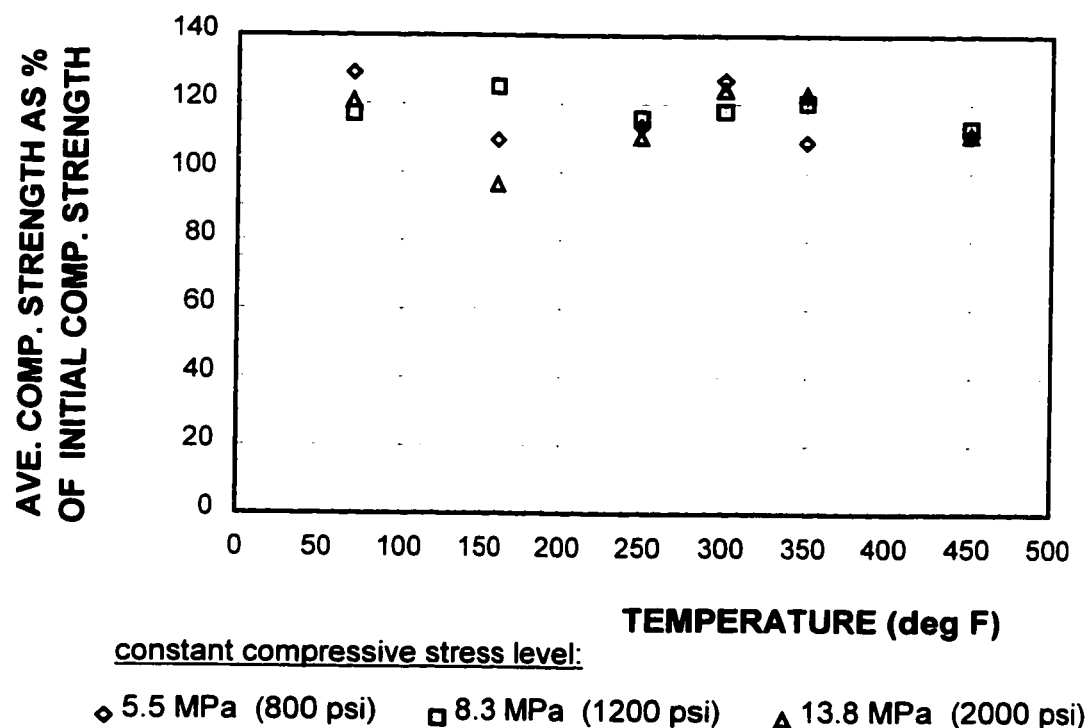


Figure 4.7 Compressive strength of 50% fly ash concrete, following completion of creep tests (sealed test specimens), as a percentage of the strength at the initial application of external stress.

4.4 Modulus of Elasticity Test Results

For the static modulus of elasticity (E), tests were performed on 75x150 mm cylindrical specimens. These tests consisted of simultaneous recording of the stress and strain of the concrete specimen at a constant rate of load application as recommended by ASTM C-469 standard. Afterwards, a stress-strain curve was plotted and the secant modulus of elasticity was computed according to ASTM C-469, using stress and strain values representing 50 per cent of the ultimate compressive strength.

In the present program, using data from the stress-strain curve to compute the modulus of elasticity (E), provides the actual experimental value for higher strength concrete containing a large volume of fly ash replacement. This procedure is long and time consuming compared to the quick and easy method for determining the compressive strength of the concrete. For this reason simple expressions have been formulated and they are used to relate the modulus of elasticity of concrete to its compressive strength. However, in a study on the prediction of modulus of elasticity in high strength concrete, Baalbaki et al. (1992) concluded that the use of equations recommended by some codes provides unreliable results. In a comparison of measured values of modulus of elasticity and computed values using code equations, Ghosh (1994), found that for high strength concrete containing no mineral admixtures, the American (ACI 318) code formulation provided a close estimate. However, for concretes containing fly ash and/or silica fume, the same study (Ghosh, 1994) reported overestimated values for the modulus of elasticity when using the ACI formulation. Hence, as proposed by Baalbaki et al. (1992), until a better relationship linking HSC modulus of elasticity to its compressive strength and other factors has been developed, the best and most reliable way to obtain HSC modulus of elasticity is by direct experimental measurement.

The measured static modulus of elasticity was related to the ultimate compressive strength of concrete, at ages ranging between 1 and 91 days. These measurements were performed for concrete containing 50% fly ash and for the control mixture, using 75x150 mm (3x6 in) cylindrical specimens cured under standard conditions of temperature and humidity. A comparison of the moduli of elasticity for plain and fly ash concretes, is shown in Figure 4.8. The static elastic modulus of both concretes increased in the same direction as their compressive strength. The plot in Figure 4.8 indicates that the modulus of elasticity values of concrete containing 50% fly ash are comparable to those of the control mixture and that no significant difference exists between the two concretes.

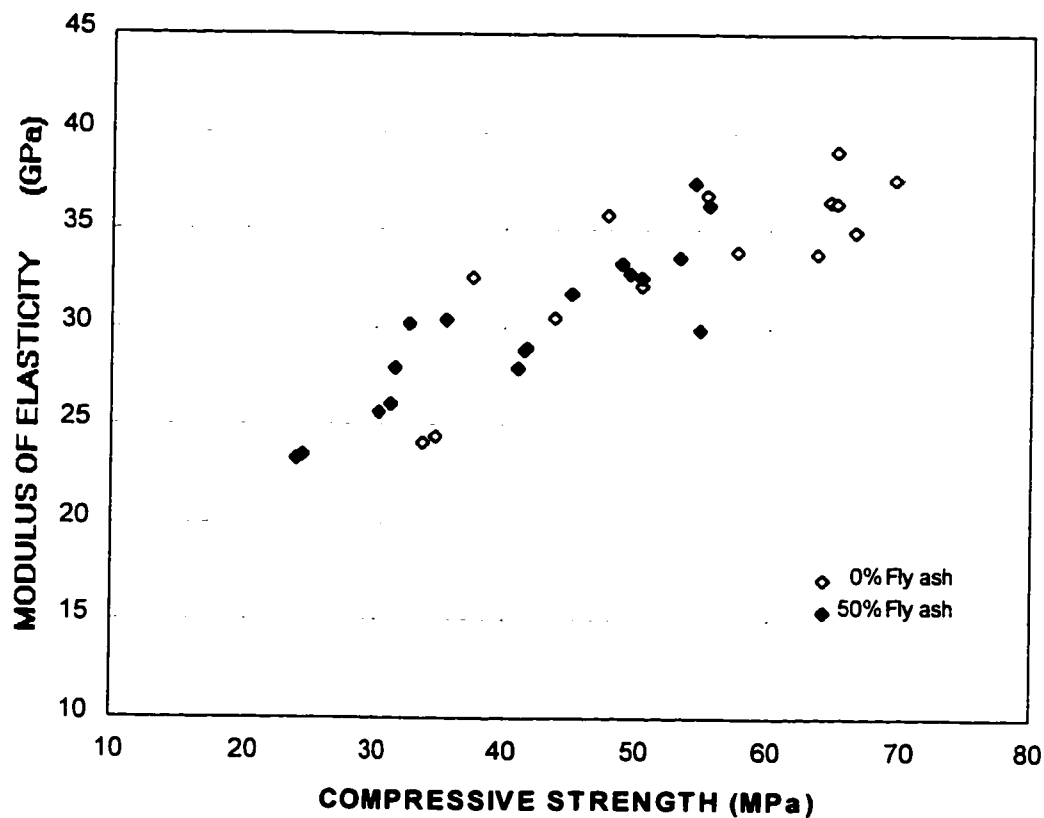


Figure 4.8 Comparison of modulus of elasticity for plain and fly ash concretes.

4.5 Long-Term Deformation Test Results

Creep and shrinkage are interrelated material properties that affect the long-term performance of a designed structure. The numerical values for creep and shrinkage strains are similar and their magnitudes are such that they are structurally significant.

The conditions of testing the long-term deformation of the fly ash and the control concretes as well as the experimental set-ups for these measurements have been described in the previous chapter. In this chapter, the results of the two different experiments studying moisture and high temperature effects are presented separately.

Shrinkage is directly related to loss of moisture to the surroundings whereas creep is not. In addition, creep does not occur independent of shrinkage, especially when concrete is exposed to drying conditions. For these reasons, it makes sense to discuss the shrinkage results first.

4.5.1 Moisture Influence on Shrinkage Characteristics

Shrinkage is the deformation of concrete during drying in the absence of an external load. The effect of a 50% replacement of cement with fly ash on the shrinkage strains of the hardened concrete was studied under high and low moisture levels. The results were compared to the shrinkage strains of the control concrete containing 100% portland cement and subjected to the same experimental conditions. Sealed specimens were used for shrinkage measurements under high moisture conditions, encountered in mass concrete, while unsealed ones were used to study the effect of drying. Both types of test specimens were tested at room temperature of 21° C (70° F). A very small shrinkage occurred in the sealed test specimens and it was considered to be negligible for both concretes. This is referred to, by Xi and Jennings (1992), as autogenous shrinkage and it

is a small deformation that occurs during the hydration of cement in sealed specimens. The drying shrinkage results from the unsealed specimens alone are presented and analyzed in this section.

A comparison between the fly ash and the control concretes, for the shrinkage strain data at different times, is illustrated in Figure 4.9. The strain at every age is the average of three measurements, one from a specimen of each of the three batches of the respective concrete mixture. The shrinkage strain of each specimen is the average of three deformation values. From this comparison of the unsealed test specimens the beneficial effects of the pozzolanic admixture become evident. At the age of 400 days, the fly ash concrete shrunk about 30% less than the control mixture containing 100% portland cement. Drying shrinkage is strongly related to the quantity of water present and the motion of water (Xi and Jennings, 1992). Water becomes chemically bound as a result of the pozzolanic reaction of the fly ash and, hence, there is less evaporable moisture in the matrix of the fly ash concrete to cause drying shrinkage.

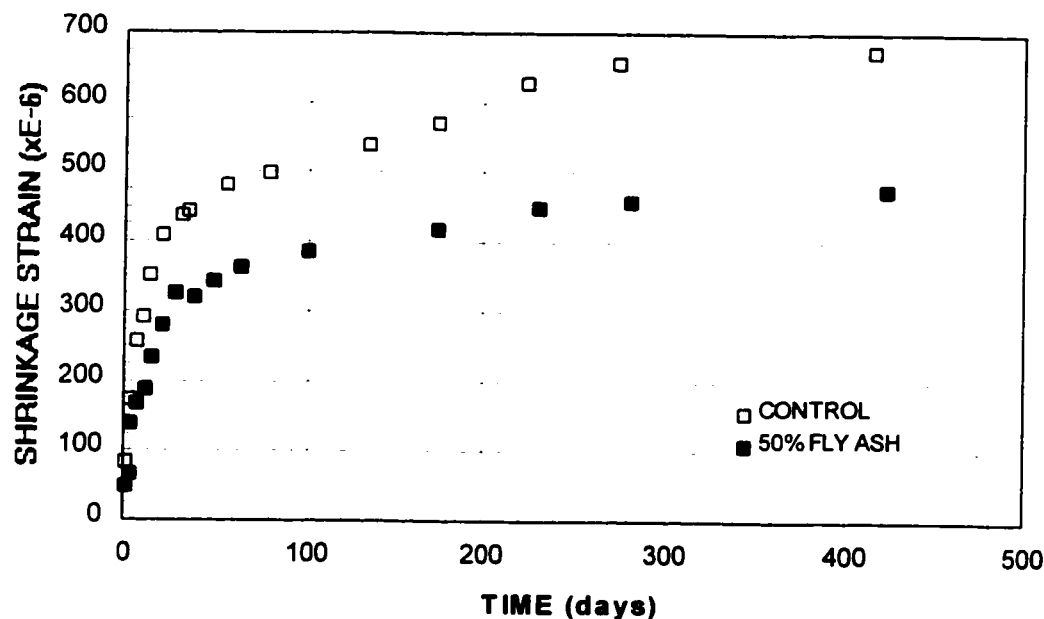


Figure 4.9 Shrinkage data for unsealed specimens of fly ash and control concretes.

4.5.2 Moisture Influence on Creep Characteristics

Creep is defined as the long-term deformation of the concrete test specimen under a constant external load. In the case where the external load is acting in the absence of drying, the deformation is called *basic creep*, whereas, in the case of simultaneous loading and drying it is called *drying creep*. The effect of a large volume of fly ash replacement on creep strains of the hardened concrete was investigated under three levels of constant compressive stress and two levels of moisture.

a. Basic Creep

In the present study, mass conditions were achieved by the use of sealed specimens and the test results represent basic creep. Basic creep was calculated as follows:

$$\epsilon_{cb} = \epsilon_t - \epsilon_i$$

where:

ϵ_{cb} = basic creep strain

ϵ_t = total time-dependent deformation (strain)

ϵ_i = initial elastic strain at time of load application t_0

Figure 4.10 represents a comparison of the basic creep strains at different times under an applied constant stress of 13.8 MPa (2000 psi) for sealed specimens. The graph illustrates that the high volume fly ash concrete produced lower creep strains compared to those of the control mixture. The same trend was evident in all of the constant compressive stress levels that were used in the study. This is indicated in Figures 4.11 and 4.12 which compare basic creep data for the fly ash and control concretes under sustained constant compressive stress levels of 8.3 MPa (1200 psi) and 5.5 MPa (800 psi)

respectively. The dependence of creep of concrete on the applied stress is evident from the above data and it is summarized in Figure 4.13 for the fly ash concrete. It is evident from Figure 4.12 that some discrepancies occurred in the readings between the ages of 21 and 49 days; but these can be ignored and the general trend remains the same.

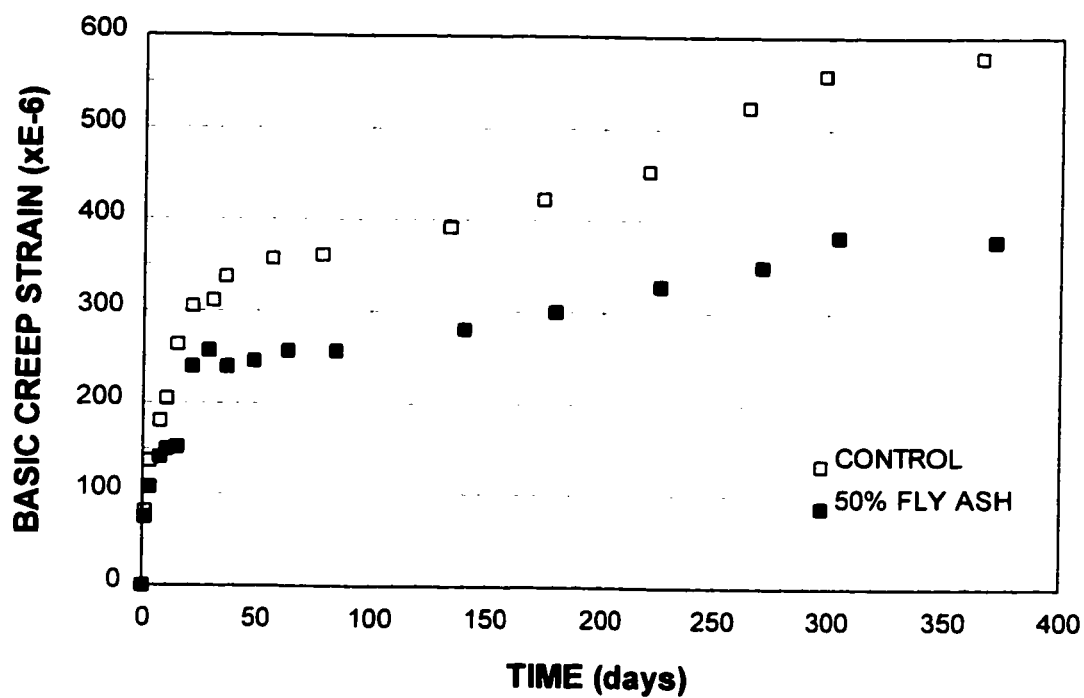


Figure 4.10 Basic creep data for sealed specimens of control and fly ash concrete under applied stress of 13.8 MPa (2000 psi).

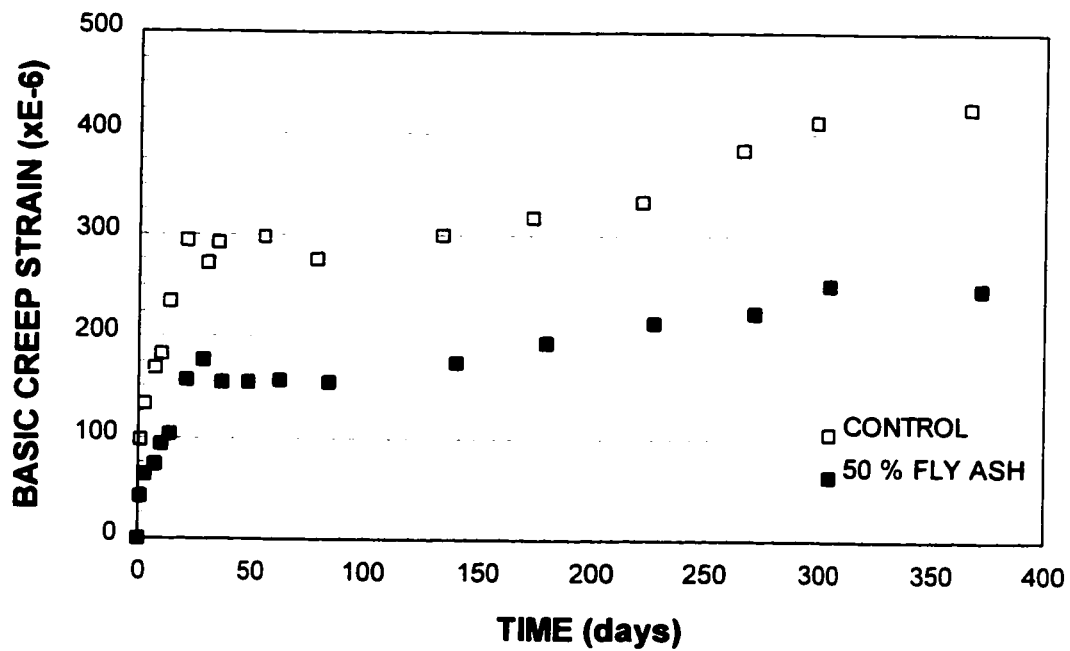


Figure 4.11 Basic creep data for sealed specimens of control and fly ash concrete under applied stress of 8.3 MPa (1200 psi).

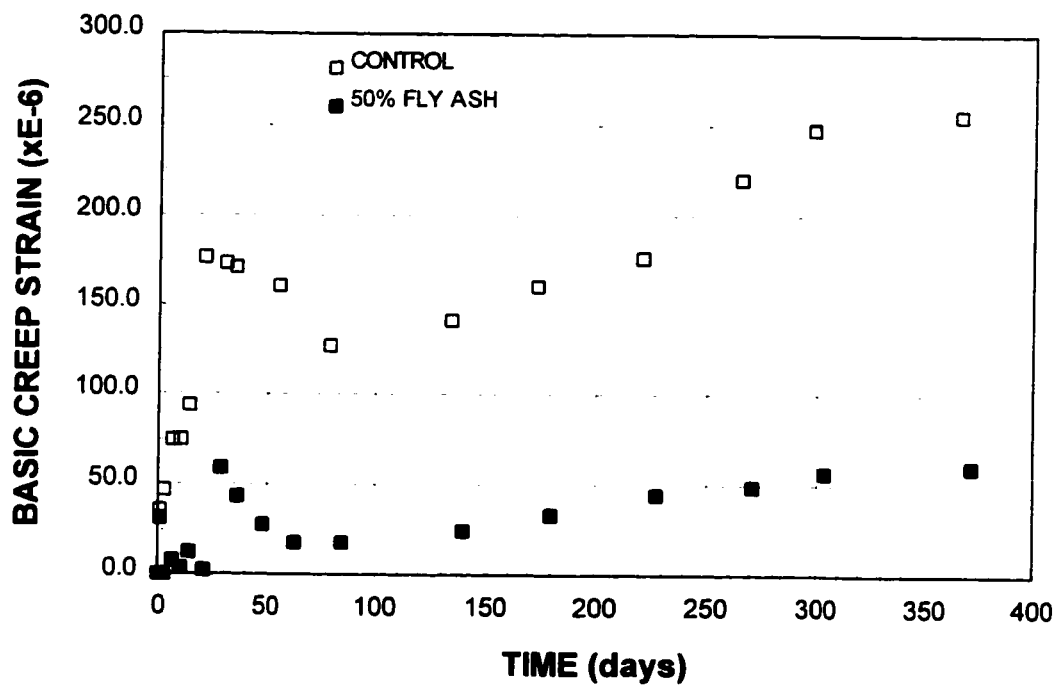


Figure 4.12 Basic creep data for sealed specimens of control and fly ash concrete under applied stress of 5.5 MPa (800 psi).

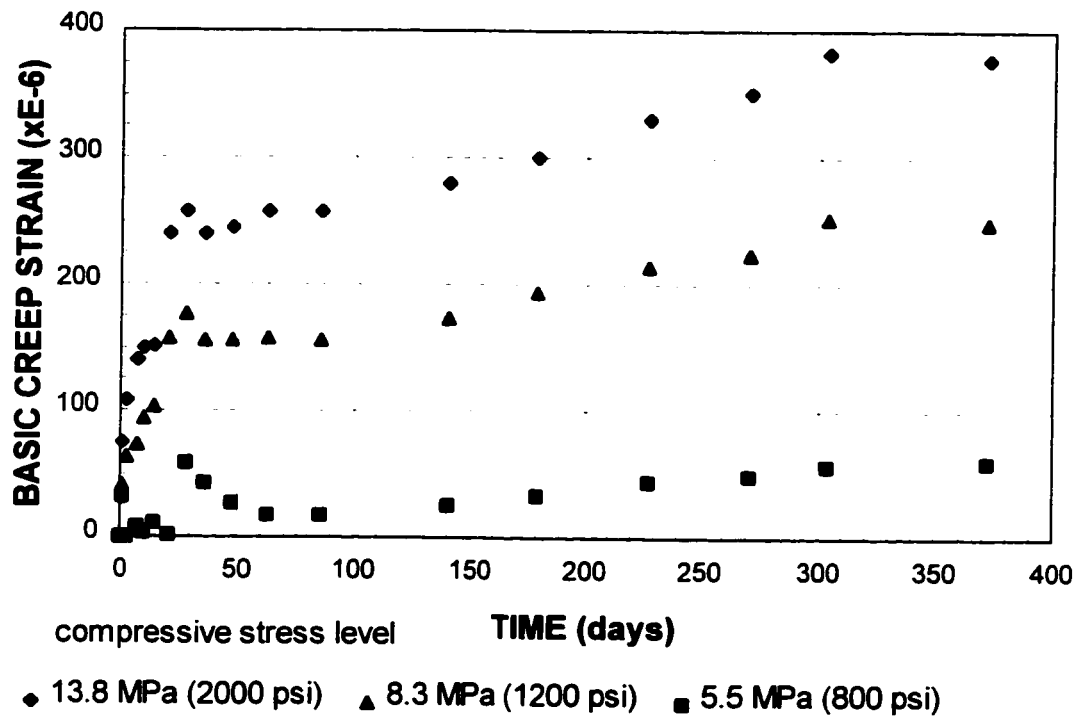


Figure 4.13 Basic creep data for 50% fly ash concrete indicating dependence on the intensity of the stress level.

b. Drying Creep

The drying creep of the fly ash and control concretes was tested by using unsealed specimens, undergoing simultaneous creep and shrinkage, a condition encountered in many actual concrete structures. Drying creep was calculated as follows:

$$\epsilon_{cd} = \epsilon_t - \epsilon_i - \epsilon_s$$

where:

ϵ_{cd} = drying creep strain

ϵ_t = total time-dependent deformation (strain)

ϵ_i = initial elastic strain at time of load application t_0

ϵ_s = shrinkage strain of an unloaded companion specimen since time t_0

As with the shrinkage and basic creep strains that were discussed above, similar trends were observed when the drying creep of the fly ash concrete was compared to the same property of the control mixture. Figure 4.14 represents a comparison of the drying creep data between the fly ash and control concretes for an externally applied compressive stress intensity level of 13.8 MPa (2000 psi). The same comparison is made between the two concretes for stress levels of 8.3 MPa (1200 psi) and 5.5 MPa (800 psi) in Figures 4.15 and 4.16 respectively. Figure 4.17 indicates the proportionality between the drying creep of the fly ash concrete and the intensity of the applied stress level. From these graphs it is evident that the high volume fly ash concrete yielded lower drying creep strains compared to the control mixture. From Figure 4.14 it may seem that at a higher applied stress (13.8 MPa), the fly ash and control concretes yielded similar creep strains. However, the two concretes were tested under the same level of applied compressive stress but their strengths at the time of the external stress application were not equal; at 28 days, the fly ash mixture had a lower compressive strength than the control concrete. For this reason the creep data are analyzed with respect to the stress-strength ratio. Figure 4.18 illustrates a comparison between the fly ash and the control concretes, using the total drying creep strains of the unsealed specimens for the different stress-strength ratios used in this study. It is verified from this graph that concrete containing 50% fly ash cement replacement has lower creep strains than the control mixture for all of the stress-strength ratios that were considered.

Under the combined effect of sustained load and simultaneous drying, a concrete specimen produces a drying creep that exceeds the sum of the individual effects of drying shrinkage and basic creep. This intriguing phenomenon exhibited by concrete was documented in 1942 (Pickett, 1942) and it is appropriately named the Pickett effect. The excess deformation that is produced by simultaneous drying is observed in concrete containing 50% fly ash replacement of the cement and it is illustrated in Figure 4.19.

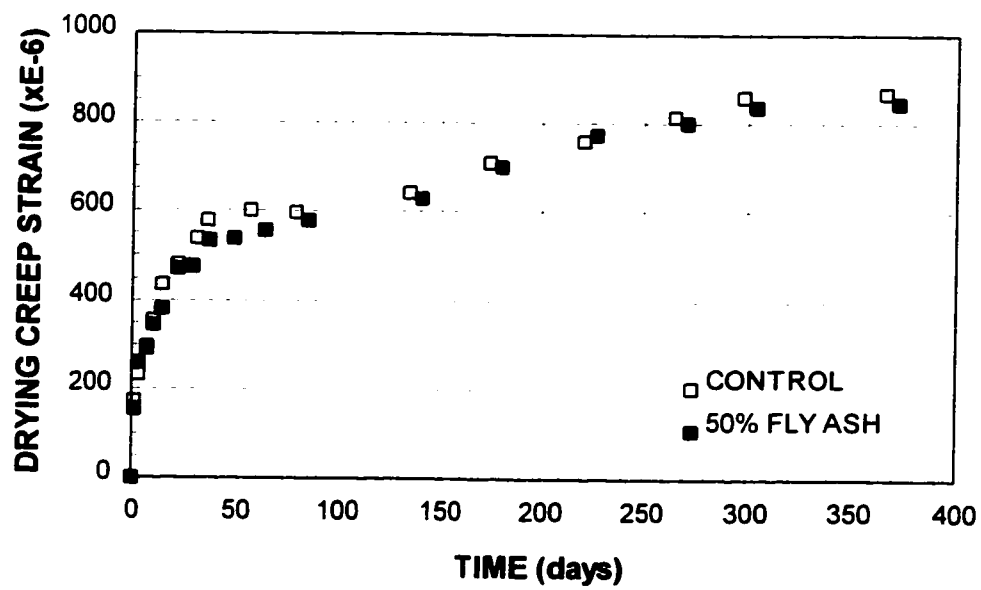


Figure 4.14 Drying creep data for unsealed specimens of control and fly ash concrete under applied stress of 13.8 MPa (2000 psi).

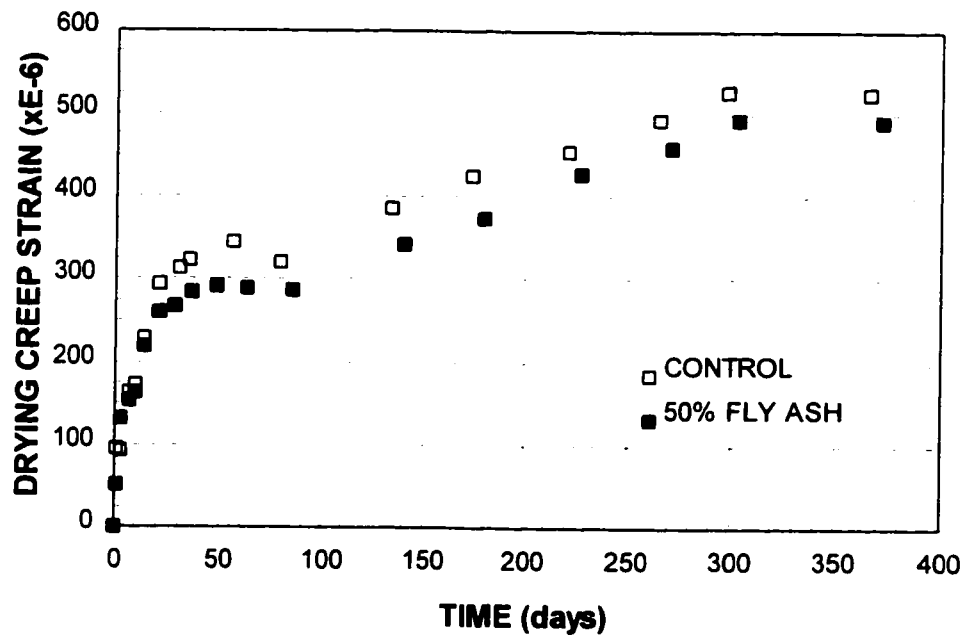


Figure 4.15 Drying creep data for unsealed specimens of control and fly ash concrete under applied stress of 8.3 MPa (1200 psi).

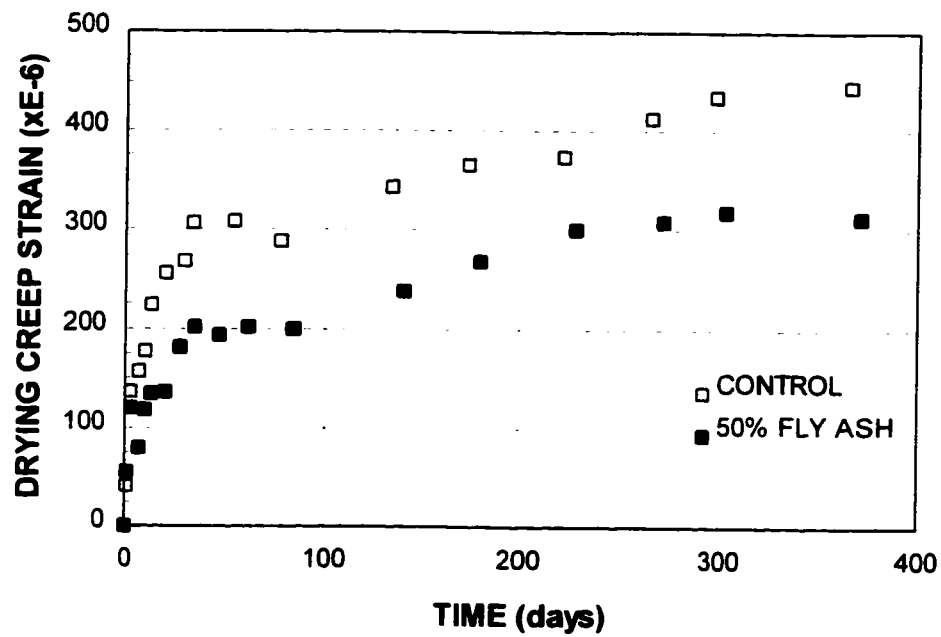


Figure 4.16 Drying creep data for unsealed specimens of control and fly ash concrete under applied stress of 5.5 MPa (800 psi).

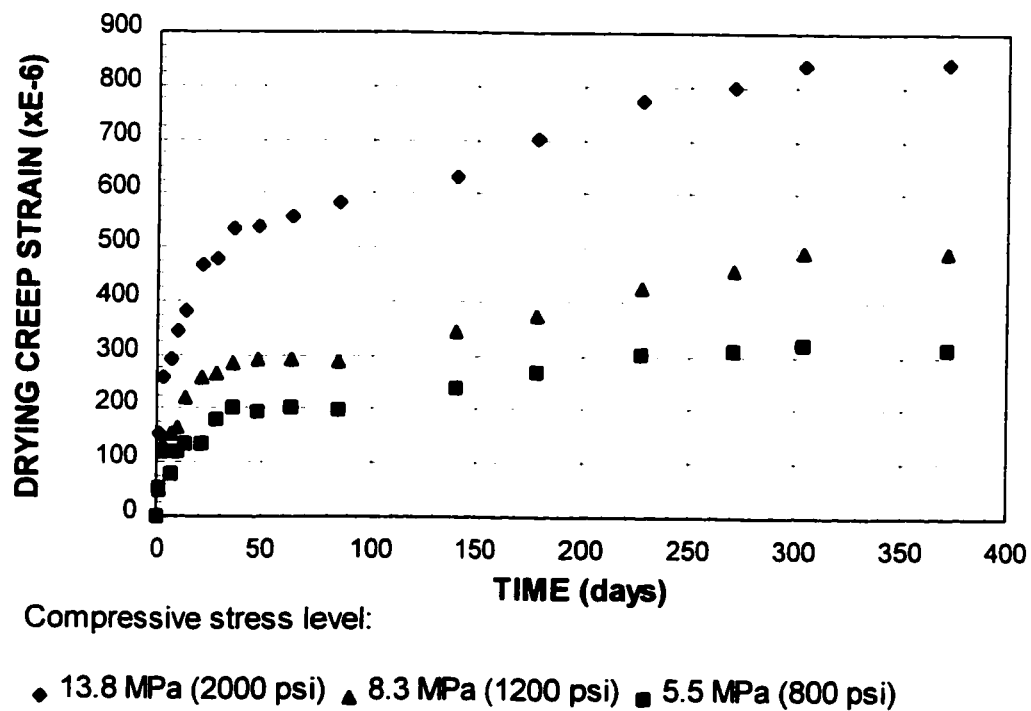


Figure 4.17 Drying creep data for 50% fly ash concrete indicating proportionality to the intensity of the stress level.

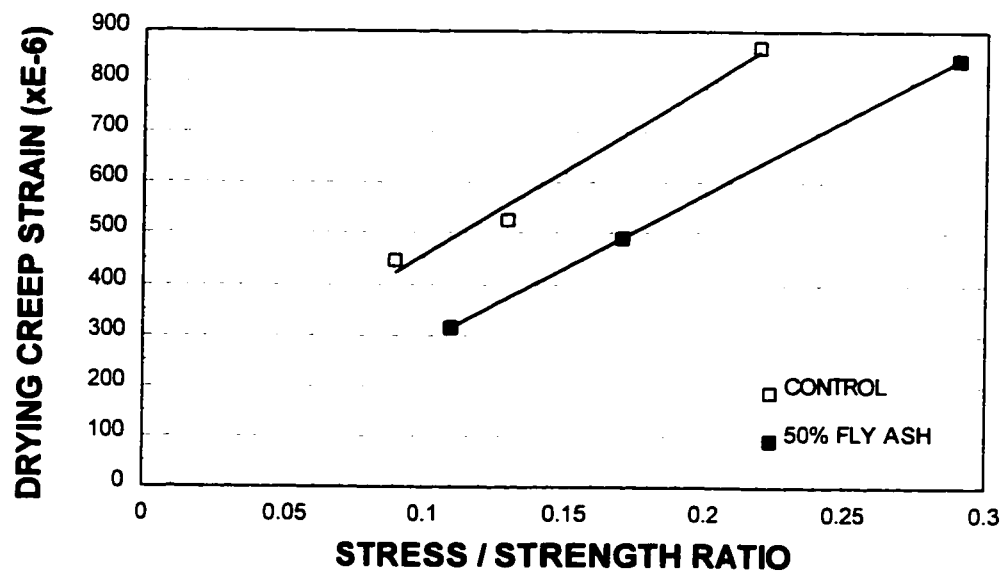
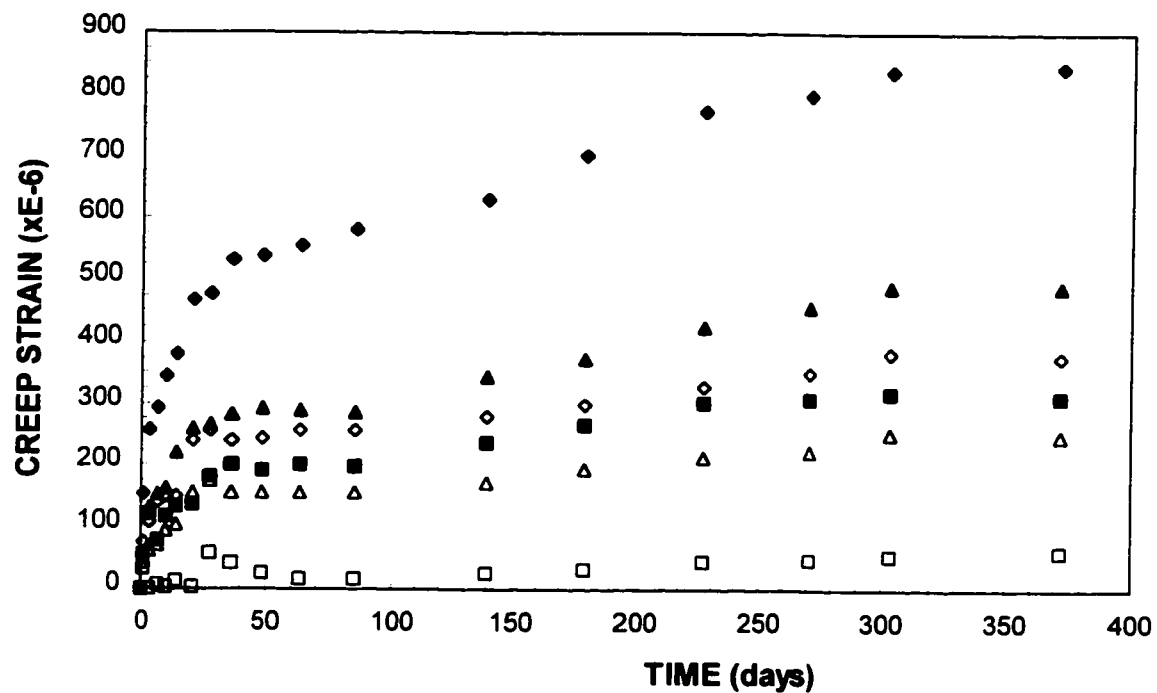


Figure 4.18 Comparison of total drying creep strains for control and fly ash concrete with respect to the stress-strength ratio.



Compressive stress level:

- ◆ 13.8 MPa (drying creep) ▲ 8.3 MPa (drying creep) ■ 5.5 MPa (drying creep)
- ◇ 13.8 MPa (basic creep) △ 8.3 MPa (basic creep) □ 5.5 MPa (basic creep)

Figure 4.19 Comparison between basic and drying creep for 50% fly ash concrete for all stress intensity levels used in the study (the Pickett effect).

4.5.3 Moisture Influence on Creep Recovery

Following observation of the creep behaviour of the control and fly ash concretes under sealed and unsealed conditions, the sustained load was released and the creep recovery period was studied for 47 days. The unloaded specimens instantaneously recovered the elastic strain and at subsequent time intervals very little creep recovery was noted. The typical creep recovery behaviour of the fly ash concrete under sealed and unsealed conditions for the stress levels of the present study is shown in Figure 4.20. The dependence of the creep recovery on the level of applied stress is evident from this figure.

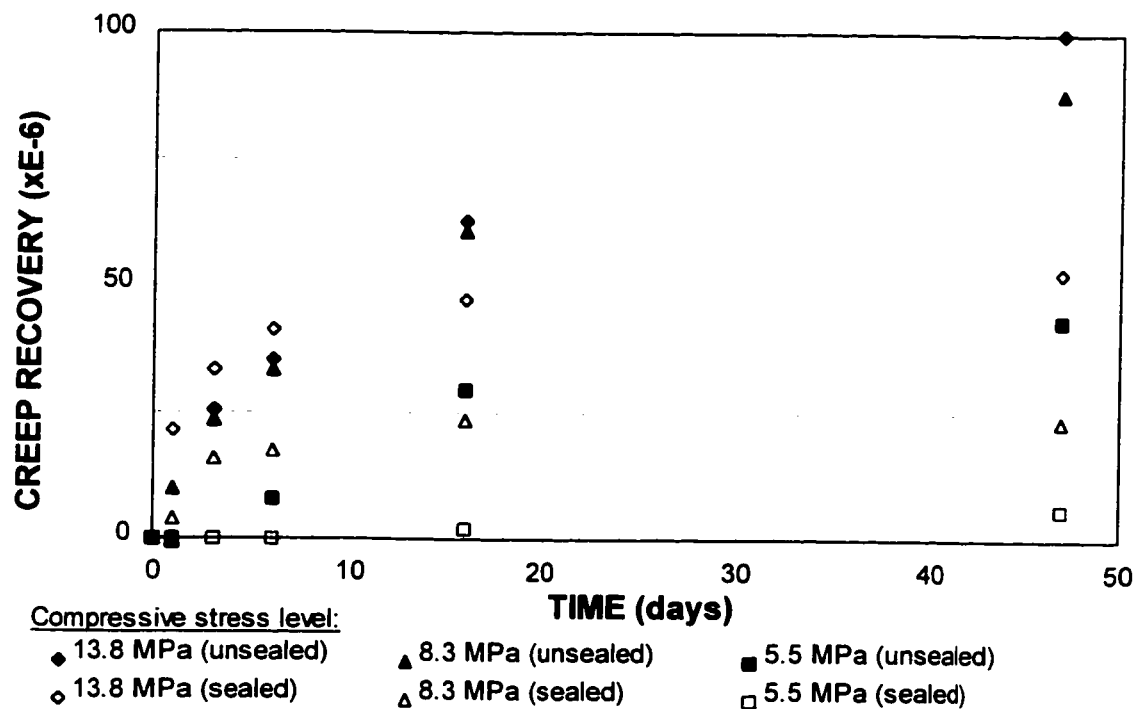


Figure 4.20 Creep recovery of 50% fly ash concrete after 372 days of creep loading under sealed and unsealed conditions.

4.5.4 Temperature Influence on Creep Characteristics

Concrete containing 50% fly ash was tested for creep at elevated temperatures in an experiment that was described in the previous chapter. The specimens were tested under sealed conditions and for this reason their drying shrinkage was negligible. In this section, only the basic creep at high temperatures is discussed. The temperature levels that were used included 71, 121, 149, 177 and 232° C (160, 250, 300, 350 and 450° F), and they were combined with three levels of externally applied compressive stress at 5.5, 8.3 and 13.8 MPa (800, 1200 and 2000 psi). The deformation of the concrete specimens was monitored for one year. The experimental results are summarized in the figures below for the three levels of compressive stress. Figure 4.21 represents a comparison over time of the creep strains at different temperatures under an applied constant stress of 13.8 MPa (2000 psi). For comparison purposes, the graph includes the results from the sealed specimens of 50% fly ash concrete that were tested for basic creep at room temperature of 21° C (70° F). It is evident from this figure that the creep of concrete increases with increasing temperatures. Similar trends about the effect of sustained high temperatures on the long term deformation of fly ash concrete are evident for all of the compressive stress levels that were used. This is indicated in Figures 4.22 and 4.23 which compare the creep strain data for different temperatures under sustained stress levels of 8.3 and 5.5 MPa (1200 and 800 psi) respectively.

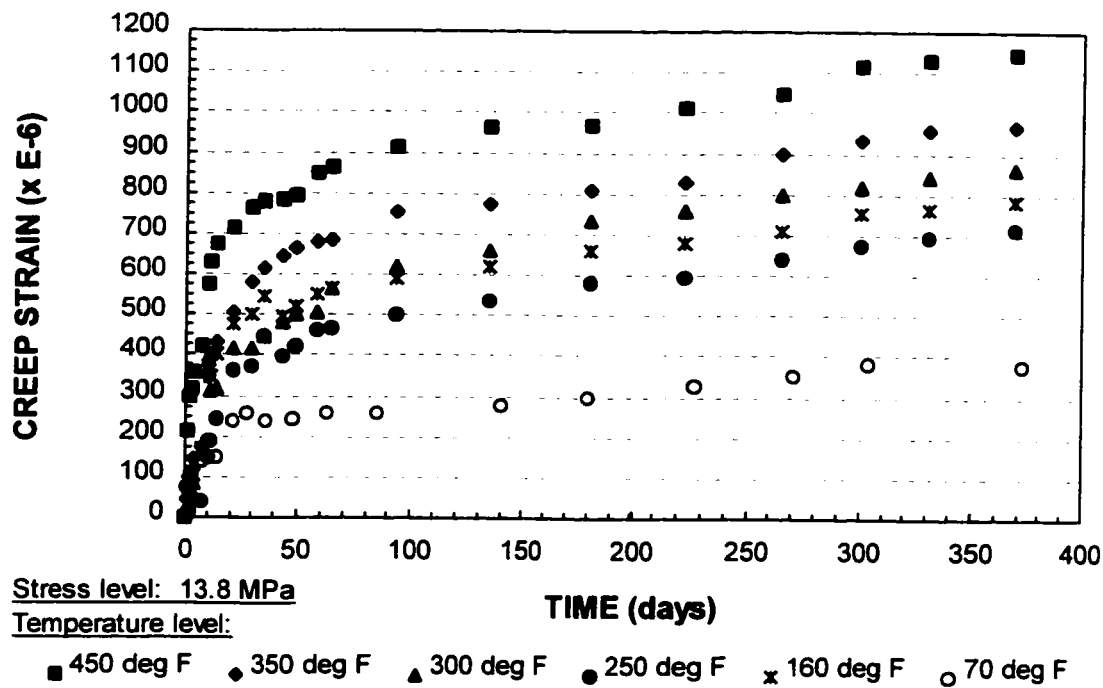


Figure 4.21 Total strain data for 50% fly ash concrete under external applied stress of 13.8 MPa (2000 psi) for various levels of high temperature.

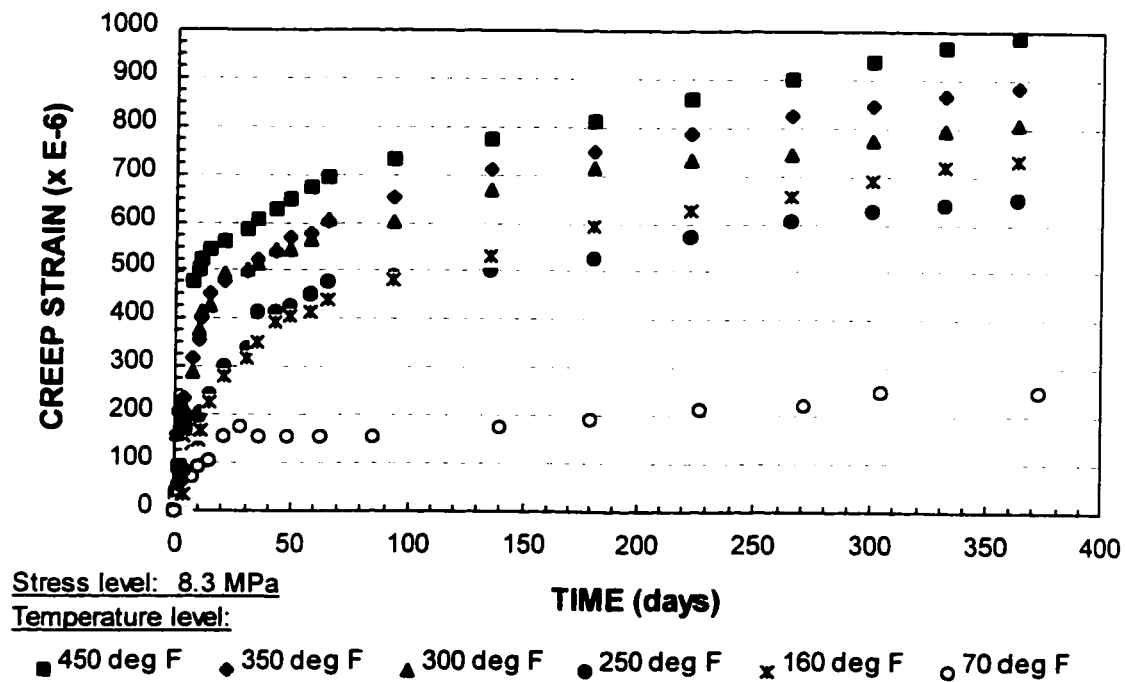
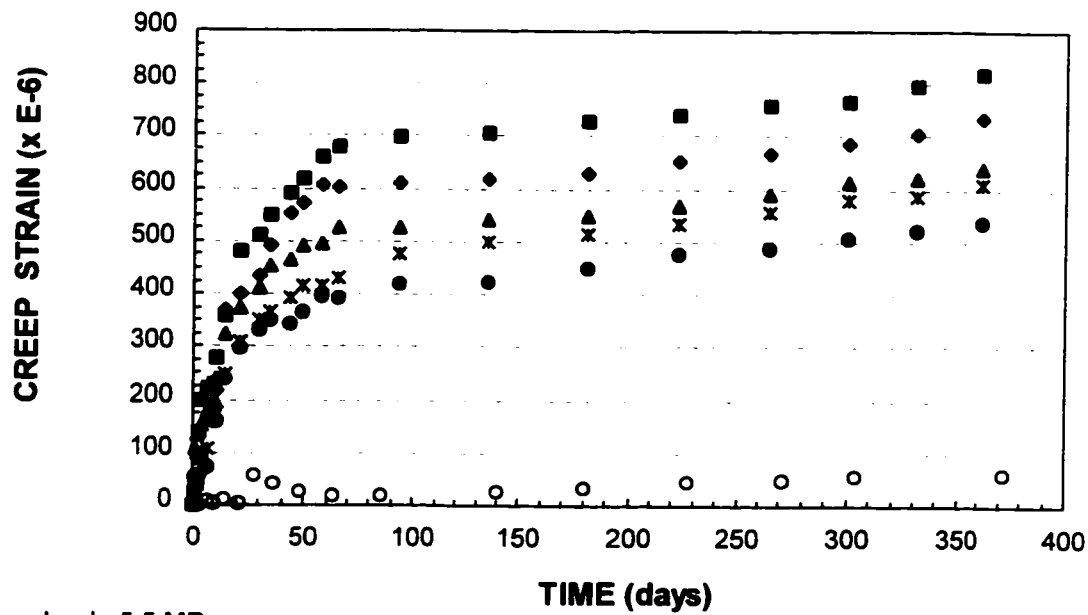


Figure 4.22 Total strain data for 50% fly ash concrete under external applied stress of 8.3 MPa (1200 psi) for various levels of high temperature.



Stress level: 5.5 MPa

Temperature level:

■ 450 deg F ◆ 350 deg F ▲ 300 deg F ● 250 deg F x 160 deg F ○ 70 deg F

Figure 4.23 Total strain data for 50% fly ash concrete under external applied stress of 5.5 MPa (800 psi) for various levels of high temperature.

Figures 4.21 to 4.23 indicate that the level of 71° C (160° F) produces a localized peak in the creep of concrete for temperatures up to 121° C (250° F). This observation is in agreement with Neville (1981) postulating that up to 71° C (160° F) the rate of creep increases; between 71° C and 96° C (205° F), the rate drops and beyond this temperature it increases again with increased temperatures. This is more clearly illustrated in Figure 4.24, representing the influence of temperature on the total creep of the fly ash concrete specimens of this study. It is evident from this figure that the creep of concrete increases to a peak value at 71° C (160° F), while the temperature of 121° C (250° F) represents a low point on the creep graph. The same trend is observed for all levels of applied stress used in this experiment.

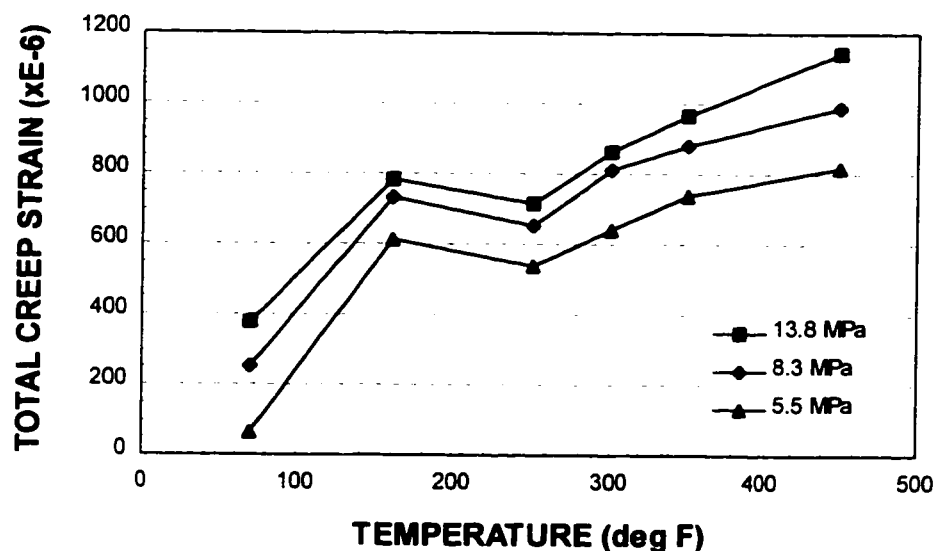


Figure 4.24 Effect of temperature on the total creep of 50% fly ash concrete for the external applied stresses used in this study under sealed conditions.

The dependence of creep strains on the intensity of the applied stress is summarized in Figure 4.25, for the temperature levels of this study with respect to the stress-strength ratio. For comparison purposes, the basic creep strains of the fly ash and the control concretes tested for creep at room temperature are also included in the same figure for their respective stress-strength ratios. Creep is considered to be more or less proportional to the applied stress level, for stresses less than about 0.4 - 0.5 of the compressive strength of the concrete (Hansen and Young, 1991). This proportionality is illustrated in Figure 4.25 within the limits of experimental errors.

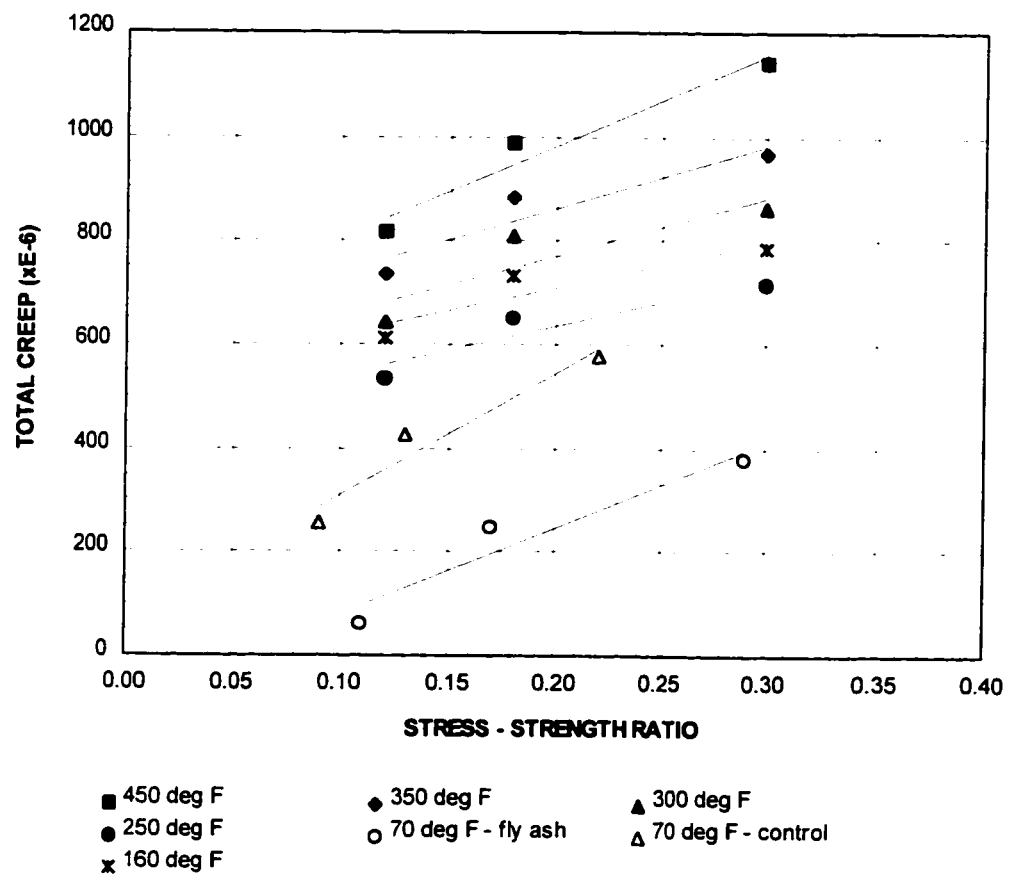


Figure 4.25 Comparison of the total creep strains of 50% fly ash concrete, for various temperature levels, with respect to the stress-strength ratio.

4.6 Frost Resistance

Testing was carried out in accordance to ASTM C-666 standard (Procedure A). A durable concrete is often defined as the one that can withstand 300 cycles of rapid freezing-and-thawing while its dynamic modulus of elasticity does not deteriorate below 60% of the initial value. In the previous chapter the two series of frost resistance experiments were explained and the specimen preparation and experimental set-ups were described.

The results from the first series of freezing-thawing testing indicated the detrimental effects of the lack of air-entrainment on the durability of both, fly ash and the control concretes. Three types of concrete mixtures were tested in this series. The two fly ash concretes tested, contained 30 and 50% cement replacements. A control concrete containing 100% portland cement was used for comparison purposes. The average 28-day compressive strengths of the two batches of each one of the concretes were 53.7 MPa (7790 psi) for the control concrete, 44.7 MPa (6485 psi) for the 30% fly ash concrete and 46.2 MPa (6700 psi) for the 50% fly ash concrete. The corresponding splitting tensile strengths were 5.3 MPa (773 psi), 4.7 MPa (680 psi) and 4.6 MPa (670 psi) for the control, 30% and 50% fly ash concretes respectively. None of the mixtures contained air-entrainment and as a result none of them tested satisfactorily. The assumed failure value of 60% of the initial dynamic modulus of elasticity was reached at less than 70 cycles, well below the accepted 300 cycles for durable concrete. At the same time a significant weight gain of the specimens indicated the presence of internal cracking and deterioration, with subsequent absorption of water. The performance of the non-air-entrained control concrete and the two fly ash mixtures is compared in Figure 4.26. All three concretes without an air entraining agent performed very poorly when exposed to the effects of rapid freezing-and-thawing. The control concrete and the mixture containing 30% fly ash replacement performed slightly better than the concrete

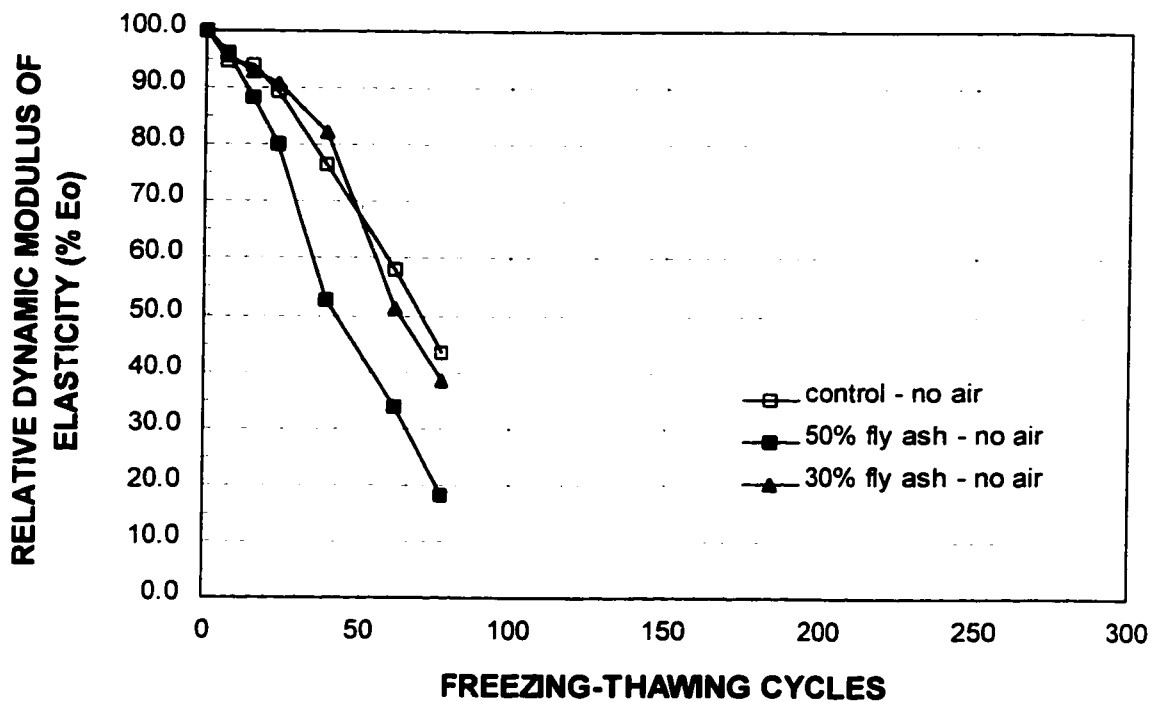


Figure 4.26 Performance of non-air-entrained concrete exposed to rapid freezing-and-thawing according to ASTM C-666 standard.

containing 50% fly ash.

A second series of concrete prism specimens was tested using a control concrete as well as a mixture containing 50% fly ash replacement. Both concretes contained micro-air to achieve entrained air contents of 6.8 - 9.8%. Some difficulty was encountered in entraining air in the fly ash concrete and for this reason several batches were discarded before an acceptable value of approximately 7% air was achieved. The complete air void parameters of the hardened concrete are presented in Table C.1 in Appendix C. Compared to the non-air-entrained concrete, the 28-day compressive strength of the air entrained concrete was lower due to the higher air content. The average 28-day compressive strength of the two batches of each one of the concretes was 27.6 MPa (4000 psi) and 30.1 MPa (4370 psi) for the fly ash and the control mixtures

respectively. The corresponding splitting tensile strength was 3.4 MPa (490 psi) and 3.7 MPa (530 psi) for the fly ash and the control mixtures respectively.

The performance of the fly ash and control concretes exposed to 300 cycles of rapid freezing-and-thawing is shown in Figure 4.27. The test results from each of the concrete batches is shown in this graph separately. The relative dynamic modulus of elasticity at each cycle interval represents the average of three concrete prisms. The graph indicates that the concrete containing 50% fly ash replacement performed at least as well as the control mixture with regards to loss of dynamic modulus of elasticity. Visual inspection after 300 cycles, showed a significant surface deterioration that developed during testing for both concretes; the surface damage included cracks, exposed aggregates and scaling. The results of the frost resistance testing that was performed at the PFRA Laboratory were comparable to the results presented above.

Satisfactory durability results have also been reported by Ghosh (1994) for concretes containing up to 50% fly ash replacements in addition to 10% silica fume. In the same study it was found that for fly ash replacement beyond the 50% level, the frost resistance of concrete was reduced substantially.

The durability factor (DF) is a simple quantity for assessing the resistance of concrete against repeated cycles of rapid freezing-and-thawing and in this study it was calculated from the observed data in accordance to ASTM C-666. Even though there are no established criteria for acceptance or rejection of concrete based on the durability factor, it is used primarily for comparative evaluation of different concretes (Neville, 1981). Figure 4.28 is a plot of the computed durability factors for the air-entrained fly ash and control mixtures showing each one of the prisms separately. The durability factors from the freezing-thawing experiment that was performed at the PFRA Laboratory are shown in Figure C.1 in Appendix C.

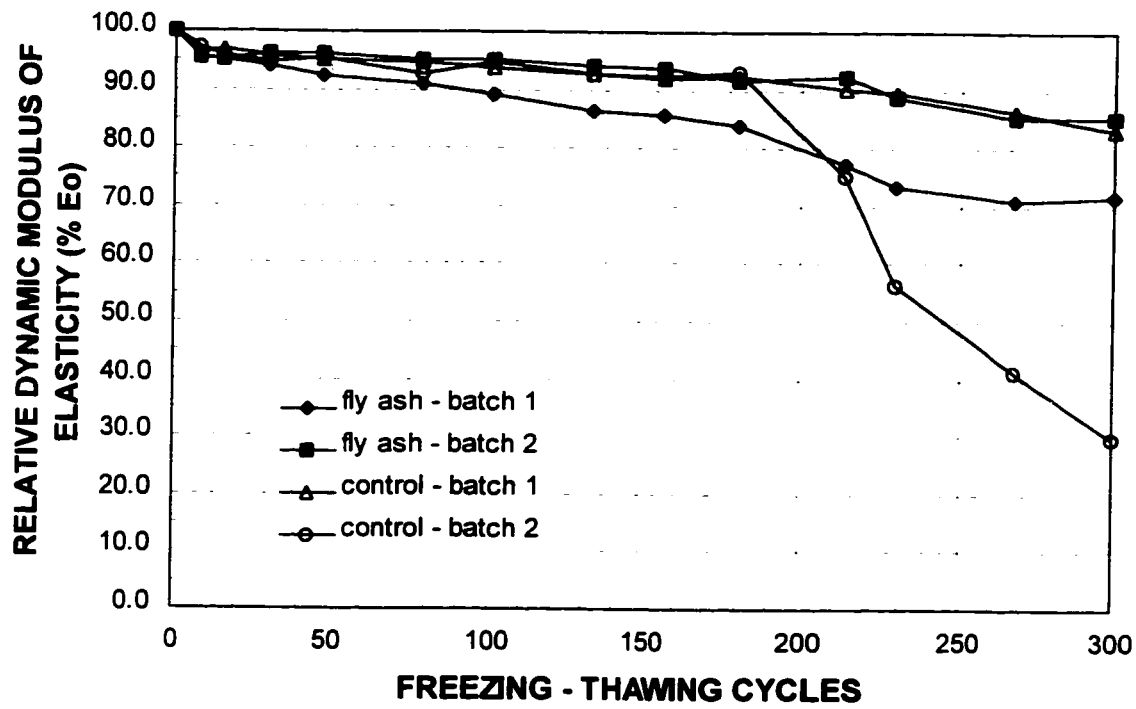


Figure 4.27 Performance of air-entrained fly ash and control concrete exposed to 300 cycles of rapid freezing-and-thawing according to ASTM C-666 standard.

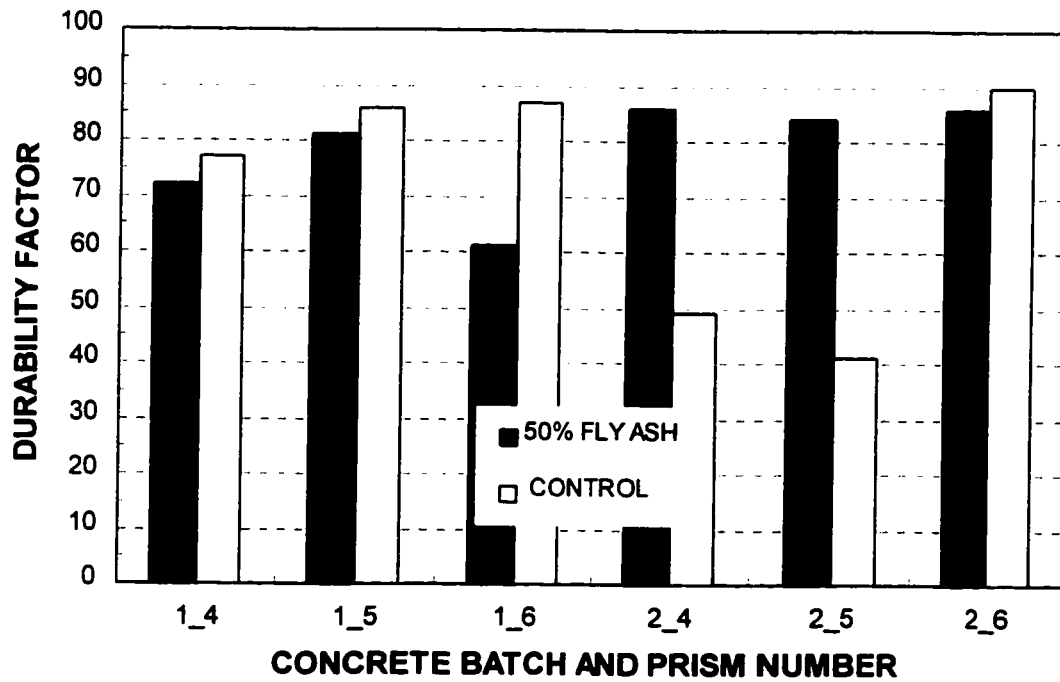


Figure 4.28 Durability Factors of air-entrained fly ash and control concretes following exposure to 300 cycles of freezing-and-thawing according to ASTM C-666 standard.

Figure 4.29 averages the freezing-thawing data of both batches of the air-entrained fly ash and the control concrete shown in Figure 4.27. For comparison purposes, the graph also includes the freezing-thawing data of the non-air-entrained 50% fly ash concrete from Figure 4.26. To illustrate the effect of longer curing, an extra batch of non-air-entrained 50% fly ash concrete was cast and it was cured in lime saturated water for 81 days before it was exposed to rapid freezing-and-thawing at the same time as the air-entrained concrete. The results are included in Figure 4.29 for comparison. It is obvious that longer curing time improved the performance of the non-air-entrained fly ash concrete somewhat, however, the specified failure value of the relative dynamic modulus of elasticity was reached at less than 100 cycles which is well below the accepted 300 cycles for durable concrete.

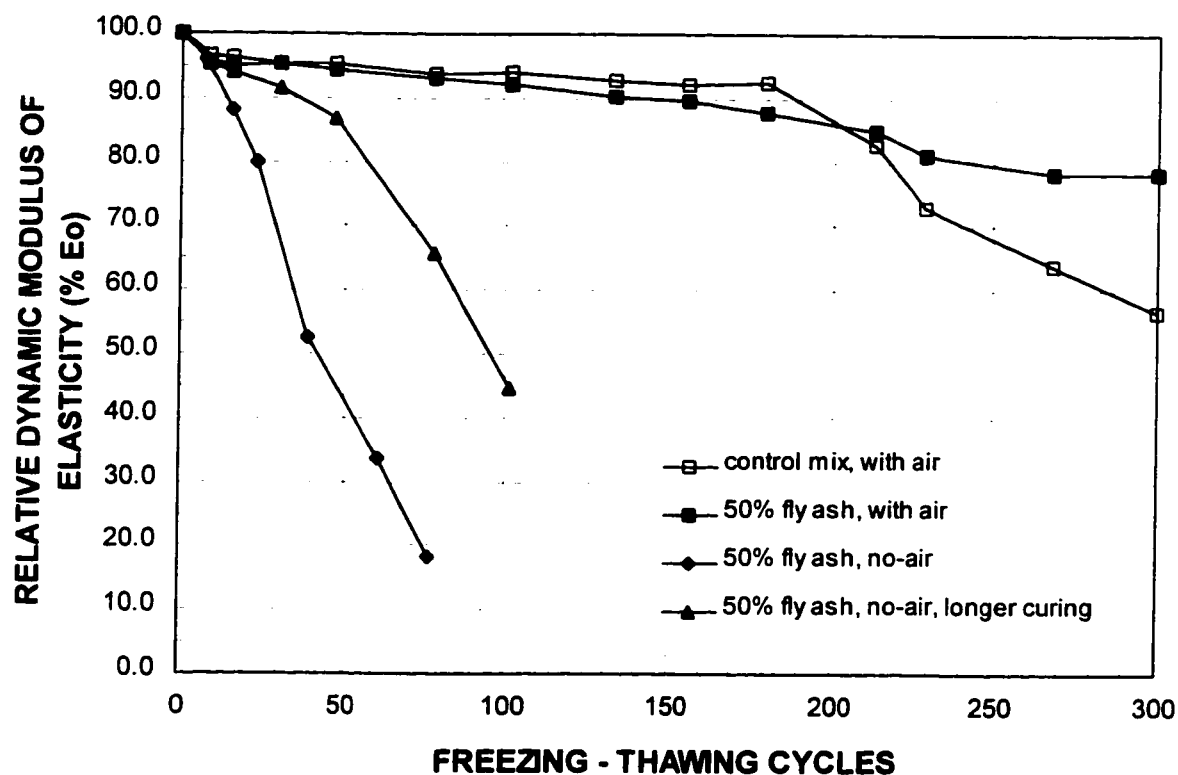


Figure 4.29 Comparison of the freezing-thawing durability of air- and non-air-entrained fly ash and control concrete.

4.7 Sulphate Resistance

The prism specimens that were prepared for this purpose were immersed in a sodium sulphate solution for one year and their length and weight changes were monitored periodically as described in the previous chapter. At the end of the test period, visual inspection indicated no surface damage in any of the specimens with either fly ash or control concretes. Following immersion in the sulphate solution, a comparison of the percent linear expansion of fly ash and control concretes is presented in Figure 4.30. The figure indicates that the presence of fly ash improves the sulphate resistance of the hardened concrete. A similar behaviour of fly ash concrete in an aggressive environment has been reported in previous research work (Tikalsky and Carrasquillo, 1993, Ghosh, 1994). The same trend is observed in the percent weight gain of the fly ash and control concrete specimens. From Figure 4.31, it is evident that concrete containing 50% fly ash replacement performed better than the control mixture in the presence of sulphate ions.

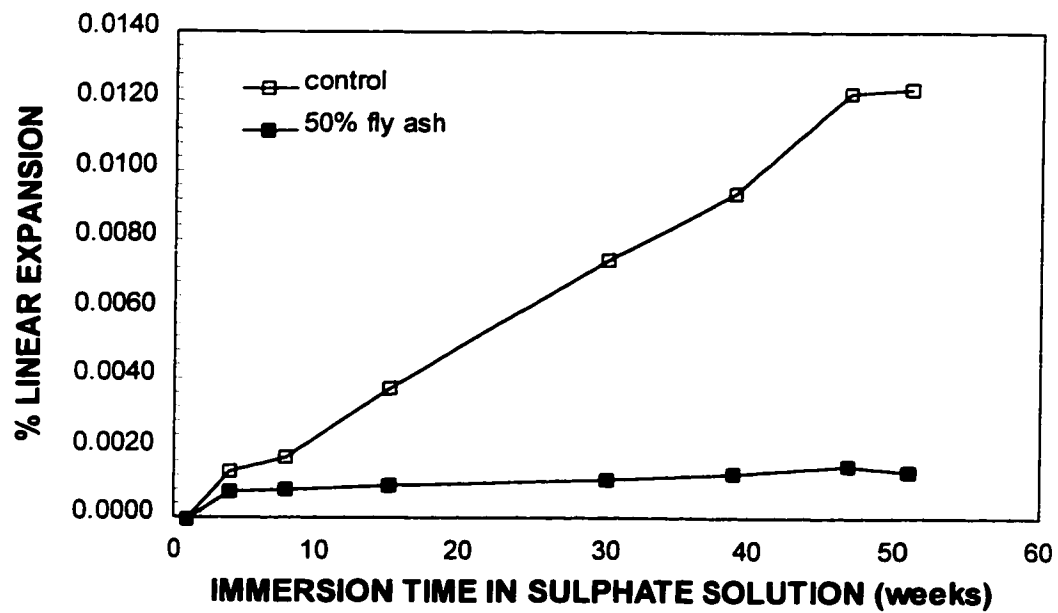


Figure 4.30 Comparison of the linear expansion of fly ash and control concretes in sulphate solution.

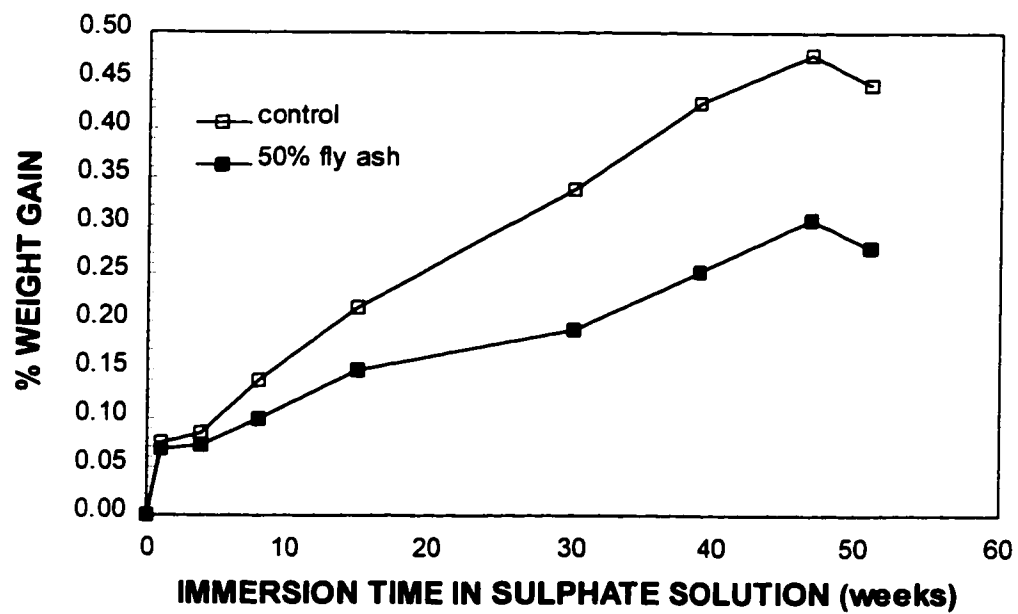


Figure 4.31 Comparison of the percent weight gain of fly ash and control concretes in sulphate solution.

CHAPTER 5

Microstructural Analysis

5.1 Introduction

Mechanical testing has traditionally been the main method by which engineers investigated and evaluated the performance and durability of concrete. While these tests provide valuable information on the mechanical properties, scientists are looking elsewhere for insight on the causes of failure and deterioration of the concrete. Increased attention is presently focused on the structure of the material and various analytical methods are available for characterization of the microstructural features of the constituent phases of the concrete.

High performance concrete is routinely produced by replacing part of the cement with fly ash, silica fume, slag, used singly or in combination, and by reducing the water demand by utilizing low and high range water reducers. The use of supplementary cementing materials in the development of high performance concrete has inevitably produced a more complex microstructure. In order to fully assess the effect of these mineral admixtures on the behaviour and long term durability of concrete, it is imperative to understand the resulting microstructure. While considerable progress has been made in understanding the development of the microstructure during cement hydration, the available literature relating the microstructure and engineering properties is minimal and far from clear (Pratt, 1987).

In this chapter, the experimental results as they relate to compressive strength, static modulus of elasticity, creep, shrinkage and durability pertaining to frost and sulphate resistance are discussed with reference to the structure of the concrete on a microscale. The analysis is focused on the microstructure of the bulk paste and interfacial regions using Scanning Electron Microscopy and Electron Probe Microanalysis on fractured and polished sections respectively. Fractured surfaces were examined using secondary electron imaging which clearly shows the topography of the sample, the density of the paste, crystals of Ca(OH)_2 and ettringite. Polished concrete surfaces were studied using backscattered electron imaging which distinguishes between the various phases of the cement paste including unhydrated cement, porosity, fly ash spheres and any reaction rims around them. A comparison is made between the microstructural features of the fly ash and control concretes.

5.2 Compressive Strength and Static Modulus of Elasticity

The inter-dependence of the compressive strength and stiffness of concrete has been well documented and it is widely accepted by various building codes that use the compressive strength to predict the static modulus of elasticity. The elastic modulus increases with the compressive strength of the concrete (Neville, 1981) and the validity of this relationship for the fly ash and control concrete mixtures of this study, was demonstrated in the previous chapter. The influence of the microstructural characteristics on the mechanical properties of the concrete has been recognized by many researchers (Aïtcin, et al., 1987, Sarkar, 1994, Pratt, 1987). The compressive strength of the concrete has been linked to structural features at a coarser scale including the total porosity and pore size distribution, the presence of flaws and the homogeneity or heterogeneity of the system (Mindess, 1985).

The high levels of compressive strength that were achieved in this study for the fly ash and the control concrete mixtures are the result of the low porosity in the cement paste. The effect of the superplasticizer on the workability of the fresh concrete allowed low water/cement ratios to be used and the result was a dense matrix in both concretes. This is revealed from the study of the cement paste microstructure using Scanning Electron Microscopy. Figures 5.1 and 5.2 represent secondary electron image (SEI) micrographs of fractured samples from the fly ash and control mixtures respectively and a dense paste is clearly visible in both concretes.

At a higher magnification than the figures above, the two concretes show a different composition and physical characteristics of the matrix. Figure 5.3 represents a SEI (secondary electron image) micrograph of a mature paste containing 100% portland cement (control mixture). The presence of hexagonal plates of calcium hydroxide crystals is evident in the bulk paste and massive depositions of the same crystals are present on the interior surface of air voids as it is indicated in Figure 5.4. By contrast, SEI micrographs of concrete with a 50% fly ash content revealed no evidence of Ca(OH)_2 (noted as CH in cement chemistry) crystals in the bulk paste and only a very small amount was found present inside air voids as it is shown in Figures 5.5 and 5.6 respectively.

The structure of bulk cement paste is very significant for the evaluation and prediction of the mechanical properties of concrete. However, since there is little "bulk" matrix in the concrete, it is important to concentrate on the microstructural features that occur near boundaries of the cement paste with aggregates or other foreign materials incorporated in concrete (Diamond, 1987).

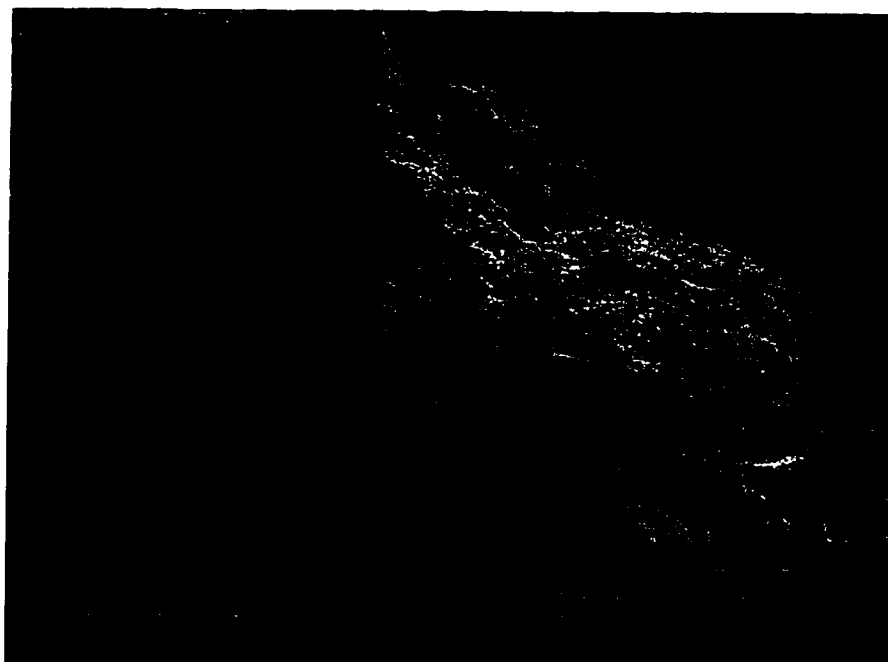


Figure 5.1 Secondary electron image micrograph of cement paste, in contact with quartz aggregate, in concrete containing 50% fly ash (Magnification 150x).

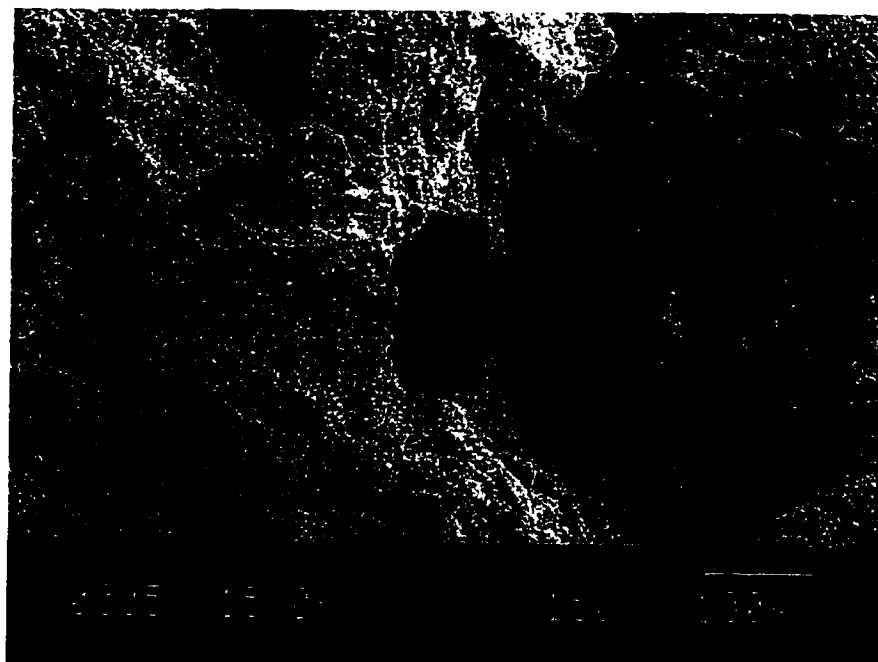


Figure 5.2 Secondary electron image micrograph of bulk paste of 100% portland cement concrete (Magnification 150x).

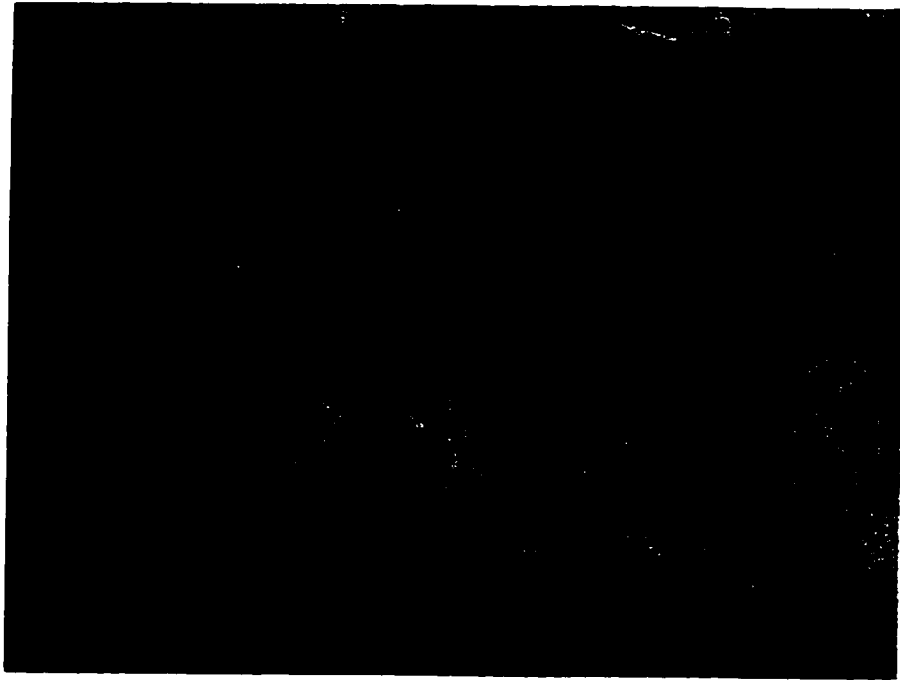


Figure 5.3 Secondary electron image micrograph of bulk paste at a paste/aggregate interface of 100% portland cement concrete (Magnification 400x).



Figure 5.4 SEI micrograph of an air void interior of 100% portland cement concrete showing a massive deposition of Ca(OH)_2 crystals (Magnification 200x).

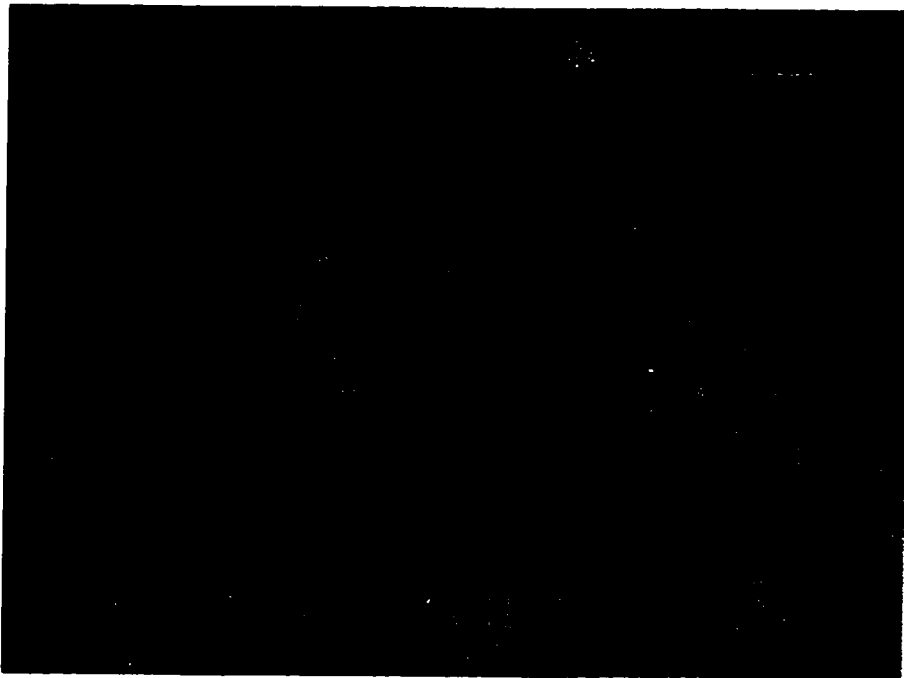


Figure 5.5 Secondary electron image micrograph at a paste/aggregate interface of a concrete specimen containing 50% fly ash (Magnification 1000x).

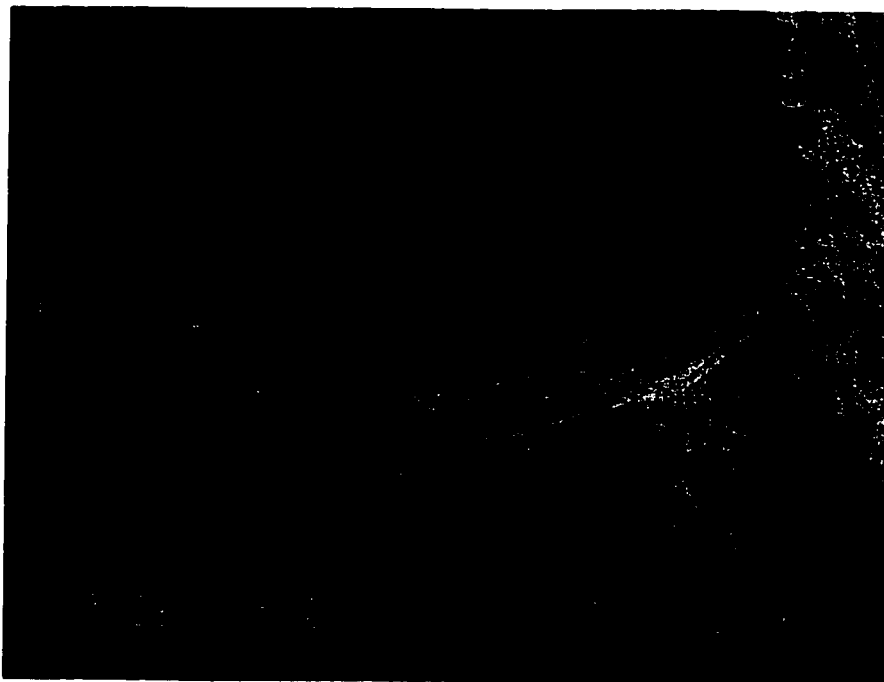


Figure 5.6 SEI micrograph of an air void interior of a concrete specimen containing 50% fly ash showing a minimal amount of Ca(OH)_2 crystals (Magnification 150x).

In an effort to correlate the microstructure and mechanical properties of concrete, Mitsui, et al., (1994), studied the paste-aggregate interface using backscattered electron imaging and found that the porosity of the interfacial region is largely influenced by the water-cement ratio. They concluded that the microstructure of the interface could be improved significantly by using lower water-cement ratio and incorporating mineral admixtures, like silica fume, into the cement paste matrix.

Figures 5.3 and 5.5 above reveal information about the physical characteristics of bonding between paste and aggregate at the interface, for the two concretes in comparison. The interfacial region of the control concrete (Figure 5.3) is characterized by a narrow gap between the paste and aggregate and this accounts for weaker bonding that has a negative effect on the strength of the composite material. Figure 5.5 represents a secondary electron image of a mature paste of concrete containing 50% fly ash. The effect of the pozzolanic reaction at the interface is evident. The CH crystals have been consumed and transformed into Calcium-Silicate-hydrate (C-S-H), the strength contributing phase. In the process, the fine gap between paste and aggregate is filled with C-S-H and a denser matrix with better bonding capacity develops at the interface. As the pozzolanic reaction continues to take place with time, the strength of the fly ash concrete develops at a faster rate than the strength of the control mixture and eventually becomes higher or equal to it.

It was shown in Chapter 4 that the compressive strength of concrete containing a low volume of fly ash (20% replacement) surpasses the strength of the control concrete within 28 days. The strength of the high volume fly ash (50% replacement) concrete does not reach the same level; instead, it approaches the compressive strength of the control mixture after three months of curing. The study of the microstructure of concrete containing 50% fly ash revealed a large number of unreacted fly ash particles in the matrix. The fine water gap separating the fly ash particle from the paste in the matrix in

Figure 5.5, does not allow for a very good bond between the paste and unreacted fly ash and this brings about a loss in compressive strength. By comparison, concrete containing only 20% fly ash reached a considerably higher strength level. A previous study of the microstructure of a similar concrete with 20% fly ash content did not show any remaining unreacted fly ash particles in the matrix (Ghosh, 1994), so, the negative effect on the compressive strength due to the poor bond between paste and unreacted fly ash particles is eliminated.

5.3 Long-Term Deformation

Neville (1981) indicates that the compressive strength has a significant influence on creep behaviour and that creep is inversely proportional to the strength of the concrete at the time of loading. This relationship was discussed in the previous chapter and supporting data for the fly ash and control concretes were presented. It was shown that the fly ash concrete produced lower creep strains even though its compressive strength at the time of loading was lower than the strength of the control concrete. This is in agreement with research results on the creep properties of concrete incorporating large volumes of Class F fly ash (Sivasundaram, et al., 1991).

Since creep is dependent on the compressive strength of the concrete, the microstructural features that affect the strength development, as they were described in the previous section, will indirectly influence the creep behaviour as well. Xi and Jennings (1992) postulated that the mechanisms of creep and shrinkage are associated with changes at the microstructural level, but models, especially those consisting of mathematical formulations, are lacking a microstructural interpretation. They (Xi and Jennings, 1992) consider the cement paste to be a composite material in itself with a varied spatial distribution of C-S-H, CH, aluminate phases, anhydrous cement and

aggregates. Shrinkage is not a property of any of the above phases alone but rather it is a process that depends on the spatial distribution of all of the phases present in the paste. In the following section, fractured and polished surface samples from the fly ash and control test specimens for creep and shrinkage are examined for any microstructural features that affect long term behaviour. The two concretes are compared and the differences in their microstructure are noted.

5.3.1 Moisture Influence on Creep Characteristics

a. Low Moisture Conditions

Figures 5.7 and 5.8 represent backscattered electron image (BEI) micrographs from polished sample surfaces of the fly ash and the control concretes respectively. The samples originated from unsealed specimens that were tested for creep under a constant compressive stress of 13.8 MPa (2000 psi). In the magnified micrographs, the coarse features of the samples are shown and they are distinguished by means of their gray level. The larger dark areas shown are sand grains, while the surrounding matrix consists of hydration products and unhydrated cement, recognized by the lightest colour grains. Using the electron probe microanalyzer and energy dispersive spectroscopy (EDS), the composition of the two tone matrix is presented in Figures 5.9 and 5.10 for the control concrete paste and unhydrated cement respectively. The corresponding information for the hydrated paste in the fly ash concrete is shown in Figure 5.11. A number of observations may be made from the above figures.

From the EDS spectrums of the hydrated paste (C-S-H), a comparison is made between the fly ash and the control concretes for their respective contents in calcium and silica. Even though the spectrums show the same approximate qualitative composition of

the hydrated cement paste, the two concretes differ substantially in their quantitative analysis. For this purpose, the ratio between the Ca-peak and the Si-peak is calculated and compared. The Ca-Si ratio in the control concrete is 1.95 while the fly ash concrete indicates a more silica-rich paste with a Ca-Si count ratio of 1.28. Microstructural studies on high strength concrete containing silica fume (Regourd, 1985, Aïtcin, et al., 1987, Roberts, 1989) have reported similarly silica-rich hydration products due to the pozzolanic reaction. Regourd (1987), reported a Ca-Si ratio between 1.0 and 1.5 in pastes containing fly ash. She also found that the C-S-H in fly ash concrete is more amorphous and it has a higher aluminum content. A higher Al content is also evident from the EDS spectrum of the fly ash concrete in the present study as shown in Figure 5.11 and compared to the equivalent spectrum of the control concrete in Figure 5.9. It is possible that the densified C-S-H gel in the fly ash concrete is more stable under sustained stresses due to its different chemical composition and for this reason it produces lower creep and shrinkage strains.

A comparison between Figures 5.7 and 5.8 indicates a more extensive fracture pattern in the control concrete. By contrast, the fly ash concrete, even though it was cured and tested under identical conditions as the control, shows a much finer crack pattern at the same magnification. In the control concrete, fractures propagate around sand grains and a wide gap that is visible at the low magnification of the micrograph indicates poor bonding and weak interfaces. It has been suggested that the anhydrous material is stronger than the cement gel and could act as a crack arrester (Pratt, 1987). However, this is not indicated by the fracture patterns in the two concretes of this comparison where the anhydrous cement cores do not seem to interfere with crack propagation.

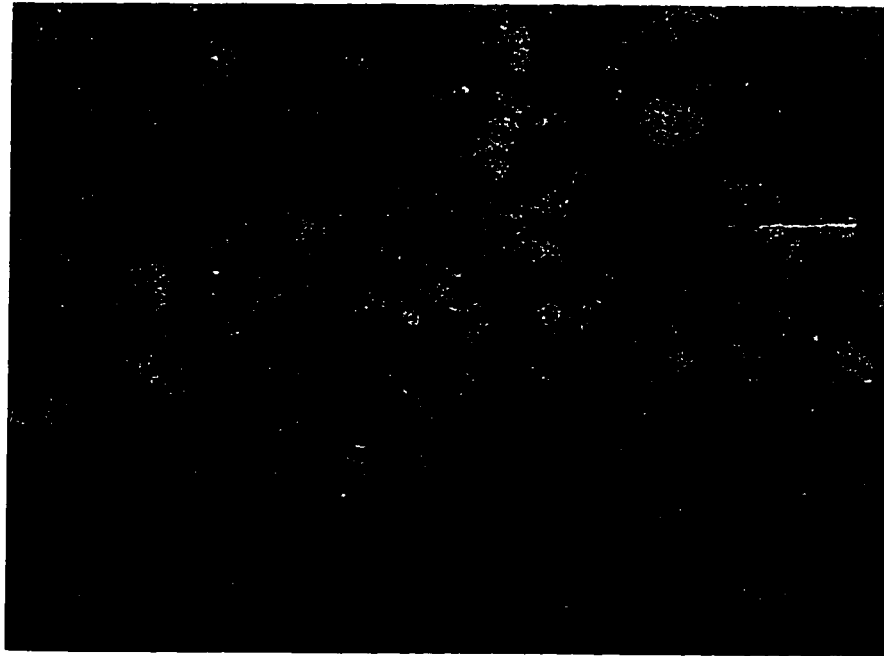


Figure 5.7 Backscattered electron micrograph of a polished surface of fly ash concrete. Specimen was unsealed and tested at 13.8 MPa (Magnification 150x).

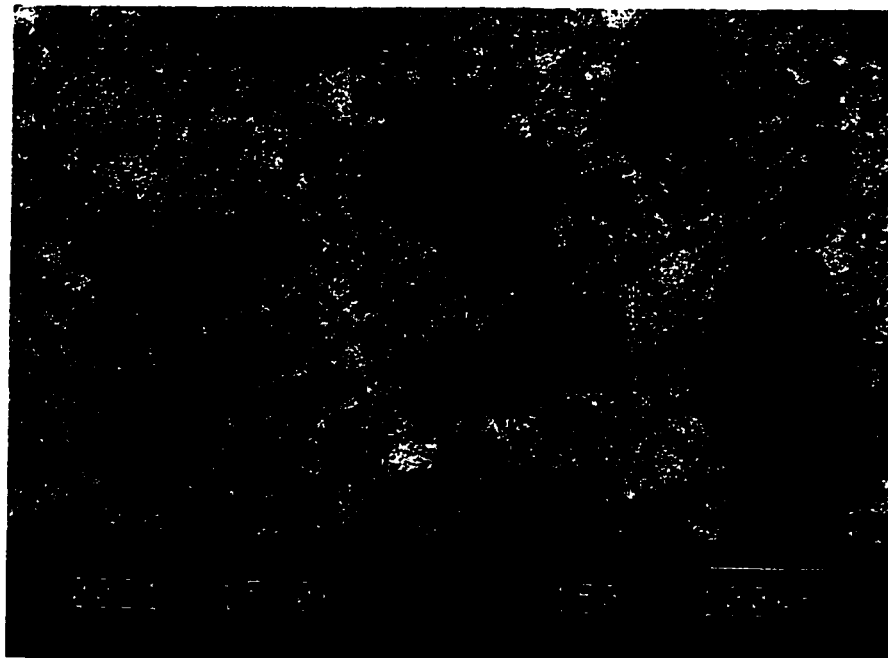


Figure 5.8 Backscattered electron micrograph of a control concrete polished surface. Specimen was unsealed and tested at 13.8 MPa (Magnification 150x).

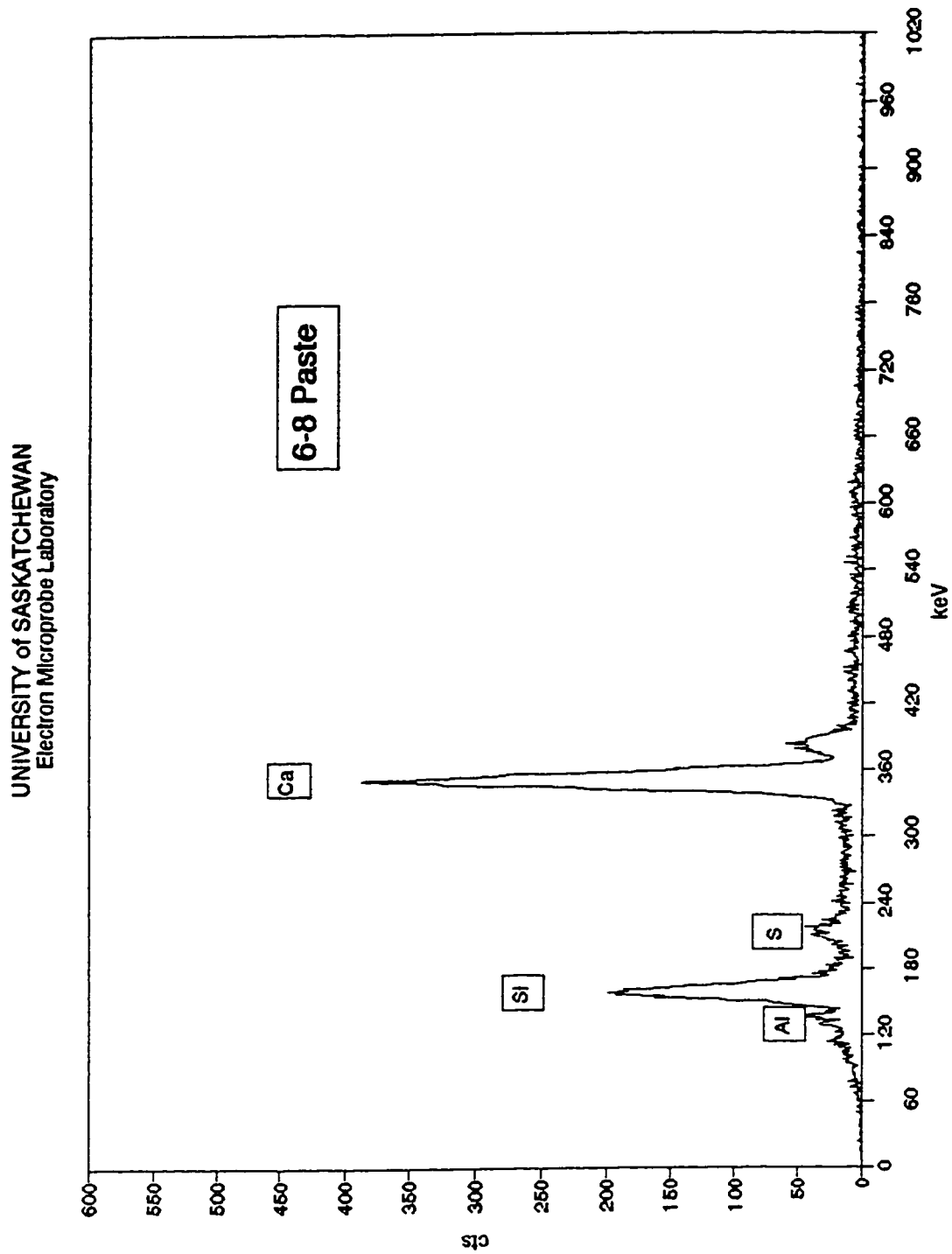


Figure 5.9 EDS spectrum of hydrated cement paste from a polished surface of a control concrete specimen.

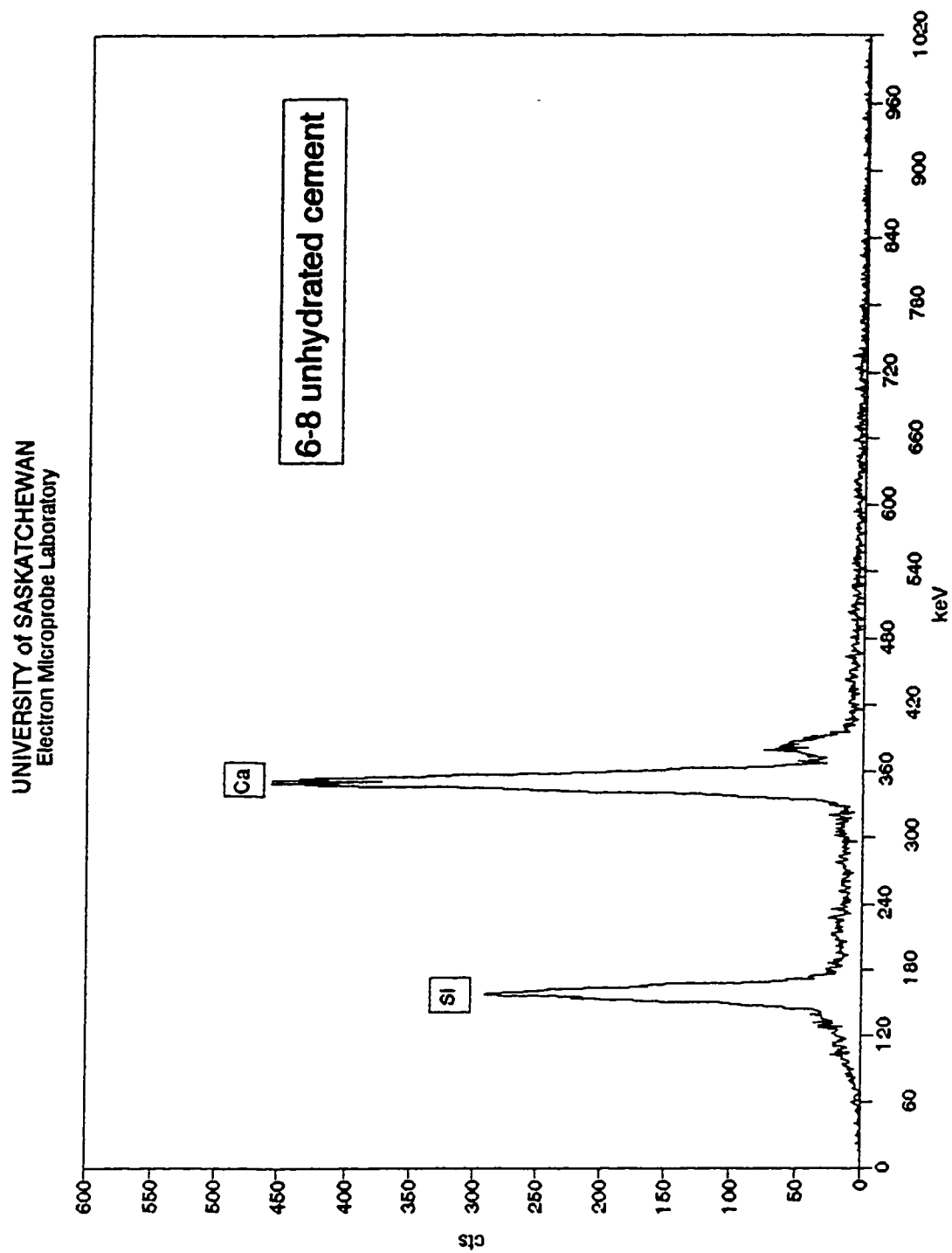


Figure 5.10 EDS spectrum of anhydrous cement grains from a polished surface of a control concrete specimen.

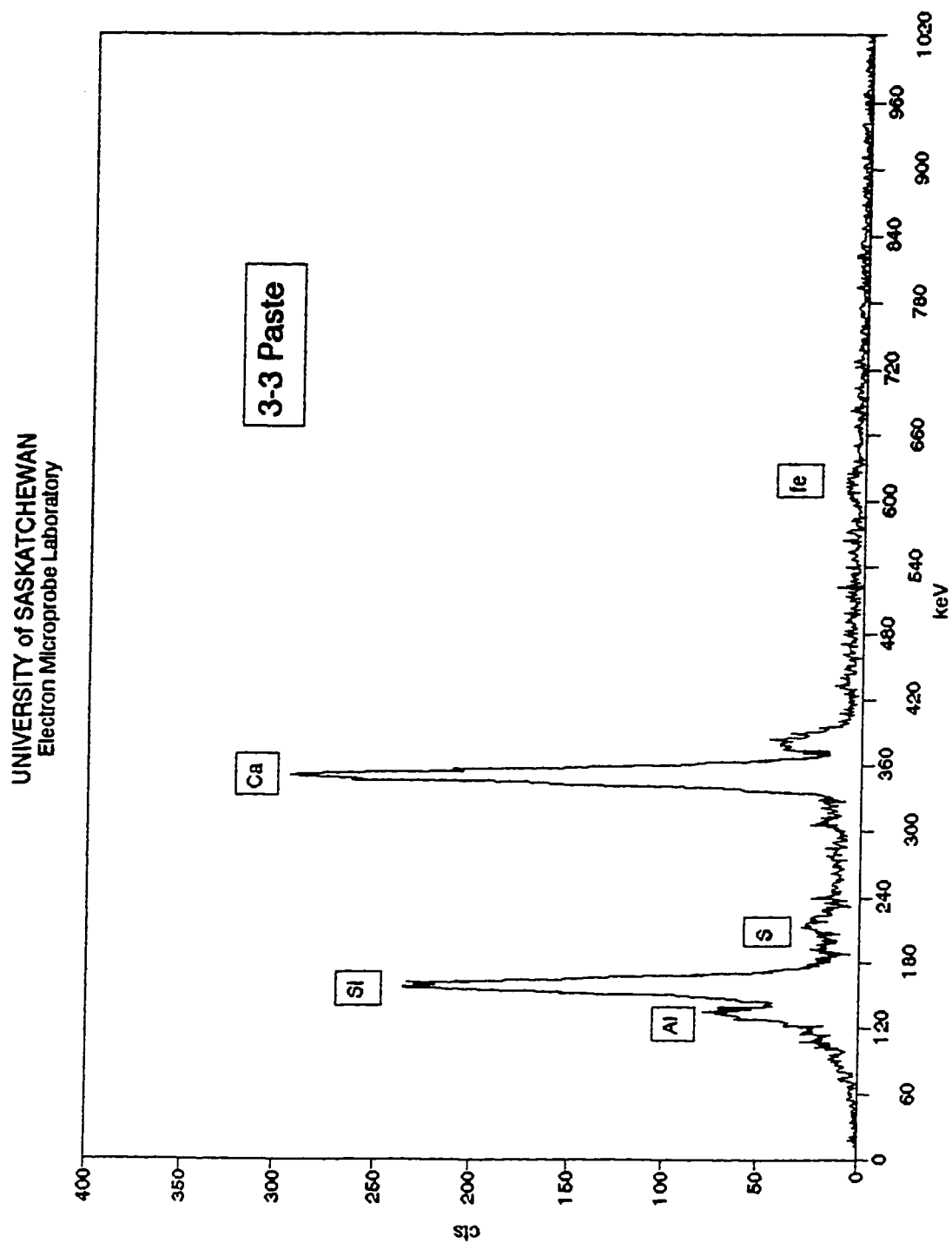


Figure 5.11 EDS spectrum of hydrated cement paste from a polished surface of a 50% fly ash concrete specimen.

Using Figures 5.7 and 5.8 to compare the anhydrous phase content, a considerably higher amount of unhydrated cement is seen in the control concrete. Anhydrous cement cores affect the drying creep of concrete indirectly by providing a restraining effect since they do not shrink on drying (Xi and Jennings, 1992). It is therefore implied that a paste with a higher content of unreacted cement would produce lower shrinkage strains and hence, the drying creep of such cement paste would also be lower. However, as it was presented in the previous chapter, the fly ash concrete of this study produced lower strains than the control. In the fly ash concrete the restraining effect of the anhydrous cement cores is supplemented by a similar effect due to the fly ash particles which do not shrink on drying. In addition, the numerous unreacted fly ash particles are considerably harder than the surrounding paste and they provide additional restraining effect acting as fine aggregate. This is evident from Figures 5.12 and 5.13 representing secondary electron image micrographs showing the topography of a polished surface of the fly ash concrete. The surface was polished without using epoxy to stabilize the matrix, as it was done for the samples that were prepared for backscattered electron image (BEI) studies. When viewed in the SEI mode, the fly ash particles are clearly visible as being more resistant to polishing, therefore, harder than the cement paste, and hence, they produce smaller long term deformations.

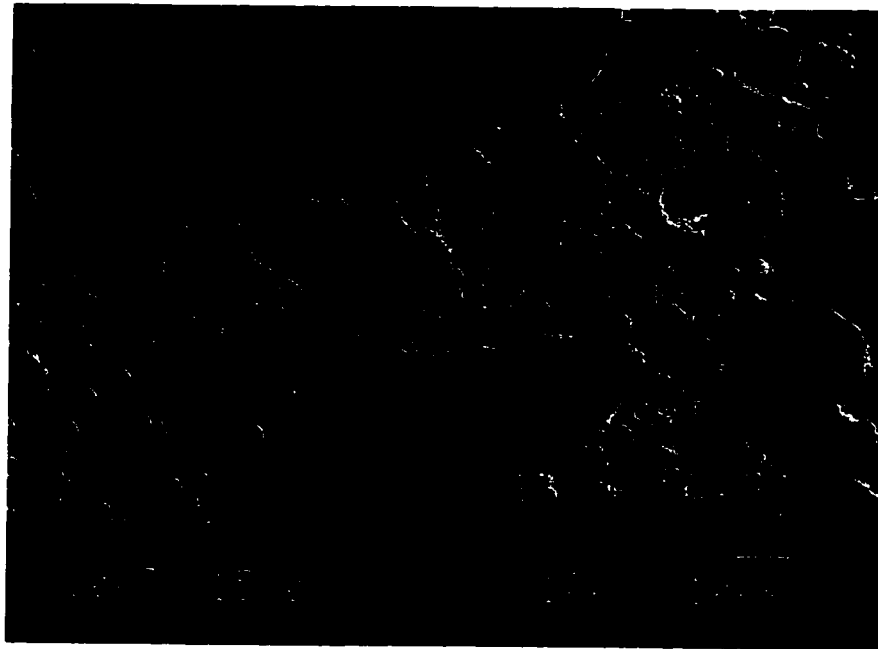


Figure 5.12 SEI micrograph of a polished surface of fly ash concrete showing fly ash particles being resistant to polishing (Magnification 100x).

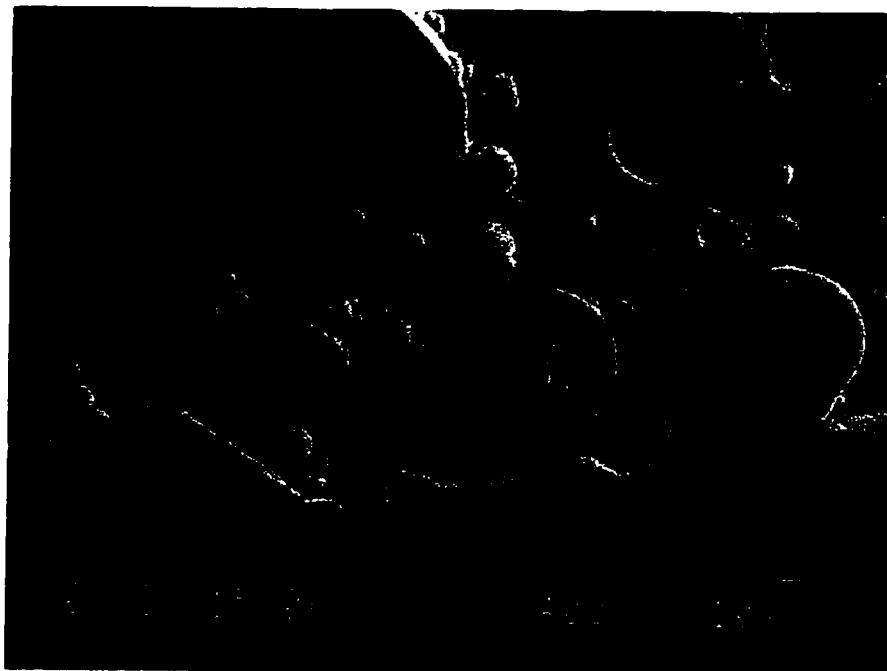


Figure 5.13 SEI micrograph of a polished surface of fly ash concrete showing fly ash particles being resistant to polishing (Magnification 400x).

b. High Moisture Conditions

Similar differences in microstructural characteristics that affect the long term deformation of the concrete are shown in Figures 5.14 and 5.15 which represent BEI micrographs from fly ash and control concretes tested for creep under a constant stress of 13.8 MPa (2000 psi) and high moisture conditions using sealed specimens.

From the secondary electron image (SEI) micrograph in Figure 5.16, the presence of calcium hydroxide and ettringite needles is evident in large quantities in the control concrete, while total absence of $\text{Ca}(\text{OH})_2$ and ettringite is noted in the bulk paste of the fly ash concrete as seen in Figure 5.17. It is noted (Taylor, 1990) that because of the cleavage planes of calcium hydroxide, preferred orientation of the crystals occurs easily at the paste-aggregate interface. The preferred orientation of the CH crystals in the control concrete is shown in Figure 5.16 in the place of a detached aggregate. Roberts (1989) indicates that as the concentration of calcium hydroxide decreases and the amount of C-S-H increases near the interface, due to the pozzolanic activity, the cleavage strength of the concrete increases as well. While it is noted by Xi and Jennings (1992) that CH provides a restraining effect since it does not shrink on drying, the instability of its structure due to cleavage planes makes it susceptible to yielding under internal stresses that develop due to shrinkage or externally applied loads.

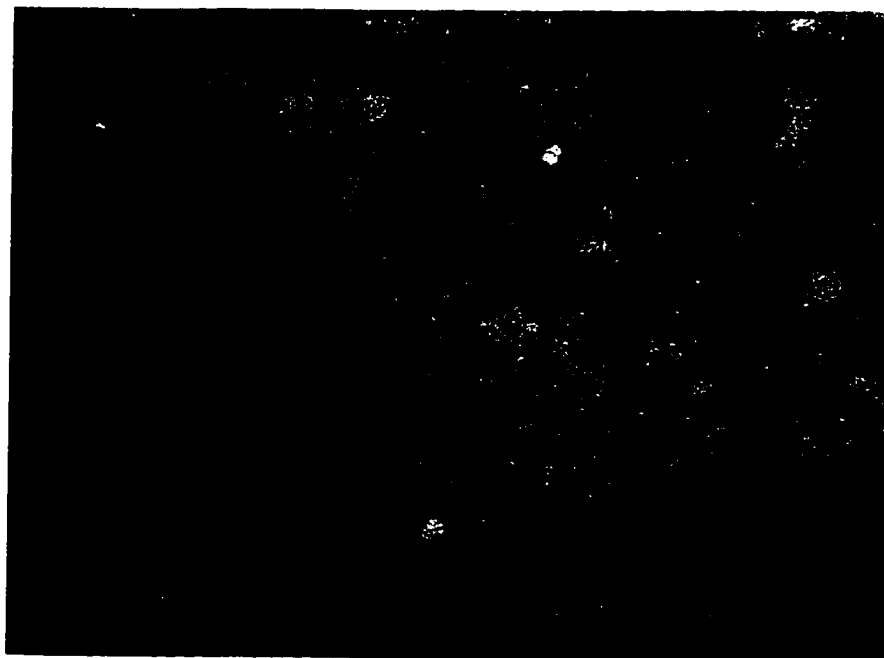


Figure 5.14 Backscattered electron micrograph of a polished surface of fly ash concrete. Specimen was sealed and tested at 13.8 MPa (Magnification 150x).

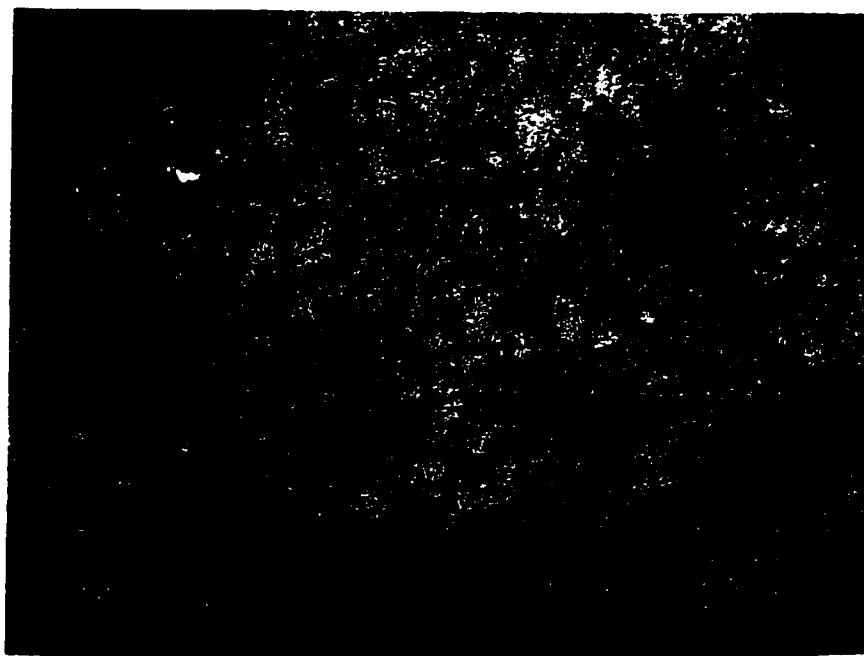


Figure 5.15 Backscattered electron micrograph of a control concrete polished surface. Specimen was sealed and tested at 13.8 MPa (Magnification 150x).

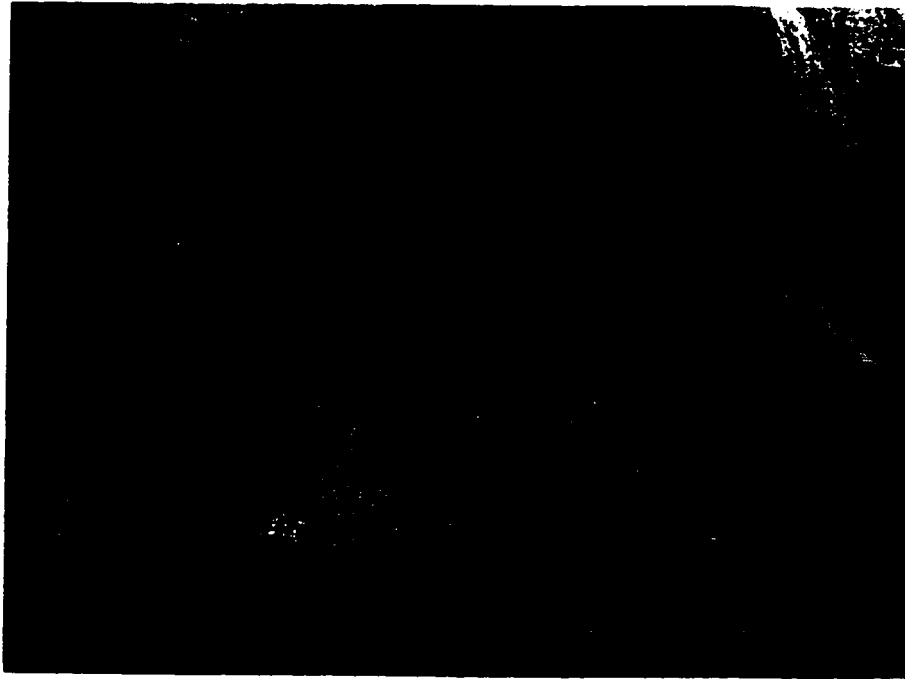


Figure 5.16 SEI micrograph of a fractured surface of the control concrete. Specimen was tested sealed at 8.3 MPa (Magnification 400x).

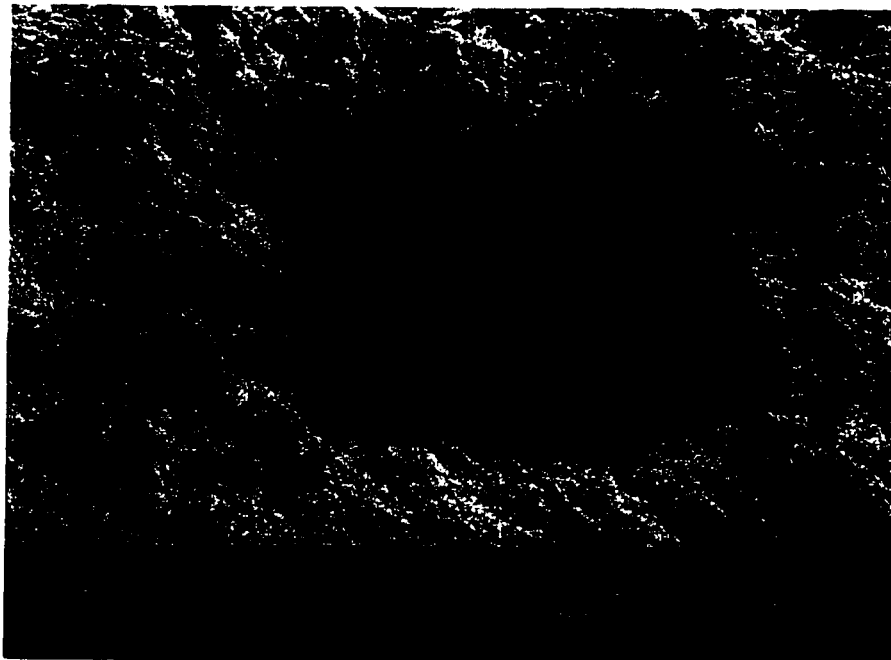


Figure 5.17 SEI micrograph of a fractured surface of the fly ash concrete. Specimen was tested sealed at 13.8 MPa (Magnification 400x).

5.3.2 Temperature Influence on Creep Characteristics

As it was presented in the previous chapter, the effect of high temperature on the creep of fly ash concrete was tested using 75x225 mm (3x9 in) cylindrical specimens in sealed compartments, at five levels of constant temperature and three levels of applied compressive strength. The creep behaviour of the fly ash concrete under elevated temperatures was compared to the basic creep of the fly ash concrete that was tested at room temperature of 21° C (70° F) using sealed concrete specimens. It was shown that high temperatures produced considerably higher creep strains in the fly ash concrete.

An investigation was undertaken to understand the microstructural features of the high temperature creep specimens and to compare them to the microstructure of the fly ash concrete specimens that were tested for creep at room temperature. The study was performed on fractured and polished sample surfaces. Secondary electron imaging (SEI) was used with the fractured sample surfaces to provide information on the topography and the microstructural features of the concrete sample. Information on the chemical composition of the constituent phases of the cement paste was obtained from the polished sample surfaces using backscattered electron imaging (BEI) and electron probe microanalysis. The following explanations are offered for the observed creep behaviour and the changes that occur under the effect of elevated temperatures.

Using energy dispersive spectroscopy on polished surfaces, the anhydrous phase of the cement paste is recognised by means of its grey level. It is identified as the lightest (almost white) grains due to a high number of backscattered electrons. A comparison between a sealed concrete specimen tested for creep at room temperature 21° C (70° F) shown in Figure 5.14 and one tested at a temperature of 149° C (300° F) shown in Figure 5.18, indicates that the fly ash concrete subjected to higher temperatures contains a lower amount of unhydrated cement. The restraining effect of the anhydrous phase was

discussed in the previous section on drying creep. Any shrinkage that occurs in sealed specimens is affected by the unhydrated cement, and it is lower at room temperature.

The other extreme of the grey spectrum (almost black) is associated with the porosity of the paste. A comparison between Figures 5.14 and 5.18 indicates that fly ash concrete that is subjected to high temperatures develops a paste matrix with a higher degree of porosity. According to previously published literature (Mitsui, et al., 1994) an image magnification of 400x is better suited for the study of cement paste porosity. A comparison of the porosity at the various levels of temperature, using the magnification suggested above, is made in Figures 5.19 through 5.23. The micrographs show that the paste-aggregate interface has a very low porosity and this is due to the low water-cement ratio used in the mixture (Mitsui, et al., 1994). It is also seen from the same micrographs that the bulk cement paste at elevated temperatures is significantly more porous than the fly ash concrete tested at room temperature. The micrograph in Figure 5.23 shows larger and more continuous porous regions in the paste at 177° C (350° F), by comparison to Figure 5.21 which represents a cement paste subjected to a lower temperature of 71° C (160° F). At a higher magnification, Figure 5.24 shows an unreacted fly ash particle surrounded by a highly porous interfacial region. It is expected that a higher degree of porosity produces higher creep and for this reason, higher temperatures produce higher creep strains in the fly ash concrete.



Figure 5.18 BEI micrograph of a polished surface of fly ash concrete at 149° C (Magnification 150x)



Figure 5.19 BEI micrograph of a polished surface of fly ash concrete. Specimen was tested sealed at 21° C and 5.5 MPa (Magnification 400x).



Figure 5.20 BEI micrograph of a polished surface of fly ash concrete. Specimen was tested sealed at 71° C and 5.5 MPa (Magnification 400x).

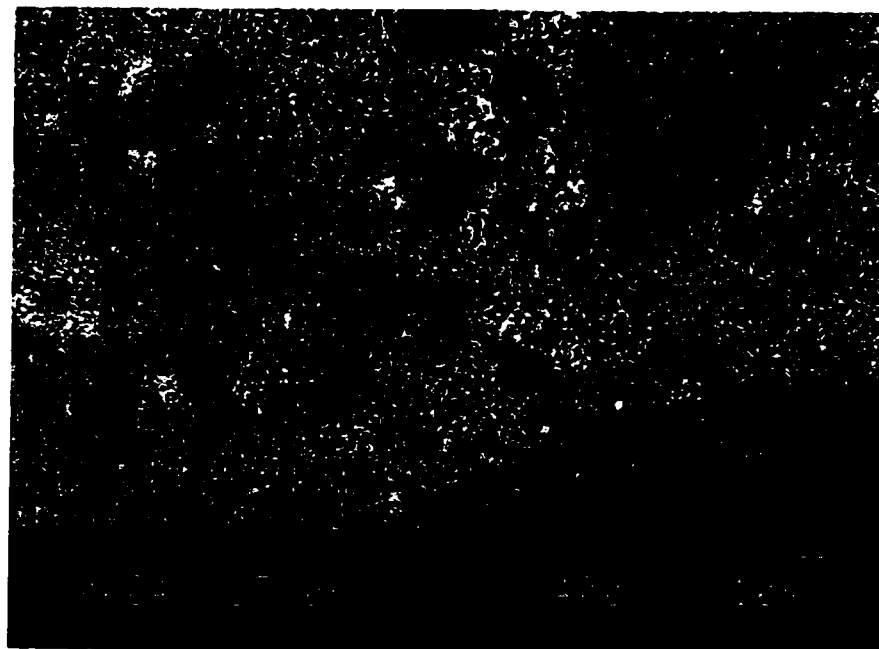


Figure 5.21 BEI micrograph of a polished surface of fly ash concrete. Specimen was tested sealed at 71° C and 13.8 MPa (Magnification 400x).

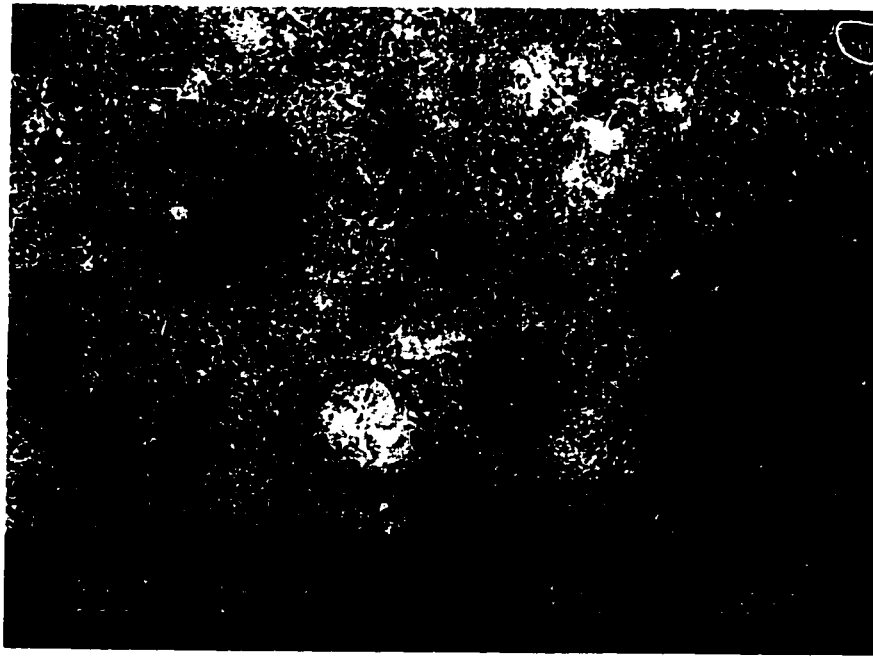


Figure 5.22 BEI micrograph of a polished surface of fly ash concrete. Specimen was tested sealed at 177° C and zero stress (Magnification 400x).

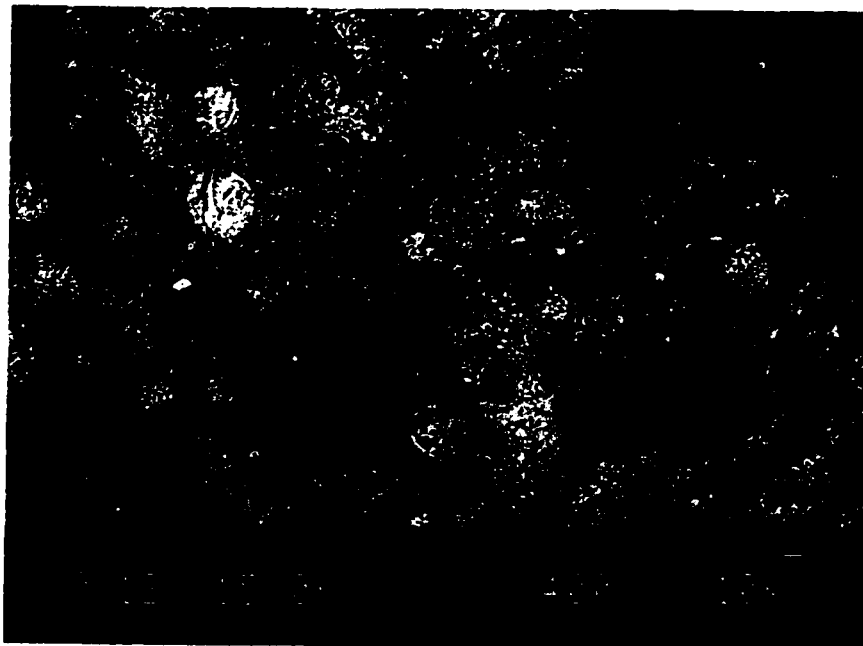


Figure 5.23 BEI micrograph of a polished surface of fly ash concrete. Specimen was tested sealed at 177° C and 13.8 MPa (Magnification 400x).



Figure 5.24 BEI micrograph of a polished surface of fly ash concrete. Specimen was tested sealed at 177° C and 13.8 MPa (Magnification 1000x).

Combining the scanning electron microscope with the electron probe microanalyzer, the composition of the cement paste matrix is identified and the Ca-Si peak ratio is calculated and compared at the various levels of temperature. This comparison is represented by the EDS spectrums of Figures 5.25 and 5.26. Comparing these spectrums of fly ash concrete tested at 149° C (300° F) and 177° C (350° F) respectively, to the paste spectrum of the same mixture tested at 21° C (70° F), in Figure 5.11, it is evident that elevated temperatures cause a chemical transformation producing a paste matrix of a significantly lower Ca content compared to Si. The Ca-Si peak ratio becomes lower as the temperature rises from 21° C to 149° C and 177° C and it assumes values of 0.8 and 0.67 respectively, well below the value of 1.28 found at room temperature.

Secondary electron imaging is used with gold coated fractured samples in order to examine the microstructure of the paste at higher temperatures and compare it to the paste of the fly ash concrete that was tested at 21° C (70° F). Figure 5.27 indicates a more fibrous structure of the cement paste at 71° C (160° F) compared to concrete tested for creep at room temperature (Figures 5.5 and 5.17). Crystals of calcium hydroxide with a preferred orientation to the surface of a removed aggregate are present in the bulk cement paste at the area marked (A) in Figure 5.27. At a higher magnification, Figure 5.28 indicates a fibrous reaction product surrounding a partly exposed fly ash particle. The presence of Ca(OH)_2 crystals with preferred orientation is also evident in the bulk matrix of concrete tested at 232° C (450° F) shown in Figure 5.29. The EDS spectrum of the parallel "fibres" of Figure 5.29 is shown in Figure 5.30. It was seen in the previous section that at room temperature there was no evidence of Ca(OH)_2 in the bulk paste of fly ash concrete and only a very minor amount was present inside air voids. The presence of calcium hydroxide in the bulk paste of the fly ash concrete at elevated temperatures, produces a more unstable matrix that undergoes higher creep strains.

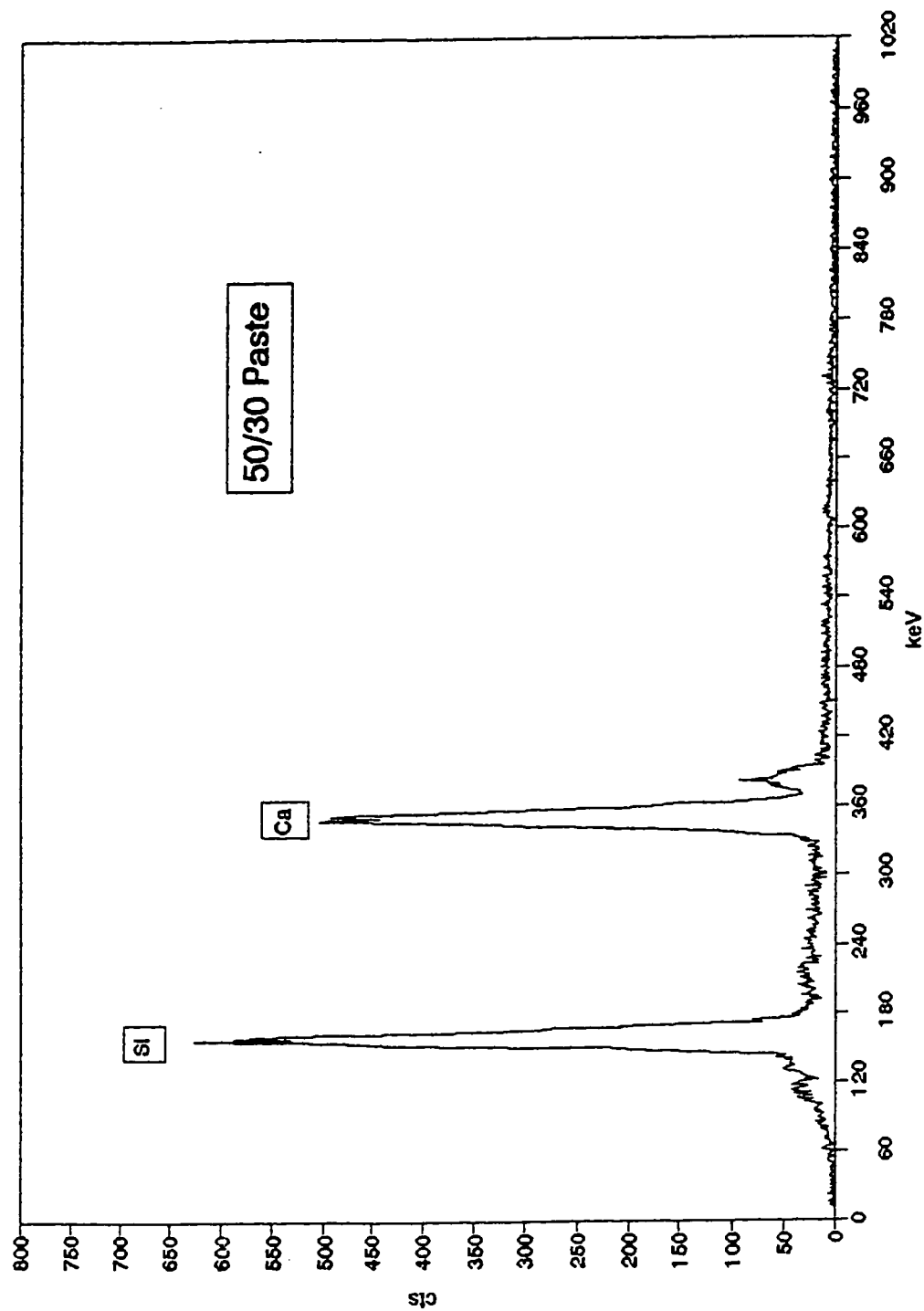


Figure 5.25 EDS spectrum of hydrated cement paste from a polished surface of a 50% fly ash concrete. Specimen was subjected to 149° C.

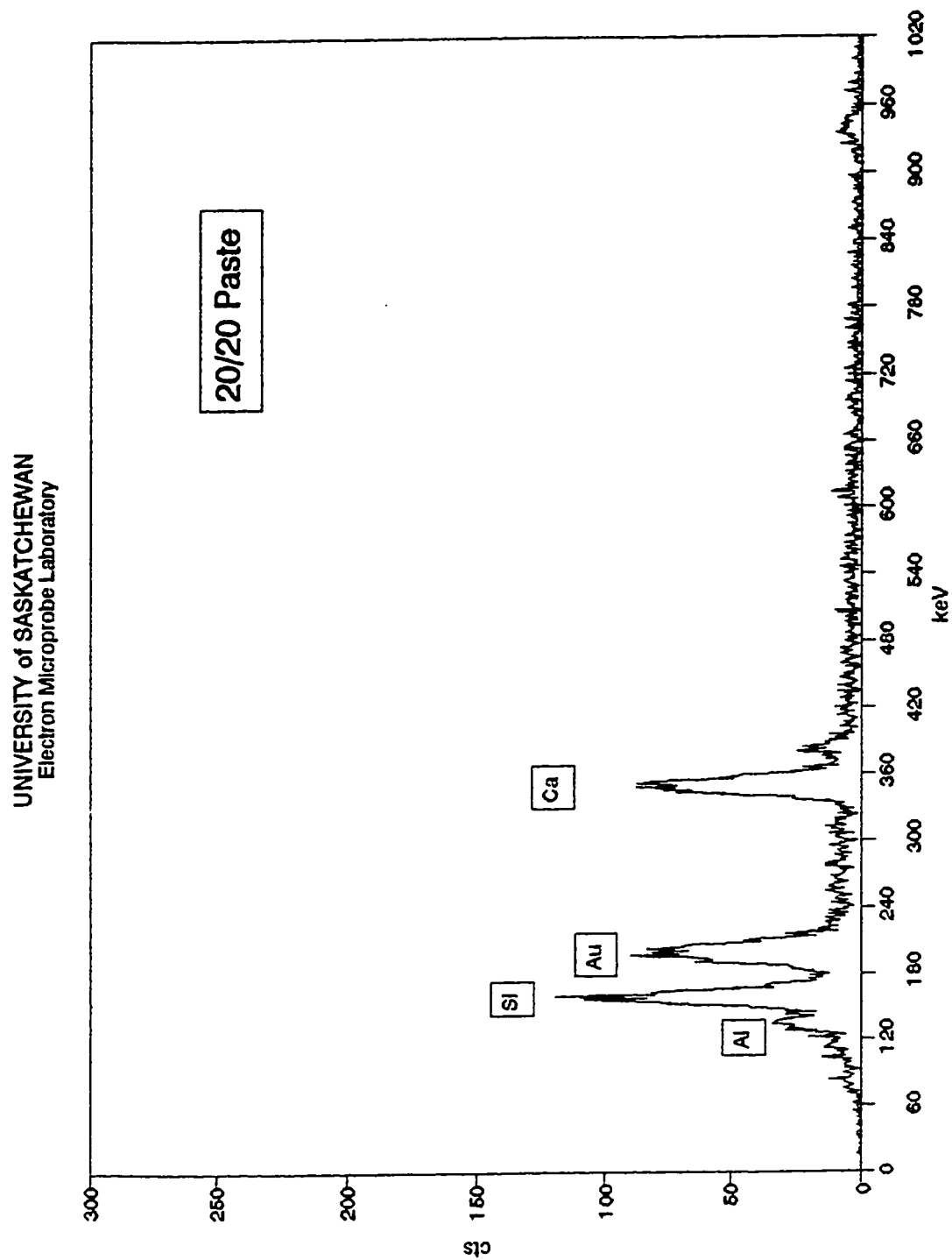


Figure 5.26 EDS spectrum of hydrated cement paste from a fractured surface of a 50% fly ash concrete. Specimen was subjected to 177° C.

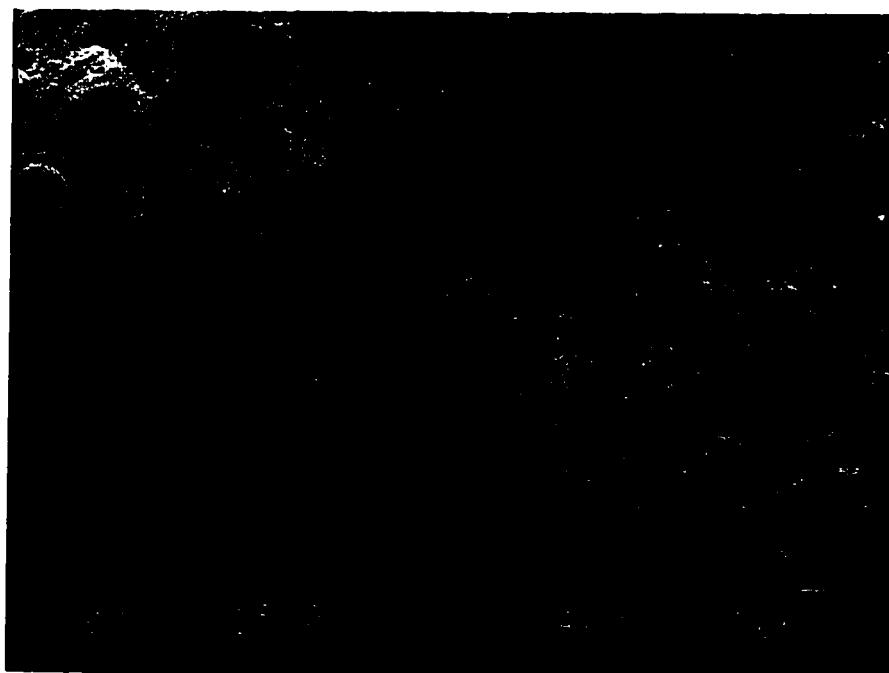


Figure 5.27 SEI micrograph of a fractured surface from 50% fly ash concrete tested for creep at 71° C and a stress level of 13.8 MPa (Magnification 400x).

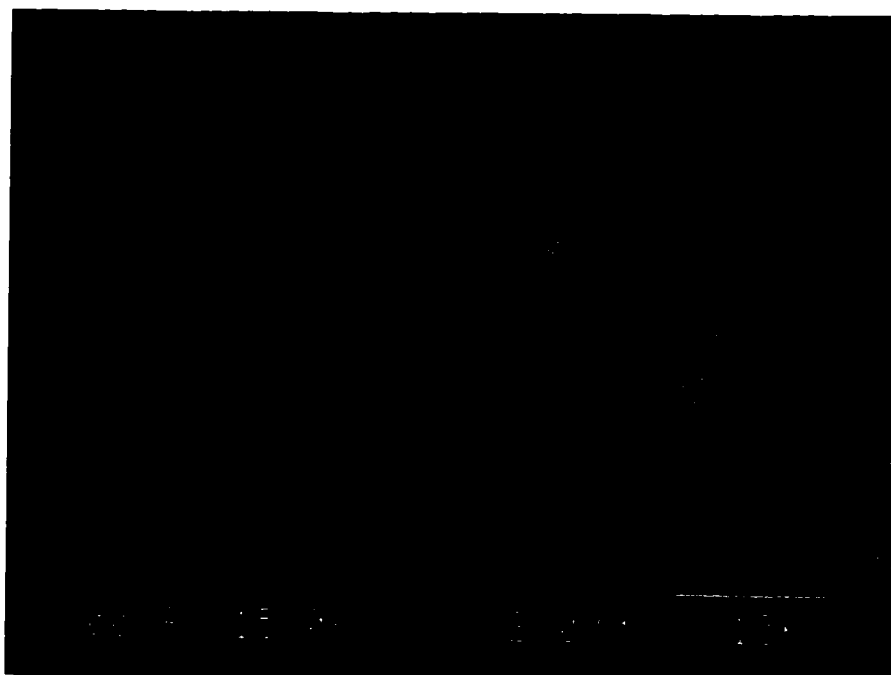


Figure 5.28 SEI micrograph of a fractured surface from 50% fly ash concrete tested for creep at 71° C and a stress level of 13.8 MPa (Magnification 2000x).

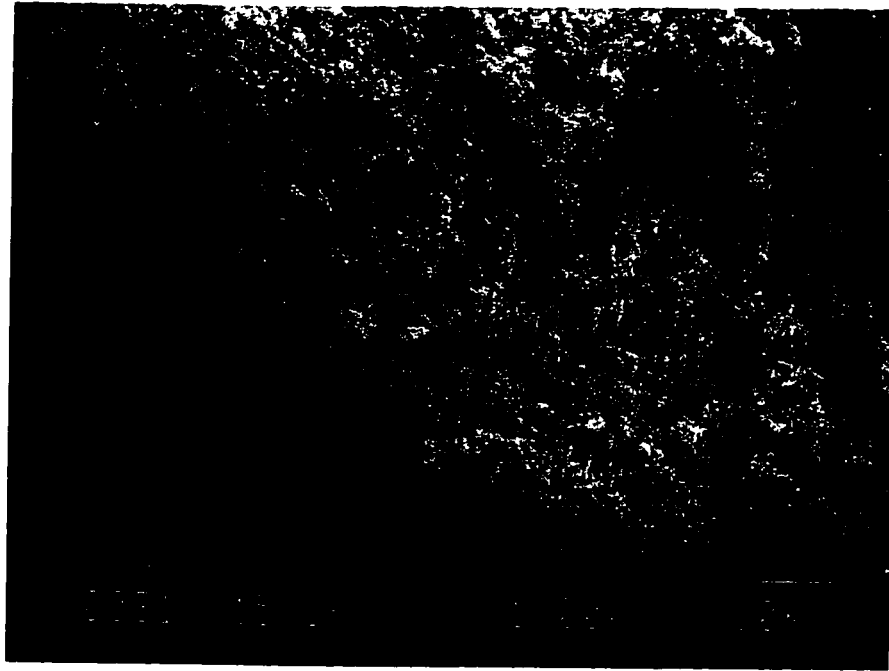


Figure 5.29 SEI micrograph of a fractured surface from 50% fly ash concrete tested at 232° C and a zero stress level (Magnification 1000x).

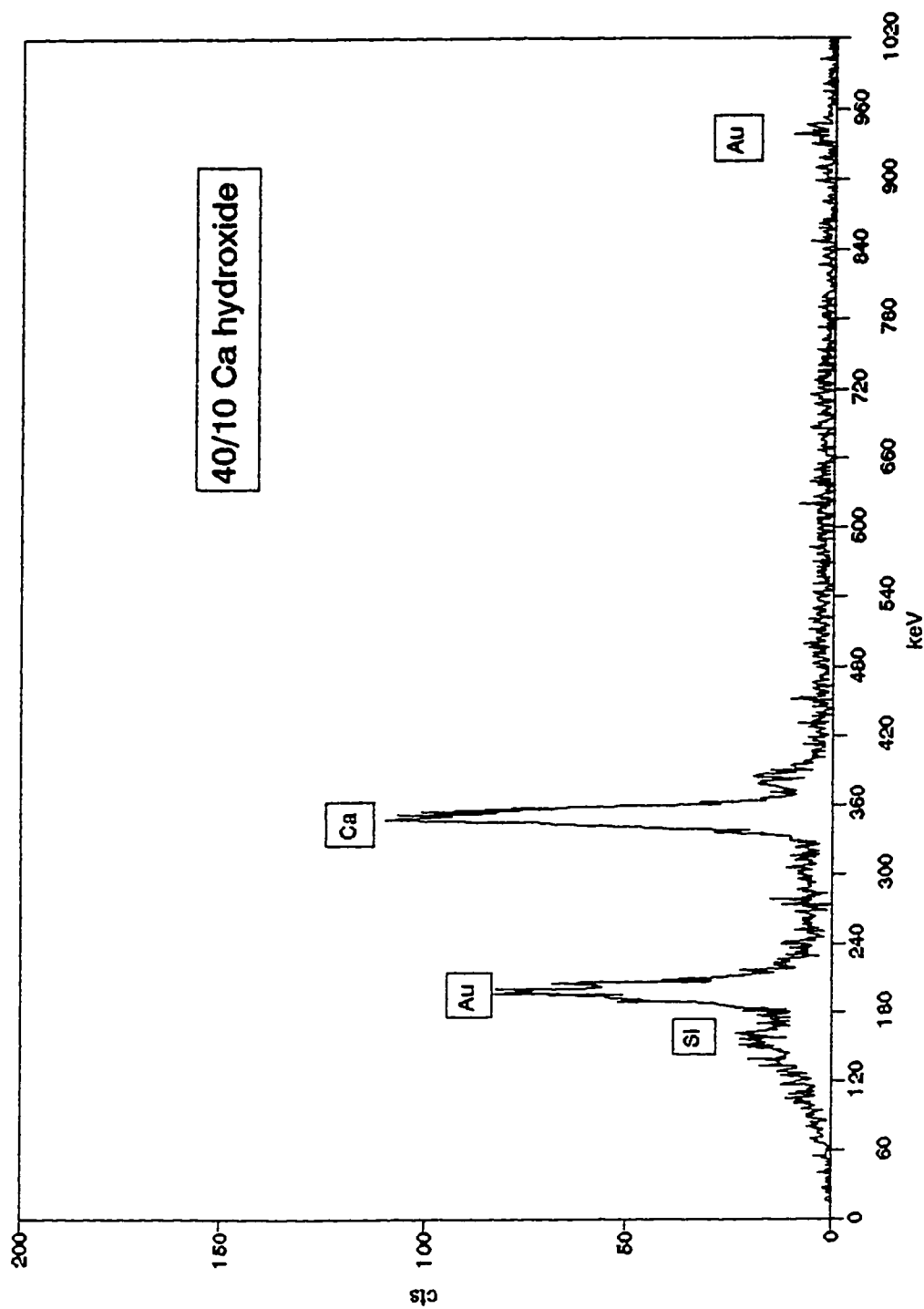


Figure 5.30 EDS spectrum of calcium hydroxide crystals from the fractured surface of fly ash concrete shown in Figure 5.29. Specimen was subjected to 232° C.

5.4 Frost Resistance

The mechanism by which repeated cycles of freezing-and-thawing affect concrete, is cracking and loosening of bonds between aggregate and cement paste. This is the physical effect from the formation of ice within the pore system of the cement paste. The beneficial effects of adequate air entrainment against the tensile forces that develop due to the freezing and expansion of water have been established from theoretical studies at the Portland Cement Association during 1940-60. Minute air bubbles act as "relaxation chambers" for the pressures caused by ice formation (Powers and Brownnyard, 1948). Mather (1990) outlined the importance of the combined effects of air-entrainment and low water/cement ratio for concrete that is frost resistant. He indicated that a lower water/cement ratio (0.5 compared to 0.8) increases the durability of air-entrained concrete significantly. At the same time Mather discussed that non-air-entrained concrete barely reached a durability factor of 10, while a lower water/cement ratio (0.5) and compressive strengths in excess of 48 MPa (7000 psi) improved the frost resistance of such concrete marginally. In the same report, Mather concluded that concrete will resist the effects of freezing-and-thawing provided it contains sound aggregate, it has an adequate air-void system through the use of an air-entraining agent and that when subjected to freezing-and-thawing it is mature enough to have attained a compressive strength of 28 MPa (4000 psi).

Low porosity or a refined and discontinuous pore system has an important bearing on the frost resistance of concrete. A dense matrix that prevents moisture from saturating the concrete, reduces the vulnerability of the material to frost deterioration. Studies on blended cement concretes indicated that a lower permeability was achieved with a 20% replacement of the cement with Class F fly ash compared to a similarly cured plain concrete (Saricimen, et al., 1995). Using a high volume Class C fly ash replacement, Naik, et al., (1995), obtained very high durability factors. Porosity measurements

concluded that fly ash cement blends are characterized by relatively large but discontinuous pores that replace continuous capillary porosity (Regourd, 1987). A higher total porosity is related to the gaps around fly ash particles as well as the pores inside the particles.

The test results of the air-entrained as well as the non-air-entrained fly ash and control concretes of the present study have been discussed in the previous chapter and the beneficial effect of the air-entrainment on the durability of both concretes has been demonstrated. Both concretes were produced with a very low water-cement ratio, thus, having a very dense matrix with low porosity. In addition, the pozzolanic reaction of the fly ash produces a further densified matrix with a refined pore system. From the EDS spectrums in preceding figures that compare the composition of the matrix in the fly ash and control concretes, it was shown that the C-S-H in the fly ash concrete is more silica rich and it has a lower Ca/Si ratio. Regourd (1987) reported a Ca/Si ratio in fly ash concrete between 1 and 1.50. C-S-H of low Ca-Si ratio has been described to have a higher degree of polymerization and a lower density (Roberts, 1989). This reaction product is able to fill more capillary space than normal C-S-H and to further refine the pore structure of the paste, thus, producing concrete with increased impermeability and higher strength (Roberts, 1989). For this reason the air-entrained fly ash concrete of this study demonstrated a frost resistance behaviour that was comparable to that of the control concrete.

The microstructure that developed in the two concretes following 300 cycles of alternating freezing-and-thawing is described in the following SEI micrographs. Figure 5.31 shows the structure of the non-air-entrained fly ash concrete. Partly reacted fly ash particles are surrounded by crystals of calcium hydroxide and ettringite. Ettringite needles are also evident in the control concrete as shown in Figure 5.32 growing on the surface of a quartz grain. The microstructure of the air-entrained fly ash concrete is

described in Figure 5.33. A fairly dense matrix is indicated with a notable absence of calcium hydroxide crystals. At a higher magnification, Figure 5.34 indicates a fibrous type of material, at the aggregate interface, resembling ettringite needles. However, energy dispersive spectroscopy indicates that this material has the same composition as the paste. This is verified in Figure 5.35 which represents the EDS spectrum of the fibrous material indicating a C-S-H composition with a low Ca/Si ratio. It is also noted from the same figure that aluminum is absent from the needle-like form of the matrix. By contrast, the EDS spectrum for ettringite is characterized by strong peaks of calcium, sulphur and aluminum as it is indicated in Figure 5.36.

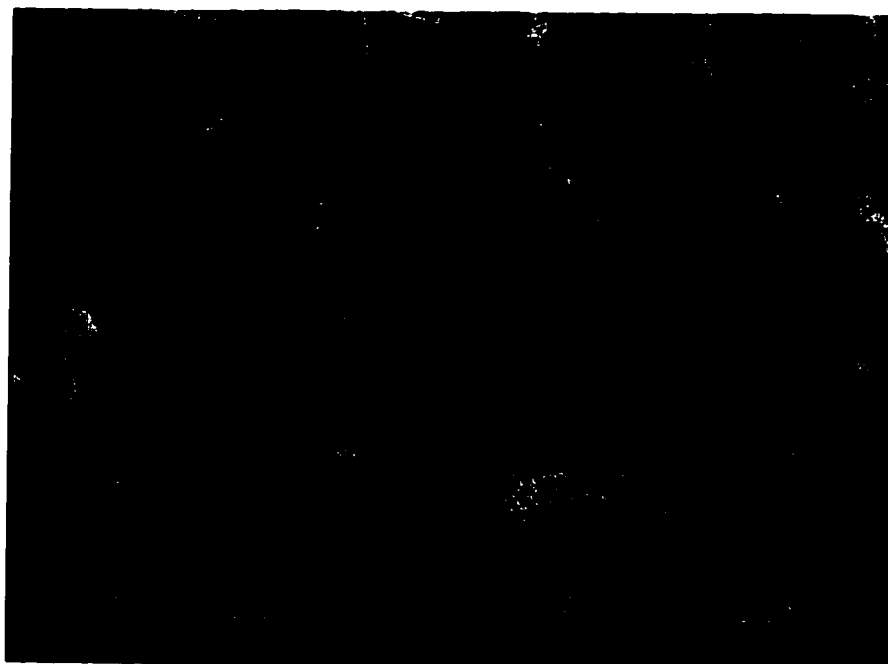


Figure 5.31 SEI micrograph of a fractured surface of non-air-entrained fly ash concrete following freezing-and-thawing (Magnification 400x).



Figure 5.32 SEI micrograph of a fractured surface of air-entrained control concrete following 300 cycles of freezing-and-thawing (Magnification 400x).

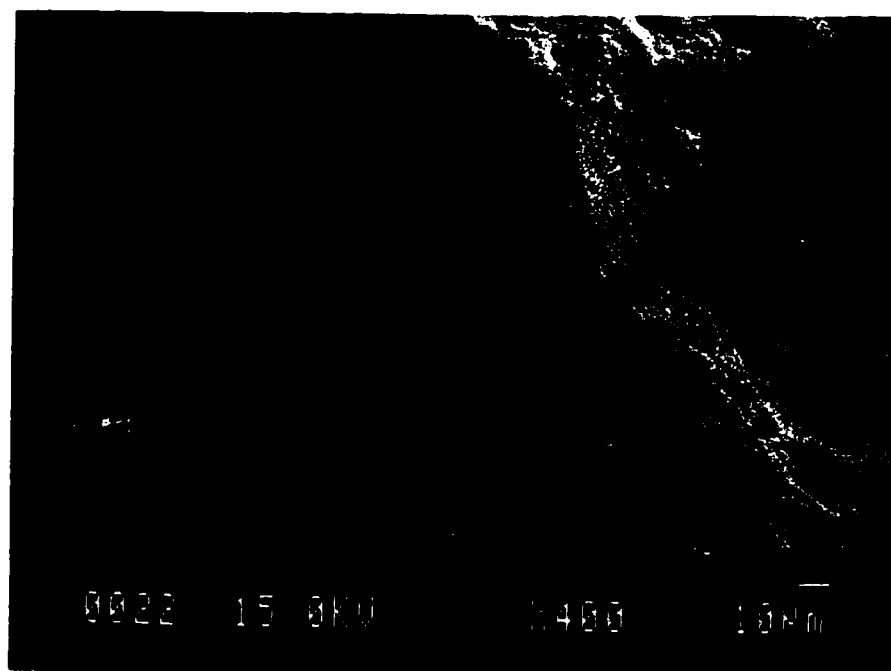


Figure 5.33 SEI micrograph of a fractured surface of air-entrained fly ash concrete following 300 cycles of freezing-and-thawing (Magnification 400x).

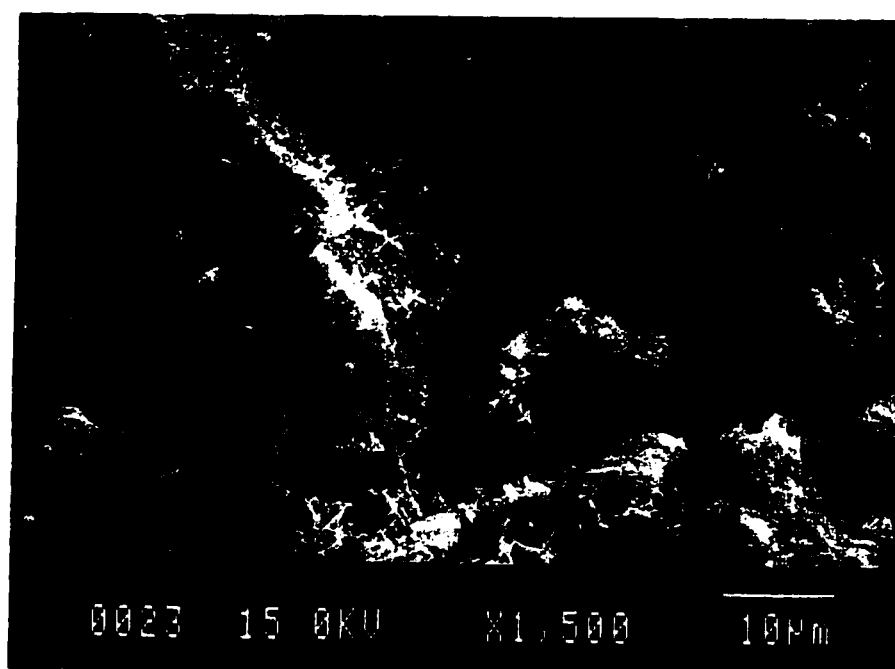


Figure 5.34 SEI micrograph of a fractured surface of air-entrained fly ash concrete following 300 cycles of freezing-and-thawing (Magnification 1500x).

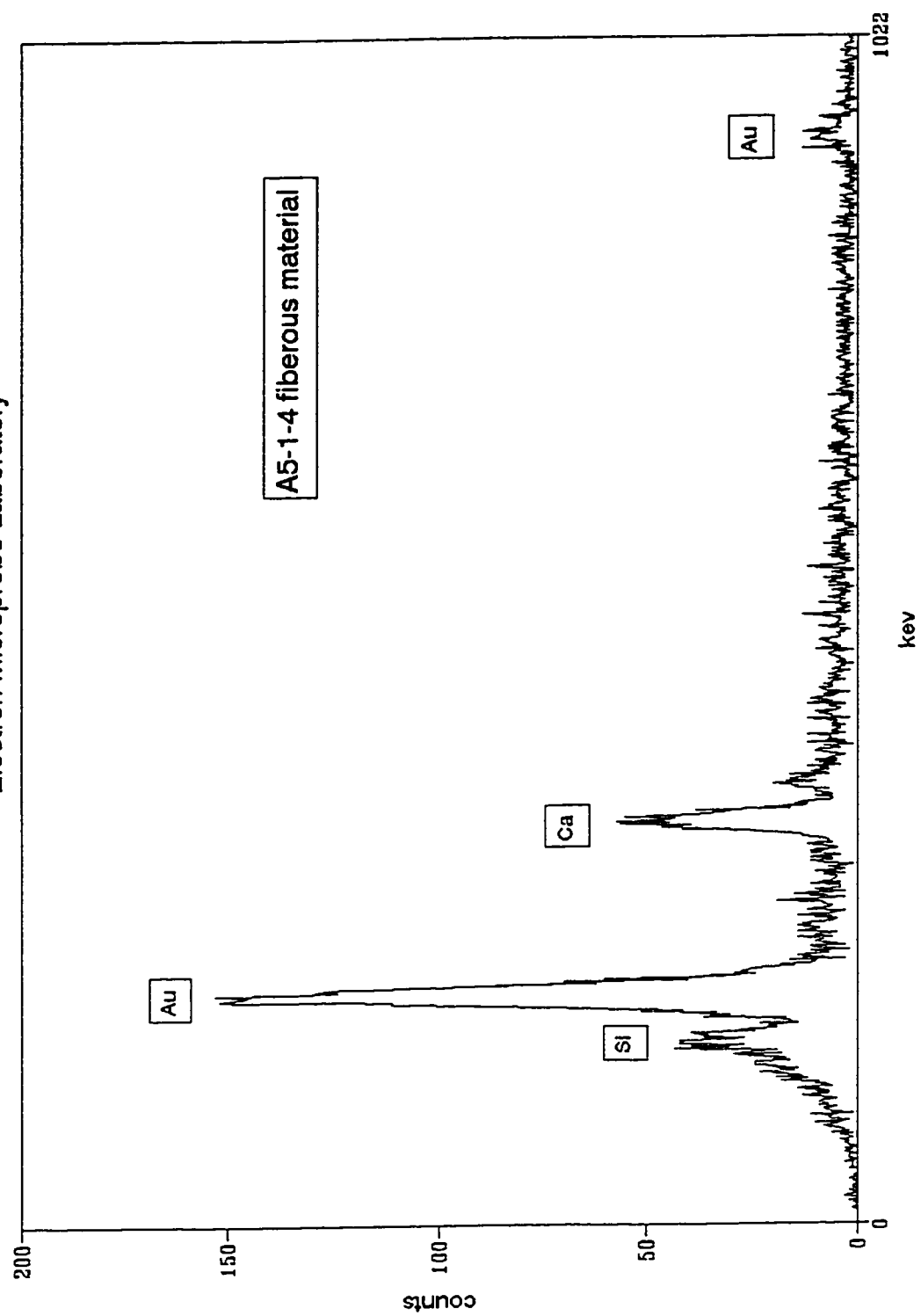


Figure 5.35 EDS spectrum of the fibrous material of Figure 5.34.

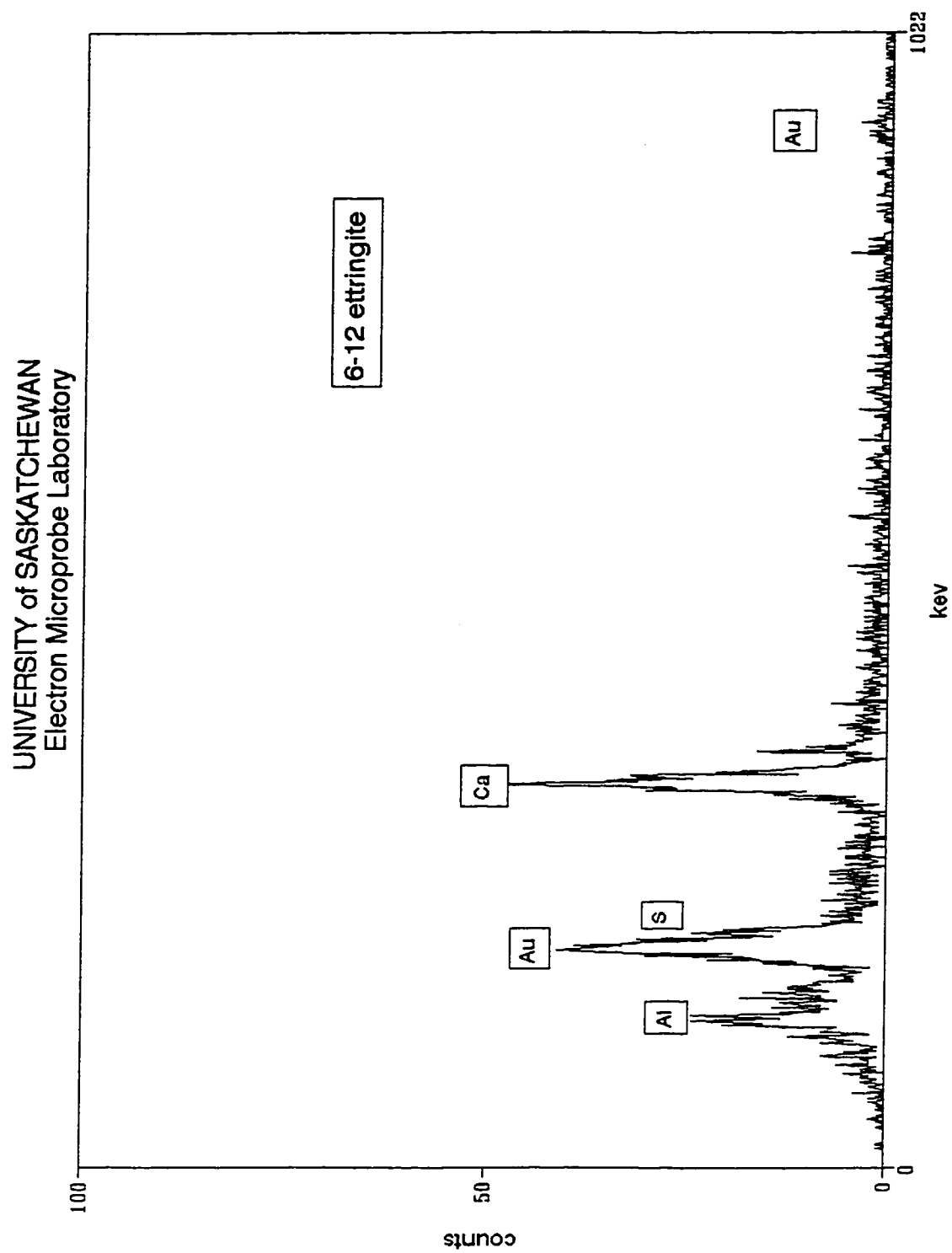


Figure 5.36 EDS spectrum of ettringite.

5.5 Resistance to Sulphate Attack

The mechanism of deterioration of concrete exposed to a hostile environment containing sulphates is attributed to the expansion of the paste and disruption of the concrete due to crack formation as it has been described in various publications (Lea, 1976, Neville, 1981, Mehta, 1992, Bonen and Sarkar, 1993). This occurs when the Ca(OH)_2 , that is present as a by-product of hydration of the cement components, reacts with the sulphate ions to form gypsum. Also the calcium-aluminate-hydrate phase reacts chemically with the sulphate ions forming calcium sulfoaluminate ($3\text{CaO}\cdot\text{Al}_2\text{O}_3\cdot3\text{CaSO}_4\cdot31\text{H}_2\text{O}$), commonly called ettringite. Both substances, gypsum and ettringite, have a volume that is considerably greater than the volume they replace and the tensile stresses that develop in the process are sufficient to cause cracking and hence, disruption of the paste. Use of cement with a low content in the aluminate phase, is intended to restrain sulphate attack by controlling the chemistry of the cement.

More effective ways have been suggested to improve the sulphate resistance of concrete (Mehta, 1992, Neville, 1981). The permeability of the concrete is a very significant factor in preventing sulphate attack. A low water-cement ratio produces a denser paste and prevents sulphate ions from penetrating the interior of the concrete. Partial replacement of cement with pozzolanic mineral admixtures is also effective in reducing the vulnerability of the concrete to sulphate deterioration owing to the absence of Ca(OH)_2 in the paste. The beneficial effect of fly ash on the sulphate resistance of concrete has been documented in various publications (Nasser and Lai, 1991, Tikalsky and Carrasquillo, 1992, Tikalsky and Carrasquillo, 1993).

The microstructural features of the control and fly ash concretes, following completion of the sulphate resistance testing, were studied using secondary electron imaging on fractured samples. Also backscattered electron imaging on polished sample

surfaces was used to study the composition of the various phases of the paste. In addition, X-ray maps were generated from the polished surfaces to detect any deposition of unusually large amounts of sulphur (as in gypsum and ettringite) in the bulk matrix and at the paste-aggregate interfaces. The X-ray maps were generated by positioning a wavelength spectrometer to the sulphur position and scanning the sample (generally at a magnification of 200x) for 10 minutes. For this study, the surfaces were prepared by mounting the sample in a plastic ring and impregnating with cold epoxy under vacuum. The samples were then ground flat on a dry 200 grit lap grinder. Final polish was achieved with 0.1 micron diamond polish on a lap polisher.

From the secondary electron image (SEI) micrographs the presence of crystals of Ca(OH)_2 and ettringite is evident in the cement paste of the control concrete. In the interior surface of an air void, Figure 5.37 shows crystals of ettringite with their characteristic needle-like structure growing among hexagonal plates of Ca(OH)_2 in a control concrete specimen that was immersed in the Na_2SO_4 solution for 330 days. Similarly, Figure 5.38 shows needles of ettringite growing among large hexagonal crystals of Ca(OH)_2 in the control concrete that was immersed in distilled water for the same duration of time (330 days) and was used as reference for length changes and development of microstructural features.

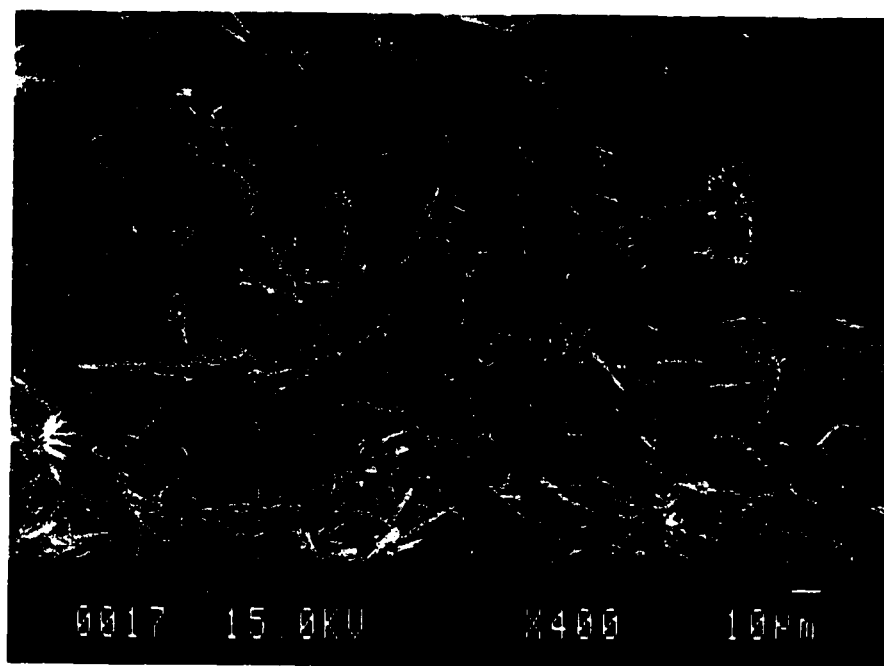


Figure 5.37 SEI micrograph of a fractured surface of the control concrete. Specimen was immersed in Na_2SO_4 solution for 330 days. (Magnification 400x).

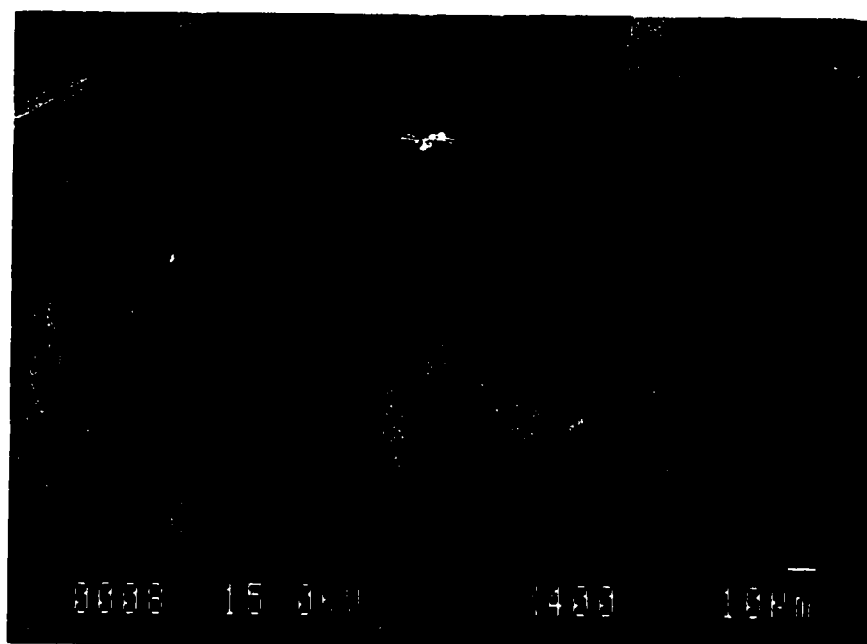


Figure 5.38 SEI micrograph of a fractured surface of the control concrete. Specimen was immersed in distilled water for 330 days. (Magnification 400x).

The morphology of the fly ash concrete, after being immersed in the sodium sulphate solution for 330 days, is shown in Figure 5.39. A dense paste is evident, interspersed with areas of a sheet-like material that is shown at a higher magnification in Figure 5.40. Even though this material resembles plates of calcium hydroxide, the EDS spectrum indicates a high content of alumina and silica. This analysis is shown in Figure 5.41 indicating strong peaks of Al and Si leading to the conclusion that this is a structure that the paste assumes and it is possibly the hexagonal form of calcium aluminate hydrate as described by Neville (1981). A similar sheet-like structure of the paste is shown in Figure 5.42 in the fly ash concrete that was immersed in distilled water as it is indicated from the EDS analysis in Figure 5.43. Nowhere in the above samples of fly ash concrete was there evidence of ettringite or Ca(OH)_2 due to the effect of the pozzolanic reaction.

Following immersion of the prism test specimens in the sulphate solution for 330 days, the composition of the cement paste in the control and fly ash concretes was studied by using samples from the inner core of the prisms as well as samples from the outer edge. X-ray maps of sulphur, as described above, were also generated using the polished surfaces from the interior and exterior of the concrete specimens. A higher concentration of sulphur would be expected around aggregates due to the higher content of calcium hydroxide at the interfaces. Bonen and Sarkar (1993), generated backscattered electron images of similarly prepared polished surfaces of plain concrete with a 0.4 water-cement ratio. They presented BEI micrographs showing gypsum deposits up to 50 microns thick surrounding the aggregate at the interface with the paste.

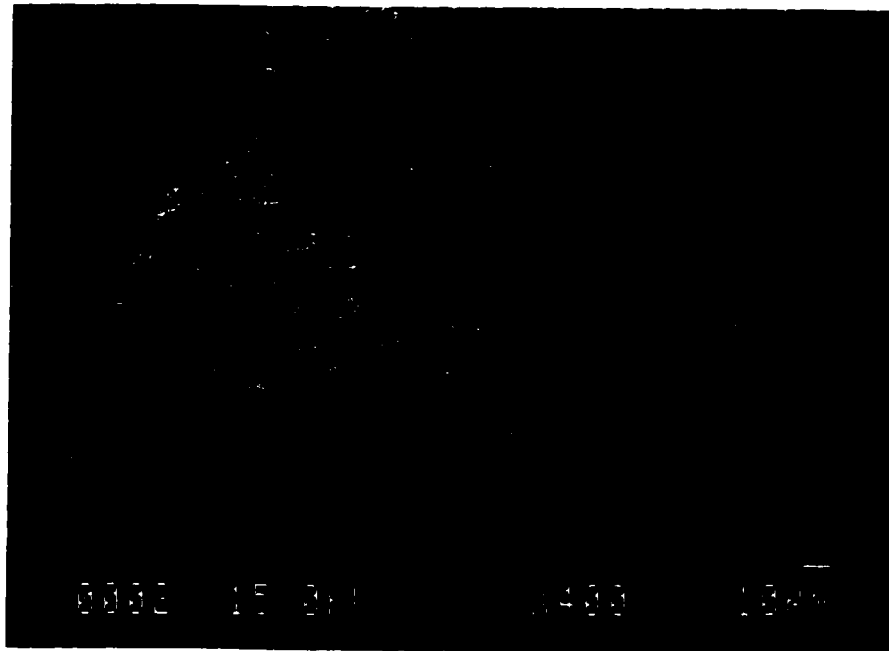


Figure 5.39 SEI micrograph of a fractured surface of fly ash concrete. Specimen was immersed in Na_2SO_4 solution for 330 days. (Magnification 400x).

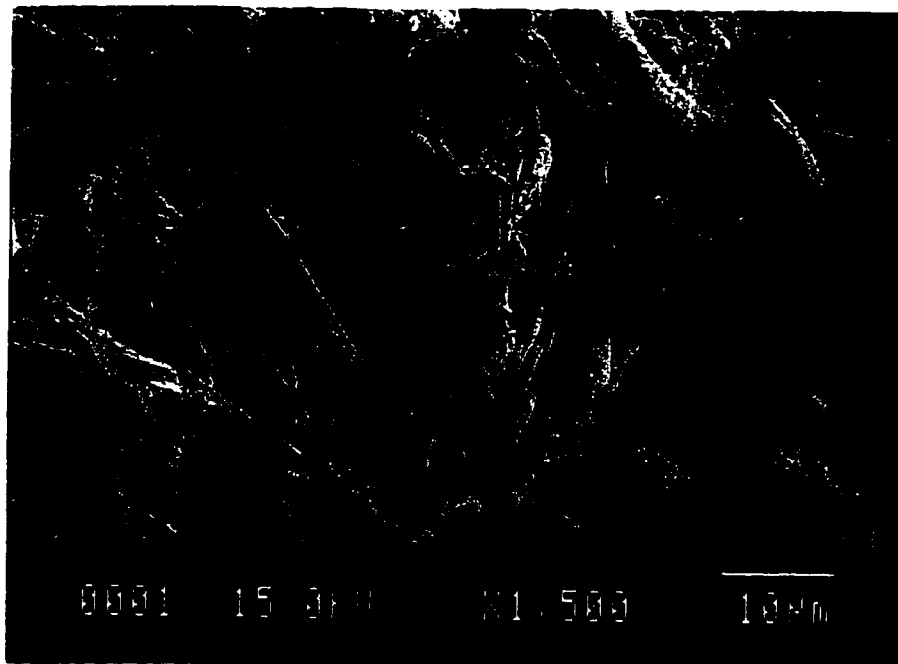


Figure 5.40 SEI micrograph of a fractured surface of fly ash concrete. Specimen was immersed in Na_2SO_4 solution for 330 days. (Magnification 1500x).

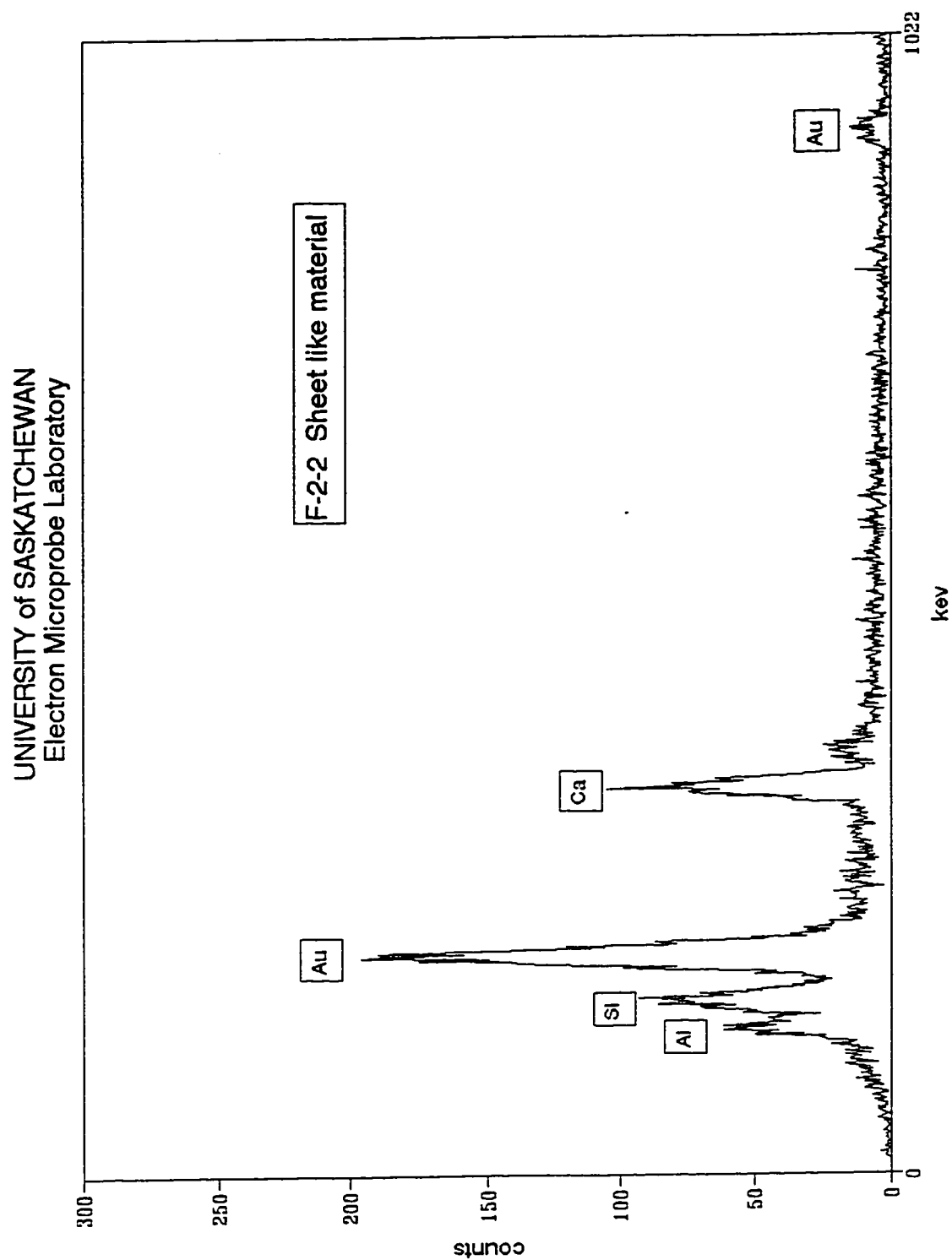


Figure 5.41 EDS spectrum of the sheet-like material shown in Figure 5.40 in a fly ash concrete specimen that was immersed in Na_2SO_4 solution for 330 days.

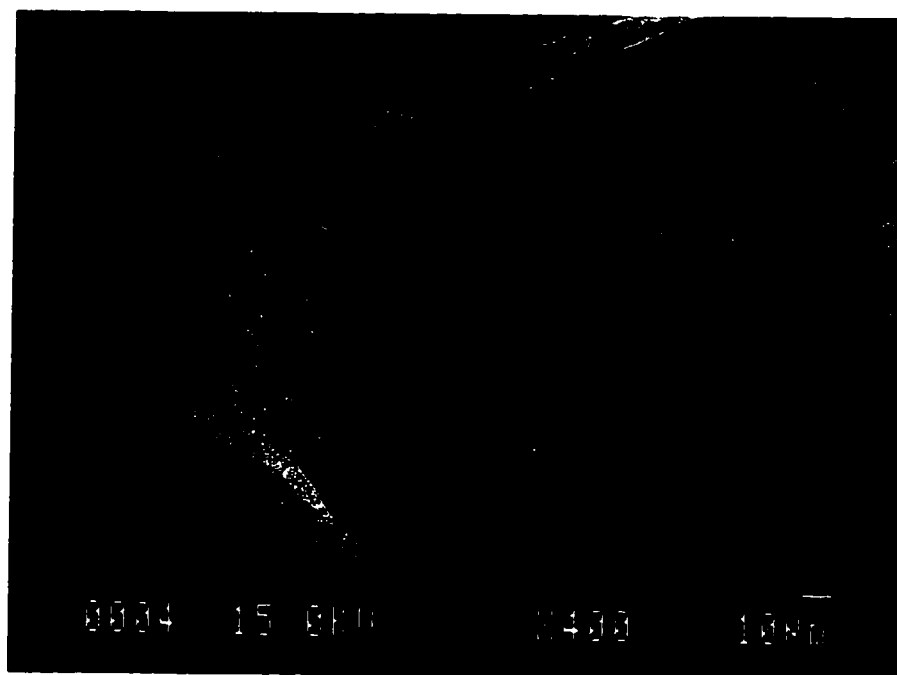


Figure 5.42 SEI micrograph of a fractured surface of fly ash concrete. Specimen was immersed in distilled water for 330 days. (Magnification 400x).

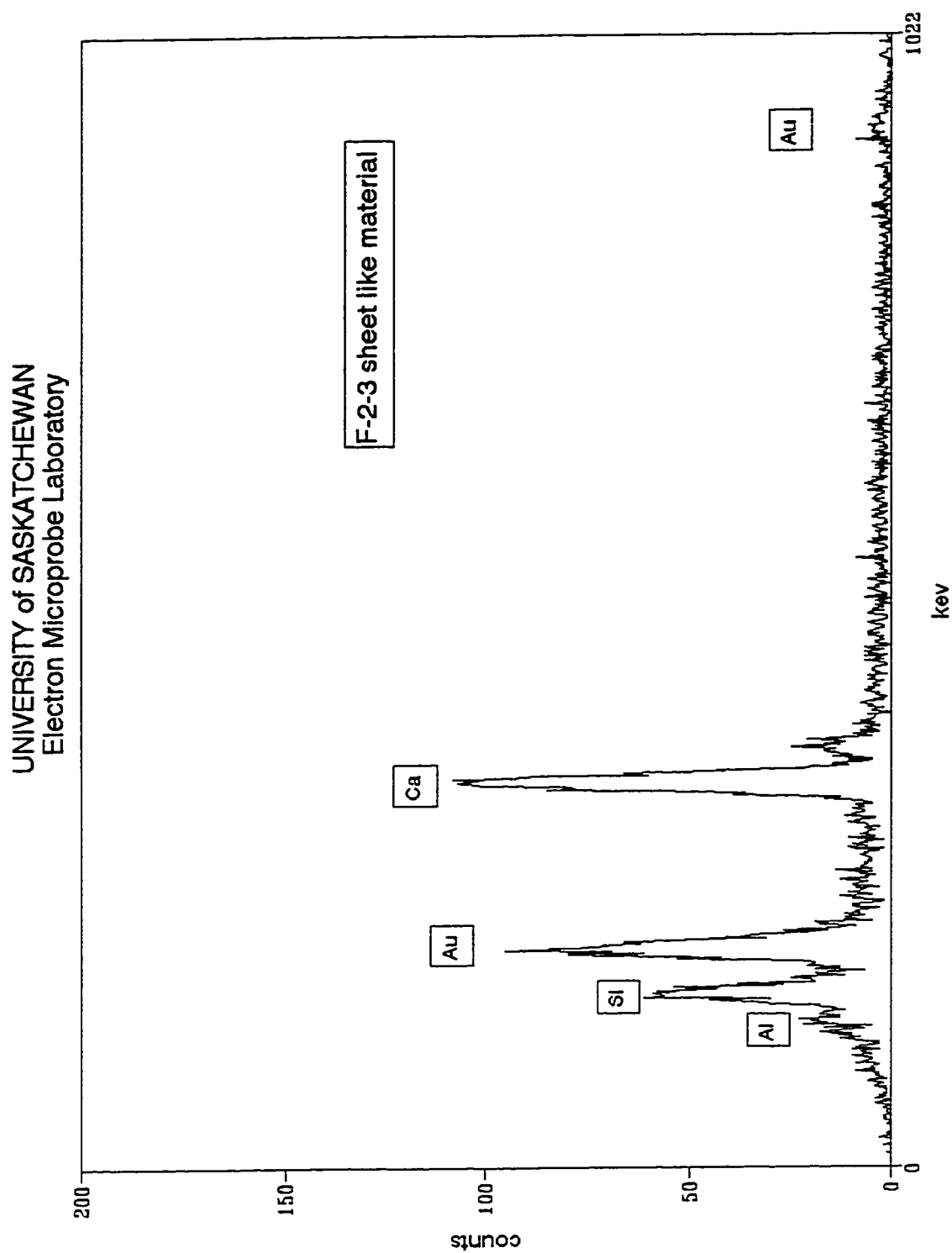


Figure 5.43 EDS spectrum of the sheet-like material shown in Figure 5.42 in a fly ash concrete specimen that was immersed in distilled water for 330 days.

The X-ray maps of sulphur and their corresponding BEI micrographs for the control and fly ash concretes of the present study are shown in Figures 5.44 through 5.55. A very low concentration of sulphur is noted from the above figures in both concretes. The X-ray maps of sulphur indicate a uniform distribution of sulphur counts throughout the matrix and there appears to be no higher concentration at the aggregate interfaces with the cement paste in either the control or the fly ash concrete samples. The water-cement ratio in the concrete of the present study was kept at a low level of approximately 0.3, thus forming a very dense matrix with a low permeability. For this reason, the sulphate ions could not penetrate the cement paste and there was no gypsum or ettringite deposits in the paste or around aggregates.

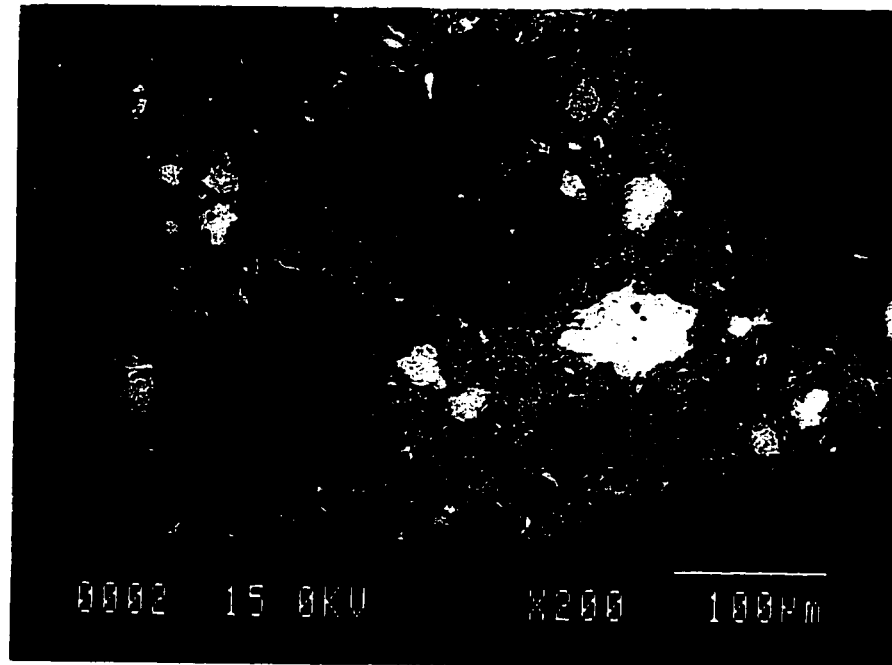


Figure 5.44 BEI micrograph of a polished surface from the inner core of control concrete. Specimen was immersed in Na_2SO_4 solution for 330 days (Magnification 200x).

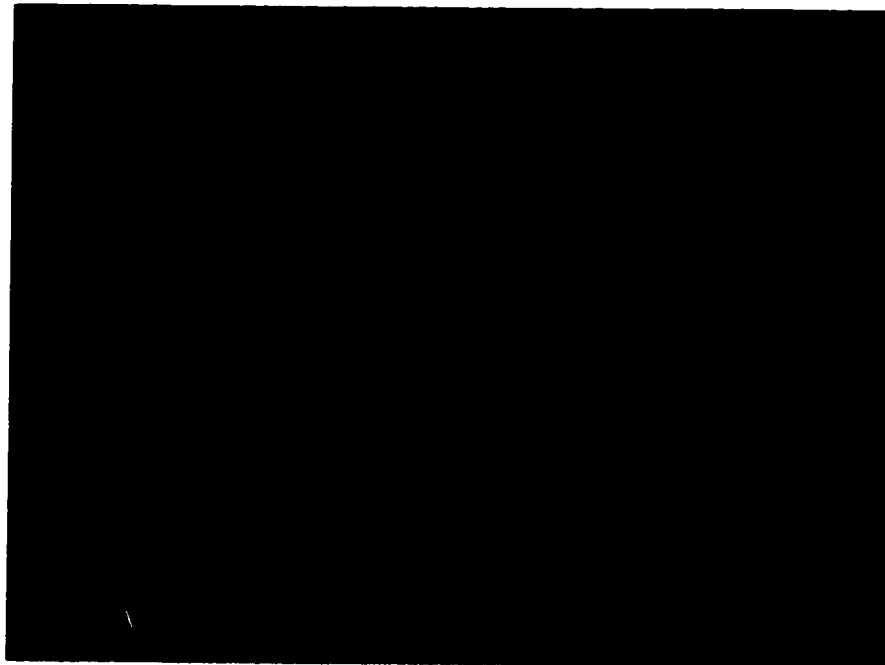


Figure 5.45 X-ray map of sulphur corresponding to the BEI micrograph above (Magnification 200x).

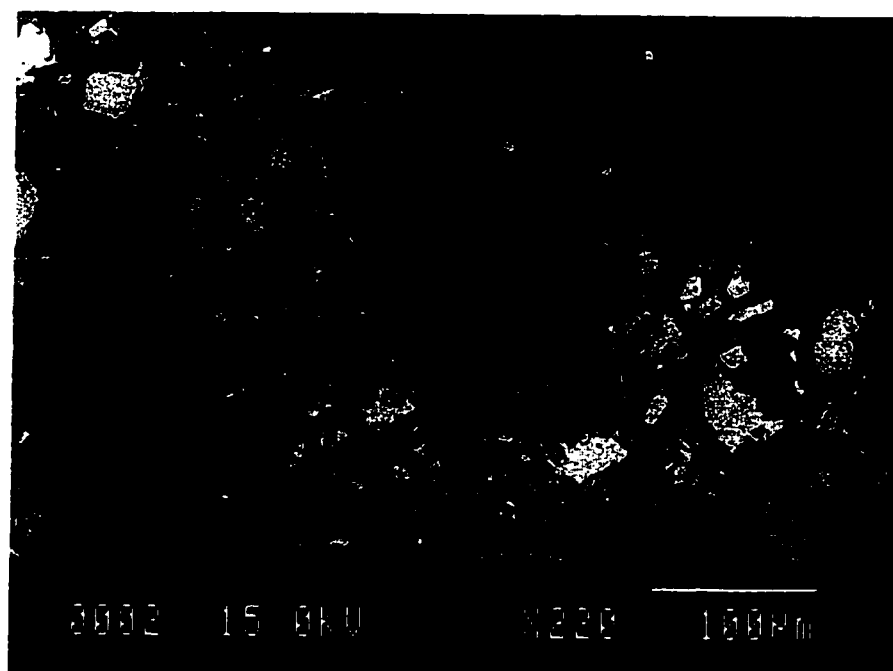


Figure 5.46 BEI micrograph of a polished surface from the outer edge of control concrete. Specimen was immersed in Na_2SO_4 solution for 330 days (Magnification 200x).



Figure 5.47 X-ray map of sulphur corresponding to the BEI micrograph above (Magnification 200x).

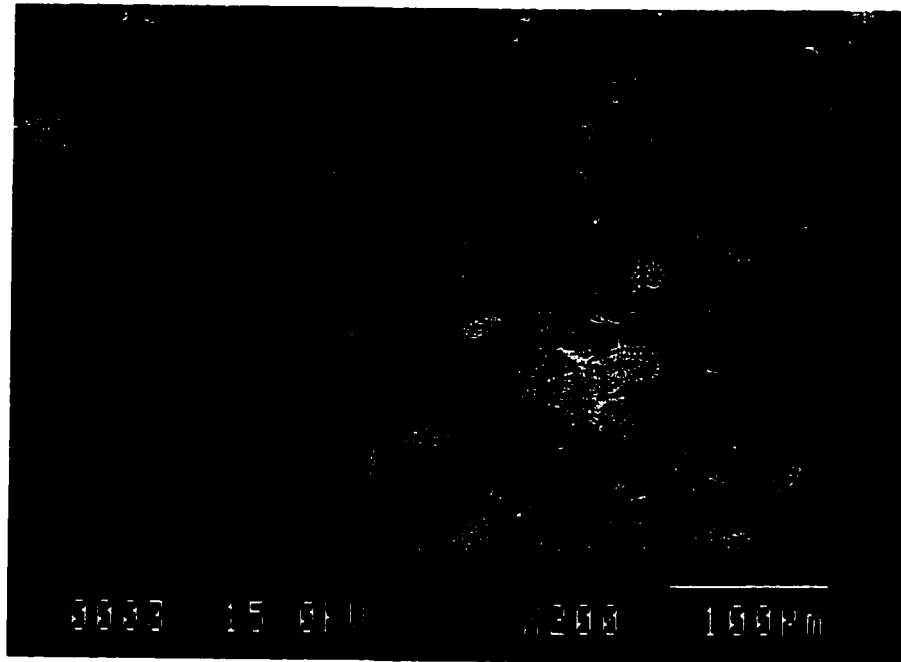


Figure 5.48 BEI micrograph of a polished surface from the outer edge of control concrete. Specimen was immersed in distilled water for 330 days (Magnification 200x).



Figure 5.49 X-ray map of sulphur corresponding to the BEI micrograph above (Magnification 200x).

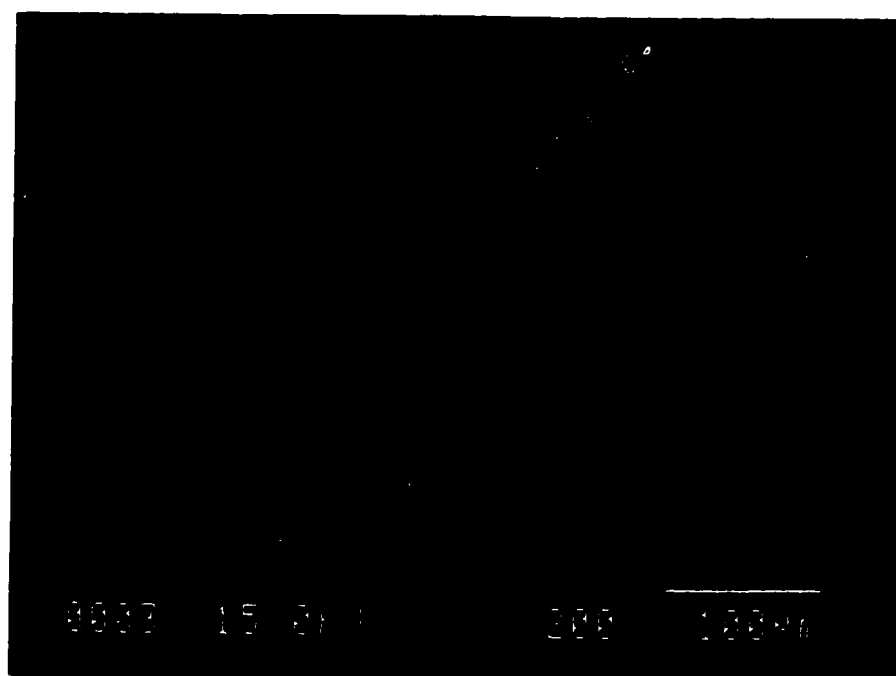


Figure 5.50 BEI micrograph of a polished surface from the inner core of fly ash concrete. Specimen was immersed in Na_2SO_4 solution for 330 days (Magnification 200x).2

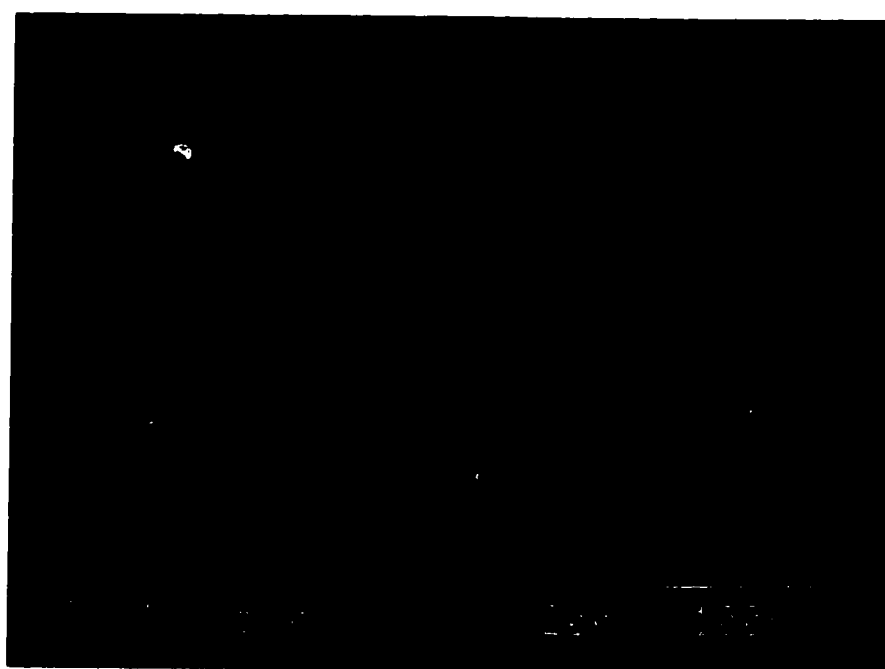


Figure 5.51 X-ray map of sulphur corresponding to the BEI micrograph above (Magnification 200x).

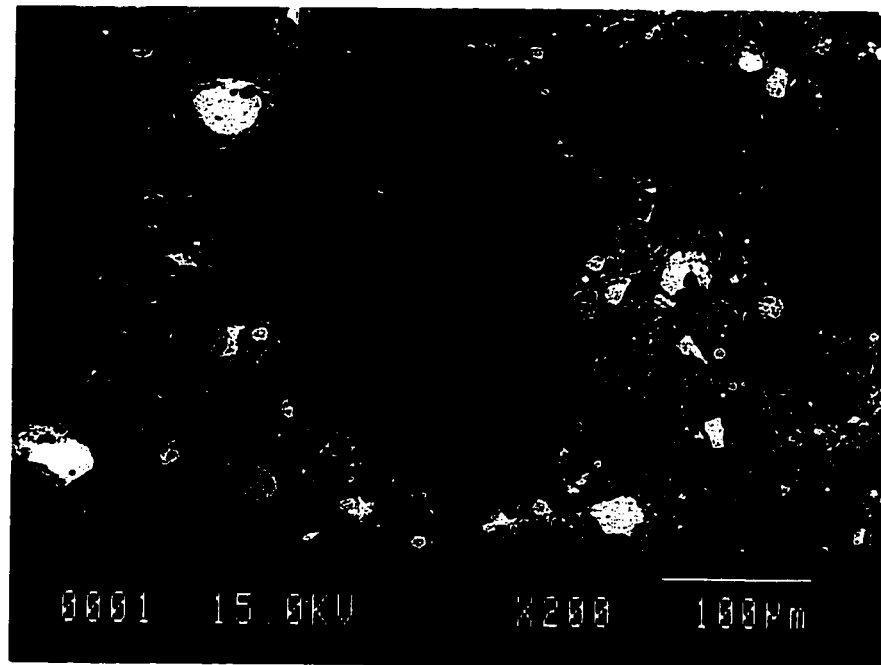


Figure 5.52 BEI micrograph of a polished surface from the outer edge of fly ash concrete. Specimen was immersed in Na_2SO_4 solution for 330 days (Magnification 200x).

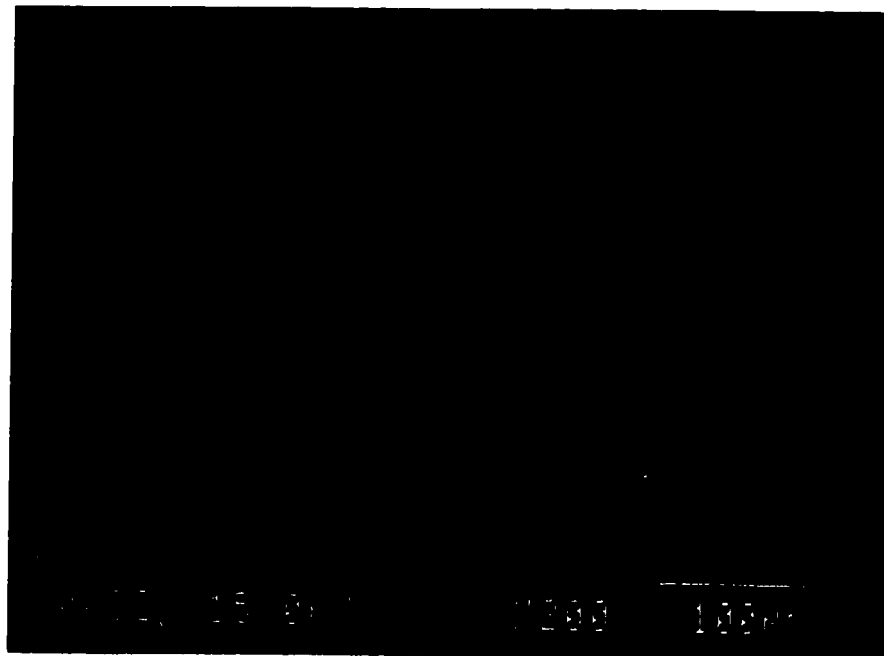


Figure 5.53 X-ray map of sulphur corresponding to the BEI micrograph above (Magnification 200x).

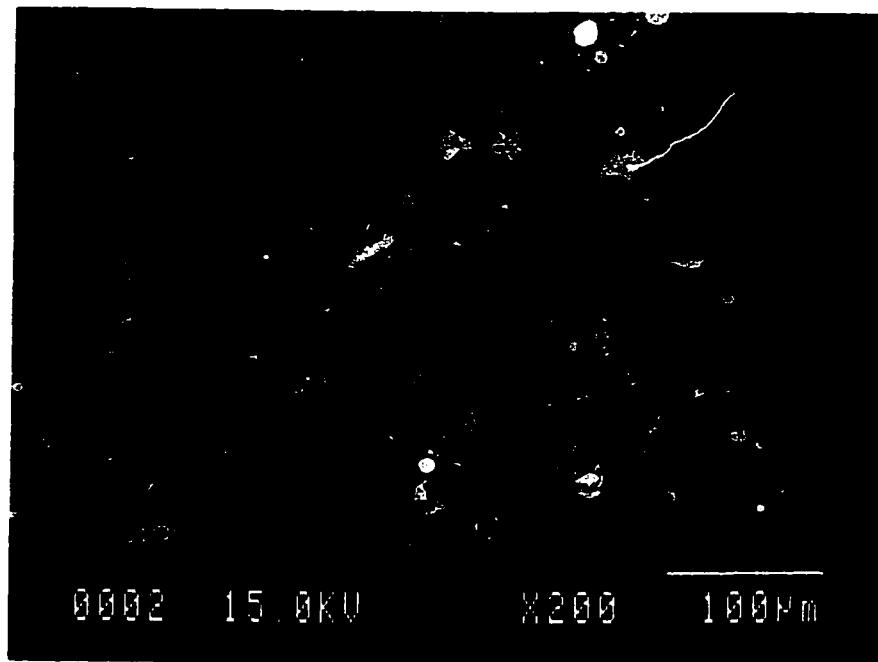


Figure 5.54 BEI micrograph of a polished surface from the outer edge of fly ash concrete. Specimen was immersed in distilled water for 330 days (Magnification 200x).

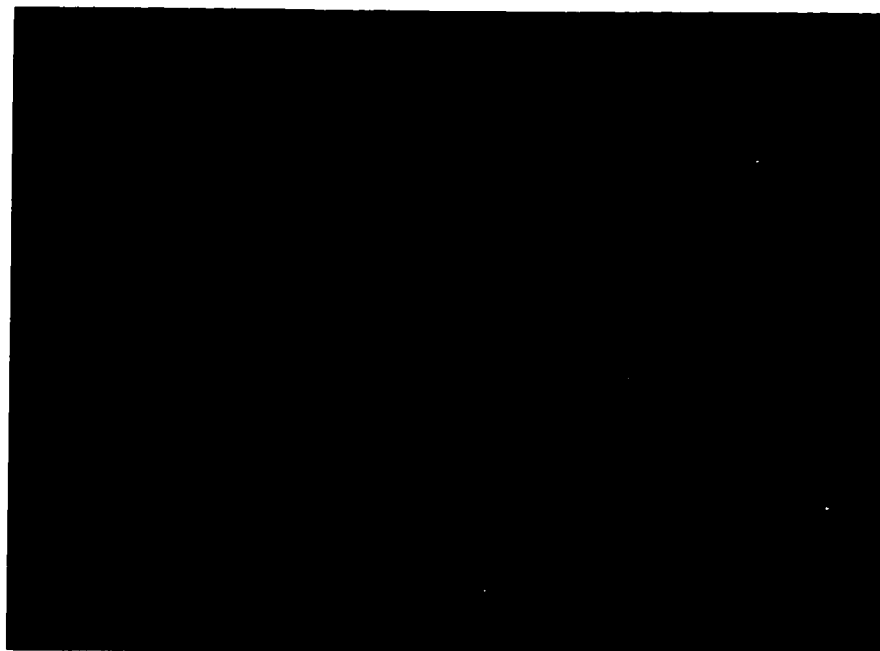


Figure 5.55 X-ray map of sulphur corresponding to the BEI micrograph above (Magnification 200x).

CHAPTER 6

Conclusions and Recommendations

6.1 Summary

This investigation was undertaken to include large volumes of fly ash in concrete to optimize its mechanical properties and reduce its cost. Superplasticizer was used in order to achieve good workability and high levels of compressive strength.

Concrete mixtures using a coarse/fine aggregate ratio of 1.22 and an aggregate/cementitious materials ratio of 5.0 were studied. Fly-ash was used as partial replacement of Type 10 Portland cement at levels ranging between 10-60% by the weight of cementitious material in the mixture. Use of Rheobuild 1000 superplasticizer allowed a reduction of water/cementitious materials ratio to 0.28-0.33, while the K-slump of fresh concrete was kept at a practical level of 25%. The effect of fly-ash on the development of the compressive strength of the hardened concrete was investigated. Concrete with a compressive strength approaching 50 MPa was obtained at 28 days, by using the water reducing properties of superplasticizer and replacing 50% of the cement with fly ash. A cost analysis indicates that these levels of strength are reached at a price below that of plain concrete.

Based on compressive strength results and cost, a mixture containing equal weights of cement and fly ash was selected for further assessment of its mechanical properties. The selected mixture containing 50% Class C fly ash was tested for its

engineering properties of strength, elasticity, creep, shrinkage, freezing-and-thawing durability and sulphate resistance. The results were compared to the same properties of a control concrete mixture containing 100% Type 10 Portland cement.

The test program consisted of compressive strength and modulus of elasticity tests at various ages from 5 hours to three months, using 75x150 mm (3x6 in) concrete cylinders containing various levels of fly ash replacement of the cement. Following the selection of a concrete mixture according to an optimum fly ash/cement ratio, two series of tests were performed using 75x225 mm (3x9 in) cylinders in order to evaluate the effect of fly ash on the long term deformation of concrete. The first series of tests consisted of creep evaluation at high and low moisture levels in combination with three levels of constant compressive stress under ambient conditions of temperature and humidity. A comparison was made between fly ash and control concretes.

The effect of high temperature and stress interaction on the creep and shrinkage of high volume fly ash concrete was investigated in the second series of long term deformation tests. Creep of concrete was studied using a combination of five levels of constant high temperature and three levels of constant compressive stress under sealed conditions. Companion specimens under zero stress level allowed measurement of shrinkage strains under the same conditions of moisture and temperature used in the long term deformation tests.

The durability of the fly ash mixture was also evaluated and compared to the control concrete. Freezing-and-thawing tests were performed according to ASTM C-666 (Procedure A) standard and the effect of air-entrainment was studied. Sulphate resistance tests were set-up according to ASTM C-1012 standard using a solution of 5% Na_2SO_4 and the performance of high volume fly ash and control concrete specimens was monitored for 11 months.

A microstructural investigation was undertaken to explain the performance of the fly ash concrete compared to the control mixture. Studies were performed using Scanning Electron Microscopy and Electron Probe Microanalysis on fractured and polished samples respectively and the microstructural features of the two concrete types were compared. Also, X-ray maps of sulphur were generated from polished surfaces, in order to evaluate the sulphate resistance of the two concretes. The effect of the fly ash on the modification of the microstructural features of the concrete was studied and the influence of the hardness of fly ash particles on mechanical measurements was considered.

6.2 Conclusions

Based on the analysis of the experimental results and observations from the microstructural analytical techniques used, the following conclusions are derived from this study:

1. Replacement of cement with high calcium Class C fly ash at various levels, generally provided a concrete with good strength development. Concrete containing a low volume (20%) of fly ash developed a compressive strength that surpassed the strength of the control mixture from 28 days onwards. The compressive strength of the 50% fly ash concrete developed at a slower rate than the control initially; at ages of 56 days onwards, the two concretes achieved strength levels that were statistically equivalent. A fly ash replacement level of 60% did not develop a high enough strength to be of practical significance.
2. By replacing 50% of the cement with high calcium Class C fly ash, concrete with high compressive strengths was obtained by using superplasticizers and low

water/binder ratios. The resultant concrete had a 28-day strength which is approximately 80% of the strength of a control mixture containing 100% Type 10 Portland cement. At 56 and 91 days, the strength of the fly ash concrete is over 85% and 90% of the control mixture respectively.

3. The static modulus of elasticity values of concrete containing 50% fly ash were comparable to those of the control mixture. The elastic modulus increased with an increase in the compressive strength and the relationship between modulus and compressive strength was very similar for both concretes.
4. The compressive strength of 50% fly ash concrete following one year of sustained external stresses and high temperatures, up to 232° C (450° F), remained virtually unaffected by these parameters when compared to the 28-day strength at the initial application of the external load.
5. The performance of concrete with 50% fly ash replacement was superior to that of the control mixture containing 100% Portland cement with respect to shrinkage. The total shrinkage strain of the fly ash concrete was lower than the control by approximately 25-30%.
6. The fly ash concrete of this study produced lower basic and drying creep strains compared to the control mixture at room temperature of 21° C (70° F). For a stress-strength ratio of 0.22, it was found that the total creep strain was lower in the fly ash concrete by approximately 35% and 25%, for sealed and unsealed specimens respectively.
7. Following release of the sustained load, the fly ash and control concrete test specimens underwent very little creep recovery.

8. Creep of the fly ash concrete under sealed conditions was studied at high temperatures ranging from 71° C (160° F) to 232° C (450° F). The general trend was that creep of concrete increased with rising temperatures, with the exception that a temperature of 71° C (160° F) produced a higher creep than the 121° C (250° F) level.
9. Fly ash concrete achieved a level of durability comparable to the control mixture for frost and sulphate resistance. A 50% replacement of the cement with fly ash produced concrete with satisfactory frost resistance provided air-entrainment was used and a 28-day proper curing period preceded exposure to rapid freezing-and-thawing.
10. The microstructural analysis showed a dense matrix with a marked absence of calcium hydroxide for the fly ash concrete. Also a dense matrix at the interfaces was responsible for a better bonding capacity and hence, development of high strength levels.
11. The long term deformation of the fly ash concrete is also affected by the density of the bulk paste and the bonding at the interfacial regions. Quantitative analysis of the paste composition of the two concretes, using the electron probe microanalyzer, indicated a lower Ca-Si peak ratio for the fly ash mixture compared to the control concrete. In addition a higher content of unhydrated cement was revealed in the paste of the control concrete. In the fly ash concrete the restraining effect of the anhydrous cement cores is supplemented by a similar effect from the presence of numerous unreacted fly ash particles. Secondary Electron Image (SEI) micrographs revealed a large number of fly ash particles being highly resistant to polishing and hence harder than the cement paste.
12. Very dense cement paste matrix is developed in the fly ash concrete at room temperature of 21° C (70° F). Backscattered Electron Image (BEI) micrographs

showed that higher temperatures, between 71° C (160° F) and 232° C (450° F), produce a bulk paste of higher porosity which then undergoes greater creep strains. Energy Dispersive Spectroscopy (EDS) indicated a physicochemical transformation at higher temperatures producing a paste of a significantly lower Ca content compared to Si. SEI micrographs revealed a more fibrous bulk matrix and a higher content of Ca(OH)_2 crystals with a preferred orientation.

13. A dense matrix and a noted absence of Ca(OH)_2 crystals in the fly ash mixture, produce concrete with a satisfactory frost resistance. The same microstructural features are responsible for the satisfactory performance of the fly ash concrete in a sulphate environment.

6.3 Recommendations

6.3.1 Optimum Mixture Using Class C Fly Ash

High calcium Class C fly ash affects the strength development of the concrete according to the level of cement replacement in the mixture. Concrete containing a low volume (20%) of fly ash developed a compressive strength that surpassed the strength of the control mixture at 28 days. At a higher fly ash content (50%), the strength was lower than that of the control at 28 days, but it was statistically equivalent to it at later ages. Assessment of other mechanical properties such as elasticity, shrinkage, creep, frost durability and sulfate resistance was needed before a final recommendation was made regarding the commercial application of concrete containing a large volume of Class C fly ash. From the preceding experimental and microstructural analysis it was indicated that improved mechanical properties were achieved with a 50% fly ash replacement and proper curing of the concrete. Based on the above conclusions, a mixture may be

recommended to the concrete industry if at the same time it is economical. A comparison of the present market rates of fly ash cement and silica fume was presented in a previous chapter. While previous studies have shown that high performance concrete with superior properties is achieved with a small replacement of cement with silica fume, the cost of such concrete makes its practical applications prohibitive. Within the limits of the present research program, an optimum fly ash concrete mixture may be recommended as follows:

1. Based on results on engineering properties, as well as economic and environmental considerations, concrete containing equal weights of cement and high calcium Class C fly ash with an aggregate/cementitious material ratio of 5 is a cost effective mixture. This mixture shows satisfactory performance with respect to strength, elastic stiffness, creep, shrinkage and sulphate resistance.
2. Where the frost resistance of concrete is of prime importance, the above mixture may be recommended provided that an air-entraining agent is incorporated and the concrete is properly cured for a minimum of 28 days. Longer curing periods have shown a slight improvement against freezing-and-thawing for non-air-entrained fly ash concrete. It is possible that a curing period longer than 28 days will have a positive effect on the frost resistance of air-entrained concrete containing 50% Class C fly ash.

6.3.2 Recommendations for Future Research

The following recommendations are offered for future research:

1. Determine the effect of a 40% replacement of cement with Class C fly ash in order to understand the anomaly that was observed in the present research study.
2. Study the effect of longer curing on the frost resistance of air-entrained concrete containing 50% replacement of cement with Class C fly ash.
3. Determine the effect of increasing the workability and content of fine materials in an economical fly ash concrete mixture.

REFERENCES

Aïtcin, P-C., Jolicoeur, C., and MacGregor, J.M., 1994, "Superplasticizers: How They Work and Why They Occasionally Don't," *Concrete International*, V. 16, No. 5, pp. 45-52.

Aïtcin, P-C., Sarkar, S.L., and Diatta, Y., 1987, "Microstructural Study of Different Types of Very High-Strength Concretes," *Proceedings, Materials Research Society Symposium*, V. 85, pp. 261-272.

ASTM C 1012, 1992, "Standard Test Method for Length Change of Hydraulic-Cement Mortars Exposed to a Sulfate Solution," *Annual Book of ASTM Standards*, Vol 04.01.

ASTM C 127, 1992, "Standard Test Method for Specific Gravity and Absorption of Coarse Aggregate," *Annual Book of ASTM Standards*, Vols 04.02 and 04.03.

ASTM C 128, 1992, "Standard Test Method for Specific Gravity and Absorption of Fine Aggregate," *Annual Book of ASTM Standards*, Vols 04.02 and 04.03.

ASTM C 136, 1992, "Standard Method Sieve Analysis of Fine and Coarse Aggregate," *Annual Book of ASTM Standards*, Vols 04.02 and 04.03.

ASTM C 138, 1992, "Test Method for Unit Weight, Yield and Air Content (Gravimetric) of Concrete" *Annual Book of ASTM Standards*, Vol 04.02.

ASTM C 150, 1992, "Specifications for Portland Cement" *Annual Book of ASTM Standards*, Vols 04.01 and 04.02.

ASTM C 192, 1992, "Practice for Making and Curing Concrete Test Specimens in the Laboratory," *Annual Book of ASTM Standards*, Vol 04.02.

ASTM C 215, 1992, "Standard Test Method for Fundamental Transverse, Longitudinal, and Torsional Frequencies of Concrete Specimens" *Annual Book of ASTM Standards*, Vol 04.02.

ASTM C 457, 1990, "Standard Test Method for Microscopical Determination of Parameters of the Air-Void System in Hardened Concrete," *Annual Book of ASTM Standards*, Vol 04.02.

ASTM C 469, 1992, "Test Method for Static Modulus of Elasticity and Poisson's Ratio of Concrete in Compression," *Annual Book of ASTM Standards*, Vol 04.02.

ASTM C 494, 1992, "Specifications for Chemical Admixtures for Concrete," *Annual Book of ASTM Standards*, Vol 04.02.

ASTM C 494, 1992, "Specifications for Chemical Admixtures in Concrete" *Annual Book of ASTM Standards*, Vol 04.02.

ASTM C 494, 1992, "Specifications for Fly Ash and Raw or Calcined Natural Pozzolan for Use as Mineral Admixtures in Portland Cement Concrete" *Annual Book of ASTM Standards*, Vol 04.02.

ASTM C 666, 1992, "Standard Test Method for Resistance of Concrete to Rapid Freezing and Thawing," *Annual Book of ASTM Standards*, Vol 04.02.

Baalbaki, W., Aïtcin, P-C., and Ballivy, G., 1992, "On Predicting Modulus of Elasticity in High-Strength Concrete," *ACI Materials Journal*, V. 89, No. 5, pp. 517-520.

Bentz, D.P., and Garboczi, E.J., 1991, "Simulation Studies of the Effects of Mineral Admixtures on the Cement Paste - Aggregate Interfacial Zone," *ACI Materials Journal*, V. 88, No. 5, pp. 518-529.

Berry, E.E., and Malhotra, V.M., 1986, *Fly Ash in Concrete*, Special Publication SP85-3, Canada Centre for Mineral and Energy Technology (CANMET), Energy, Mines and Resources, Canada, 175pp.

Berry, E.E., and Malhotra, V.M., 1987, "Fly Ash in Concrete", *Supplementary Cementing Materials for Concrete*, V.M. Malhotra, ed., Canada Centre for Mineral and Energy Technology (CANMET), Energy, Mines and Resources, Canada, pp. 37-163.

Berry, E.E., Hemmings, R.T., Zhang, M.H., Cornelius, B.J., and Golden, D.M., 1994, "Hydration in High-Volume Fly Ash Concrete Binders," *ACI Materials Journal*, V. 91, No. 4, pp. 382-389.

Bickis, M., personal discussions (unpublished).

Bilodeau, A., Sivasundaram, V., Painter, K.E., and Malhotra, V.M., 1994, "Durability of Concrete Incorporating High Volumes of Fly Ash from Sources in the U.S.," *ACI Materials Journal*, V. 91, No. 1, pp. 3-12.

Bisaillon, A., Rivest, M., and Malhotra, V.M., 1994, "Performance of High-Volume Fly Ash Concrete in Large Experimental Monoliths," *ACI Materials Journal*, V. 91, No. 2, pp. 178-187.

Bonen, D., and Sarkar, S.L., 1993, "Replacement of Portlandite by Gypsum in the Interfacial Zone and Cracking Related to Crystallization Pressure," *Ceramic Transactions*, Vol. 37: *Cement-Based Materials: Present, Future and Environmental Aspects*, M. Moukwa, S.L. Sarkar, K.Luke, M.W. Grutzeck, ed., The American Ceramic Society, Westerville Ohio, pp. 49-59.

Brown, T.L., LeMay, H.E.Jr., and Bursten, B.E., 1991, *Chemistry: The Central Science*, Prentice Hall, Fifth Edition.

Callister, W.D.Jr., 1991, *Materials Science and Engineering: An Introduction*, John Wiley and Sons Inc., Second Edition.

Carette, G., Bilodeau, A., Chevrier, R.L., and Malhotra, V.M., 1993, "Mechanical Properties of Concrete Incorporating High Volumes of Fly Ash from Sources in the U.S.," *ACI Materials Journal*, V. 90, No. 6, pp. 535-544.

Carette, G.G., and Malhotra, V.M., 1987, "Characterization of Canadian Fly Ashes and their Relative Performance in Concrete," *Canadian Journal of Civil Engineering*, V. 14, No. 5, pp. 667-682.

Chanda, M., *Science of Engineering Materials, Structure of Matter, Volume 1*, The MacMillan Press, 1979.

Cheng-yi, Huang, and Feldman, R.F., 1985, "Influence of Silica Fume on the Microstructural Development in Cement Mortars," *Cement and Concrete Research*, V. 15, No. 2, pp. 285-294.

Clifton, J.R., Brown, P.W., Frohnsdorff, G.B., 1979, "Reactivity of Fly Ashes with Cement," *Cement Research Progress*, American Ceramic Society, pp. 321-341.

Davis, R.E., Carlson, R.W., Kelly, J.W., and Davis, H.E., 1937, "Properties of Cements and Concretes Containing Fly Ash," *ACI Journal Proceedings*, V.33, No. 3, pp. 577-612.

Day, R.L., and Haque, M.N., 1993, "Correlation between Strength of Small and Standard Concrete Cylinders," *ACI Materials Journal*, V. 90, No. 5, pp. 452-462.

Diamond, S., 1987, "Cement Paste Microstructure in Concrete," *Proceedings, Materials Research Society Symposium*, V. 85, pp. 21-31.

Diamond, S., Ravina, D., Lovell, J., 1980, *Cement and Concrete Research*, Vol. 10, pp. 297-300.

Dikeou, J.T., 1975 "Fly Ash Increases Resistance of Concrete to Sulfate Attack," *Research Report No. 23*, U.S. Bureau of Reclamation, Denver, 17 pp.

Feldman, R.F., and Cheng-yi, Huang, 1985, "Properties of Portland Cement-Silica Fume Pastes. II. Mechanical Properties," *Cement and Concrete Research*, V. 15, No. 6, pp. 943-952.

Feldman, R.F., Beaudoin, J.J., 1976, *Cement and Concrete Research*, Vol. 6, pp. 389.

Flinn, R.A., Trojan, P.K., *Engineering Materials and their Applications*, Houghton Mifflin Company, 1990.

Gabriel, B.L., 1985, *SEM: A User's Manual for Materials Science*, American Society for Metals, Metals Park, Ohio.

Garboczi, E.J., and Bentz, D.P., 1991, "Digital Simulation of the Aggregate-Cement Paste Interfacial Zone in Concrete," *Journal of Materials Research*, V. 6, No. 1, pp. 196-201.

Ghosh, S., 1994, "Engineering Properties of High Strength Concrete Containing Silica Fume and Lignite Fly Ash," Ph.D. Thesis, Department of Civil Engineering, University of Saskatchewan, Saskatoon, Canada.

Glasser, F.P., Diamond, S., Roy, D.M., 1987, "Hydration Reactions in Cement Pastes Incorporating Fly Ash and Other Pozzolanic Materials," *Proceedings, Materials Research Society Symposium*, V. 85, pp. 167-186.

Goldstein, J.I. and Yakowitz, H. ed., 1975, *Practical Scanning Electron Microscopy*, Plenum Press, New York.

Halse, Y., Pratt, P.L., Dalzeil, J.A., Gutteridge, W.A., 1984, "Development of Microstructure and Other Properties in Flyash OPC Systems," *Cement and Concrete Research*, Vol. 14, No. 4, pp. 491-498.

Hansen, Will, and Young, J. Francis, 1991, "Creep Mechanisms in Concrete," in *Materials Science of Concrete II*, Edited by J.P. Skalny and S. Mindess, pp. 185-200.

Haque, M.N., Kayyali, O.A., and Gopalan, M.K., 1992, "Fly Ash Reduces Harmful Chloride Ions in Concrete," *ACI Materials Journal*, V. 89, No. 3, pp. 238-241.

Helmouth, R.A., 1987, "Water-Reducing Properties of Fly Ash in Cement Pastes, Mortars and Concretes: Causes and Test Methods," ACI SP-91, pp. 723-740.

Idorn, G.M., Johansen, V., Thaulow N., 1992, "Assessment of Causes of Cracking in Concrete," in *Materials Science of Concrete III*, Edited by J.P. Skalny, pp. 71-104.

- Jambor, J., 1974, in Proceedings of the Sixth International Congress on the Chemistry of Cement, Moscow.
- Jastrzebski, Z.D., 1987, *The Nature and Properties of Engineering Materials*, John Wiley & Sons.
- Lai, P.S.H., 1986, "Behavior of Concrete Containing 50% Fly Ash," M.Sc. Thesis, Department of Civil Engineering, University of Saskatchewan, Saskatoon, Canada.
- Lai, P.S.H., 1989, "Study on the Durability of Concrete Containing Lignite Fly Ash," Ph.D. Thesis, Department of Civil Engineering, University of Saskatchewan, Saskatoon, Canada.
- Lea, F.M., 1976, *The Chemistry of Cement and Concrete*, Edward Arnold (Publishers) Ltd., Third Edition.
- Lohtia, R.P., 1968, "The Effect of Temperature on the Creep, Strength and Elasticity of Mass Concrete," Ph.D. Thesis, Department of Civil Engineering, University of Saskatchewan, Saskatoon, Canada.
- Malhotra, V.M., 1987, "Properties of Fresh and Hardened Concrete Incorporating Ground Granulated, Blast-Furnace Slag," *Supplementary Cementing Materials for Concrete*, V.M. Malhotra, ed., Canada Centre for Mineral and Energy Technology (CANMET), Energy, Mines and Resources, Canada, pp. 291-333.
- Marzouk, H.E., 1979, "Effect of High Temperature on the Creep of Concrete Containing Fly Ash," Ph.D. Thesis, Department of Civil Engineering, University of Saskatchewan, Saskatoon, Canada.
- Mather, B., 1990, "How to Make Concrete that will be Immune to the Effects of Freezing and Thawing," *Paul Klieger Symposium on Performance of Concrete*, ACI SP-122, pp. 1-18.
- Mehta, P.K., 1986, *Concrete: Structure, Properties and Materials*, Prentice-Hall, Inc.,

- Mehta, P.K., 1987, "Natural Pozzolans," *Supplementary Cementing Materials for Concrete*, V.M. Malhotra, ed., Canada Centre for Mineral and Energy Technology (CANMET), Energy, Mines and Resources, Canada, pp. 3-33.
- Mehta, P.K., 1989, "Pozzolanic and Cementitious By-Products in Concrete - Another Look", SP114-1, Proceedings on the Third International Conference on *Fly Ash, Silica Fume Slag and Natural Pozzolans in Concrete*, Trondheim, Norway, Vol. 1, pp. 1-43.
- Mehta, P.K., 1992, "Sulfate Attack on Concrete - A Critical Review," in *Materials Science of Concrete III*, Edited by J.P. Skalny, pp. 105-130.
- Mills, R.H., Buenfeld, N., 1987, "Restricted Hydration of Mass-Cured Concrete Containing Fly Ash," *Proceedings, Materials Research Society Symposium*, V. 85, pp. 235-243.
- Mindess, S., 1985, "Relationship Between Strength and Microstructure for Cement-Based Materials," *Proceedings, Materials Research Society Symposium*, V. 42, pp. 53-68.
- Mindess, S., and Young J.F., 1981, *Concrete*, Prentice-Hall Inc., Englewood Cliffs, New Jersey.
- Mitsui, K., Zongjin, L., Langue, D.A., and Shah, S.P., 1994, "Relationship between Microstructure and Mechanical Properties of the Paste-Aggregate Interface," *ACI Materials Journal*, V. 91, No. 1, pp. 30-39.
- Moffat, W.G., Pearsall, G.W., Wulff, J., 1964, *The structure and Properties of Materials, Structure, Volume 1*, John Wiley & Sons.
- Monteiro, P.J.M., Maso, J.C., Ollivier, J.P., 1985, "The Aggregate-Mortar Interface," *Cement and Concrete Research*, V. 15, No. 6, pp. 953-958.
- Montgomery, D.C., 1991, *Design and Analysis of Experiments*, Third Edition, John Wiley and Sons.

Naik, T.R., Ramme, B.W., and Tews, J.H., 1995, "Pavement Construction with High-Volume Class C and Class F Fly Ash Concrete," *ACI Materials Journal*, V. 92, No. 2, pp. 200-210.

Nasser, K.W., 1976, "New and Simple Tester for Slump of Concrete," *ACI Journal*, V. 73, No. 10, pp. 561-565.

Nasser, K.W., and Al-Manasser, A.A., 1987, "It's time for a Change from 6x12 to 3x6 in Cylinders," *ACI Materials Journal*, V. 84, No. 3, pp. 213-216.

Nasser, K.W., and Kenyon, J.C., 1984, "Why not 3x6 inch Cylinders for Testing Concrete Compressive Strength," *ACI Materials Journal*, V. 81, No. 1, pp. 47-53.

Nasser, K.W., and Lai, P.S.H., 1991, "Effect of Sulphates on Concrete Containing Flyash," Second CANMET/ACI International Conference on Durability of Concrete, Montreal, Canada, pp 817-838.

Nasser, K.W., and Lai, P.S.H., 1992, "Resistance of Fly Ash Concrete to Freezing and Thawing," Fourth CANMET/ACI Conference Proceedings *Fly Ash, Silica Fume, Slag and Natural Pozzolanas in Concrete*, V. 1, SP-132, pp 205-226.

Nasser, K.W., and Malhotra, V.M., 1990, "Accelerated Testing of Concrete: Evaluation of the K-5 Method," *ACI Materials Journal*, V. 87, No. 6, pp. 588-593.

Neville, A.M., 1957, "The Measurement of Creep of Mortar under Fully-Controlled Conditions," *Magazine of Concrete Research*, Vol. 9, No. 25, pp. 9-12.

Neville, A.M., 1981, *Properties of Concrete*, Third Edition, The Pitman Press.

Owens, P.L., 1979, "Fly Ash and its Usage in Concrete," *Journal, Concrete Society (England)*, Vol. 13, No. 7, pp. 21-26.

Philleo, R.E., 1991, "Concrete Science and Reality," in *Materials Science of Concrete II*, Edited by J.P. Skalny, pp. 1-8.

- Pickett, G., 1942, "The Effect of Change in Moisture Content on the Creep of Concrete under a Sustained Load," *ACI Journal*, V. 38, pp. 333-356.
- Pommersheim, J.M., 1987, "Effect of Particle Size Distribution on Hydration Kinetics," *Proceedings, Materials Research Society Symposium*, V. 85, pp. 301-306.
- Popovics, S., *Concrete-Making Materials*, Hemisphere Publishing Corporation, 1979.
- Powers, T.C., and Brownyard, T.L., 1948, "Studies of the Physical Properties of Hardened Portland Cement Paste," Research Laboratories of the Portland Cement Association, Bulletin 22, Chicago.
- Pratt, P.L., 1987, "Relationships Between Microstructure and Engineering Properties," *Proceedings, Materials Research Society Symposium*, V. 85, pp. 145-155.
- Regourd, M., 1985, "Microstructure of High Strength Cement Paste Systems," *Proceedings, Materials Research Society Symposium*, V. 42, pp. 3-17.
- Regourd, M., 1987, "Microstructure of Cement Blends Containing Fly Ash, Silica Fume, Slag and Fillers," *Proceedings, Materials Research Society Symposium*, V. 85, pp. 187-200.
- Roberts, L.R., 1989, "Microsilica in Concrete, I," in *Materials Science of Concrete I*, Edited by J.P. Skalny, pp. 197-222.
- Robertson, Vernon E., 1990, *Introduction to the Principles of Operation and Applications of the Scanning Electron Microscope and Electron Microprobe*, JEOL USA Inc., Peabody, Massachusetts.
- Saricimen, H., Maslehuddin, M., Al-Tayyib, A.J., and Al-Mana, A.I., 1995, "Permeability and Durability of Plain and Blended Concretes Cured in Field and Laboratory Conditions," *ACI Materials Journal*, V. 92, No. 2, pp. 111-116.
- Sarkar S.L., 1994, "The Importance of Microstructure in Evaluating Concrete," *Advances in Concrete Technology*, second edition, V.M. Malhotra, ed., Canada Centre for Mineral

and Energy Technology (CANMET), Energy, Mines and Resources, Canada, pp. 125-160.

Scrivener, K.L., 1984, Ph.D. Thesis, Imperial College, University of London, England.

Scrivener, K.L., Patel, H.H, Pratt, P.L., and Parrott, L.J., 1987, "Analysis of Phases in Cement Paste Using Backscattered Electron Images, Methanol Adsorption and Thermogravimetric Analysis," *Proceedings, Materials Research Society Symposium*, V. 85, pp. 67-76.

Sivasundaram, V., Carrette, G.G., and Malhotra, V.M., 1991, "Mechanical Properties, Creep, and Resistance to Diffusion of Chloride Ions of Concretes Incorporating High Volumes of ASTM Class F Fly Ashes from Seven Different Sources," *ACI Materials Journal*, V. 88, No. 4, pp. 407-416.

Taylor, H.F.W., 1990, *Cement Chemistry*, Academic Press.

Tikalsky, P.J., and Carrasquillo, R.L., 1992, "Influence of Fly Ash on the Sulfate Resistance of Concrete," *ACI Materials Journal*, V. 89, No. 1, pp. 69-75.

Tikalsky, P.J., and Carrasquillo, R.L., 1993, "Fly Ash Evaluation and Selection for Use in Sulfate Resistant Concrete," *ACI Materials Journal*, V. 90, No. 6, pp. 545-551.

Xi, Yunping, and Jennings, H.M., 1992, "Relationships Between Microstructure and Creep and Shrinkage of Cement Paste," in *Materials Science of Concrete III*, Edited by J.P. Skalny, pp. 37-69.

Young, J. Francis, and Hansen, Will, 1990, "Volume Relationships for CSH Formation Based on Hydration Stoichiometry," *Proceedings, Materials Research Society Symposium*, V. 85, pp. 313-322.

Appendix A

Chemical and Physical Properties of Materials

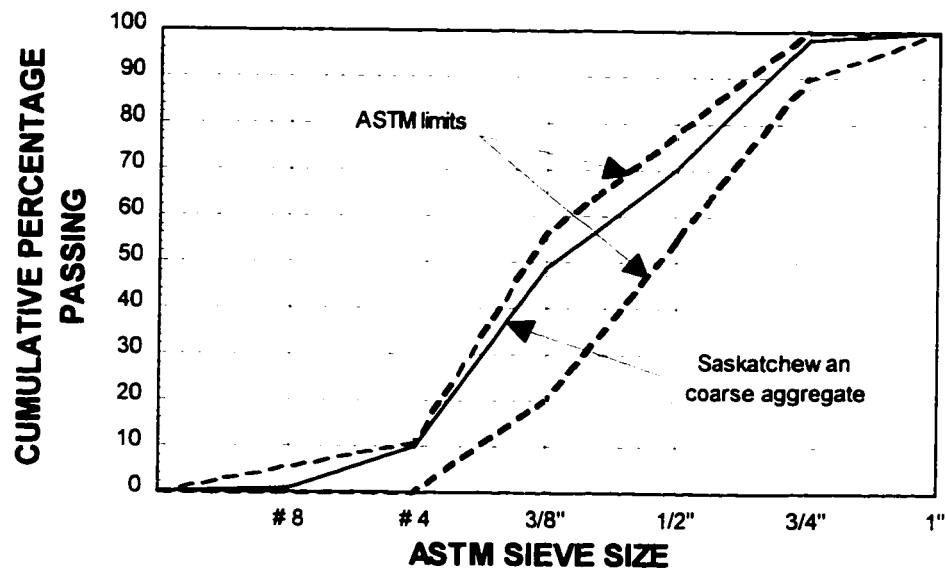


Figure A.1 Grading curve for 19 mm (3/4") Saskatchewan coarse aggregate.

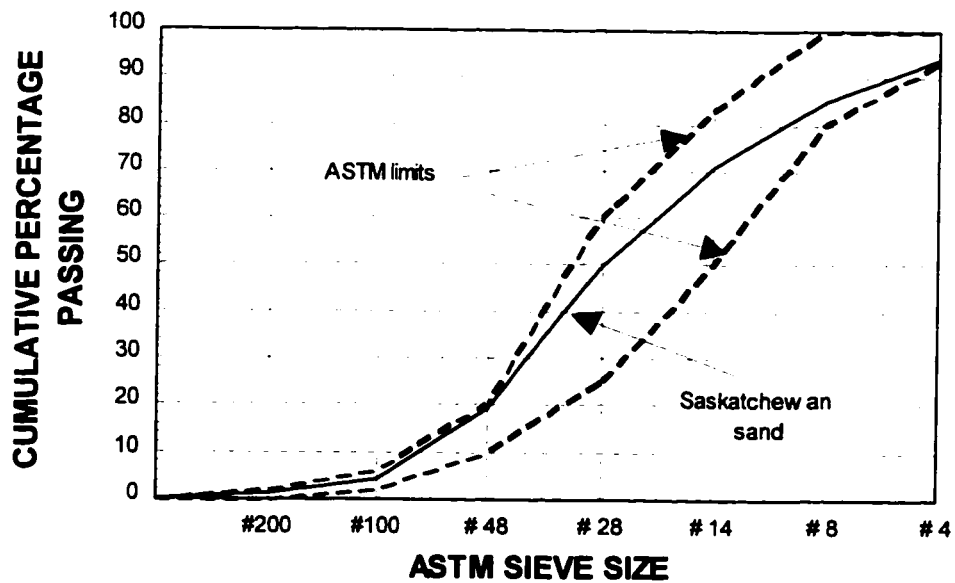


Figure A.2 Grading curve for Saskatchewan fine aggregate.

Table A.1 Chemical Analysis and Physical Properties of Portland Cement.

Chemical Analysis	Type 10 Portland Cement	
	%	ASTM C150
SiO ₂	21.19	--
Al ₂ O ₃	4.10	--
Fe ₂ O ₃	2.34	--
CaO, total	62.84	--
CaO, free	0.99	--
SO ₃	2.56	3.0 max
MgO	4.56	6.0 max
Alkalis as Na ₂ O	0.66	
C ₃ S	56.60	--
C ₂ S	18.10	--
C ₃ A	6.90	--
C ₄ AF	7.10	--
Loss on ignition	1.40	3.0 max
Insoluble residue	0.20	0.75 max
Physical Properties		
Autoclave Expansion, %	0.74	0.8 max
Time Vicat, minutes	75.00	45 - 375
Compressive Strength:		
at 3 days, Mpa (psi)	24.5 (3550)	12.4 (1800)
7 days, Mpa (psi)	31.7 (4600)	19.3 (2800)
28 days, Mpa (psi)	37.0 (5370)	27.6 (4000)
45-mm sieve passing	90.5	--
Blaine Fineness, m ² /Kg	401	--

Table A.2 Chemical Analysis and Physical Properties of Class C Fly Ash (Sundance, Alberta)

Chemical Analysis	Class C Fly Ash	
	%	ASTM C618
SiO ₂	47.40	--
Al ₂ O ₃	21.50	--
Fe ₂ O ₃	5.30	--
CaO	14.40	--
Total, SiO ₂ + Al ₂ O ₃ + Fe ₂ O ₃	74.20	50.5 min
SO ₃	0.58	5.0 max
MgO	2.90	5.0 max
Available alkalis as Na ₂ O	1.77	1.5 max
Loss on ignition	0.65	6.0 max
Moisture content	0.09	3.0 max
Physical Properties		
Soundness - Autoclave Expansion, %	0.13	0.8 max
Fineness: 45 mm sieve retained, %	26.32	34 max
Drying shrinkage increase at 28 days, %	0.09	0.03 max
Specific gravity	2.21	--
Pozzolanic activity index:		
w/ portland cement at 28 days, % of control	82.00	75.0 min
w/ lime at 7 days (psi)	871	800 min
Water requirement, % of control	94	105 max

Table A.3 Chemical Analysis of anhydrous sodium sulphate (supplied by manufacturer)

Composition	%
Na ₂ SO ₄	99.8799
Chloride (Cl)	0.0004
Nitrogen compound (as N)	0.0003
Arsenic (As)	0.00001
Calcium, magnesium and R ₂ O ₃ ppt	0.004
Heavy metals (as Pb)	0.0001
Iron (Fe)	0.0002
Insoluble matter	0.005
Loss on ignition	0.11
pH of a 5% solution at 25° C	6.1

Table A.4 Chemical Analysis of Tap Water Used for Mixing

Composition	mg/L
Total dissolved solids (by evaporation)	205
Bicarbonates, as CO ₃	77
Carbonates, as CO ₃	7
Chlorides, as Cl	7
Sulphates, as SO ₄	78
Nitrates, as NO ₃	0.35
Iron	<0.05
Total hardness	120
Calcium hardness	60
Magnesium hardness	60
Phenolphthalein alkalinity	7
Total alkalinity	77
Fluorides	0.85
Manganese	<0.03
Sodium	22
Potassium	2
pH	9.2
Appearance	clear
Odour	nil

Appendix B

Statistical Analysis of Compressive Strength

The development of the compressive strength of the fly ash and control concretes was analyzed by writing a program in Statistical Analysis System (SAS) on the VAX/VMS mainframe computer. Complete details on the use of SAS can be found in SAS/STAT® User's Guide, Version 6, vol. 2, SAS Institute Inc., 1989.

The program is based on a procedure in the General Linear Model (GLM). It performs the analysis of variance (ANOVA) by test day and establishes significant or non-significant differences between the compressive strengths of the two concretes. The program in SAS calls the data file (infile) which is input in a separate file with a .DAT extension in the VAX/VMS computer. The program output, including the fitted (predicted) values and the residuals, is automatically stored in a new file with a .LIS extension. For the analysis of variance, SAS is programmed to use the batch average values for calculation of the error sum of squares term (FA*BATCH), thus, recognizing the dependence of the strength values for test specimens that originated from the same batch of concrete.

A PLOT procedure is also programmed in SAS for plotting the residuals against the fitted values. The plot of residuals is important since it will indicate if there are any data that should be discarded as outliers (i.e., values that are so different that they should be suspected as being errors). In addition, the plot of residuals will show if there are any trends that are present and will indicate what type of transformation (for example square root or logarithmic transformation) has to be performed on the data before the analysis is done. A cloud scatter-plot diagram of the residuals around the horizontal axis indicates

that the data may be fitted into a general linear model without any transformation being necessary.

The SAS program and output are given in the following pages.


```

TITLE "ANALYSIS OF STRENGTH FOR CONTROL MIXES (11,17)
      AND 50% FLYASH (13, 15, 16) -
      ANALYSIS DONE BY DAY";
OPTIONS LS=78 PS=40;
/* FILENAME FA14; */
DATA;
      INFILE FA14;
INPUT  FA
      BATCH
      CYLINDER
      LOAD
      DAY ;
PSI=LOAD/7.07;
MPA=PSI/145;

/* HALF_MPA=MPA*.5;
LOG_MPA=LOG(MPA); */

PROC GLM;
      BY DAY;
CLASS FA BATCH CYLINDER DAY;
MODEL MPA = FA BATCH FA*BATCH/SS1;
MEANS FA BATCH FA*BATCH;

TEST H=FA
      E=FA*BATCH/HTYPE=1;
OUTPUT OUT=FITRES
      PREDICTED=F0
      RESIDUAL=R0;
DATA; SET;
LABEL  F0='FITTED VALUE UNTRANSFORMED'
      /* F1='FITTED VALUE SQUARE ROOT TRANSFORMATION'
      F2='FITTED VALUE LOG TRANSFORMATION' */
      R0='RESIDUAL VALUE UNTRANSFORMED'
      /* R1='RESIDUAL VALUE SQUARE ROOT TRANSFORMATION'
      R2='RESIDUAL VALUE LOG TRANSFORMATION'*/ ;
PROC PLOT;
      TITLE2 "RESIDUAL VERSUS FITTED PLOT";
PLOT R0%F0=FA
      /* R1%F1=FA
      R2%F2=FA */
      /VREF=0;

```

ANALYSIS OF STRENGTH FOR CONTROL MIXES (11,17) AND 50% FLYASH (13, 15, 16) -
 16/18 Friday, March 19, 1991

----- DAY=14 -----

General Linear Models Procedure
 Class Level Information

Class	Levels	Values
FA	2	0 50
BATCH	5	11 13 15 16 17
CYLINDER	3	1 2 3
DAY	1	14

Number of observations in by group = 15

ANALYSIS OF STRENGTH FOR CONTROL MIXES (11,17) AND 50% FLYASH (13, 15, 16) -
 14:18 Friday, March 19, 1993

----- DAY=14 -----

General Linear Models Procedure

Dependent Variable: MPA

Source	DF	Sum of Squares	Mean Square	F Value	Pr > F
Model	4	846.6677428	211.6669357	71.60	0.0001
Error	10	29.5610479	2.9561048		
Corrected Total	14	876.2287907			
	R-Square	C.V.	Root MSE		MPA Mean
	0.966263	3.735322	1.719333		46.0290

Source	DF	Type I SS	Mean Square	F Value	Pr > F
FA	1	825.3448811	825.3448811	279.20	0.0001
BATCH	3	21.3228618	7.1076206	2.40	0.1285
FA*BATCH	0	0.0000000	.	.	.

ANALYSIS OF STRENGTH FOR CONTROL MIXES (11,17) AND 50% FLYASH (13, 15, 16) -
 16:18 Friday, March 19, 199

----- DAY=14 -----

General Linear Models Procedure

Level of FA	N	-----MFA----- Mean	SD
0	6	55.1138858	1.44685139
50	9	39.9724702	2.24769368

Level of BATCH	N	-----MFA----- Mean	SD
11	3	54.3009966	1.12637228
13	3	40.8720675	1.12496343
15	3	38.0106976	3.17938403
16	3	41.0346453	0.39423030
17	3	55.9267749	1.40796534

Level of FA	Level of BATCH	N	-----MFA----- Mean	SD
0	11	3	54.3009966	1.12637228
0	17	3	55.9267749	1.40796534
50	13	3	40.8720675	1.12496343
50	15	3	38.0106976	3.17938403
50	16	3	41.0346453	0.39423030

ANALYSIS OF STRENGTH FOR CONTROL MIXES (11,17) AND 50% FLYASH (13, 15, 16) -
13:18 Friday, March 19, 1993

----- DAY=14 -----

General Linear Models Procedure

Dependent Variable: MPA

Tests of Hypotheses using the Type I MS for FA*BATCH as an error term

Source	DF	Type I SS	Mean Square	F Value	Pr > F
FA	1	825.3448811	825.3448811	.	.

ANALYSIS OF STRENGTH FOR CONTROL MIXES (11,17) AND 50% FLYASH (13, 15, 16) -
16:18 Friday, March 19, 1991

----- DAY=28 -----

General Linear Models Procedure
Class Level Information

Class	Levels	Values
FA	2	0 50
BATCH	5	11 13 15 16 17
CYLINDER	3	1 2 3
DAY	1	28

Number of observations in by group = 15

ANALYSIS OF STRENGTH FOR CONTROL MIXES (11:17) AND 50% FLYASH (13: 15: 16) -
16:18 Friday, March 19, 1991

----- DAY#28 -----

General Linear Models Procedure

Dependent Variable: MPA

Source	DF	Sum of Squares	Mean Square	F Value	Pr > F
Model	4	713.6519081	178.4129770	28.27	0.0001
Error	10	63.1185465	6.3118547		
Corrected Total	14	776.7704547			
	R-Square	C.V.	Root MSE		MPA Mean
	0.918742	4.754817	2.512340		52.83780

Source	DF	Type I SS	Mean Square	F Value	Pr > F
FA	1	634.6215672	634.6215672	100.54	0.0001
BATCH	3	79.0303409	26.3434470	4.17	0.0370
FA*BATCH	0	0.0000000	.	.	.

ANALYSIS OF STRENGTH FOR CONTROL MIXES (11-17) AND 50% FLYASH (13, 15, 16) -
16:13 Friday, March 19, 1997

----- DAY:28 -----

General Linear Models Procedure

Level of FA	N	-----MPA----- Mean	SD
0	6	60.8041100	4.72539684
50	9	47.5269202	1.95262679

Level of BATCH	N	-----MPA----- Mean	SD
11	3	57.3899755	4.50548910
13	3	46.9849941	1.01529825
15	3	48.9359281	0.28159307
16	3	46.6598384	3.09752376
17	3	64.2182445	0.74502523

Level of FA	Level of BATCH	N	-----MPA----- Mean	SD
0	11	3	57.3899755	4.50548910
0	17	3	64.2182445	0.74502523
50	13	3	46.9849941	1.01529825
50	15	3	48.9359281	0.28159307
50	16	3	46.6598384	3.09752376

ANALYSIS OF STRENGTH FOR CONTROL MIXES (11-17) AND 50% FLYASH (13, 15, 16) -
 16:18 Friday, March 19, 1993

----- DAY=28 -----

General Linear Models Procedure

Dependent Variable: MPA

Tests of Hypotheses using the Type I MS for FA*BATCH as an error term

Source	DF	Type I SS	Mean Square	F Value	Pr > F
FA	1	634.6215672	634.6215672	.	.

ANALYSIS OF STRENGTH FOR CONTROL MIXES (11,17) AND 50% FLYASH (13, 15, 16) -
16:18 Friday, March 19, 1991

----- DAY=56 -----

General Linear Models Procedure
Class Level Information

Class	Levels	Values
FA	2	0 50
BATCH	5	11 13 15 16 17
CYLINDER	3	1 2 3
DAY	1	56

Number of observations in by group = 15

NOTE: Due to missing values, only 7 observations can be used in this analysis.

ANALYSIS OF STRENGTH FOR CONTROL MIXES (11,17) AND 50% FLYASH (13, 15, 16) :
15:18 Friday, March 19, 1993

----- DAY=56 -----

General Linear Models Procedure

Dependent Variable: MPA

Source	DF	Sum of Squares	Mean Square	F Value	Pr > F
Model	2	79.03003886	39.51501943	10.19	0.0265
Error	4	15.50369123	3.87592281		
Corrected Total	6	94.53373009			
	R-Square	C.V.	Root MSE		MPA Mean
	0.835998	3.486612	1.968736		56.46560

Source	DF	Type I SS	Mean Square	F Value	Pr > F
FA	1	71.41458006	71.41458006	18.43	0.0107
BATCH	1	7.61545881	7.61545881	1.96	0.2333
FA*BATCH	0	0.00000000	.	.	.

ANALYSIS OF STRENGTH FOR CONTROL MIXES (11,17) AND 50% FLYASH (13,15,16) .
 16:18 Friday, March 19, 1993

----- DAY=56 -----

General Linear Models Procedure

Level of FA	N	-----MPA----- Mean	SD
0	3	60.1537986	1.12637228
50	4	53.6994586	2.61926968

Level of BATCH	N	-----MPA----- Mean	SD
11	3	60.1537986	1.12637228
13	1	56.0893528	.
15	3	52.9028272	2.54619935

Level of FA	Level of BATCH	N	-----MPA----- Mean	SD
0	11	3	60.1537986	1.12637228
50	13	1	56.0893528	.
50	15	3	52.9028272	2.54619935

ANALYSIS OF STRENGTH FOR CONTROL MIXES (11-17) AND 50% FLYASH (13-15, 16) 1
 16:18 Friday, March 19, 1993

----- DAY=56 -----

General Linear Models Procedure

Dependent Variable: MPA

Tests of Hypotheses using the Type I MS for FA*BATCH as an error term

Source	DF	Type I SS	Mean Square	F Value	Pr > F
FA	1	71.41458006	71.41458006	.	.

ANALYSIS OF STRENGTH FOR CONTROL MIXES (11,17) AND 50% FLYASH (13, 15, 16) -
16:18 Friday, March 19, 1991

----- DAY=91 -----

General Linear Models Procedure
Class Level Information

Class	Levels	Values
FA	2	0 50
BATCH	5	11 13 15 16 17
CYLINDER	3	1 2 3
DAY	1	91

Number of observations in by group = 15

NOTE: Due to missing values, only 6 observations can be used in this analysis.

ANALYSIS OF STRENGTH FOR CONTROL MIXES (11-17) AND DAY FLYASH (15, 17-19) :
 14:12 Friday, March 19, 1997

----- DAY-91 -----

General Linear Models Procedure

Dependent Variable: MPA

Source	DF	Sum of Squares	Mean Square	F Value	Pr > F
Model	1	17.48447175	17.48447175	2.53	0.1866
Error	4	27.59454045	6.89863511		
Corrected Total	5	45.07901220			
	R-Square	C.V.	Root MSE		MPA Mean
	0.387863	4.396053	2.626525		59.74735

Source	DF	Type I SS	Mean Square	F Value	Pr > F
FA	1	17.48447175	17.48447175	2.53	0.1866
BATCH	0	0.00000000	.	.	.
FA*BATCH	0	0.00000000	.	.	.

ANALYSIS OF STRENGTH FOR CONTROL MIXES (11+13) AND 50% FLYASH (17+19+13) 1
 16:18 Friday, March 19, 1990

----- DAY=91 -----

General Linear Models Procedure

Level of FA	N	-----MPA----- Mean	SD
0	3	61.4544213	2.53433762
50	3	58.0402868	2.71558521

Level of BATCH	N	-----MPA----- Mean	SD
11	3	61.4544213	2.53433762
13	3	58.0402868	2.71558521

Level of FA	Level of BATCH	N	-----MPA----- Mean	SD
0	11	3	61.4544213	2.53433762
50	13	3	58.0402868	2.71558521

ANALYSIS OF STRENGTH FOR CONTROL MIXES (11,17) AND 50% FLYASH (13, 15, 16) at
14:18 Friday, March 12, 1993

----- DAY 91 -----

General Linear Models Procedure

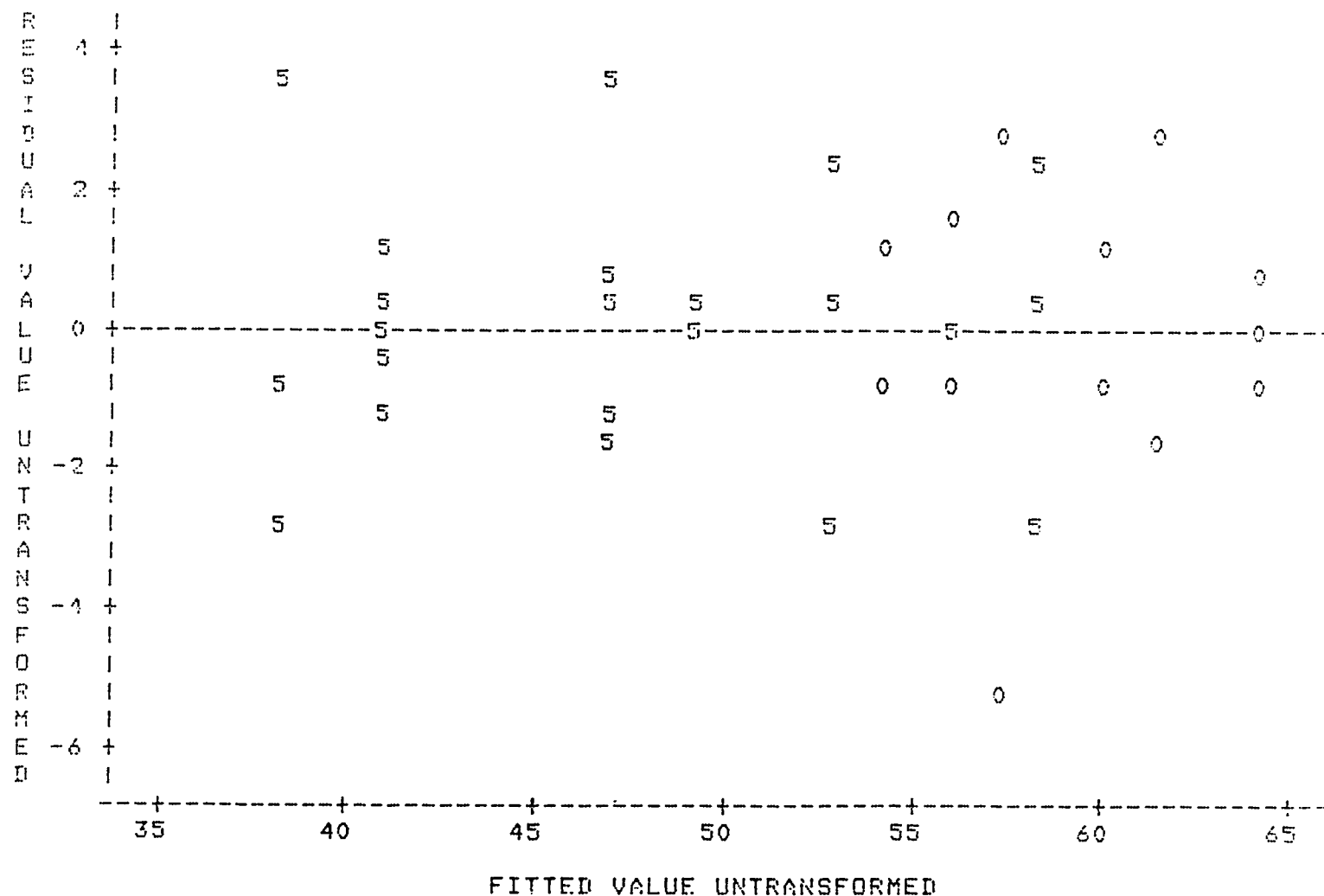
Dependent Variable: MPA

Tests of Hypotheses using the Type I MS for FA%BATCH as an error term

Source	DF	Type I SS	Mean Square	F Value	Pr > F
FA	1	17.48447175	17.48447175	.	.

ANALYSIS OF STRENGTH FOR CONTROL MIXES (11,17) AND 50% FLYASH (13, 18, 19)
 RESIDUAL VERSUS FITTED PLOT
 16:18 Friday: March 19: 1977

Plot of R0*F0. Symbol is value of FA.



Appendix C

Freezing-and-Thawing Results

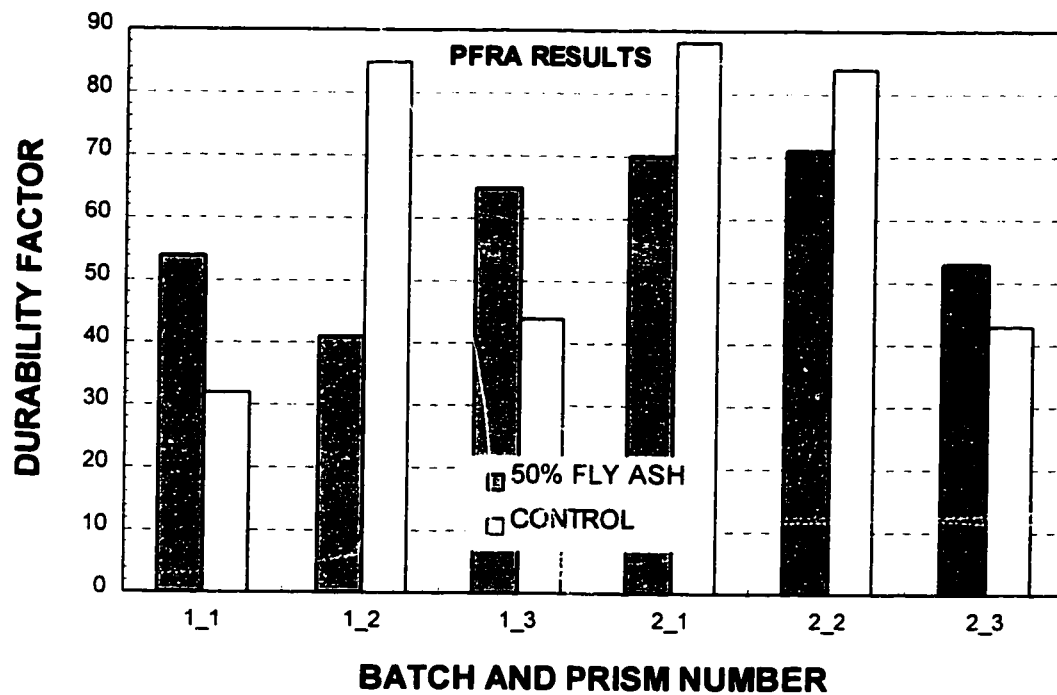


Figure C.1 Durability factors of air-entrained fly ash and control concretes following exposure to 270 cycles of freezing-and-thawing according to ASTM C-666 standard. Testing was performed at the PFRA laboratory, on the UofS campus.

Table C.1 Air void characteristics of hardened fly ash and control concretes, measured according to ASTM C-457 standard.

Concrete Mixture	Air Content %	Void Frequency n	Specific Surface 1/mm	Paste Content %	Ave. Chord Length mm	Spacing Factor μm
AC-1-7	7.459	0.3452	18.511	16.81	0.216	121.7
AC-2-7	9.567	0.5218	21.817	18.59	0.183	89
A5-1-7	6.756	0.3733	22.097	16.43	0.181	110
A5-2-7	9.351	0.4494	19.225	18.59	0.208	103.4

The notation used for the mixture numbering system means:

AC-1-7 Air-Entrained Control concrete, batch 1, prism 7

A5-2-7 Air-Entrained 50% fly ash concrete, batch 2, prism 7

Table C.2 Density and K-Slump of fresh concrete.

Mixture	Unit weight kg/m^3	K-Slump %
AC-1-7	2265	45
AC-2-7	2255	58
A5-1-7	2266	21
A5-2-7	2271	17

The notation used for the mixture numbering system was the same as in Table C.1.